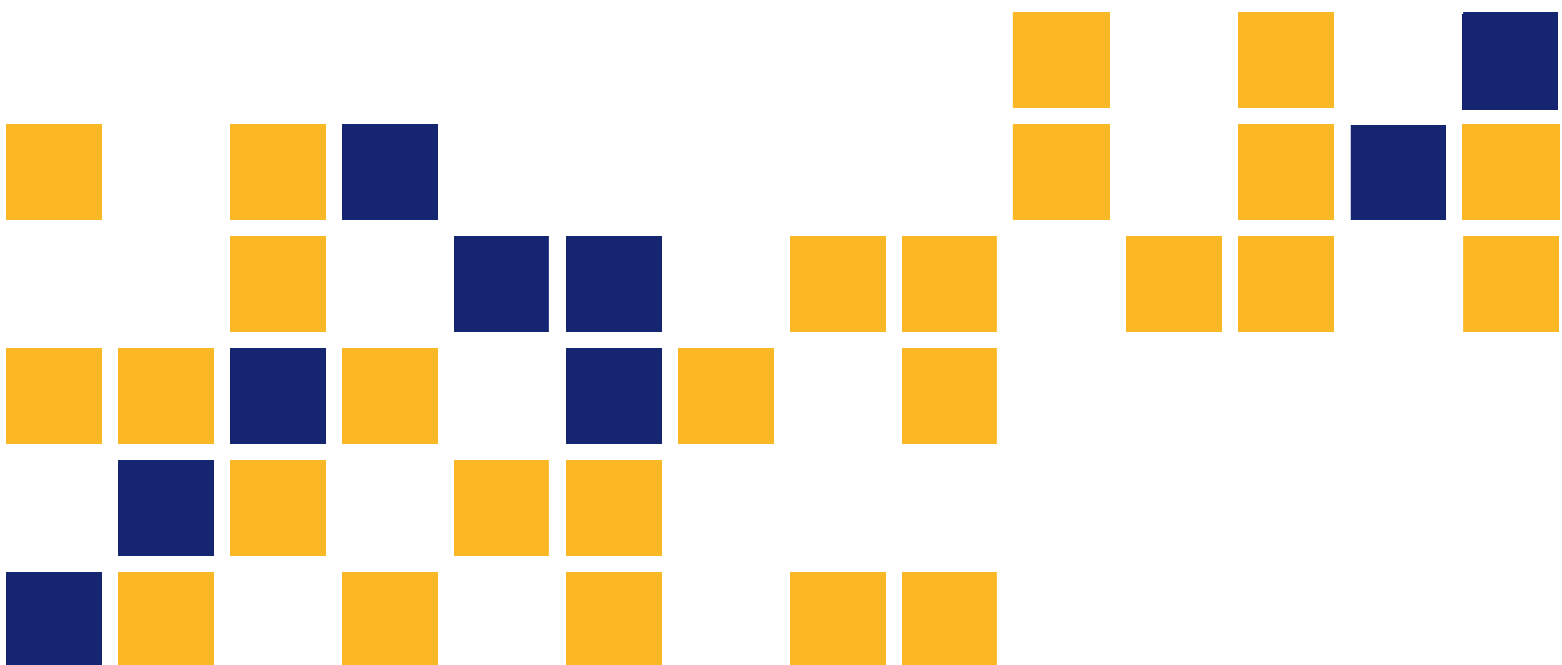


A Comparison Study of One- and Two-Dimensional Hydraulic Models for River Environments

Evan C. Deal
A. David Parr, Ph.D.
C. Bryan Young, Ph.D., P.E.

The University of Kansas



| | | | |
|-----------------------------------------------------------------------------------------------------------------------------------------------------------------------------------------------------------------------------------------------------------------------------------------------------------------------------------------------------------------------------------------------------------------------------------------------------------------------------------------------------------------------------------------------------------------------------------------------------------------------------------------------------------------------------------------------------------------------------------------------------------------------------------------------------------------------------------------------------------------------------------------------------------------------------------------------------------------------------------------------------------------------------------------------------------------------------------------------------------------------------------------------------------------------------------------------------------------------------------------------------------------------------------------------------------------------------------------------------------------------------------------------------------------------------------------------------------------------------------------------------------------------------------------------------------------------------------------------------------------------|------------------------------------------------------------------|---------------------------------------------------------------------------------------------------------------------------------------------------------------------------------------------------|------------------------------------------------|
| 1 Report No. KS-17-02 | 2 Government Accession No. | 3 Recipient Catalog No. | |
| 4 Title and Subtitle A Comparison Study of One- and Two-Dimensional Hydraulic Models for River Environments | | 5 Report Date May 2017 | 6 Performing Organization Code |
| 7 Author(s) Evan C. Deal, A. David Parr, Ph.D., C. Bryan Young, Ph.D., P.E. | | 7 Performing Organization Report No. | |
| 9 Performing Organization Name and Address The University of Kansas Department of Civil, Environmental and Architectural Engineering 1530 West 15th St Lawrence, Kansas 66045-7609 | | 10 Work Unit No. (TRAIS) | 11 Contract or Grant No. C2062 |
| 12 Sponsoring Agency Name and Address Kansas Department of Transportation Bureau of Research 2300 SW Van Buren Topeka, Kansas 66611-1195 | | 13 Type of Report and Period Covered Final Report January 2015–December 2016 | 14 Sponsoring Agency Code RE-0681-01 |
| 15 Supplementary Notes For more information write to address in block 9. | | | |
| <p>Computer models are used every day to analyze river systems for a wide variety of reasons vital to the public interest. For decades most hydraulic engineers have been limited to models that simplify the fluid mechanics to the unidirectional case. With the advent of higher quality data and greater computational power, two-dimensional hydrodynamic models have become practical for widespread use. Two such models are considered in this report: HEC-RAS v.5.0, v.5.0.1, and v.5.0.3, and SRH-2D v.3.0. These two-dimensional models were compared to the most common one-dimensional model (HEC-RAS). While the latest version of HEC-RAS is capable of both one- and two-dimensional analyses, previous versions were restricted to one-dimensional flow. Findings in this report include: differences in the flow divisions for multiple opening bridges for all three models, less subjectivity in the construction of the 2D models than for the 1D, differences in the sensitivity of each 2D model to the Manning's roughness coefficient, great similarity in the expansion and contraction rates at bridges for the 2D models when using the full momentum equations with HEC-RAS 2D, differences in the response of the two-dimensional models at steady state conditions to vortex shedding through bridge openings with cylindrical piers, shorter computation times for HEC-RAS 2D than SRH-2D using highly comparable model setups, and in general, higher depths predicted by SRH-2D than HEC-RAS 1D but the highest depths overall predicted by the HEC-RAS 2D full momentum model.</p> | | | |
| 17 Key Words Hydraulic Modeling, One-Dimensional Hydraulic Model, Two-Dimensional Hydraulic Model | | 18 Distribution Statement No restrictions. This document is available to the public through the National Technical Information Service www.ntis.gov . | |
| 19 Security Classification (of this report) Unclassified | 20 Security Classification (of this page) Unclassified | 21 No. of pages 252 + Appendix | 22 Price |

Form DOT F 1700.7 (8-72)

This page intentionally left blank.

A Comparison Study of One- and Two-Dimensional Hydraulic Models for River Environments

Final Report

Prepared by

Evan C. Deal
A. David Parr, Ph.D.
C. Bryan Young, Ph.D., P.E.

The University of Kansas

A Report on Research Sponsored by

THE KANSAS DEPARTMENT OF TRANSPORTATION
TOPEKA, KANSAS

and

THE UNIVERSITY OF KANSAS
LAWRENCE, KANSAS

May 2017

© Copyright 2017, Kansas Department of Transportation

NOTICE

The authors and the state of Kansas do not endorse products or manufacturers. Trade and manufacturers names appear herein solely because they are considered essential to the object of this report.

This information is available in alternative accessible formats. To obtain an alternative format, contact the Office of Public Affairs, Kansas Department of Transportation, 700 SW Harrison, 2nd Floor – West Wing, Topeka, Kansas 66603-3745 or phone (785) 296-3585 (Voice) (TDD).

DISCLAIMER

The contents of this report reflect the views of the authors who are responsible for the facts and accuracy of the data presented herein. The contents do not necessarily reflect the views or the policies of the state of Kansas. This report does not constitute a standard, specification or regulation.

Abstract

Computer models are used every day to analyze river systems for a wide variety of reasons vital to the public interest. For decades most hydraulic engineers have been limited to models that simplify the fluid mechanics to the unidirectional case. With the advent of higher quality data and greater computational power, two-dimensional hydrodynamic models have become practical for widespread use. Two such models are considered in this report: HEC-RAS v.5.0, v.5.0.1, and v.5.0.3, and SRH-2D v.3.0. These two-dimensional models were compared to the most common one-dimensional model (HEC-RAS). While the latest version of HEC-RAS is capable of both one- and two-dimensional analyses, previous versions were restricted to one-dimensional flow. Findings in this report include: differences in the flow divisions for multiple opening bridges for all three models, less subjectivity in the construction of the 2D models than for the 1D, differences in the sensitivity of each 2D model to the Manning's roughness coefficient, great similarity in the expansion and contraction rates at bridges for the 2D models when using the full momentum equations with HEC-RAS 2D, differences in the response of the two-dimensional models at steady state conditions to vortex shedding through bridge openings with cylindrical piers, shorter computation times for HEC-RAS 2D than SRH-2D using highly comparable model setups, and in general, higher depths predicted by SRH-2D than HEC-RAS 1D but the highest depths overall predicted by the HEC-RAS 2D full momentum model.

Acknowledgements

The authors would like to thank the Kansas Department of Transportation (KDOT) for their support of this project. Project Monitor Mike Orth, P.E., provided guidance and feedback throughout the course of the project; his input was critical to the success of the project. We thank Gary Brunner, P.E., Senior Hydraulic Engineer at the U.S. Army Corps of Engineers (USACE) Hydrologic Engineering Center (HEC). Gary Brunner provided valuable insight into the continuing development of HEC-RAS, the bridge flume model study (Chapter 6), and the selection of Manning *n*-values in HEC-RAS 2D. Dr. Yong Lai, Hydraulic Engineer with the Bureau of Reclamation, provided assistance early on with our implementation of SRH-2D.

Table of Contents

| | |
|-------------------------------------------------------------------------|-----|
| Abstract | v |
| Acknowledgements | vi |
| Table of Contents | vii |
| List of Tables | x |
| List of Figures | xii |
| Chapter 1: Introduction | 1 |
| Chapter 2: Theory | 3 |
| 2.1 Overview of the Model Theory and Hydraulics | 3 |
| 2.2 Model Equations | 9 |
| 2.2.1 One-Dimensional HEC-RAS Equations | 9 |
| 2.2.2 Two-Dimensional HEC-RAS Equations | 14 |
| 2.2.3 SRH-2D Equations..... | 17 |
| Chapter 3: Computation Test and Basic Flow Around a Bend..... | 20 |
| 3.1 Overview of the Computation Test and Basic Flow Around a Bend | 20 |
| 3.2 Computational Test Results | 24 |
| 3.3 Basic Flow around a Bend | 29 |
| Chapter 4: Turbulence and Roughness Sensitivity Tests..... | 35 |
| 4.1 Overview of the Turbulence and Roughness Sensitivity Tests | 35 |
| 4.2 Results of Sensitivity Tests..... | 39 |
| Chapter 5: Mixed Flow Regime Test..... | 43 |
| 5.1 Overview of the Mixed Flow Regime Test | 43 |
| 5.2 Direct Step Method and Solution Procedure for Test Reach..... | 44 |
| 5.3 Direct Step Method Results | 47 |
| 5.4 Equations Used for Depth Step Method | 48 |

| | |
|----------------------------------------------------------------------------------------------|-----|
| 5.5 SRH-2D Hydraulic Jump Test Terrain Setup and Determining Results for Comparison .. | 49 |
| 5.6 SRH-2D Hydraulic Jump Test Results from Simulation with Square 1-Foot Elements | 51 |
| 5.7 One-Dimensional HEC-RAS Hydraulic Jump Test | 59 |
| 5.8 Two-Dimensional HEC-RAS Hydraulic Jump Test..... | 68 |
| Chapter 6: Bridge Flume Modeling Study | 76 |
| 6.1 Background for the Bridge Flume Modeling Study | 76 |
| 6.2 HEC-RAS 2D Model of Type One Bridge from Flume Study (Short Model)..... | 88 |
| 6.3 SRH-2D Model of Type One Bridge from Flume Study (Short Model)..... | 95 |
| 6.4 Summary of Water Surface Profiles for the Type One Bridge Experiments..... | 103 |
| 6.5 Calibration of the Two-Dimensional Models to the Laboratory Results (Short Model).. | 104 |
| 6.6 HEC-RAS 2D Modeling of Type One Bridge Experiments from Flume Study (Long Model)..... | 109 |
| 6.7 SRH-2D Modeling of Type One Bridge Experiments from Flume Study (Long Model)..... | 119 |
| 6.8 Runtime Comparison | 124 |
| Chapter 7: Neodesha Floodplain Study | 125 |
| 7.1 Background for the Neodesha Floodplain Study..... | 125 |
| 7.2 One-Dimensional HEC-RAS Model for Neodesha | 133 |
| 7.2.1 One-Dimensional HEC-RAS Neodesha Model Setup..... | 133 |
| 7.2.2 One-Dimensional HEC-RAS Neodesha Model Results | 136 |
| 7.3 Two-Dimensional HEC-RAS Full Momentum Model for Neodesha | 139 |
| 7.3.1 Two-Dimensional HEC-RAS Full Momentum Neodesha Model Setup..... | 139 |
| 7.3.2 Two-Dimensional HEC-RAS Full Momentum Neodesha Model Results | 143 |
| 7.4 SRH-2D Model for Neodesha..... | 150 |
| 7.4.1 SRH-2D Neodesha Model Setup | 150 |
| 7.4.2 SRH-2D Neodesha Model Results..... | 153 |

| | |
|----------------------------------------------------------------------------|-----|
| 7.5 Summary of the Neodesha Floodplain Study Hydraulic Model Results | 157 |
| 7.6 Runtime Comparison | 163 |
| Chapter 8: Sumner County Site | 165 |
| 8.1 Background for the Floodplain Study..... | 165 |
| 8.2 HEC-RAS 1D Model..... | 167 |
| 8.3 HEC-RAS 2D Model..... | 169 |
| 8.4 SRH-2D Model | 183 |
| 8.5 Runtime Comparison | 186 |
| Chapter 9: Butler County Site..... | 187 |
| 9.1 Background for the Floodplain Study..... | 187 |
| 9.2 Preparation of Terrain Data | 190 |
| 9.2.1 Create a Polygon for the Flat Area of the LIDAR Data | 192 |
| 9.2.2 Creating the Trapezoidal Channel Raster | 194 |
| 9.2.3 Merge the Channel Raster and the LIDAR Raster..... | 197 |
| 9.3 Create HEC-RAS Terrain in RAS Mapper..... | 199 |
| 9.3.1 1D HEC-RAS Model | 202 |
| 9.4 2D HEC-RAS Model | 205 |
| 9.5 Summary | 218 |
| Chapter 10: Conclusions | 220 |
| References | 227 |

Due to file size, the Appendix (Notes on SRH-2D Model Construction using the Surface Water Modeling System (SMS) v.12.1.7) is available in a separate file located at:

<https://kdotapp.ksdot.org/kdotlib/kdotlib2.aspx>

or by contacting the KDOT Library at KDOT#Research.Library@ks.gov.

List of Tables

| | | |
|-------------|-------------------------------------------------------------------------------------------------------------------------|-----|
| Table 3.1: | Major Inputs and Results of the Computational Tests | 25 |
| Table 3.2: | Estimation of Calculation Speed for Each Model | 26 |
| Table 3.3: | Solution of Equation 3.8 (Henderson's 7.17) with Data from SRH-2D Model | 34 |
| Table 3.4: | Solution of Equation 3.8 (Henderson's 7.17) with Data from HEC-RAS 2D Model..... | 34 |
| Table 4.1: | Change in Depth from Upstream to Downstream Normalized by the Channel Length..... | 42 |
| Table 5.1: | Depth Step Method Spreadsheet with Incorrect Solution | 45 |
| Table 5.2: | Depth Step Method Spreadsheet with Correct Solution..... | 45 |
| Table 5.3: | Depth Step Method Results for M1 Profile from Station 500 to 900..... | 46 |
| Table 5.4: | Combined Depth Step Method Results for S2 and S1 Profiles from Station 300 to 500 | 46 |
| Table 5.5: | Depth Step Method Results for M2 Profile from Station 0 to 300..... | 47 |
| Table 5.6: | SRH-2D Froude Numbers at Station 300 for Hydraulic Jump Test..... | 59 |
| Table 6.1: | Stations for Short and Long Lab and Prototype Piezometer Locations | 78 |
| Table 6.2: | Lab and Prototype Station–Elevation Points for Figure 6.1 | 79 |
| Table 6.3: | WSE Values from Lab Experiments Expressed in 20-Scale Prototype Dimensions (Q in cfs)..... | 82 |
| Table 6.4: | Ordinates of Hydrographs Used for Type One Bridge Study 2D Simulations | 87 |
| Table 6.5: | Determination of Upstream EGL from Flume Data for HEC-RAS 2D Simulations | 89 |
| Table 6.6: | Results for Averaging Process at the Most Upstream Point for SRH-2D Bridge Flume Simulations..... | 101 |
| Table 6.7: | Summary of Water Surface Profiles for the Type One Bridge Experiments | 104 |
| Table 6.8: | HEC-RAS 2D Results for Time-Averaged Depth at a Point Upstream of the Bridge | 107 |
| Table 6.9: | SRH-2D Results for Time-Averaged Depth at a Point Upstream of the Bridge.... | 107 |
| Table 6.10: | Comparison of the Calibration Test Results from Both Two-Dimensional Models to the Laboratory Depth of 17.77 feet | 108 |

| | |
|---------------------------------------------------------------------------------------------------------------------------------|-----|
| Table 6.11: HEC-RAS Grid Cell Parameters | 115 |
| Table 6.12: DSBC for Long Model for $D = 0.2$ seconds | 116 |
| Table 6.13: Comparison of Runtimes | 124 |
| Table 7.1: Flow Divisions for the Hydraulic Structures of the HEC-RAS 1D Neodesha Floodplain Model | 138 |
| Table 7.2: Flow Divisions at the Final Timestep for the Hydraulic Structures of the HEC-RAS 2D Neodesha Floodplain Models | 145 |
| Table 7.3: Flow Divisions at the Final Timestep for the Hydraulic Structures of the SRH-2D Neodesha Floodplain Model..... | 154 |
| Table 7.4: Summary of Flooded Area for All Three Models for the Neodesha Test Site..... | 158 |
| Table 7.5: Summary of Flow Divisions for all Models through the Hydraulic Structures within the Neodesha Test Site | 159 |
| Table 7.6: Runtime Comparison for Neodesha | 164 |
| Table 8.1: Timesteps for Different Δx -Values and Velocities..... | 175 |
| Table 8.2: Parameters for SRH-2D and HEC-RAS 2D 1-Second Timestep Models | 184 |
| Table 8.3: Comparison of Runtimes | 186 |
| Table 9.1: Discharges from FEMA FIS for El Dorado Bridge No 54-8-271 | 188 |
| Table 9.2: Floodplain Areas | 217 |
| Table 10.1: Considerations for Model Selection | 223 |
| Table 10.2: Considerations for 2D Modeling | 225 |

List of Figures

| | | |
|--------------|----------------------------------------------------------------------------------------------|----|
| Figure 2.1: | Plan View of Typical HEC-RAS 1D Model | 3 |
| Figure 2.2: | Selection of Example Cross Section 1589.255 | 4 |
| Figure 2.3: | Representation of Assumed Flow Directions for a Single Cross Section | 5 |
| Figure 2.4: | HEC-RAS 1D Interpretation of Given Cross Section | 5 |
| Figure 2.5: | Schematic of a Typical HEC-RAS 1D Reach Model | 6 |
| Figure 2.6: | Geometric Data Editor Window for HEC-RAS 5.0 Bald Eagle Creek Dam Break Example Project..... | 7 |
| Figure 2.7: | Zoomed-In View for HEC-RAS 2D Bald Eagle Creek Example Project Showing Mesh Details | 8 |
| Figure 2.8: | SRH-2D Mesh Viewed in SMS 12.1 for a Site in Crawford County, KS | 8 |
| Figure 2.9: | Zoomed-In View of SRH-2D Mesh from Figure 2.8 Showing Elevation Values at Corner Nodes..... | 9 |
| Figure 2.10: | Diagram Showing Terms Used in HEC-RAS 1D Energy Equation | 10 |
| Figure 2.11: | Channel Subdivisions Used in HEC-RAS 1D Cross Section Model | 11 |
| Figure 2.12: | Square Mesh Element atop Grid with Elevation Contours Spaced at 0.2' Intervals | 15 |
| Figure 2.13: | Three-Dimensional Representation of the Mesh Element from Figure 2.12 | 15 |
| Figure 2.14: | View from Upstream Looking Downstream | 15 |
| Figure 2.15: | View Perpendicular to That in Figure 2.14 Looking Towards the Main Channel Flowline..... | 16 |
| Figure 3.1: | Significant Properties of the Machine Used to Perform the Computational Tests | 20 |
| Figure 3.2: | Plan View Showing Geometric Basis for Computational Test Reach | 21 |
| Figure 3.3: | Close-Up of View Describing Straight Segments of Computational Test Reach... .. | 22 |
| Figure 3.4: | Elevation View of Geometric Basis for Cross Sections of the Computational Test Reach | 23 |
| Figure 3.5: | Representative Cross Sections for the Computational Test Terrain | 24 |
| Figure 3.6: | Comparison of the Six Trials Performed for the Computational Test | 25 |
| Figure 3.7: | Steady State Profiles for Channel Centerline for Computational Tests | 28 |

| | | |
|--------------|--------------------------------------------------------------------------------------------------------------------------|----|
| Figure 3.8: | View from SMS 12.1 of Cross Section Used for Analysis of Basic Flow around a Bend..... | 30 |
| Figure 3.9: | SRH-2D Data for Cross Section at Station 1253.81 | 30 |
| Figure 3.10: | HEC-RAS 2D Data for Cross Section at Station 1253.81 | 31 |
| Figure 3.11: | Detailed SRH-2D Data for Cross Section at Station 1253.81 | 32 |
| Figure 3.12: | Detailed HEC-RAS 2D Data for Cross Section at Station 1253.81 | 33 |
| Figure 4.1: | Plan View of the Geometric Basis for Tests with $l = 6$ feet..... | 36 |
| Figure 4.2: | SMS 12.1 Project Overview and Grid Display for SRH-2D Sensitivity Tests | 37 |
| Figure 4.3: | Representative Plan View from HEC-RAS 2D Showing Typical Flow Patterns from the Simulations (Flow Left to Right)..... | 37 |
| Figure 4.4: | HEC-RAS 2D Flow Area Elements for Sensitivity Tests..... | 38 |
| Figure 4.5: | Triangulated Irregular Network for Model Elevations for HEC-RAS 2D Sensitivity Tests as Seen in RAS Mapper..... | 38 |
| Figure 4.6: | SRH-2D Roughness Coefficient Tests with Parabolic Turbulence Equal to 0.7 for all Trials | 40 |
| Figure 4.7: | SRH-2D Parabolic Turbulence Constant Tests with Manning's Roughness Coefficient Equal to 0.01 for all Tests | 40 |
| Figure 4.8: | HEC-RAS 2D Roughness Coefficient Tests | 41 |
| Figure 4.9: | Comparison between Roughness Coefficient Test Results for SRH-2D and HEC-RAS 2D | 41 |
| Figure 5.1: | Elevation View of Reach with Exaggerated Z-Scale | 43 |
| Figure 5.2: | Representative Cross Section for Channel | 44 |
| Figure 5.3: | Locating Hydraulic Jump on the Hydraulically Steep Section | 47 |
| Figure 5.4: | Composite Water Surface Profile from the Depth Step Method..... | 48 |
| Figure 5.5: | Raster and Lines Denoting Channel Slope Changes | 50 |
| Figure 5.6: | Plan View in SMS 12.1 with Color Fill Contours of SRH-2D Hydraulic Jump Trial Results Using Square 4-Foot Elements | 50 |
| Figure 5.7: | Plan View in SMS 12.1 with Color Fill Contours of SRH-2D Hydraulic Jump Trial Results Using Square 2-Foot Elements | 51 |
| Figure 5.8: | Plan View in SMS 12.1 with Color Fill Contours of SRH-2D Hydraulic Jump Trial Results Using Square 1-Foot Elements | 51 |

| | |
|-------------------------------------------------------------------------------------------------------------------------------------------------------------------|----|
| Figure 5.9: SMS 12.1 Output for Centerline Water Surface Elevation Data from Hydraulic Jump Test with 1-Foot Square Mesh Elements..... | 52 |
| Figure 5.10: Oblique View of Simulation Output without Exaggerated Z-Scale..... | 52 |
| Figure 5.11: Complete Water Surface Profile along Channel Centerline for SRH-2D Hydraulic Jump Test | 53 |
| Figure 5.12: Data from Figure 5.11 near the Location of the Hydraulic Jump | 54 |
| Figure 5.13: Velocity Details near Hydraulic Jump from SRH-2D Viewed in SMS | 55 |
| Figure 5.14: Close-Up of Recirculating Flow Where Extents Are Defined in Figure 5.13 | 56 |
| Figure 5.15: Froude Number Data across Cross Section at Station 408.50..... | 57 |
| Figure 5.16: Gradually Varied Flow Profiles for Hydraulic Jump Test Reach from Step Method and SRH-2D..... | 57 |
| Figure 5.17: Detailed Summary of Cross Section at Station 300 | 58 |
| Figure 5.18: Graphical Representation of HEC-RAS 5.0 1D Cross Sections for Hydraulic Jump Test at 8-Foot Spacing | 60 |
| Figure 5.19: Poor Results of Hydraulic Jump Test for 1D HEC-RAS Simulation Using Subcritical Flow Regime Option..... | 61 |
| Figure 5.20: Initial HEC-RAS 1D Simulation to Locate Hydraulic Jump Using 8-Foot Spacing for Cross Sections..... | 62 |
| Figure 5.21: HEC-RAS 1D Simulation to Locate Hydraulic Jump Using 4-Foot Spacing for Cross Sections | 63 |
| Figure 5.22: Conveyance Sections for Normal Depth on the Hydraulically Mild Portion of the Hydraulic Jump Test Reach with Incorrect Placement of Bank Points..... | 64 |
| Figure 5.23: Proper Placement of HEC-RAS Bank Points on the Trapezoidal Channel | 65 |
| Figure 5.24: HEC-RAS 1D Simulation to Locate Hydraulic Jump Using 4-Foot Spacing for Cross Sections and Proper Placement of Bank Points | 66 |
| Figure 5.25: Cross Section Data Showing Adjusted Bank Points and No Contraction or Expansion Loss Coefficients | 67 |
| Figure 5.26: 2D Flow Area for HEC-RAS Hydraulic Jump Test Model | 68 |
| Figure 5.27: Default Manning's Roughness Coefficient and Grid Spacing for 2D Flow Area... <td>69</td> | 69 |
| Figure 5.28: Boundary Conditions for the HEC-RAS 2D Hydraulic Jump Test | 69 |
| Figure 5.29: Hydrograph Used for the HEC-RAS 2D Hydraulic Jump Test | 70 |
| Figure 5.30: Option for Sub- and Supercritical Flow in the Unsteady Flow Analysis Menu | 71 |

| | |
|---------------------------------------------------------------------------------------------------------------------------|----|
| Figure 5.31: Options Leading to the Governing Equations Used for 2D Simulation..... | 72 |
| Figure 5.32: Tab Including Options for Selecting Equations of Fluid Motion..... | 72 |
| Figure 5.33: RAS Mapper Window Showing Results of the Simulation Using the Diffusion Wave Equation | 73 |
| Figure 5.34: Water Surface Profile for HEC-RAS 2D Hydraulic Jump Test Using Simplified Equation of Fluid Motion | 73 |
| Figure 5.35: Water Surface Profile for HEC-RAS 2D Hydraulic Jump Test Using St. Venant Equation | 74 |
| Figure 5.36: Both Water Surface Profiles from HEC-RAS 2D Simulations for Hydraulic Jump Test | 74 |
| Figure 5.37: Summary of Profiles from Hydraulic Jump Tests..... | 75 |
| Figure 6.1: Plan View of Laboratory Model..... | 76 |
| Figure 6.2: Location of Piezometers in Lab and Prototype Stations | 76 |
| Figure 6.3: Piezometric Surface for Flume Experiment | 77 |
| Figure 6.4: Section C–C (Figure 6.1) through Bridge Abutment | 78 |
| Figure 6.5: Cross Section Data for Sections A–A and B–B of Figure 6.1 | 80 |
| Figure 6.6: Results from Previous Study for the Type One Bridge Configuration Using HEC-RAS 4.1..... | 83 |
| Figure 6.7: Comparison of Lab and Modified, Undistorted 1D HEC-RAS 5.0.1 Models from Previous Study for 3620 cfs | 84 |
| Figure 6.8: Comparison of Lab and Modified, Undistorted 1D HEC-RAS 5.0.1 Models from Previous Study for 4400 cfs | 85 |
| Figure 6.9: Comparison of Lab and Modified, Undistorted 1D HEC-RAS 5.0.1 Models from Previous Study for 5600 cfs | 86 |
| Figure 6.10: View from ArcScene of TIN for Type One Bridge Experiments with Elevations Given in Feet | 86 |
| Figure 6.11: Hydrographs Used for Type One Bridge Study 2D Simulations | 87 |
| Figure 6.12: HEC-RAS 2D Cell Face on Bridge Piers for Flume Study..... | 88 |
| Figure 6.13: Lab and HEC-RAS 2D Full Momentum Equation Model Results for Type One Bridge Configuration and 3620 cfs | 90 |
| Figure 6.14: Lab and HEC-RAS 2D Full Momentum Equation Model Results for Type One Bridge Configuration and 4400 cfs | 90 |

| | |
|---------------------------------------------------------------------------------------------------------------------------------------------------------------------------------------|-----|
| Figure 6.15: Lab and HEC-RAS 2D Full Momentum Equation Model Results for Type One Bridge Configuration and 5600 cfs | 91 |
| Figure 6.16: Velocity Contour Maps Ranging for 0 to 15 fps with Tracers for the Third High Discharge Profile Using Two Different Upstream EGLs | 92 |
| Figure 6.17: Time Series of Velocity Contour Maps Ranging from 0 to 15 fps for the Second Middle Discharge Profile | 93 |
| Figure 6.18: Water Surface Elevation Contour Map for the Final Timestep of the Second Middle Discharge Profile | 94 |
| Figure 6.19: Depth Map with Tracers for the Second Middle Discharge Profile Showing Typical Expansion and Contraction Ratios | 95 |
| Figure 6.20: Before and After Manual Mesh Adjustment for SRH-2D Bridge Flume Model.... | 96 |
| Figure 6.21: Oblique View from SMS 12.1 of the SRH-2D Computational Mesh Used for Type One Bridge Flume Simulations..... | 97 |
| Figure 6.22: Lab and SRH-2D Model Results for Type One Bridge Configuration and 3620 cfs | 98 |
| Figure 6.23: Lab and SRH-2D Model Results for Type One Bridge Configuration and 4400 cfs | 98 |
| Figure 6.24: Lab and SRH-2D Model Results for Type One Bridge Configuration and 5600 cfs | 99 |
| Figure 6.25: Time Series Showing Water Surface Elevation for the Third High Discharge Profile SRH-2D Simulation | 100 |
| Figure 6.26: Froude Number Contour Map from SMS 12.1 for the Third High Discharge Profile SRH-2D Simulation | 102 |
| Figure 6.27: Water Surface Profiles at the Cross Section 90 feet Upstream for the Final Timestep of the Profile with a Discharge of 4400 cfs and a Tailwater Depth of 15.43 feet..... | 105 |
| Figure 6.28: Example of Depth at a Discrete Time Mapped to an Observation Point in the RAS Mapper..... | 106 |
| Figure 6.29: HEC-RAS 2D Terrain | 110 |
| Figure 6.30: Polyline Z Lines in GIS Used to Create the Land Raster..... | 111 |
| Figure 6.31: ArcScene Illustration of Combining Land and Pier Rasters to Create the HEC-RAS 2D Terrain | 111 |

| | |
|---------------------------------------------------------------------------------------------------------------------------------------------------------------------------------------------------|-----|
| Figure 6.32: Creating the Pier Raster..... | 112 |
| Figure 6.33: Pier Raster Used in this Study..... | 112 |
| Figure 6.34: HEC-RAS 2D Breaklines..... | 113 |
| Figure 6.35: HEC-RAS 2D Grid Cells and Breaklines | 113 |
| Figure 6.36: HEC-RAS Grid Cell Parameters | 115 |
| Figure 6.37: HEC-RAS 2D Long Model Results for $\Delta t = 0.5$ seconds | 117 |
| Figure 6.38: HEC-RAS 2D Long Model Best Fit Results for Runs 7, 8, and 9 | 118 |
| Figure 6.39: Velocity Patterns and Vectors at the End of Run 1 for $\Delta t = 0.2$ seconds..... | 118 |
| Figure 6.40: Selection of \square for SRH-2D | 119 |
| Figure 6.41: SRH-2D Long Model Results for $\Delta t = 0.1$ second..... | 120 |
| Figure 6.42: HEC-RAS 2D and SRH-2D Max WSE Profiles for Runs 1, 2, and 3 | 121 |
| Figure 6.43: HEC-RAS 2D and SRH-2D Max WSE Profiles for Runs 4 and 5 | 122 |
| Figure 6.44: HEC-RAS 2D and SRH 2D Max WSE Profiles for Runs 7, 8, and 9..... | 123 |
| Figure 6.45: Computer Specifications | 124 |
| Figure 7.1: Neodesha Floodplain Study Site and Surrounding Area..... | 125 |
| Figure 7.2: Digital Elevation Model for the Neodesha Floodplain Study | 128 |
| Figure 7.3: Composite TIN of Raw Data and As-Built Plan Bridge Data for Main Bridge on Highway 400 | 130 |
| Figure 7.4: Composite TIN of Raw Data and As-Built Plan Bridge Data for Main Bridge on Highway 75 | 130 |
| Figure 7.5: Manning's Roughness Coverage Polygons for the Neodesha Floodplain Study Site..... | 132 |
| Figure 7.6: 1D HEC-RAS Geometry and Flood Map for the Neodesha Floodplain Study | 133 |
| Figure 7.7: River Station 2192.038 from the HEC-RAS 1D Model for Neodesha Floodplain Study Showing Blocked Ineffective Flow Areas Typical of the Three Most Downstream Cross Sections | 134 |
| Figure 7.8: Upstream Bounding Bridge Cross Section for Highway 400 | 135 |
| Figure 7.9: Upstream Bounding Bridge Cross Section for Highway 75 | 135 |
| Figure 7.10: Map Showing Inundated Area from HEC-RAS 1D Neodesha Floodplain Model | 137 |
| Figure 7.11: Channel Centerline Water Surface Profile from the HEC-RAS 1D Neodesha Floodplain Model | 138 |

| | |
|---------------------------------------------------------------------------------------------------------------------------------------------|-----|
| Figure 7.12: Flow Results for the Main Bridge Opening on Highway 400 for the HEC-RAS 1D Neodesha Floodplain Model | 139 |
| Figure 7.13: Inflow Hydrograph for the HEC-RAS 2D Neodesha Floodplain Model..... | 140 |
| Figure 7.14: Transparent 2D Flow Area and Aerial Imagery for the HEC-RAS 2D Neodesha Floodplain Model | 141 |
| Figure 7.15: Results of Mesh Editing and Inclusion of Breaklines at the First Relief Bridge for the HEC-RAS 2D Neodesha Model | 142 |
| Figure 7.16: Map Showing Inundated Area from HEC-RAS 2D Full Momentum Neodesha Floodplain Model | 143 |
| Figure 7.17: Disconnected Flow Areas from the HEC-RAS 2D Model for Neodesha Floodplain Model | 145 |
| Figure 7.18: Weir Flow Hydrograph from HEC-RAS 2D for the Main Bridge on Highway 75 | 146 |
| Figure 7.19: Hydrographs of the HEC-RAS 2D Hydraulic Structures for the Neodesha Floodplain Study | 147 |
| Figure 7.20: Channel Centerline Water Surface Profile from HEC-RAS 1D and 2D Neodesha Floodplain Models | 147 |
| Figure 7.21: Velocity Contours with Tracers for the HEC-RAS 2D Highway 400 Openings.. | 148 |
| Figure 7.22: Velocity Contours with Tracers for the HEC-RAS 2D Highway 75 Openings.... | 149 |
| Figure 7.23: Finite-Element Mesh for SRH-2D Neodesha Floodplain Model Viewed in SMS | 150 |
| Figure 7.24: Two Plan Views Typical of the SRH-2D Mesh Construction Near the Hydraulic Structures for the Neodesha Floodplain Model..... | 151 |
| Figure 7.25: Inflow Hydrograph for SRH-2D Neodesha Floodplain Model..... | 152 |
| Figure 7.26: Map Showing Inundated Area from SRH-2D Neodesha Floodplain Model | 153 |
| Figure 7.27: Hydrographs of the SRH-2D Hydraulic Structures for the Neodesha Floodplain Study..... | 155 |
| Figure 7.28: Channel Centerline Water Surface Profile from SRH-2D Neodesha Floodplain Model | 155 |
| Figure 7.29: Velocity Contours with Vectors for the SRH-2D Highway 400 Openings | 156 |
| Figure 7.30: Velocity Contours with Vectors for the SRH-2D Highway 75 Openings | 156 |

| | |
|------------------------------------------------------------------------------------------------------------------------------------------------------------------------------------------------------|-----|
| Figure 7.31: Comparison Map Showing the Floodplain Extents from All Three Models for the Neodesha Test Site | 157 |
| Figure 7.32: HEC-RAS 2D Flow Tracers and SRH-2D Velocity Vectors at the First Relief Bridge on Highway 400 | 160 |
| Figure 7.33: Water Surface Profiles for the Three Models at the Upstream Bounding Cross Section of Highway 400 | 161 |
| Figure 7.34: Water Surface Profiles for the Three Models at the Upstream Bounding Cross Section of Highway 75 | 161 |
| Figure 7.35: Water Surface Profiles from the Stream Centerline of the Models Tested for the Neodesha Floodplain Study – HR 1D, HR 2D (Raised Piers and High Pier <i>n</i> -Values), and SRH-2D | 163 |
| Figure 8.1: Sumner County Site | 165 |
| Figure 8.2: Bridge and Pier Details | 166 |
| Figure 8.3: Land Use Polygon | 167 |
| Figure 8.4: Survey Data Along Bridge Face and Corrected for Skew Angle..... | 168 |
| Figure 8.5: Upstream HEC-RAS Internal Bridge Cross Section for Bridge 1171 | 168 |
| Figure 8.6: Floodplain Boundary for 1D HEC-RAS Model..... | 169 |
| Figure 8.7: HEC-RAS 2D Mesh | 170 |
| Figure 8.8: Mesh around Bridge Piers for Bridges 1176 and 1171 | 171 |
| Figure 8.9: HEC-RAS 2D Terrain | 171 |
| Figure 8.10: HEC-RAS 2D Terrain at Bridge 1171 | 172 |
| Figure 8.11: HEC-RAS 2D Terrain around Bridge 1171 Piers | 172 |
| Figure 8.12: Mesh Parameters | 173 |
| Figure 8.13: Ramped Inflow Hydrograph..... | 174 |
| Figure 8.14: 2D Computation Options | 175 |
| Figure 8.15: Centerline Velocities for 1-Second Timestep Run..... | 175 |
| Figure 8.16: HEC-RAS 2D Max WSE for Different Timesteps | 176 |
| Figure 8.17: HEC-RAS 2D Max WSE (1 second) – Max WSE ($\Delta t = 3, 5, \text{ or } 10$)..... | 177 |
| Figure 8.18: HEC-RAS 2D Max WSE for Different Timesteps with HEC-RAS 1D Profile ... | 177 |
| Figure 8.19: HEC-RAS 2D Floodplain for 1-second Timestep Run | 178 |
| Figure 8.20: HEC-RAS 2D Floodplain for 1-second Timestep Run with 1D Floodplain Overlain | 179 |

| | |
|------------------------------------------------------------------------------------------------------------------------------|-----|
| Figure 8.21: HEC-RAS 1D and HEC-RAS 2D (1 second) WSEs with 2D Streamlines | 180 |
| Figure 8.22: HEC-RAS 2D (1 second) cell WSEs near DS Boundary (should be 1152.57)..... | 180 |
| Figure 8.23: Long HEC-RAS 1D Floodplain and 2D HEC-RAS ($\Delta t = 1$ second)..... | 181 |
| Figure 8.24: Streamlines at Bridge 1176 for 2D HEC-RAS ($\Delta t = 1$ second) | 182 |
| Figure 8.25: Streamlines at Bridge 1176 for 2D HEC-RAS, Several Δt -values | 183 |
| Figure 8.26: SRH-2D and HEC-RAS 2D Max WSE Profiles ($\Delta t = 1$ second) | 184 |
| Figure 8.27: SRH-2D Floodplain ($\Delta t = 1$ second) | 185 |
| Figure 8.28: SRH-2D and HEC-RAS 2D Floodplains ($\Delta t = 1$ second)..... | 185 |
| Figure 9.1: Butler County Site (El Dorado, KS)..... | 187 |
| Figure 9.2: HEC-RAS Model Area..... | 189 |
| Figure 9.3: Ramped Hydrographs for HEC-RAS 2D Models | 190 |
| Figure 9.4: Weir Location..... | 191 |
| Figure 9.5: Weir Photograph | 191 |
| Figure 9.6: Walnut River Channel Centerline Elevation Plot from LIDAR | 192 |
| Figure 9.7: RAS Mapper Floodplain for Fake Model | 193 |
| Figure 9.8: Export Inundation Area to Polygon Shapefile | 193 |
| Figure 9.9: Modify Polygon Shapefile to Include Weir Area..... | 194 |
| Figure 9.10: Create Centerline Shapefile Called trapchllines for Flat Reach of LIDAR | 195 |
| Figure 9.11: Apply Copy Parallel to Create Base and Top Width of Trapezoidal Channel..... | 195 |
| Figure 9.12: (a) Populating zus and zds fields, (b) Creating a 3D shapefile | 196 |
| Figure 9.13: Create TIN from 3D Shapefile (chl_tin) | 196 |
| Figure 9.14: A Portion of chl_tin..... | 197 |
| Figure 9.15: Chl_tin Used to Create chlras..... | 197 |
| Figure 9.16: Mosaic Function was Used to Merge the Channel Raster and the Original Raster to Create the Proj4ft_ras | 198 |
| Figure 9.17: Final Proj4ft_ras | 198 |
| Figure 9.18: Model Site | 199 |
| Figure 9.19: ARC Scene View of Piers, Weir, and the Proj4ft_ras | 200 |
| Figure 9.20: HW 54 Bridge | 200 |
| Figure 9.21: Create New Terrain in RAS Mapper..... | 201 |
| Figure 9.22: New RAS Mapper Terrain, Terrain_Final | 202 |
| Figure 9.23: 1D HR Floodplain (a) Unedited, (b) Edited..... | 203 |

| | |
|-------------------------------------------------------------------------------------------------------------------------------------------------------------------------|-----|
| Figure 9.24: 1D HR US HW 54 Bridge Section..... | 204 |
| Figure 9.25: WSE and Ground Profiles for Main Channel and Tributary..... | 204 |
| Figure 9.26: WSE and Ground Profiles for Main Channel and Tributary..... | 205 |
| Figure 9.27: Grid in Pier and Weir Regions | 206 |
| Figure 9.28: Weir and Selected Piers on Terrain_Final..... | 206 |
| Figure 9.29: Main Channel WSE Profiles for a Range of Δt -values Using the 1D HEC-RAS <i>n</i> -values (a) with CL Elevation, (b) without CL Elevation | 207 |
| Figure 9.30: Tributary WSE Profiles for a Range of Δt -values Using the 1D HEC-RAS <i>n</i> - Values (a) with CL Elevation, (b) without CL Elevation | 208 |
| Figure 9.31: Main Channel WSE Profiles for $\Delta t = 10$ seconds | 209 |
| Figure 9.32: Tributary WSE Profiles for $\Delta t = 10$ seconds (a) with CL Elevation, (b) without CL Elevation | 210 |
| Figure 9.33: Main Channel WSE Profiles for $\Delta t = 5$ seconds (a) with Ground, (b) without Ground..... | 211 |
| Figure 9.34: Tributary WSE Profiles for $\Delta t = 5$ seconds (a) with CL Elevation, (b) without CL Elevation | 212 |
| Figure 9.35: Main Channel WSE Profiles for $\Delta t = 3$ seconds (a) with Ground, (b) without Ground..... | 213 |
| Figure 9.36: Tributary WSE Profiles for $\Delta t = 3$ seconds (a) with CL Elevation, (b) without CL Elevation | 214 |
| Figure 9.37: Main Channel WSE Profiles for $\Delta t = 2$ seconds (a) with Ground, (b) without Ground..... | 215 |
| Figure 9.38: Tributary WSE Profiles for $\Delta t = 2$ seconds (a) with CL Elevation, (b) without CL Elevation | 216 |
| Figure 9.39: 1D and 2D Floodplain for $\Delta t = 10$ seconds, $n_{2D} = 0.7 n_{1D}$ | 217 |
| Figure 9.40: 1D and 2D Floodplain for $\Delta t = 5$ seconds, $n_{2D} = 0.6 n_{1D}$ | 218 |
| Figure 9.41: 1D and 2D Floodplain for $\Delta t = 2$ seconds, $n_{2D} = 0.4 n_{1D}$ | 219 |

This page intentionally left blank.

Chapter 1: Introduction

Hydraulic modeling is often required for transportation projects. Common applications include drainage structure sizing, floodplain mapping, and bridge scour evaluation. Most early hydraulic models dealt with unidirectional or one-dimensional (1D) flow, not because the mathematics to do more did not exist, but because the computational power and the availability of detailed terrain data did not. One-dimensional models, such as HEC-2 and HEC-RAS 1D, have proven exceptionally useful over the years, in large part due to the significant effort and care by researchers and practicing engineers to compensate for shortcomings of the 1D assumption.

Two-dimensional (2D) models are quickly gaining acceptance in civil engineering practice. Desktop computers are now fast enough to process 2D simulations, and the quality of and access to detailed terrain data are also increasing. A number of 2D models are currently used in practice, including:

- HEC-RAS 2D (Hydrologic Engineering Center's River Analysis System): produced by the United States Army Corps of Engineers (USACE).
- SRH-2D (Sedimentation and River Hydraulics – Two-Dimensional River Flow Model): produced by the United States Bureau of Reclamation.
- FESWMS (Finite-Element Surface-Water Modeling System): produced by the United States Geological Survey.
- FST2DH (Flow and Sediment Transport Two-Dimensional Hydraulics): a module of FESWMS sponsored by the Federal Highway Administration.
- AdH (Adaptive Hydraulics): another product of the USACE.
- TELEMAC-MASCARET: managed by a consortium of European agencies based in France, Germany, and the United Kingdom.
- FLO-2D: produced by FLO-2D Software, Inc., a privately owned company.
- RiverFlow-2D: produced by another privately owned company, Hydronia, LLC.

Water resources modeling is on the verge of great change, and care must be taken to ensure that these new 2D models are adopted responsibly. A great many structures have been designed based on the results of 1D analyses, and engineers have grown to understand and trust those designs. The adoption of 2D models may have great consequences for the public and its safety, and accordingly, such a decision should be made only with all reasonable confidence in the effectiveness of the models. This report seeks to compare these programs (HEC-RAS 1D version 4.1 and 2D, versions 5.0, 5.0.1, and 5.0.3, and SRH-2D version 3.0) in order to assess their efficacy and to provide guidance for good hydraulic modeling practices, such as those for terrain conditioning, mesh development, and model parameterization. Comparisons are made on the basis of floodplain extent and velocity calculations across the spatial domain. HEC-RAS 2D Version 5.0 and 5.0.1 were used in Chapters 3 through 7 and HEC-RAS 2D Version 5.0.3 was used in Chapters 6 (long model), 7, and 8.

Chapter 2: Theory

2.1 Overview of the Model Theory and Hydraulics

One-dimensional models are based on the assumption that all discharge through any cross section is normal to that cross section at all locations. Obviously, this is not true for an actual river, but in many cases the assumption provides quite reasonable results if the cross sections are judiciously located and constructed. To best reflect this assumption, terrain cross sections for 1D models must be delineated such that flow is normal to the cross section. This often requires that cross sections have breaks with individual line segments perpendicular to the terrain contours. The hydraulic engineer must be able to visualize the flow patterns which are likely to occur and to draw the cross sections accordingly. This can be a challenging task and one whose difficulty greatly depends upon the complexity of the terrain. In the end, engineers must rely on their best judgment to properly model a reach.

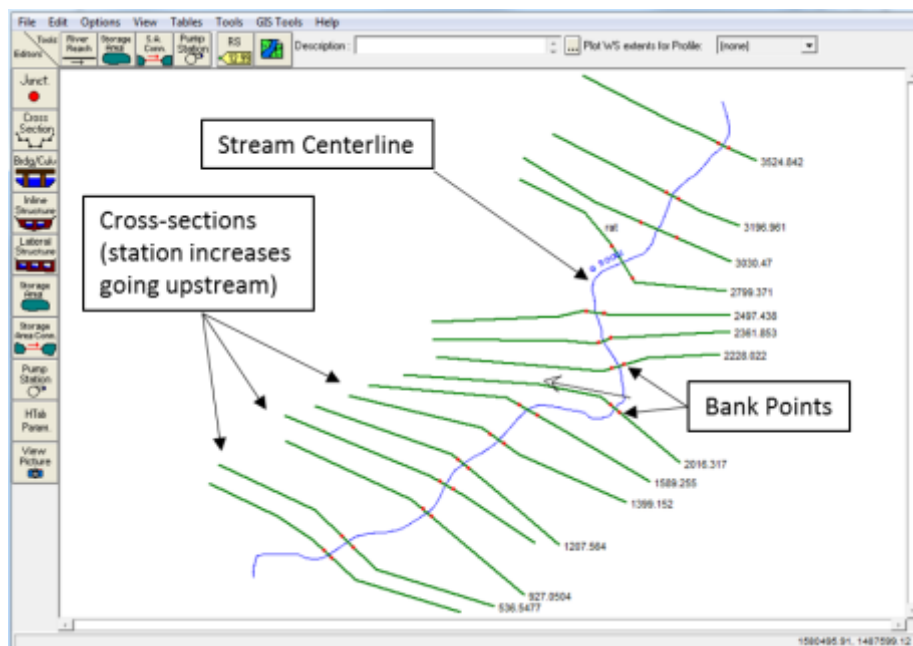


Figure 2.1: Plan View of Typical HEC-RAS 1D Model

Figures 2.1 and 2.2 show sample cross sections for a simple HEC-RAS 1D project. Each segment of each cross section is drawn so that it is perpendicular to the elevation contours, though the maximum angle recommended between segments in a cross section is 20 degrees.

Often, the direction of flow will depend on flood magnitude. For example, when flow overtops a road, then the road functions as a weir, meaning that the flow would move in a perpendicular direction to the road centerline.

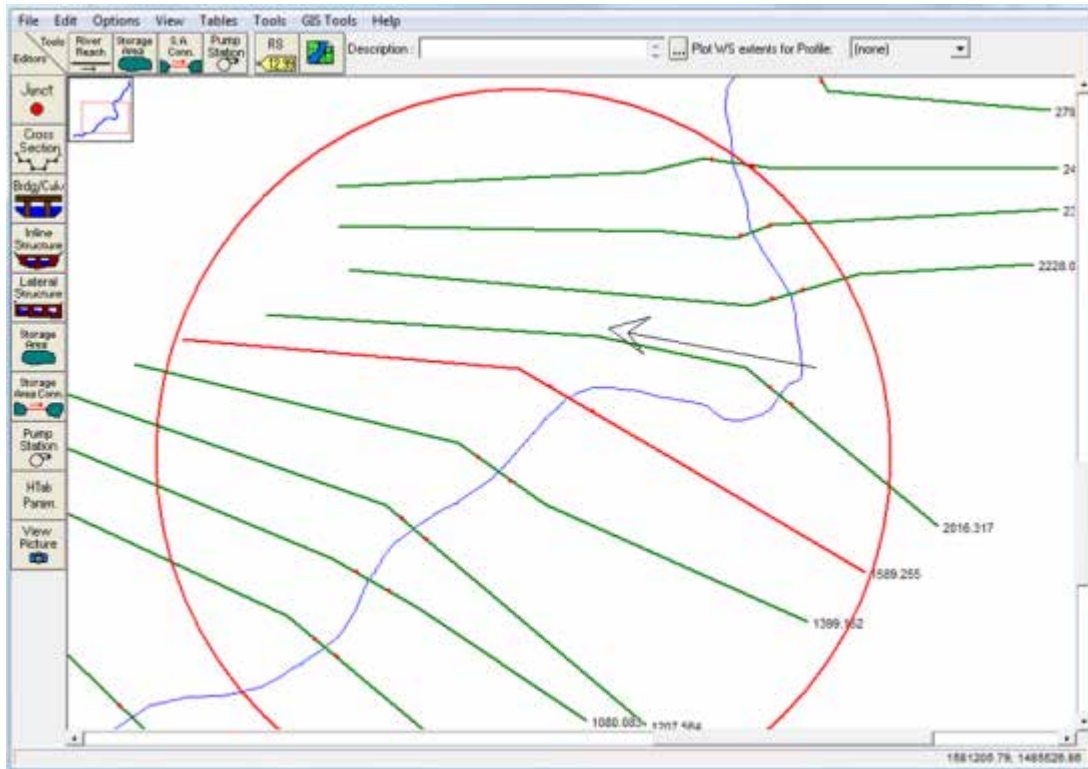


Figure 2.2: Selection of Example Cross Section 1589.255

Figure 2.3 shows the flux across a sample cross-section from a HEC-RAS 1D project. While it may seem that there are indeed two components to the velocity, this is merely an artifact of the graphical user interface (GUI) of HEC-RAS 1D.

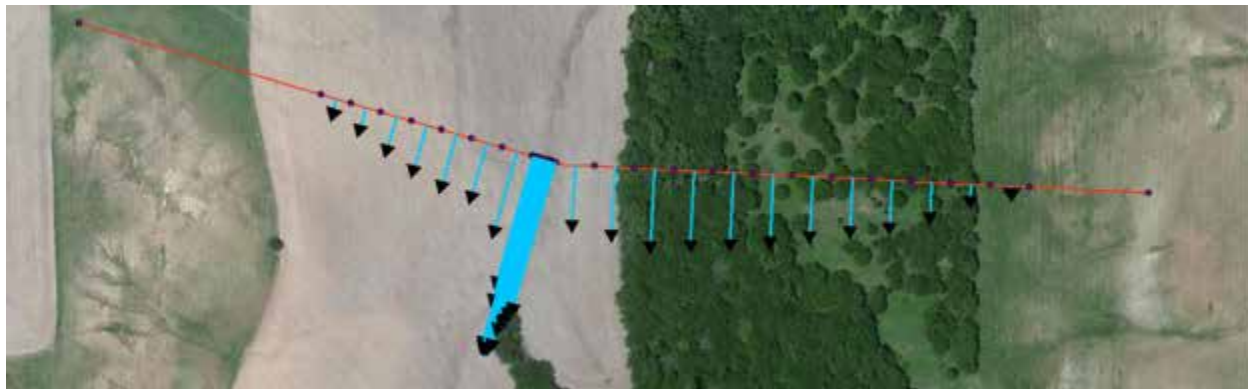


Figure 2.3: Representation of Assumed Flow Directions for a Single Cross Section

It should be noted that velocity is allowed to vary across the cross section in a HEC-RAS 1D model. In Figure 2.3, the magnitudes of the velocities correspond to the lengths of the vectors drawn from the cross section (this was accomplished manually within ArcMap in ESRI ArcDesktop 10.2). HEC-RAS 1D can compute these velocities as it determines the conveyance through each subdivision of the cross section (see Section 2.2.1 for more details). In order to see these values, displayed graphically in Figure 2.4, one must set the option in HEC-RAS 1D by going to Run > Steady Flow Data > Options > Flow Distribution Locations before running the model. Figure 2.4 also shows how HEC-RAS 1D extracts data from the underlying digital elevation model (DEM) and uses it for a cross section.

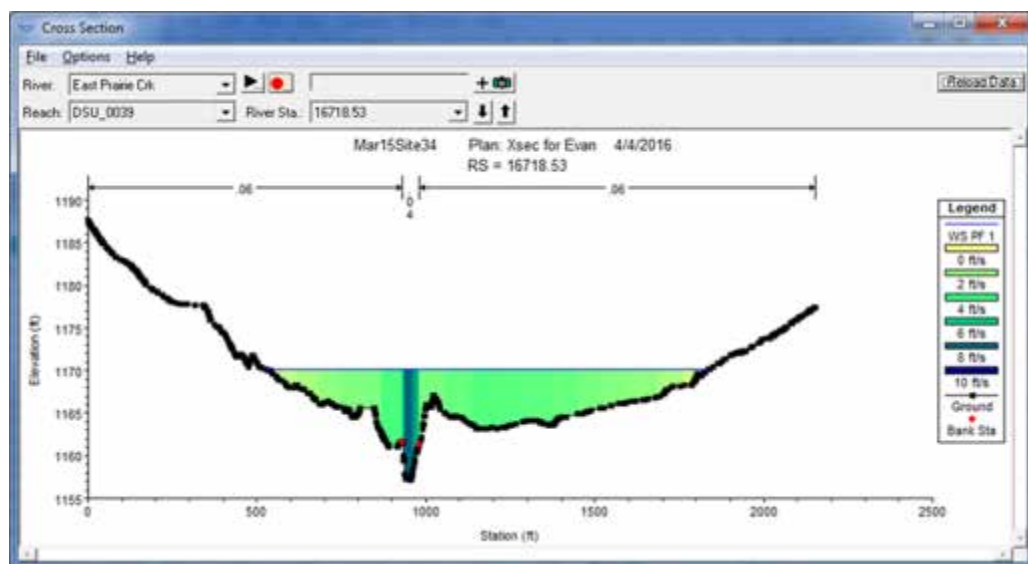


Figure 2.4: HEC-RAS 1D Interpretation of Given Cross Section

As shown in Figures 2.1 through 2.3, each cross section is made up of a single line or a line with multiple segments. This display, however, is merely for the benefit of the engineer in constructing the model and interpreting the model results. Figure 2.5 more accurately represents how HEC-RAS 1D models the reach. Mathematically, the program treats the river as if it were straight and as if all the flow were moving in one direction, albeit at different depths and velocities from one cross section to the next. HEC-RAS 1D does, however, allow for different reach lengths between cross sections for the main channel and the left and right overbanks. Another significant limitation of 1D models is that the water surface elevation (WSE) is averaged over each cross section, and thus sometimes over very long distances. This averaging of properties is not nearly so drastic when using a 2D model.

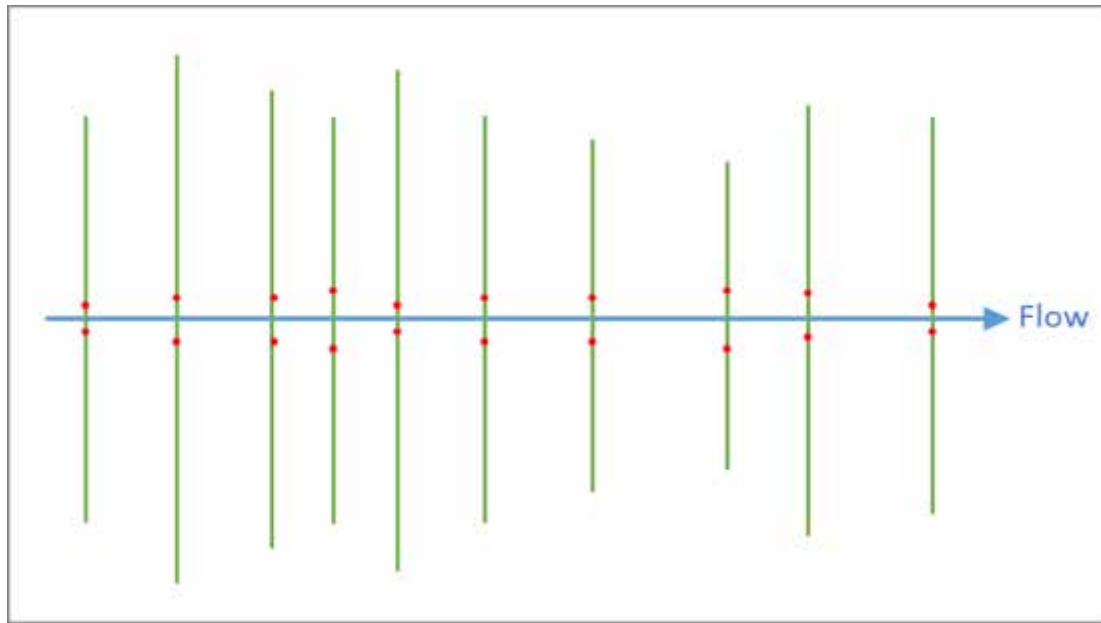


Figure 2.5: Schematic of a Typical HEC-RAS 1D Reach Model

Two-dimensional models allow for velocity vector components along a horizontal plane in two directions while neglecting any vertical component. Clearly, this mathematical treatment of flow provides a much more realistic solution of the hydraulics occurring in a given river reach.

Two-dimensional models can take different approaches in representing terrain with the computational elements. HEC-RAS 2D essentially uses scaled-down cross sections for each side

of a 2D element. In contrast, SRH-2D uses a finite-element approach to define the model space. The result of each method is that water is allowed to flow from a computational mesh element into adjacent elements. Figures 2.6 and 2.7 show a typical mesh for a HEC-RAS 2D model. Figures 2.8 and 2.9 show the mesh in SRH-2D.

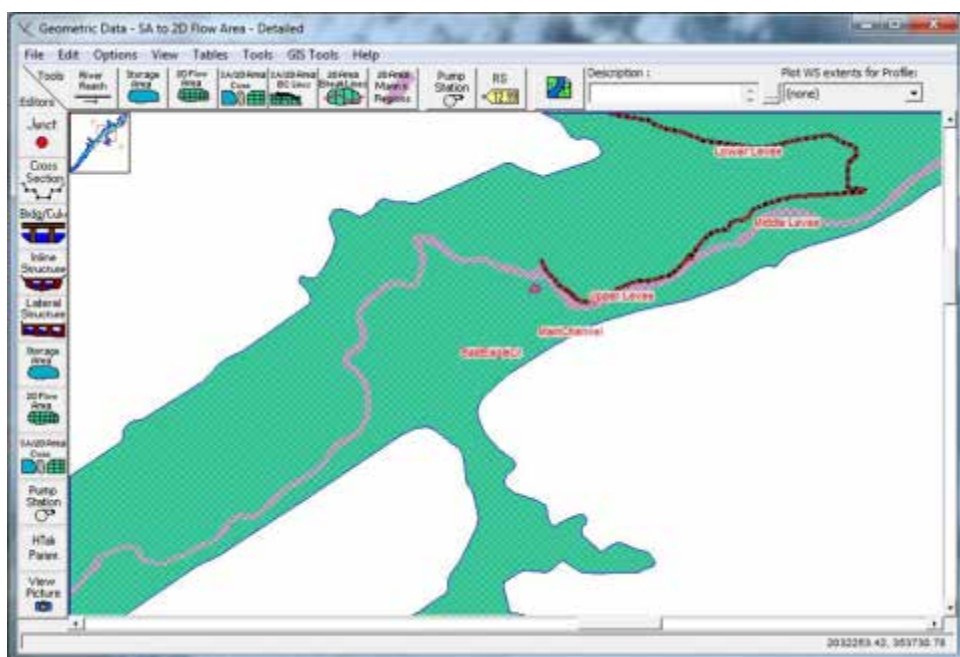


Figure 2.6: Geometric Data Editor Window for HEC-RAS 5.0 Bald Eagle Creek Dam Break Example Project

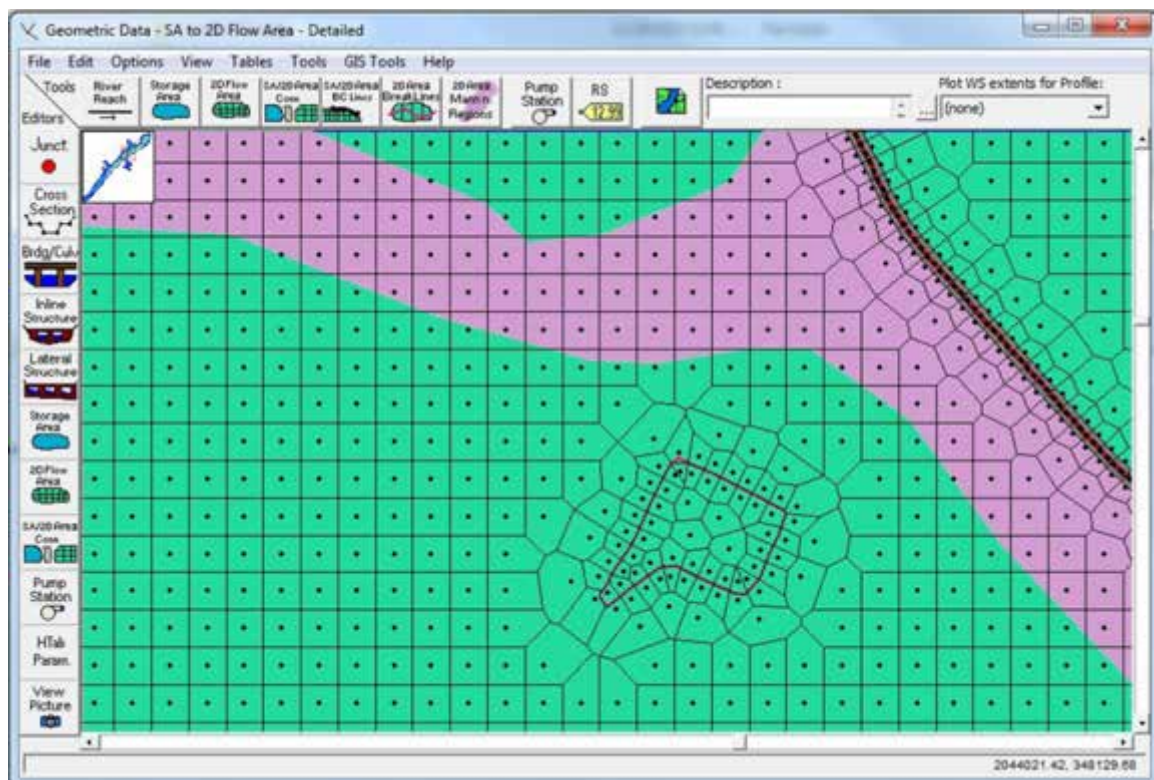


Figure 2.7: Zoomed-In View for HEC-RAS 2D Bald Eagle Creek Example Project Showing Mesh Details

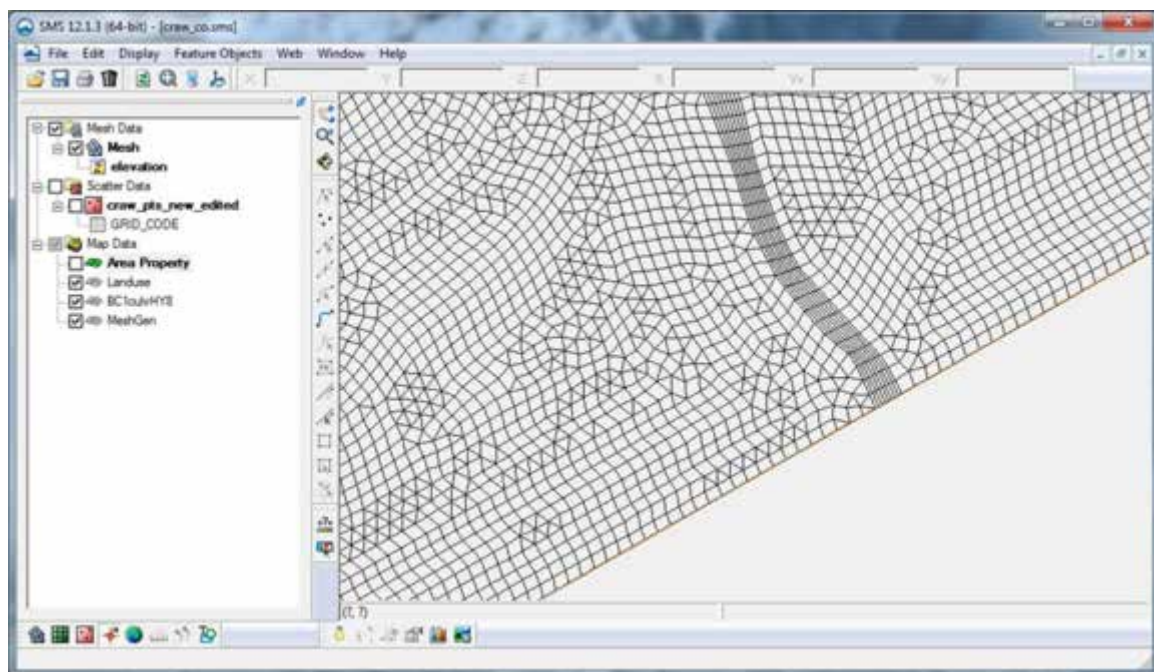


Figure 2.8: SRH-2D Mesh Viewed in SMS 12.1 for a Site in Crawford County, KS

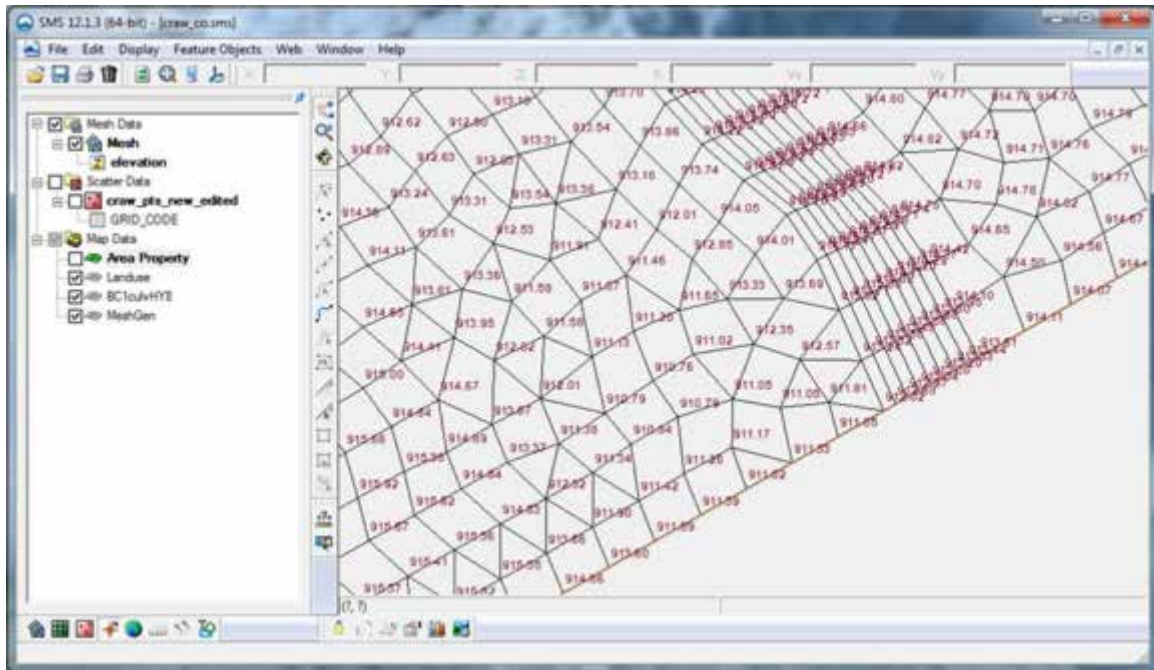


Figure 2.9: Zoomed-In View of SRH-2D Mesh from Figure 2.8 Showing Elevation Values at Corner Nodes

2.2 Model Equations

2.2.1 One-Dimensional HEC-RAS Equations

During a steady-state simulation for HEC-RAS 1D, the flow profile is determined from one cross section to the next by solving the energy equation and by employing the standard step method.

$$Z_2 + Y_2 + \frac{\alpha_2 V_2^2}{2g} = Z_1 + Y_1 + \frac{\alpha_1 V_1^2}{2g} + h_e \quad \text{Equation 2.1}$$

Where:

Z = channel invert elevation

Y = water depth

α = velocity-weighting coefficient

V = average velocity for the cross section

g = gravitational acceleration

h_e = energy loss from Section 2 to 1

The subscripts represent the cross section immediately upstream as shown in Figure 2.10.

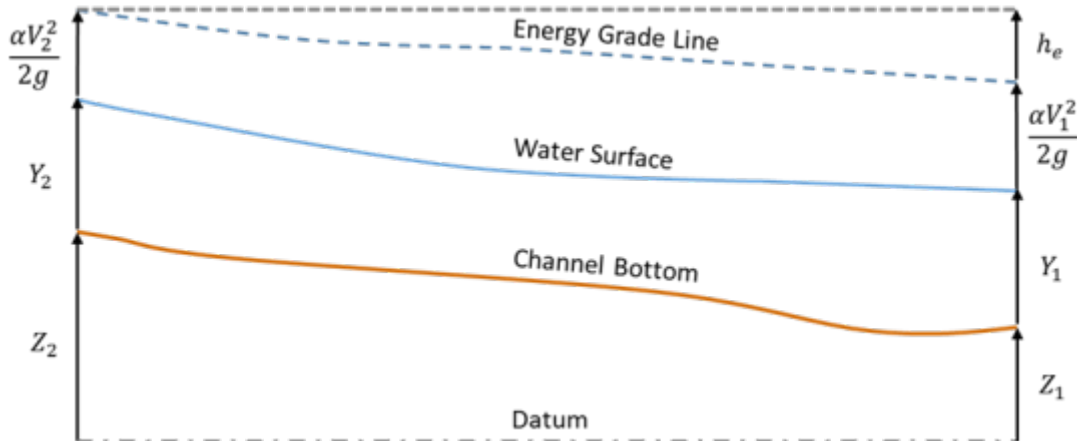


Figure 2.10: Diagram Showing Terms Used in HEC-RAS 1D Energy Equation

$$h_e = L\bar{S}_f + C \left| \frac{\alpha_2 V_2^2 - \alpha_1 V_1^2}{2g} \right| \quad \text{Equation 2.2}$$

Equation 2.2 is used to calculate head loss between sections and is required to apply the energy equation. L is the discharge-weighted reach length, \bar{S}_f is the representative friction slope, and C is either an expansion or contraction loss coefficient.

$$L = \frac{L_{lob}\bar{Q}_{lob} + L_{ch}\bar{Q}_{ch} + L_{rob}\bar{Q}_{rob}}{\bar{Q}_{lob} + \bar{Q}_{ch} + \bar{Q}_{rob}} \quad \text{Equation 2.3}$$

In Equation 2.3, the subscript “*lob*” stands for left overbank, “*ch*” for channel, and “*rob*” for right overbank. L is the cross section reach length between sections, while \bar{Q} is the arithmetic mean of discharge.

$$S_f = \left(\frac{Q}{K} \right)^2 \rightarrow \bar{S}_f = \left(\frac{Q_1 + Q_2}{K_1 + K_2} \right)^2 \quad \text{Equation 2.4}$$

By default, HEC-RAS 1D uses the arithmetic mean of the friction slope at each section to calculate the representative friction slope (although the geometric and harmonic means are also options within the program). In Equation 2.4, Q represents discharge and K the conveyance for each subdivision within an individual cross section.

$$Q = KS_f^{1/2}$$

Equation 2.5

$$K = \frac{1.486}{n} AR^{2/3}$$

Equation 2.6

As shown in Equations 2.5 and 2.6, discharge is computed for each conveyance subdivision using Manning's equation with English units. The bases for each subdivision are n -value break points within the cross section and at breaks between the overbanks and the main channel (where transitions in n -values typically occur). A is the cross-sectional area of each section, n is the Manning's roughness coefficient, and R is the hydraulic radius, which is defined as the cross-sectional area divided by the wetted perimeter ($R = A/P$).

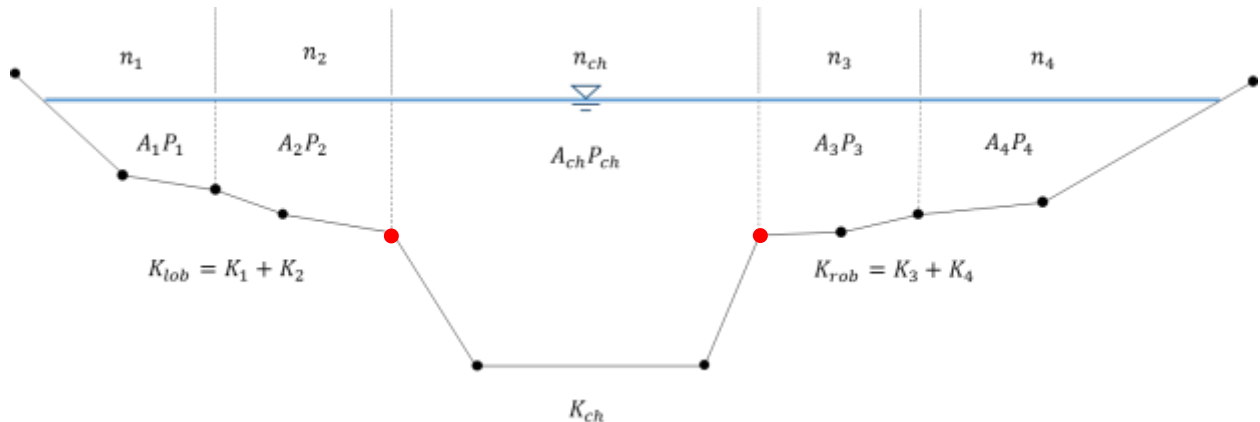


Figure 2.11: Channel Subdivisions Used in HEC-RAS 1D Cross Section Model

HEC-RAS 1D determines the total conveyance for the cross section by summing up all the incremental K -values. The Manning's n values may also vary within the main channel itself. If this is the case, Equation 2.7 is used to determine a composite roughness coefficient.

$$n_c = \left[\frac{\sum_{i=1}^N (P_i n_i^{1.5})}{P} \right]^{2/3}$$

Equation 2.7

The velocity weighting coefficient, α , used in Equation 2.1 is determined using Equation 2.8, where A_t is the total area for the cross section and K_t is the total conveyance.

$$\alpha = \frac{(A_t)^2 \left[\frac{K_{lob}^3}{A_{lob}^2} + \frac{K_{ch}^3}{A_{ch}^2} + \frac{K_{rob}^3}{A_{rob}^2} \right]}{K_t^3} \quad \text{Equation 2.8}$$

Equation 2.9 is used to determine the head losses due to either the expansion or contraction of flow. Equation 2.9 groups the terms on the right-hand side of Equation 2.2.

$$h_{ce} = C \left| \frac{\alpha_1 V_1^2}{2g} - \frac{\alpha_2 V_2^2}{2g} \right| \quad \text{Equation 2.9}$$

Whether the C -value used in the equation corresponds with the expansion or contraction coefficient for the cross-section depends on V_1 and V_2 . When the velocity upstream, V_2 , is less than the velocity downstream, the contraction coefficient is applied; when the reverse is true, the expansion coefficient is used. For more information on expansion and contraction coefficients, see Chapter 3 of the HEC-RAS 4.1 Hydraulic Reference Manual, “Basic Data Requirements.”

In a steady state HEC-RAS 1D simulation, in addition to the 1D requirement, two key assumptions are made: that the discharge is constant (steady state) and that the water surface profile is gradually varied, except at locations where the flow is rapidly varied. Such locations include channel constrictions (culverts, weirs, and bridges) and sites where a hydraulic jump may exist. Empirical equations or momentum analyses are used at these locations. The momentum equation (Equation 2.10) is shown below.

$$\frac{Q_2^2 \beta_2}{g A_2} + A_2 \bar{Y}_2 + \left(\frac{A_1 + A_2}{2} \right) LS_0 - \left(\frac{A_1 + A_2}{2} \right) LS_f = \frac{Q_1^2 \beta_1}{g A_1} + A_1 \quad \text{Equation 2.10}$$

This form of the momentum equation includes terms for the momentum flux in and out of the control volume between cross sections. It includes hydrostatic pressure terms, a term for the water weight component acting parallel to the channel bed, and a term for the frictional forces between the water and the ground opposing the motion of the water. The β terms are momentum coefficients that account for the velocity distribution in irregular channels, and \bar{Y} represents the depth measured from the water surface to the centroid of the cross-sectional area.

A discussion of the unsteady-flow routing portion of HEC-RAS 1D is especially relevant because these equations also serve as the basis for the 2D HEC-RAS model. These equations are based on the St. Venant equations, which are in turn based on the Navier-Stokes equation for an incompressible fluid.

$$\rho \frac{Du}{Dt} = -\nabla p + \rho g + \mu \nabla^2 u \quad \text{Equation 2.11}$$

In Equation 2.11, ρ is the density of the fluid. $\frac{Du}{Dt}$ is the total time differential of the velocity vector, u ; g is the gravitational acceleration expressed as a vector; μ is the dynamic viscosity of the fluid; and ∇^2 is the Laplace operator $\left(\frac{\partial^2}{\partial x^2} + \frac{\partial^2}{\partial y^2} + \frac{\partial^2}{\partial z^2}\right)$. The Navier-Stokes equation is derived from Newton's second law concerning conservation of momentum.

$$\sum F_x = \frac{d\bar{M}}{dt} \quad \text{Equation 2.12}$$

Free surface flow may be derived from the 1D St. Venant equation for shallow water (see HEC-RAS 4.1 User's Manual for more information).

$$\frac{\partial Q}{\partial t} + \frac{\partial QV}{\partial x} + gA \left(\frac{\partial z}{\partial x} + S_f \right) = 0 \quad \text{Equation 2.13}$$

If all terms in Equation 2.13 are included, then it is referred to as the *full momentum equation* within HEC-RAS 1D. (Equation 2.13 is also known as the *dynamic wave equation*.) If the first term, $\frac{\partial Q}{\partial t}$, which represents the local acceleration of the fluid, is excluded, then what remains is known as the *diffusion wave equation*. $\frac{\partial QV}{\partial x}$ represents the convective acceleration of the fluid. $\frac{\partial z}{\partial x}$ is the change in the z -direction with respect to the x -direction, and is then clearly equal to the negative of the ground slope, S_o . The friction slope, S_f , is calculated by Equation 2.14 (based on Manning's equation) when an unsteady-flow analysis is performed.

$$S_f = \frac{Q|Q|n^2}{2.208R^{4/3}A^2} \quad \text{Equation 2.14}$$

Equation 2.15 is the continuity equation for unsteady HEC-RAS 1D .

$$\frac{\partial A_T}{\partial t} + \frac{\partial Q}{\partial x} - q_l = 0 \quad \text{Equation 2.15}$$

Where:

A_T represents the total flow area, and
 q_l the lateral inflow per unit length.

2.2.2 Two-Dimensional HEC-RAS Equations

The HEC-RAS 2D system differs from the 1D model in that cross-section-like properties are defined for each cell face. In consequence, the rate at which water flows through each cell face is dependent on the face properties. This feature is important because it allows the hydraulic engineer to more accurately represent the terrain of the entire reach within the model. As a result, less averaging of the flow and terrain properties occurs in a 2D model since it embodies the properties of the entire area of interest.

The computational mesh employed within HEC-RAS 2D differs from most 2D models in that the ground elevation within an element is not assumed to be a plane. The model uses what is called a high resolution subgrid model. Within the interface, this model is referred to as the 2D Computational Mesh, which is linked to a Hydraulic Property Table. Cells can have anywhere from three to eight sides, and these edges of an element are not required to be straight lines. Various details about the cell faces—such as elevation versus wetted perimeter, area, and roughness—are stored within the hydraulic property table. The model computes discharge across a cell face using this information together with water surface elevations of adjacent cells. Figures 2.12 through 2.15 seek to clarify the nature of these cells with cross-section-like edges.

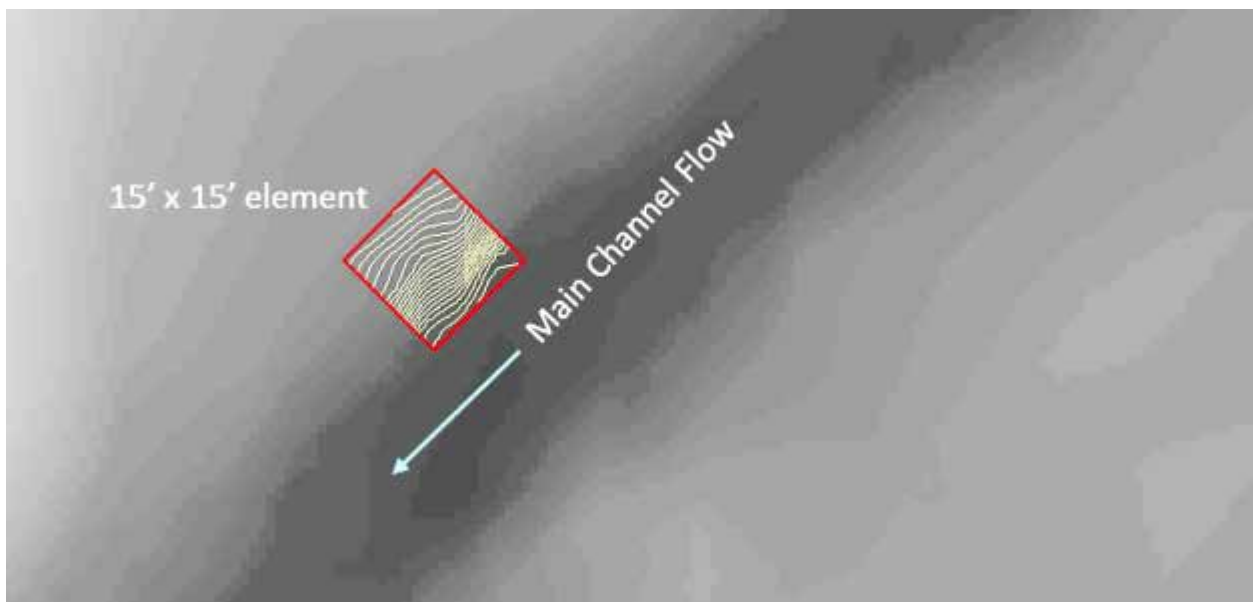


Figure 2.12: Square Mesh Element atop Grid with Elevation Contours Spaced at 0.2' Intervals

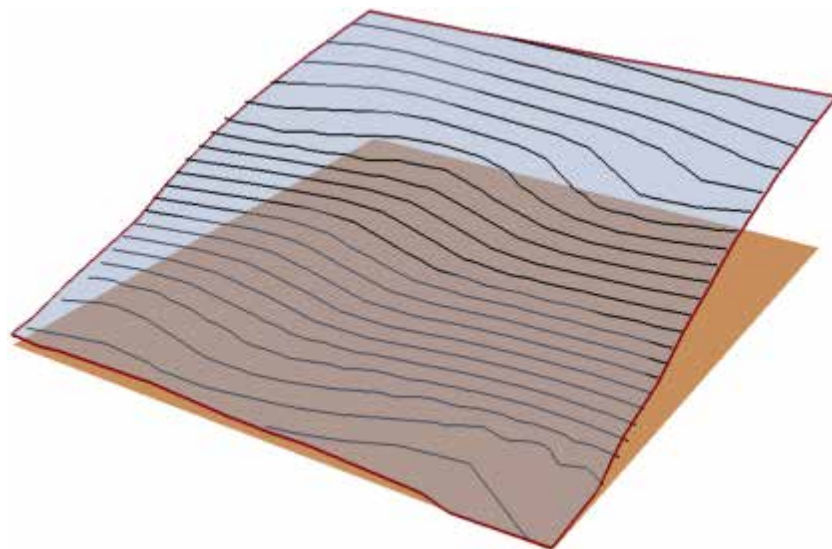


Figure 2.13: Three-Dimensional Representation of the Mesh Element from Figure 2.12

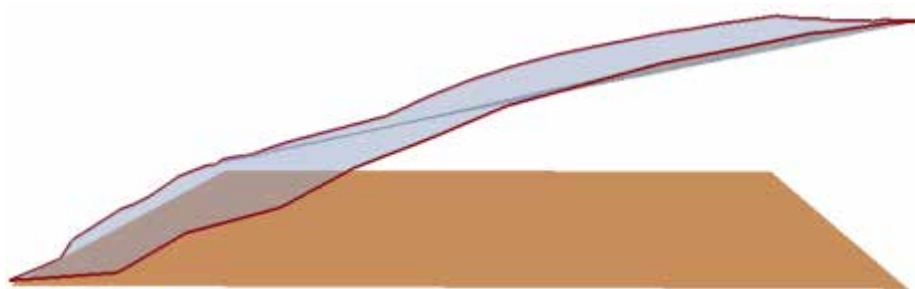


Figure 2.14: View from Upstream Looking Downstream

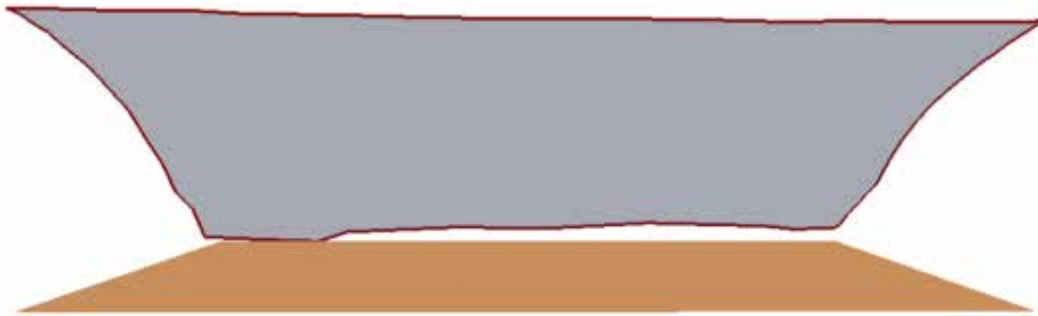


Figure 2.15: View Perpendicular to That in Figure 2.14 Looking Towards the Main Channel Flowline

Each of the four faces of the element described in Figures 2.12 through 2.15 is analogous to a 1D HEC-RAS cross section. Treating the mesh this way allows for a cell to be partially wet and yet still contain the correct volume of water. It also allows for larger mesh sizes that still accurately account for storage versus stage within an individual cell. Even if all elements within the model are 40 ft \times 40 ft, and the river being modeled is only 10 ft wide, at low flows when the water should stay in the channel the model shows it doing just that. This system makes it possible to use fewer cells as well as a larger computational timestep than do most other models, meaning fewer calculations are required, yet accurate results are still achievable.

The equations used for a HEC-RAS 2D simulation are based upon those outlined in the Section 2.2.1 for a HEC-RAS 1D unsteady-state simulation. The full momentum or the diffusive wave versions of the St. Venant equations can be selected before starting a simulation. The full momentum equation should provide more accurate solutions, but it takes more time to compute than the diffusive wave equation. Often, the results from the two equations are similar enough that either solution is acceptable, but situations exist in which the diffusive wave equation is grossly inadequate. These include places where large eddy losses occur, such as locations upstream and downstream of bridge openings where recirculating flow occurs. Usually, sections such as bridge constrictions should be handled by the 1D HEC-RAS bridge routines by creating a combined 1D and 2D HEC-RAS model, where a 1D sections upstream and downstream from the bridge are placed within 2D portions of the model. For situations where the flow does not contact or overtop the bridge deck/roadway, full 2D models have been shown to work effectively.

2.2.3 SRH-2D Equations

SRH-2D uses a finite-element approach for hydraulic calculations. Elements in the mesh can be either triangles or quadrilaterals, and a model may contain a combination of the two. Each element is a plane defined by a single elevation, although within the mesh generation application, the Surface Water Modeling System (SMS 12.1, a product of Aquaveo) interpolates elevation values to the mesh nodes on the corners of each element.

The flow equations used by SRH-2D are derived from the 3D Navier-Stokes equation presented in Section 2.2.1 by integrating across the vertical dimension, thus leading to the depth-averaged 2D St. Venant equations.

The form of the continuity equation used is shown in Equation 2.16.

$$\frac{\partial h}{\partial t} + \frac{\partial hU}{\partial x} + \frac{\partial hV}{\partial y} = e \quad \text{Equation 2.16}$$

Where:

h is the water depth;

t is time;

U and V are depth-averaged velocity components in the x and y directions, respectively; and

e is the excess rainfall rate.

$$\frac{\partial hU}{\partial t} + \frac{\partial hUU}{\partial x} + \frac{\partial hVU}{\partial y} = \frac{\partial hT_{xx}}{\partial x} + \frac{\partial hT_{xy}}{\partial y} - gh \frac{\partial z}{\partial x} - \frac{\tau_{bx}}{\rho} + D_{xx} + D_{xy} \quad \text{Equation 2.17a}$$

$$\frac{\partial hV}{\partial t} + \frac{\partial hUV}{\partial x} + \frac{\partial hVV}{\partial y} = \frac{\partial hT_{xy}}{\partial x} + \frac{\partial hT_{yy}}{\partial y} - gh \frac{\partial z}{\partial y} - \frac{\tau_{by}}{\rho} + D_{yx} + D_{yy} \quad \text{Equation 2.17b}$$

Equations 2.17a and 2.17b are the full momentum equations used by SRH-2D. T_{xx} , T_{xy} , and T_{yy} are depth-averaged turbulent stresses. D_{xx} , D_{xy} , D_{yx} , and D_{yy} are dispersion terms that arise due to depth averaging. z is the water surface elevation and is equal to z_b , the bed elevation,

plus h . ρ is the water density. τ_{bx} and τ_{by} are both frictional stresses between the water and the ground. They are calculated using Equations 2.18 and 2.19, which are based upon Manning's roughness equation.

$$\left(\frac{\tau_{bx}}{\tau_{by}}\right) = \rho C_f \left(\frac{U}{V}\right) \sqrt{U^2 + V^2} \quad \text{Equation 2.18}$$

$$C_f = \frac{gn^2}{h^{1/3}} \quad \text{Equation 2.19}$$

Equations 2.20a, 2.20b, and 2.20c are used to calculate the turbulent stresses and are based on the Boussinesq equations.

$$T_{xx} = 2(\nu + \nu_t) \frac{\partial U}{\partial x} - \frac{2}{3} k \quad \text{Equation 2.20a}$$

$$T_{xy} = (\nu + \nu_t) \left(\frac{\partial U}{\partial y} + \frac{\partial V}{\partial x} \right) \quad \text{Equation 2.20b}$$

$$T_{yy} = 2(\nu + \nu_t) \frac{\partial V}{\partial y} - \frac{2}{3} k \quad \text{Equation 2.20c}$$

Where:

ν is the kinematic viscosity of water,

ν_t is the turbulent eddy viscosity, and

k is the turbulent kinetic energy.

There are two ways of modeling turbulence within SRH-2D. One method is called the k - ϵ model. This model is not the standard setting within SRH-2D and will not be discussed (for more information see SRH-2D manual, Chapter 6). The second method, the parabolic turbulence model, is the standard in SRH-2D. In this second approach to modeling turbulence, the terms with k are dropped, and ν_t is calculated using Equation 2.21.

$$v_t = C_t U_* h$$

Equation 2.21

Where:

U_* is the bed frictional velocity, and

C_t is the parabolic turbulence constant.

While C_t can range from 0.3 to 1.0, the default is 0.7. For most applications the default value should be acceptable. Section 4.2 presents a simple test to evaluate model sensitivity to this value.

The distribution of flow in the SRH-2D model is determined according to a conveyance method described by Equation 2.22.

$$K = Q / \sum_i \frac{h_i^{5/3}}{n_i} \Delta s_i$$

Equation 2.22

Where:

i is the i -th boundary face of the inlet,

h_i is the water depth,

n_i is Manning's coefficient, and

Δs_i is the i -th boundary face distance.

The velocity at each face is calculated using Equation 2.23.

$$v_i = K h_i^{2/3} / n_i$$

Equation 2.23

Chapter 3: Computation Test and Basic Flow Around a Bend

3.1 Overview of the Computation Test and Basic Flow Around a Bend

Given the iterative nature of hydraulic modeling, the amount of time required to execute a simulation is an important practical consideration. Consider a project that involves the design of a new bridge with scour considerations. If the team designing the bridge is seeking the optimal configuration in terms of cost, structural integrity, and hydraulic performance, models with run times of several days may be impractical. 2D hydraulic models have only recently started to enter the mainstream for projects such as floodplain mapping and bridge hydraulics because of the rapidly falling cost of computers capable of producing simulation results in reasonable amounts of time and the availability of detailed terrain data.

Multiple simulations were performed in this study using HEC-RAS 2D and SRH-2D, with the parameters of the two models kept as similar as possible to gauge their differences in computation time. (HEC-RAS 1D was not considered because its simulation time is extremely short—several seconds at most—even for complicated models.) For HEC-RAS 2D, both the diffusive wave and full momentum equation sets were considered. A Dell Precision T1770 workstation with four two-thread cores was used to perform the tests.

| |
|-------------------------------------------------|
| Operating System: Windows 7 Enterprise |
| Processor: Intel ® Xeon ® CPU E3-1246 v3 |
| CPU Speed (GHz): 3.50 |
| RAM (GB): 16.0 |
| System type: 64-bit Operating System |

Figure 3.1: Significant Properties of the Machine Used to Perform the Computational Tests

As Figures 3.2 and 3.3 show, the channel used for these tests was sinusoidal in the x-y plane, and due to this feature the basic characteristics of flow around a bend as described in Section 7.3 of Henderson's (1966) *Open Channel Flow* were examined in brief. The channel was developed in ArcMap following the recommendations for developing meander patterns given in the report *Guidelines for Stream Realignment Design* (McEnroe, Young, & Shelley, 2009). A series of parallel polylines were used to define the channel through its length and across its

width. These lines were created from the generated centerline using the “Copy Parallel” tool during an editing session. Each line was assigned upstream and downstream elevation values, and these 2D polylines were converted to 3D using the 3D Analyst tool “Feature to 3D by Attribute” where the upstream elevation field was used as the required “Height Field” input and the downstream elevation field was used as the optional “To Height Field.” The resulting 3D shapefile was used to create a triangulated irregular network (TIN), and from this TIN a Raster was created on a 1×1 -ft grid (which needed to be made slightly larger than the test section to avoid errors later when the models were developed).

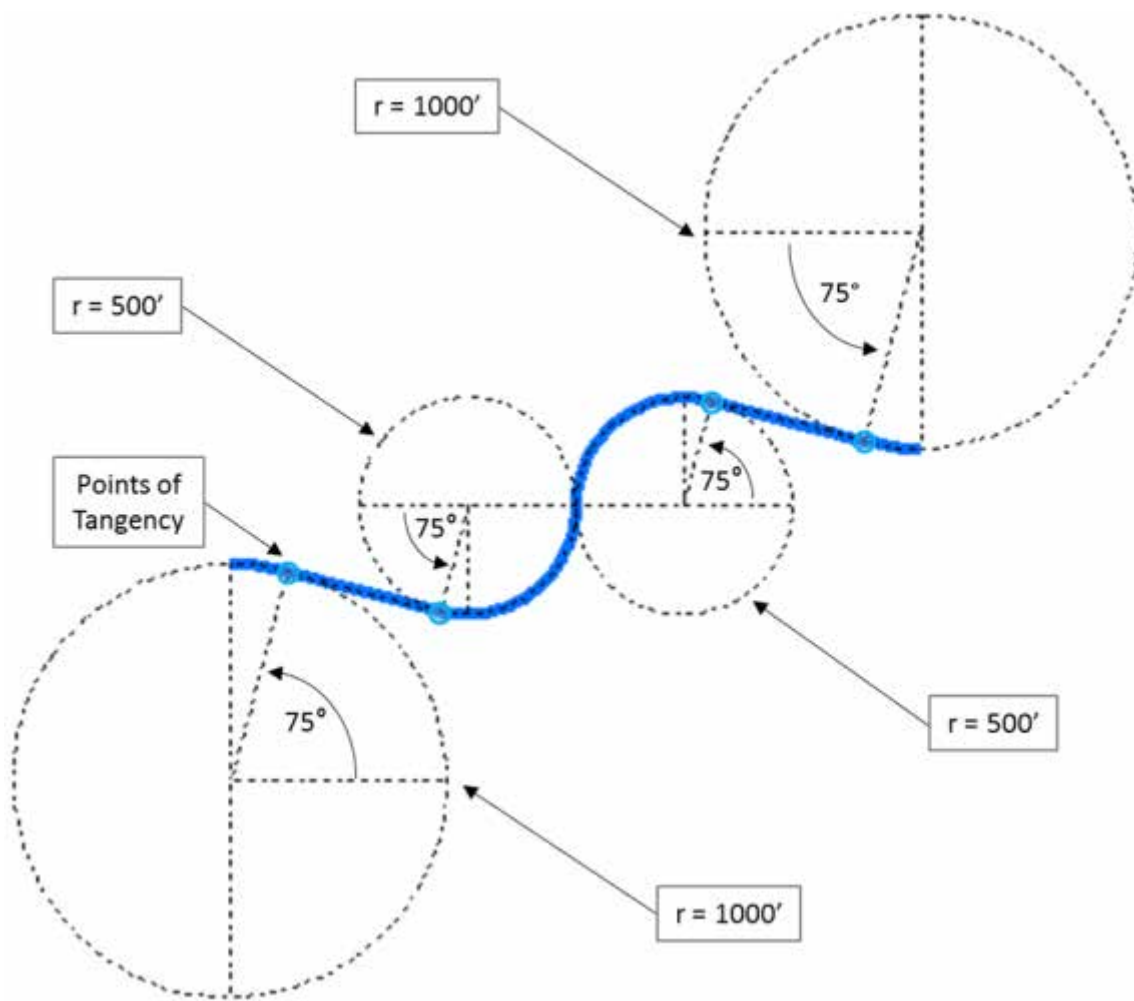


Figure 3.2: Plan View Showing Geometric Basis for Computational Test Reach

The stream centerline (represented by the blue line) was constructed from four arc segments and two straight lines. The arcs were derived from four different circles with the two types of geometry featured above: those with a radius of 500 ft and those with a radius of 1000 ft. The straight segments were connected to points of tangency on the circles corresponding to the angles in the figure. The distance in the x-direction spanned by both straight segments was based on a geometric mean of the two different radii of curvature used for this reach—that is, $\sqrt{r_{big} \cdot r_{small}} = \sqrt{1000\text{ft} \cdot 500\text{ft}} = 707\text{ft}$. The distance in the y-direction for each segment was thus dictated by this length and the angles involved (see Figure 3.3).

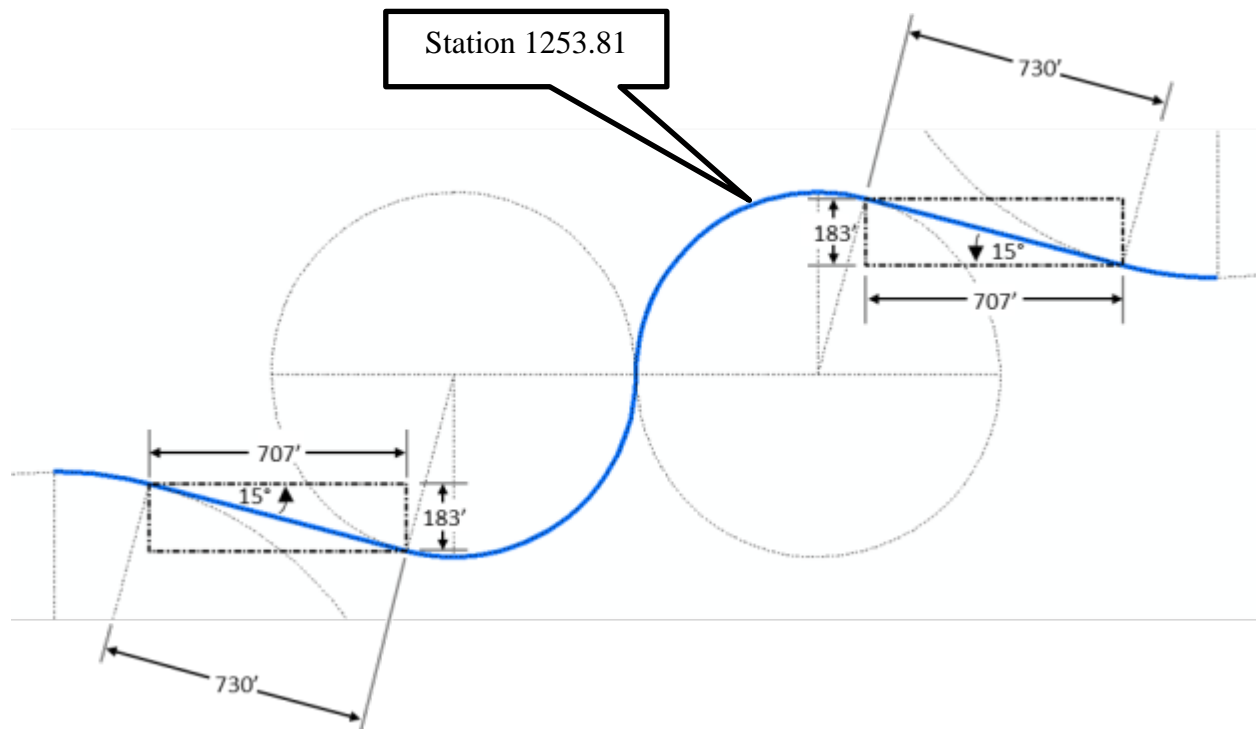


Figure 3.3: Close-Up of View Describing Straight Segments of Computational Test Reach

A representative cross section was created for the downstream end of the test reach in a Microsoft Excel spreadsheet. The channel possessed a circular bottom except out of the main-channel area where two different straight side slopes were used. The flow was not expected to be outside the main channel, but the side slopes were included in case this happened. The low point of the cross section was along its centerline, and at the downstream end this point had an

elevation of 0 ft. Equations 3.1, 3.2, and 3.3 were used to determine the elevations of points spaced every 1 ft horizontally across the cross section in the manner described by Figure 3.4. In the end, the main channel was defined for a radius of curvature equal to 40 ft and spanned a horizontal distance of 68 ft.

$$\beta_i = \sin^{-1} \left(\frac{STA_i}{r} \right) + \beta_o \quad \text{Equation 3.1}$$

$$y_i = r \cdot \sin \beta_i \quad \text{Equation 3.2}$$

$$z_i = z_o + r + y_i \quad \text{Equation 3.3}$$

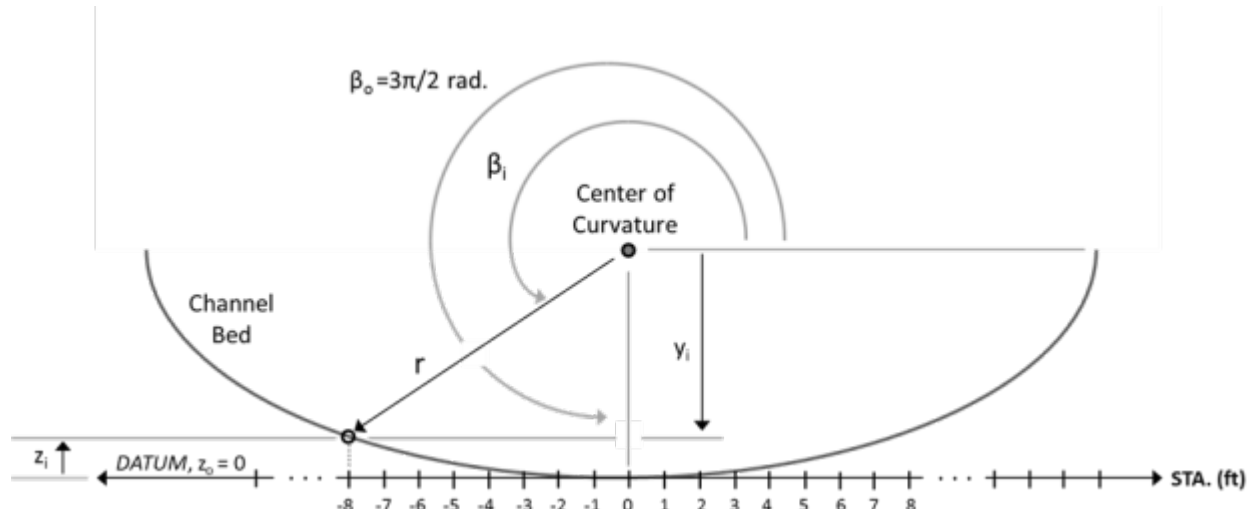


Figure 3.4: Elevation View of Geometric Basis for Cross Sections of the Computational Test Reach

Within the channel definition spreadsheet, Manning's equation was applied as if the channel were straight to estimate a roughness coefficient and discharge that would return an acceptable normal depth for the tests. Using a roughness coefficient of 0.045 and a discharge of 3001 cfs, the normal depth calculated was 16.27 ft. This value for normal depth was used as the downstream boundary condition for each simulation. The bed has a constant longitudinal slope of 0.2% and a length of 3816.34 ft (determined from ArcMap); elevations for points along the upstream cross section were calculated using Figures 3.2 through 3.4. The side slopes outside of

the circular portion of the channel were extended at first using a 1:2 (H:V) side slope for a horizontal distance of 6 ft, and then extended at 1:1 for 8 ft. Using the average velocity for uniform flow of 6.25 fps, an approximate travel time of 10.2 minutes was calculated for flow through the channel. Taking this rate into account, the hydrograph used for the simulations ramps up linearly from 150 cfs to 3000 cfs over a 15-minute period and maintains that flowrate for another 15 minutes, slightly longer than the estimated travel time of 10.2 minutes to account for discrepancies resulting from the bends. A visual check was made on all models to ensure steady state conditions had been reached.

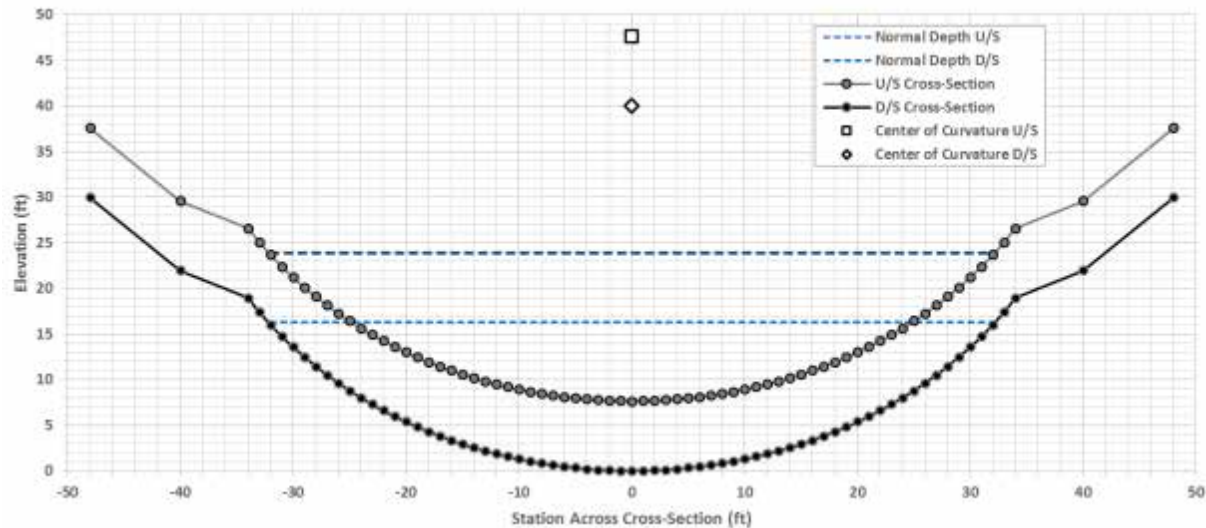


Figure 3.5: Representative Cross Sections for the Computational Test Terrain

3.2 Computational Test Results

Table 3.1 contains much of the relevant information concerning the computational tests performed. These results show that for comparable model setups, HEC-RAS 2D is faster than SRH-2D even when using the full momentum equation set. SRH-2D took from about 32% to about 149% longer than HEC-RAS 2D (using full momentum) for the models with 10-ft and 8-ft spacing, respectively.

Table 3.1: Major Inputs and Results of the Computational Tests

| Model | Timestep, Δt (s) | Spacing (ft) | Total Simulation Time, T (hr) | No. of Elements | CPU Runtime (s) | Result output time (min) | Initial Condition | Max. Cell (sq.ft) | Min. Cell (sq.ft) | Avg. Cell (sq.ft) | Approx. Courant Number |
|----------------|--------------------------------|-----------------|----------------------------------------|--------------------|-----------------------|-----------------------------------|----------------------|----------------------|----------------------|----------------------|------------------------------|
| - | (s) | (ft) | (hr) | - | (s) | (min) | - | (sq.ft) | (sq.ft) | (sq.ft) | - |
| SRH-2D | 1.0 | 10 | 0.50 | 3826 | 34.44 | 1.00 | Dry | 113.14 | 50.97 | 95.76 | 0.63 |
| | 0.5 | 8 | 0.50 | 5724 | 134.64 | 1.00 | Dry | 76.61 | 49.24 | 64.01 | 0.39 |
| HR-2D Diff. | 1.0 | 10 | 0.50 | 3476 | 10.00 | 1.00 | Dry | 184.37 | 80.35 | 105.40 | 0.63 |
| | 0.5 | 8 | 0.50 | 5495 | 23.00 | 1.00 | Dry | 135.30 | 47.61 | 66.67 | 0.39 |
| HR-2D Mom. | 1.0 | 10 | 0.50 | 3476 | 26.00 | 1.00 | Dry | 184.37 | 80.35 | 105.40 | 0.63 |
| | 0.5 | 8 | 0.50 | 5495 | 54.00 | 1.00 | Dry | 135.30 | 47.61 | 66.67 | 0.39 |

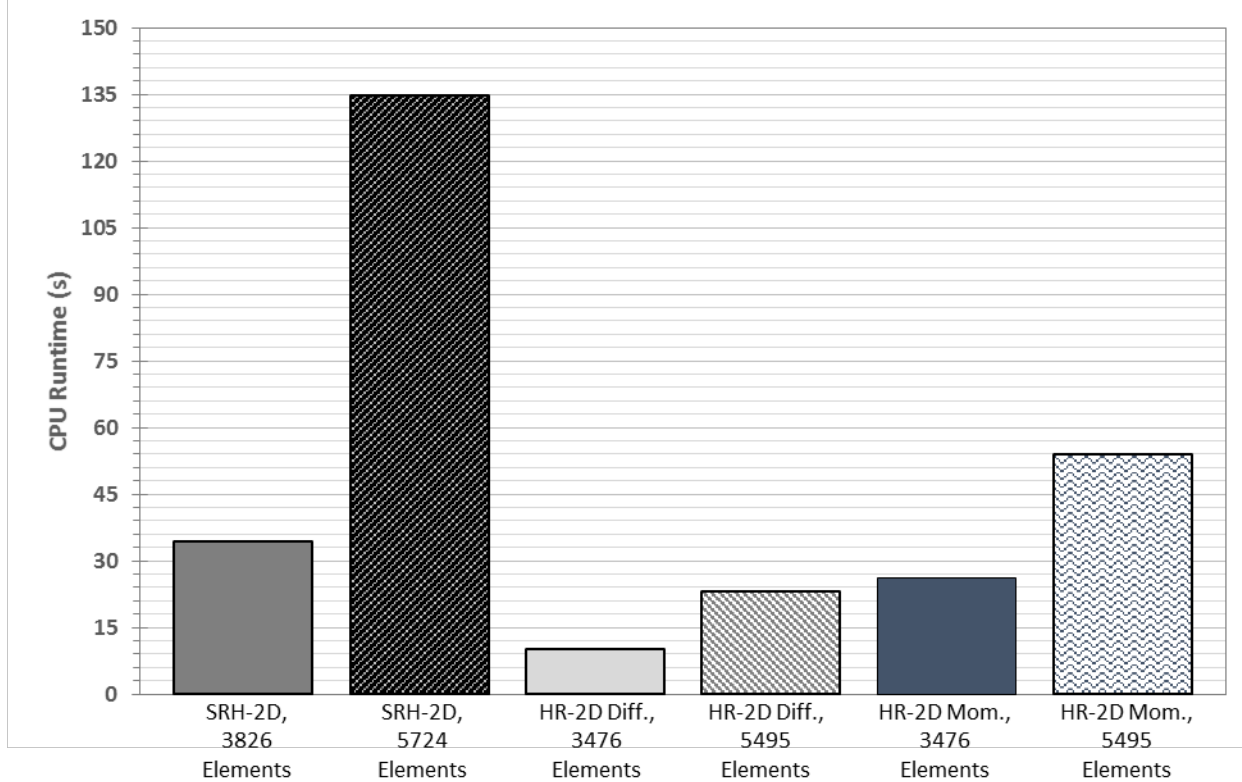


Figure 3.6: Comparison of the Six Trials Performed for the Computational Test

Figure 3.6 clearly shows that the HEC-RAS 2D model using the diffusion wave equation set (HR-2D Diff.) is by far the fastest: its longest CPU runtime in those trials is shorter than either HEC-RAS simulation using the full momentum equation set and either SRH-2D trial. However, some physics are sacrificed for that added computational benefit, the effects of which are investigated later in this chapter. It should be noted that there were no applications being run in the foreground of the operating system, and by watching the real-time system details visible

on the Performance tab of the Windows Task Manager that at no point during the simulations was either CPU usage or the physical memory in use ever significantly above 50%.

An attempt was made to quantify each model's computational speed by normalizing the rate of each simulation. By considering that each model needed to determine results for every element for every timestep for the entire duration of the simulation, a total number of element-results per simulation could be defined. By dividing this value by the CPU runtime recorded for each trial, an element-results per unit time could be determined. Equations 3.4 and 3.5 were used, and the results are included in Table 3.2.

$$\frac{\text{Total Simul. Time} * \text{No. of Elements in Model}}{\text{Timestep}} = \text{Element Results per Simulation}$$

Equation 3.4

$$\frac{\text{Element Results per Simulation}}{\text{CPU Runtime}} = \text{Element Results per Second}$$

Equation 3.5

Table 3.2: Estimation of Calculation Speed for Each Model

| Model | Timestep, Δt (s) | Total Simulation Time (hr) | No. of Elements - | CPU Runtime (s) | Element Results per Simulation | Element Results per Second |
|----------------|--------------------------------|-------------------------------------|-------------------------|-----------------------|--------------------------------------|----------------------------------|
| SRH-2D | 1.0 | 0.50 | 3826 | 34.44 | 6886800 | 199937 |
| | 0.5 | 0.50 | 5724 | 134.64 | 20606400 | 153048 |
| HR-2D Diff. | 1.0 | 0.50 | 3476 | 10.00 | 6256800 | 625680 |
| | 0.5 | 0.50 | 5495 | 23.00 | 19782000 | 860087 |
| HR-2D Mom. | 1.0 | 0.50 | 3476 | 26.00 | 6256800 | 240646 |
| | 0.5 | 0.50 | 5495 | 54.00 | 19782000 | 366333 |

The calculations presented in Table 3.2 ignore the fact that each model produces different results for each mesh element (in the case of SRH-2D) or computational cell (in the case of HEC-RAS 2D). However, there were enough similarities that a comparison of the results should be useful. The best comparison for model speed in Table 3.2 is the element results per second.

Interestingly, for SRH-2D the denser mesh with the 0.5-second timestep had fewer element results per second, while for both HEC-RAS equation sets the reverse was true. In the case of SRH-2D, this likely had to do with the Courant number (discussed below), which was larger for the less dense mesh with the longer timestep. Because the Courant number was larger, the code needed to perform more iterations for each timestep to solve for the desired variables. It is not understood why the opposite would be true for the HEC-RAS simulations.

$$\text{Courant number, } C = \frac{V\Delta t}{\Delta x} \quad \text{Equation 3.6}$$

Equation 3.6 presents the Courant number as the ratio of the distance water in the simulation could travel in a given timestep to the length of the element through which it is travelling. It is a dimensionless quantity; values less than 1 mean that the water entering an element will have at least one computational timestep coincide with its residence in that cell, while values greater than 1 indicate that the water could bypass an element entirely during a computational timestep. Generally speaking, to increase model stability, the Courant number should be decreased. Chapter 4 of the HEC-RAS 5.0 User's Manual (Brunner, 2016b) provides recommendations for the Courant number: when the full momentum equations are used, the value should be less than or equal to 1.0 (maximum of 3.0), but when the diffusion wave equations are used, a larger timestep is permissible, the recommended value being less than or equal to 2.0 (maximum of 5.0). In order to approximate a representative Courant number for these models, the average velocity for uniform flow of 6.252 fps was used in Equation 3.6 in place of V , Δt was equal to the computational timestep for each model, and the value used for Δx was the spacing criterion used when generating each mesh. Table 3.1 shows these values. Upon closer examination of the results of each model using SMS 12.1 and the RAS Mapper, the approximate Courant number calculated was quite accurate.

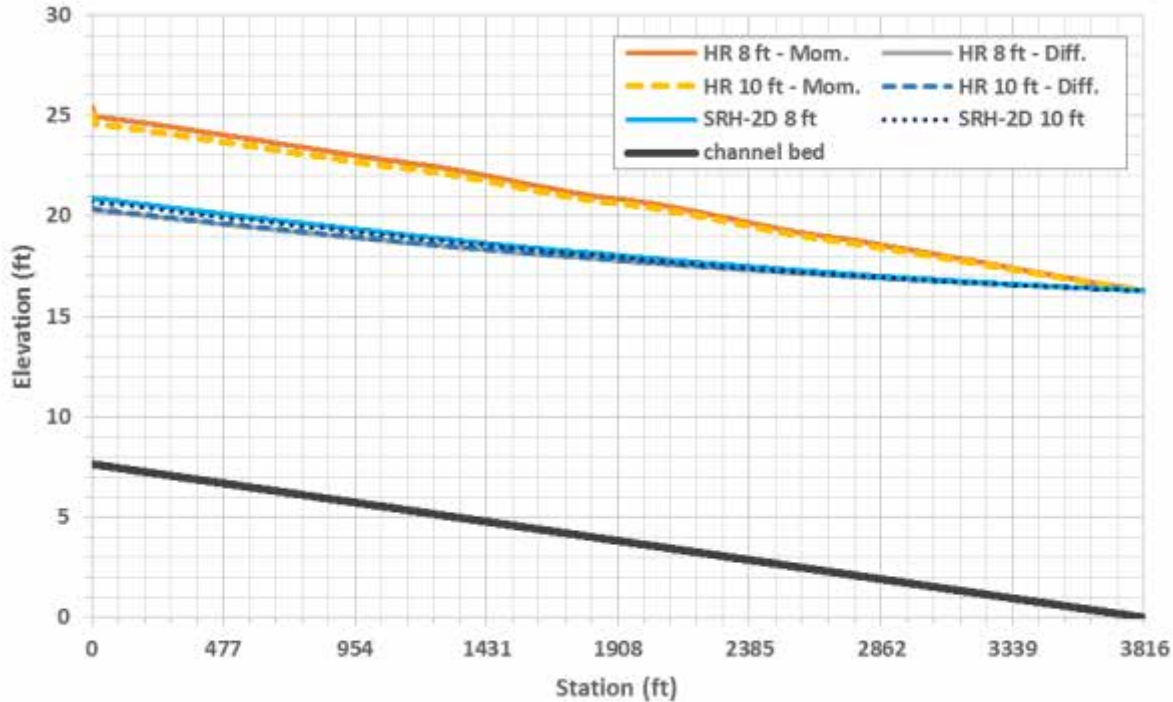


Figure 3.7: Steady State Profiles for Channel Centerline for Computational Tests

Figure 3.7 shows model results for SRH-2D and HEC-RAS 2D using both the diffusion and full momentum equations for two different mesh densities. While the differences between the simulation results are small within each model, there are obvious differences between the results of different models. Surprisingly, the HEC-RAS models using the diffusion wave equations are more similar to the SRH-2D results than they are to those from the HEC-RAS models using the full momentum equations. Both the SRH-2D and diffusion wave profiles resemble a standard M1 gradually varied flow profile in which depth increases in the downstream direction—behavior that seems entirely reasonable for this reach. However, the profiles generated by HEC-RAS 2D models using the full momentum equations enter the model space above the uniform depth of 16.27 feet, at 17.82 ft and 17.42 ft for the 8-ft and 10-ft spacing models, respectively. This is despite using an energy grade line (EGL) equal to the ground slope of 0.002 to determine conveyance at the upstream boundary condition. The HEC-RAS 2D models produce another curious result: in both HEC-RAS 2D full momentum simulations the flow enters at the depths mentioned, decreases rapidly over some relatively short distance—18.7 ft and 14.7 ft for the 8-ft and 10-ft spacing models, respectively—and then hardly

changes for the entire length of the channel, staying near 17 ft for most of the distance yet decreasing very gradually until the depth reaches the downstream boundary condition of 16.27 ft.

3.3 Basic Flow around a Bend

In natural streams, it is extremely common to see bends where the bank on the outside of the turn is steeper than that on the inside. The outside bank becomes steeper because it incurs stress from the flow of the stream as it is forced to change direction; this stress causes erosion of the bank. The water surface elevation of the flow on the outside of the bend tends to be higher than that of the flow on the inside, and because of larger hydrostatic forces near the channel bed caused by this deeper flow, a secondary, circular pattern of flow is induced through the cross section, which deposits the eroded soil on the inside bank. Henderson (1966) discusses this in his section “Changes of Direction.” While these secondary flow patterns through bends result in markedly 3D situations, the fact that flow is expected to be deeper on the outside of a channel bend can be investigated using the software discussed in this report. Only the HEC-RAS 2D full-momentum models and the SRH-2D models with 8-ft spacing were used in this analysis. All data shown are from the steady state portion of each simulation.

Data were taken from the SRH-2D and HEC-RAS 2D models at Station 1253.81 (measured in feet from the downstream boundary condition); 32.9% of the entire channel length. This location was selected to compare model results at a location on a small-radius bend. SMS could only provide values for each element, and thus gives data at approximately 8-ft spacing, while RAS Mapper writes output to the terrain used (in this case the elevation raster). Since the original terrain had a grid spacing of 1 ft × 1 ft, the RAS-2D data are much denser. In Figures 3.9 and 3.10, the lateral stationing increases from inside the bend to outside facing downstream, as is the hydraulic modeling convention.

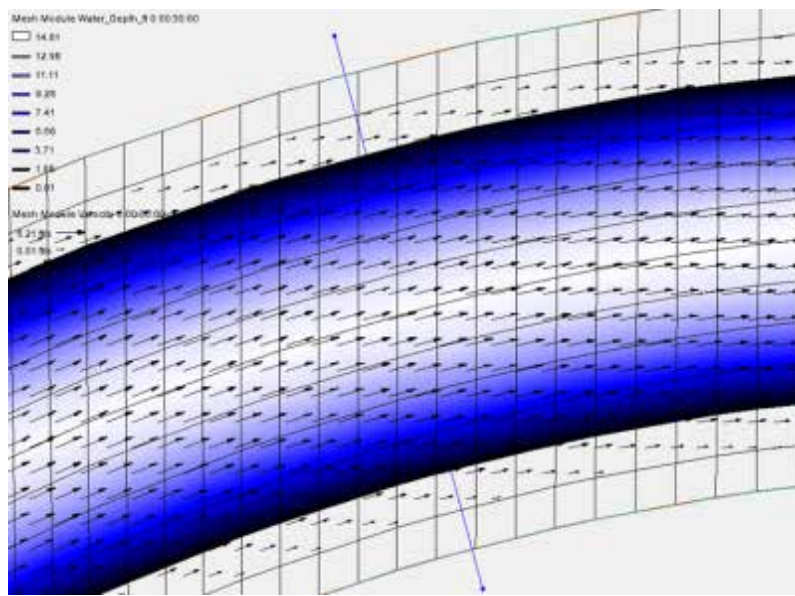


Figure 3.8: View from SMS 12.1 of Cross Section Used for Analysis of Basic Flow around a Bend

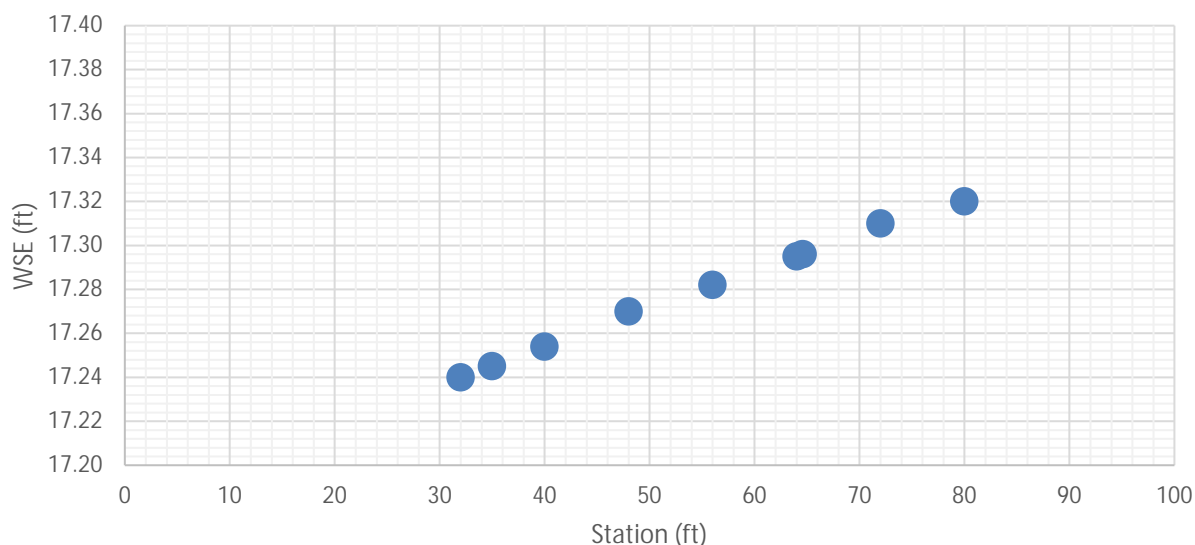


Figure 3.9: SRH-2D Data for Cross Section at Station 1253.81

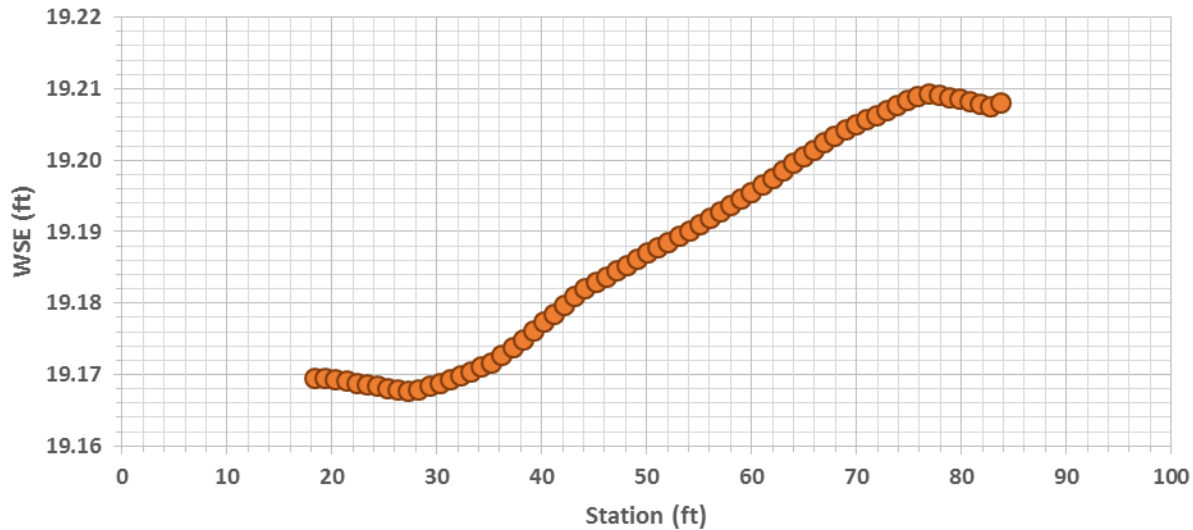


Figure 3.10: HEC-RAS 2D Data for Cross Section at Station 1253.81

Figures 3.9 and 3.10 clearly show that the water surface does indeed tend to be higher on the outside of the bend. Interestingly, this was not true for every cross section along the channel—in fact, frequently the opposite was true: the water surface was higher on the inside of the bend. This is believed to be caused by series of reflections caused by the two major bends in this channel. It appears that the cross section at Station 1253.81 is far enough away from these disturbances to be unaffected by them.

One more test was conducted using the data from this station, to check the validity of Equation 17.17 in Henderson (1966), reproduced below as Equation 3.7.

$$\frac{dv}{dn} + \frac{v}{r} = 0 \quad \text{Equation 3.7}$$

In the above equation, v is the depth averaged velocity at a point, n is the distance measured outwards across the width of the cross section, and r is the radius of curvature drawn in the horizontal plane of the streamlines at any vertical section. From the velocity vectors in Figure 3.8, it is apparent that all flow travels in a manner normal to the cross section, and thus the radius of curvature for the streamlines should be determined based on their position relative to the stream centerline, where a radius of curvature of 500 feet exists. For the purposes of this

analysis, the derivatives in Equation 3.7 were approximated using finite differences, as shown in Equation 3.8.

$$\frac{\Delta v}{\Delta n} + \frac{v}{r} = 0 \quad \text{Equation 3.8}$$

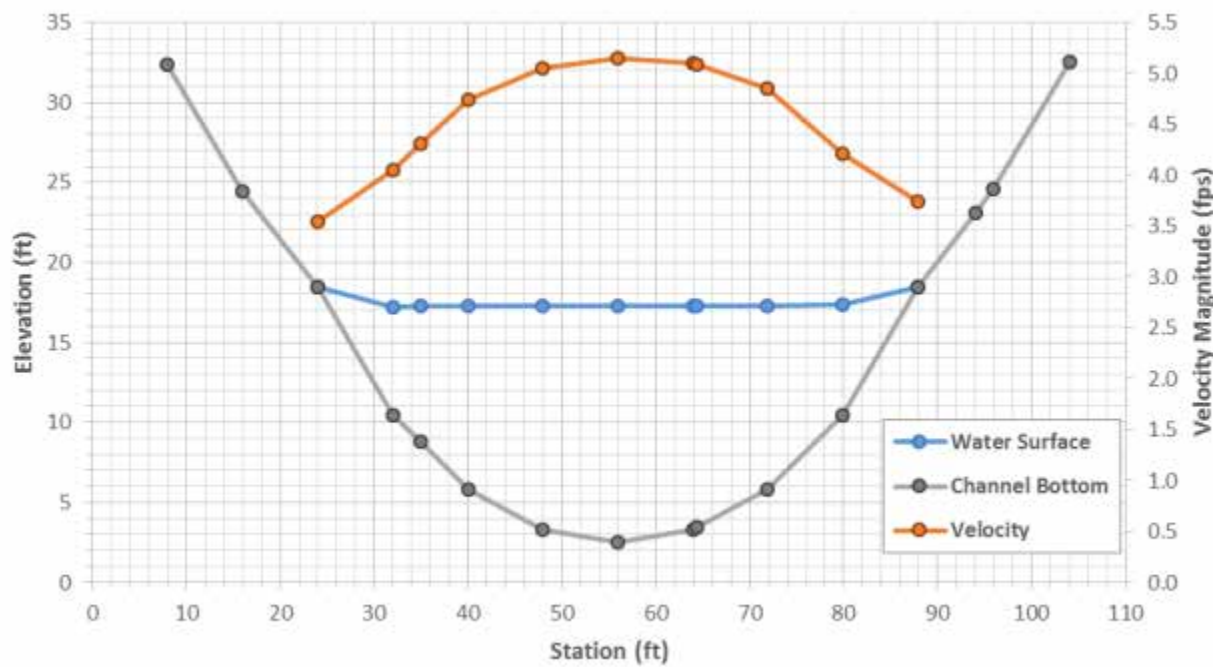


Figure 3.11: Detailed SRH-2D Data for Cross Section at Station 1253.81

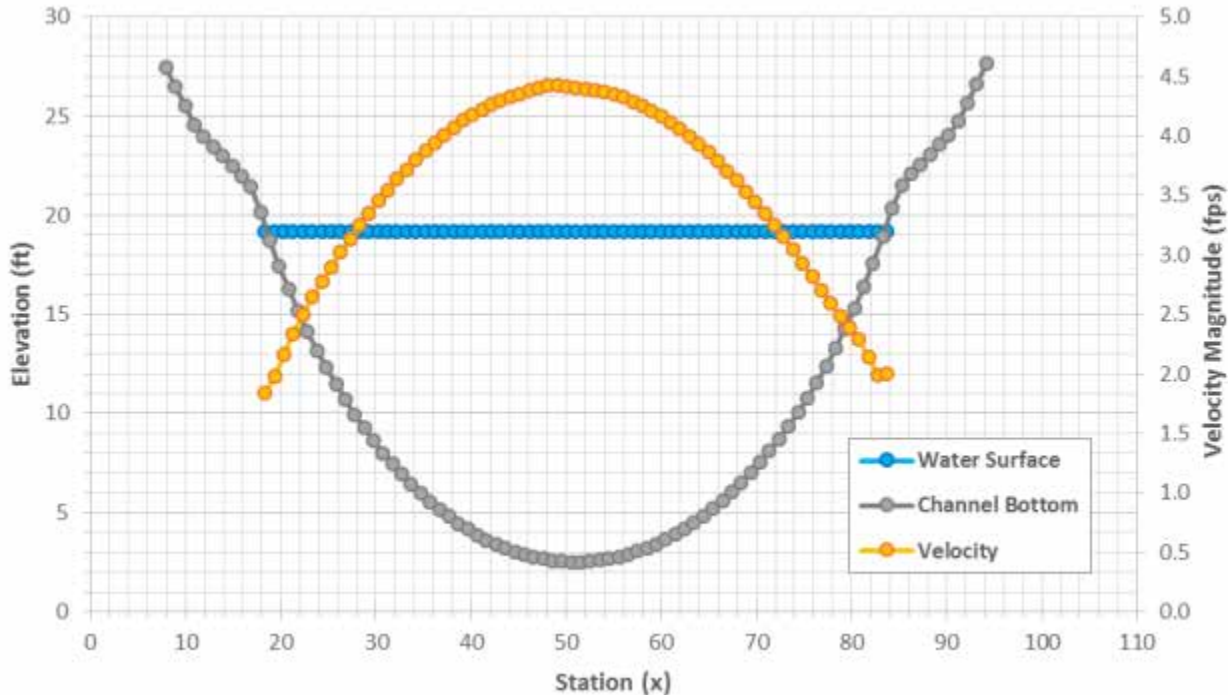


Figure 3.12: Detailed HEC-RAS 2D Data for Cross Section at Station 1253.81

Tables 3.3 and 3.4 show that the 2D models capture the general behavior of the Henderson equation. The range of values is greatest—from 0.143 to 0.000—for those determined from the data derived from the HEC-RAS 2D model, yet both sets of data yielded solutions to Equation 3.8 that were near zero. The data in Tables 3.3 and 3.4 also show that the assumption reflected in Henderson's Equation 7.14, that all stream filaments across the width will have the same total energy, is satisfied here except at the far lateral extents of the flow in the SRH-2D data.

Table 3.3: Solution of Equation 3.8 (Henderson's 7.17) with Data from SRH-2D Model

| Sta. (ft) | Elev. (ft) | Vel.Mag. (fps) | WSE (ft) | H (ft) | Δv (fps) | Δn (ft) | (7-17)* - |
|--------------|---------------|-------------------|-------------|-----------|---------------------|--------------------|--------------|
| 8.000 | 32.360 | - | - | - | - | - | - |
| 15.993 | 24.428 | - | - | - | - | - | - |
| 23.992 | 18.450 | 3.545 | 18.453 | 18.648 | - | - | - |
| 31.998 | 10.471 | 4.053 | 17.239 | 17.494 | 0.508 | 8.005 | 0.072 |
| 34.912 | 8.778 | 4.308 | 17.244 | 17.533 | 0.256 | 2.914 | 0.096 |
| 39.976 | 5.834 | 4.745 | 17.255 | 17.605 | 0.437 | 5.064 | 0.096 |
| 47.945 | 3.315 | 5.046 | 17.270 | 17.666 | 0.301 | 7.969 | 0.048 |
| 55.924 | 2.512 | 5.151 | 17.285 | 17.697 | 0.105 | 7.979 | 0.023 |
| 63.913 | 3.319 | 5.100 | 17.299 | 17.703 | -0.052 | 7.989 | 0.004 |
| 64.410 | 3.476 | 5.084 | 17.300 | 17.701 | -0.015 | 0.498 | -0.020 |
| 71.881 | 5.831 | 4.855 | 17.311 | 17.677 | -0.230 | 7.471 | -0.021 |
| 79.873 | 10.466 | 4.210 | 17.324 | 17.599 | -0.645 | 7.992 | -0.072 |
| 87.891 | 18.465 | 3.738 | 18.468 | 18.685 | -0.472 | 8.018 | -0.052 |
| 94.005 | 23.098 | - | - | - | - | - | - |
| 95.934 | 24.565 | - | - | - | - | - | - |
| 104.004 | 32.514 | - | - | - | - | - | - |

*Derivatives approximated by finite differences

Table 3.4: Solution of Equation 3.8 (Henderson's 7.17) with Data from HEC-RAS 2D Model

| Station* (ft) | WSE (ft) | Vel. Mag. (fps) | H (ft) | Δv (fps) | Δn (ft) | (7-17)** - |
|------------------|-------------|--------------------|-----------|---------------------|--------------------|---------------|
| 18.337 | 19.170 | 1.841 | 19.222 | - | - | - |
| 19.329 | 19.170 | 1.979 | 19.230 | 0.1376 | 0.991 | 0.143 |
| 20.320 | 19.169 | 2.159 | 19.242 | 0.1807 | 0.991 | 0.187 |
| 36.179 | 19.173 | 3.944 | 19.414 | 0.0684 | 0.991 | 0.077 |
| 44.108 | 19.182 | 4.327 | 19.473 | 0.0307 | 0.991 | 0.040 |
| 45.099 | 19.183 | 4.356 | 19.478 | 0.0286 | 0.991 | 0.038 |
| 46.091 | 19.184 | 4.383 | 19.482 | 0.0273 | 0.991 | 0.036 |
| 47.082 | 19.185 | 4.409 | 19.486 | 0.0259 | 0.991 | 0.035 |
| 49.064 | 19.186 | 4.422 | 19.490 | -0.0015 | 0.991 | 0.007 |
| 50.055 | 19.187 | 4.414 | 19.490 | -0.0074 | 0.991 | 0.001 |
| 51.046 | 19.188 | 4.407 | 19.489 | -0.0072 | 0.991 | 0.002 |
| 52.038 | 19.189 | 4.399 | 19.489 | -0.0085 | 0.991 | 0.000 |
| 53.029 | 19.189 | 4.386 | 19.488 | -0.0128 | 0.991 | -0.004 |
| 54.020 | 19.190 | 4.370 | 19.487 | -0.0159 | 0.991 | -0.007 |
| 82.764 | 19.208 | 1.989 | 19.269 | -0.1511 | 0.991 | -0.149 |
| 83.756 | 19.208 | 2.000 | 19.270 | 0.0112 | 0.991 | 0.015 |

*Many interior rows hidden

**Derivatives approximated by finite differences

Chapter 4: Turbulence and Roughness Sensitivity Tests

4.1 Overview of the Turbulence and Roughness Sensitivity Tests

A river model often must be calibrated against historical data such as high water marks for historical floods before it can be used to predict behavior of the reach—for example, after construction of a new bridge over the river. A proper model requires many inputs, and the collection of this data is often a large part of the modelling task. Not all of these inputs, however, are appropriate candidates for calibration. All hydraulic models must account for energy losses due to friction and turbulence. Both types of energy loss can have a large effect on flow behavior, and both are good candidates for model calibration.

Friction losses are accounted for through the use of Manning's equation in 1D river models. One important parameter in this equation is the familiar roughness coefficient, n , known as Manning's roughness coefficient. This parameter (with units of $\text{seconds} \cdot \text{feet}^{-1/3}$) depends upon the type of land cover the water is flowing over, such as concrete, dense brush, tall grass, short grass, rocky channels, or bare earth. Much research has been performed to empirically determine Manning's n values for many possible scenarios (Chow, 1959). Hydraulic engineers have used Manning's roughness coefficient for many years and are familiar with how changes in this parameter will affect their models. Because of their familiarity—and all of the time invested in laboratory work, calibration studies, and the compilation of tables of these coefficients—classic Manning's n values have been adapted for use in 2D models such as HEC-RAS 2D and SRH-2D. Losses due to turbulence must be accounted for when using the full momentum equations employed by HEC-RAS 2D and SRH-2D. HEC-RAS 2D accomplishes this by using an eddy viscosity model that can be adjusted by changing the value of the eddy viscosity coefficient (Kundu & Cohen, 2008). SRH-2D accounts for losses due to turbulence by using a parabolic-turbulence model (or a κ - ϵ model, which was not investigated in this report) with a constant coefficient that can be adjusted in the model control menu of SMS 12.1 (see Lai, 2008). The 1D HEC-RAS model attempts to account for these sorts of losses in part by use of the expansion and contraction coefficients discussed in Chapter 2 of this report.

While hydraulic engineers understand how variations in Manning's n affect 1D models, they are far less familiar with how variations in turbulence parameters will affect their 2D

models. For this reason, a simple sensitivity test was conducted for a reach using both HEC-RAS 2D and SRH-2D. Prior to version 5.0.3, in HEC-RAS 2D the eddy viscosity term could not be adjusted for use with the full momentum equation; therefore, it was not included in this study. However, the parabolic turbulence model of SRH-2D allows for adjustment of the coefficient, and both models accept changes to the Manning's roughness coefficients.

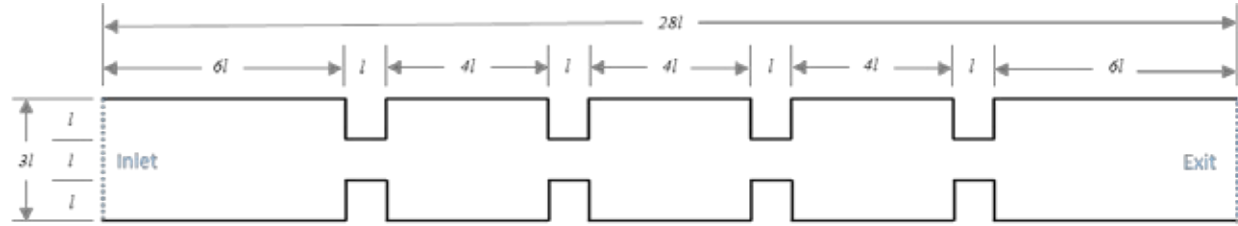


Figure 4.1: Plan View of the Geometric Basis for Tests with $l = 6$ feet

Figure 4.1 describes the layout used for these sensitivity tests. The channel has a horizontal bed, a flat bottom, and infinitely high walls perpendicular to the flat bottom. Each of four constrictions reduces the channel width by two-thirds, to 6 ft from 18 ft, before opening again to the full width. These constrictions are intended to cause many local losses due to turbulent dissipation of energy. To allow for comparison, the same channel was used for both the turbulence constant test and the roughness coefficient test. Some model preparation was performed in ArcMap for use in both SMS 12.1 and HEC-RAS 5.0. For SMS 12.1 (and thus for SRH-2D), only the shapefile defining the boundary of the channel needed definition. A raster defining the elevations for the model had to be created for use in HEC-RAS 2D, and to simulate the sheer walls of the channel, a rapidly sloping wall was used—from the channel bottom at an elevation of 0 ft to a height of 70 ft over a horizontal distance of 0.5 ft. Square mesh elements measuring 1 ft were used for both models. A computational timestep of 0.1 second was used for all tests, and the simulation time for every run was 12 minutes. The discharge for every test ramped up linearly to 2000 cfs from 20 cfs over 6 minutes, and stayed at 2000 cfs for the 6 remaining minutes of each test. The downstream boundary condition used was a constant depth of 12 ft. All profiles shown are for the channel's centerline and the final timestep at 12 minutes. To distribute the flow at the inlet in SRH-2D, the “conveyance” option was selected for the inlet

boundary. Similarly, in HEC-RAS 2D the flow was distributed according to conveyance at the inlet; however, a slope for the energy grade line had to be specified, and a value of 0.0006 was chosen, somewhat arbitrarily, for all trials. For every SRH-2D turbulence test, the Manning's roughness coefficient was set to 0.01 to minimize the influence of friction on the results.

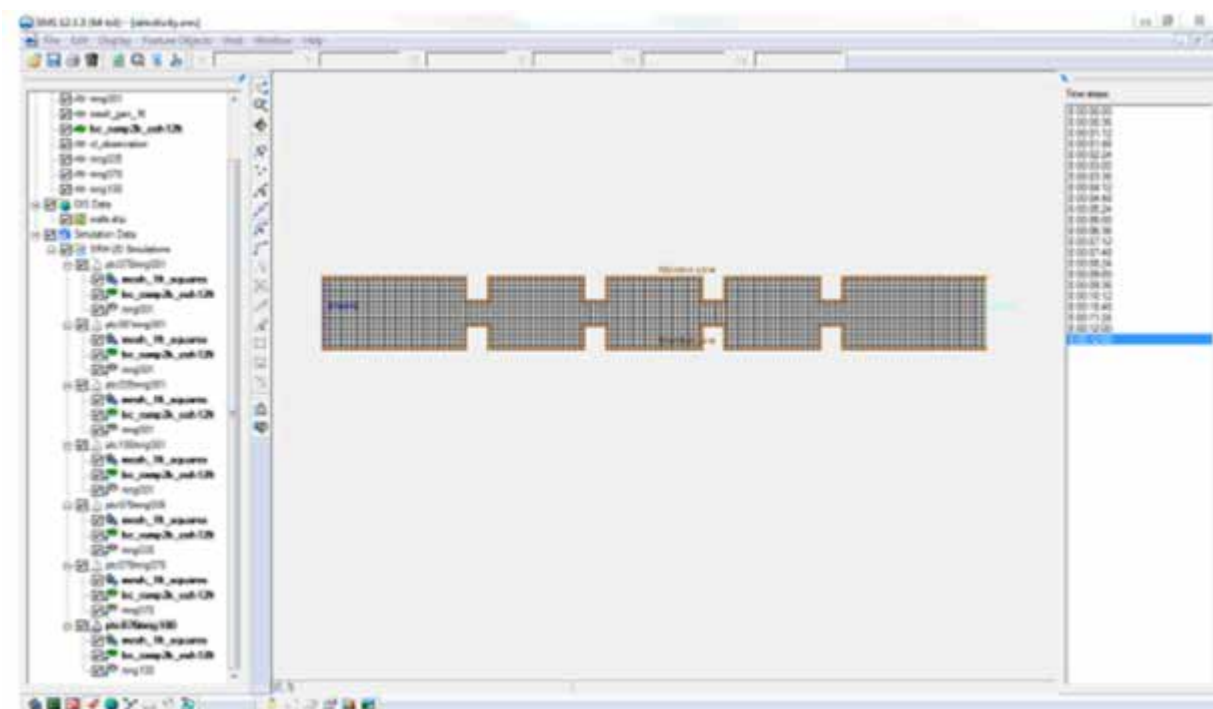


Figure 4.2: SMS 12.1 Project Overview and Grid Display for SRH-2D Sensitivity Tests



Figure 4.3: Representative Plan View from HEC-RAS 2D Showing Typical Flow Patterns from the Simulations (Flow Left to Right)

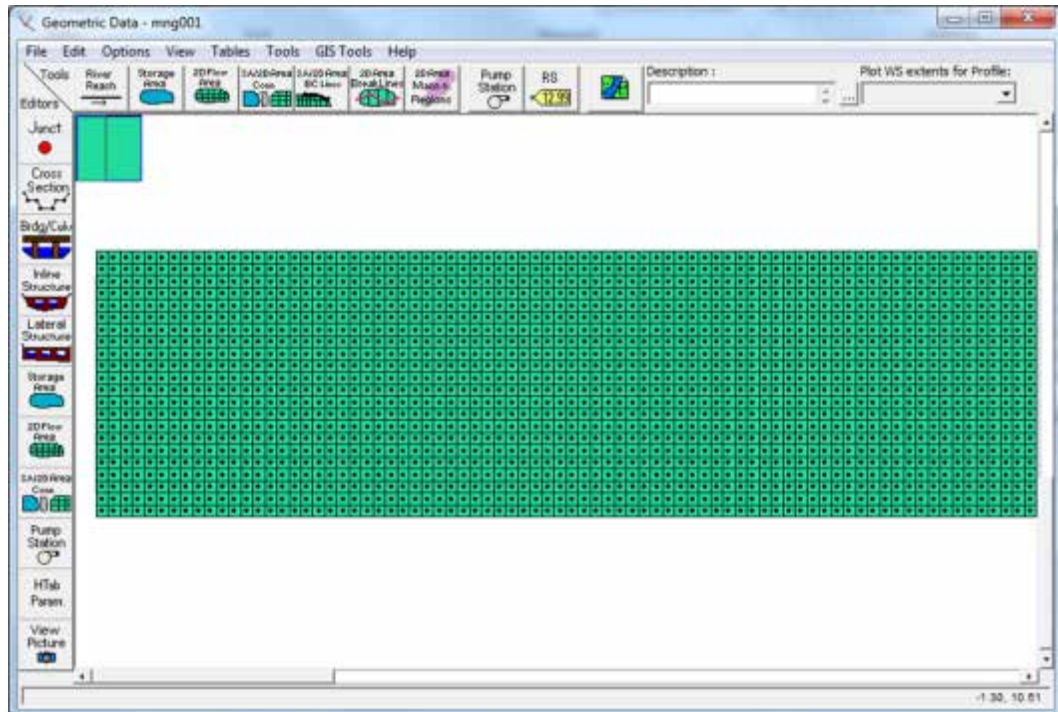


Figure 4.4: HEC-RAS 2D Flow Area Elements for Sensitivity Tests

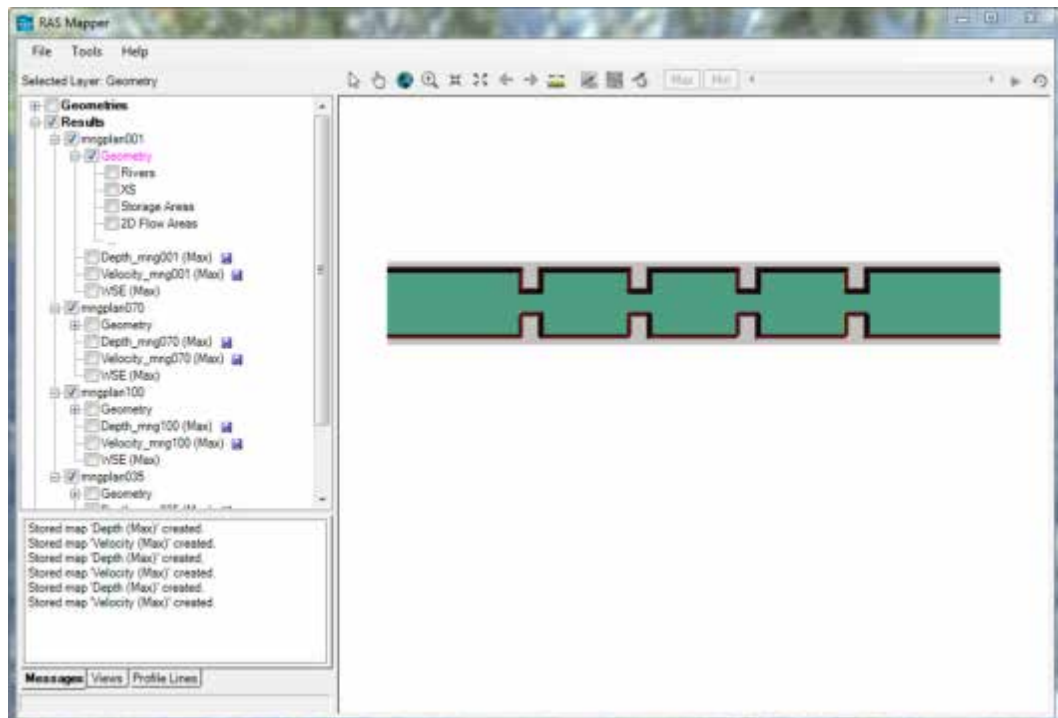


Figure 4.5: Triangulated Irregular Network for Model Elevations for HEC-RAS 2D Sensitivity Tests as Seen in RAS Mapper

4.2 Results of Sensitivity Tests

The data show that between the SRH-2D parabolic turbulence tests the increase in upstream depth from minimum to maximum trials was 36.7%, while there was an increase of 64.9% from the SRH-2D roughness trials. The increase in upstream depth between the minimum and maximum trials for the HEC-RAS 2D roughness trials was 85.3%. It should be noted, however, that for the HEC-RAS tests, the upstream depths were all lower than for the SRH-2D trials with the same roughness coefficients. This could be explained by the constant friction slope used for the HEC-RAS models to determine conveyance at the inlet; however, the results exhibit physically realistic behavior in that as roughness increases, there are more losses, and so the water must gain hydraulic head by gaining depth upstream to pass the same discharge. It is likely that the friction slope used as an input to the HEC-RAS models could itself be a source of calibration. It seems that the effect of the parabolic turbulence constant is not especially large, and unless the modeler has a special reason to do so, this parameter should not be considered when trying to calibrate a model (it should be noted that the actual value of the parabolic turbulence constant for the PTC = 1.00 test is PTC = 0.999999, the maximum value allowed by SRH-2D). Small changes in the roughness coefficient have a large impact on the depth of flow, and these coefficients can vary over an even wider range than the turbulence constant values; therefore, they should be a primary concern when calibrating a model. Moreover, the roughness coefficients are often—at least initially—simply educated guesses based upon aerial photographs of the site in question. It can be difficult to say, for example, whether the crop field seen in an image should have a roughness coefficient of 0.025 or 0.030 after consulting the descriptions within a Manning's roughness coefficient table. It is not surprising that the coefficients used within a model may require some fine-tuning.

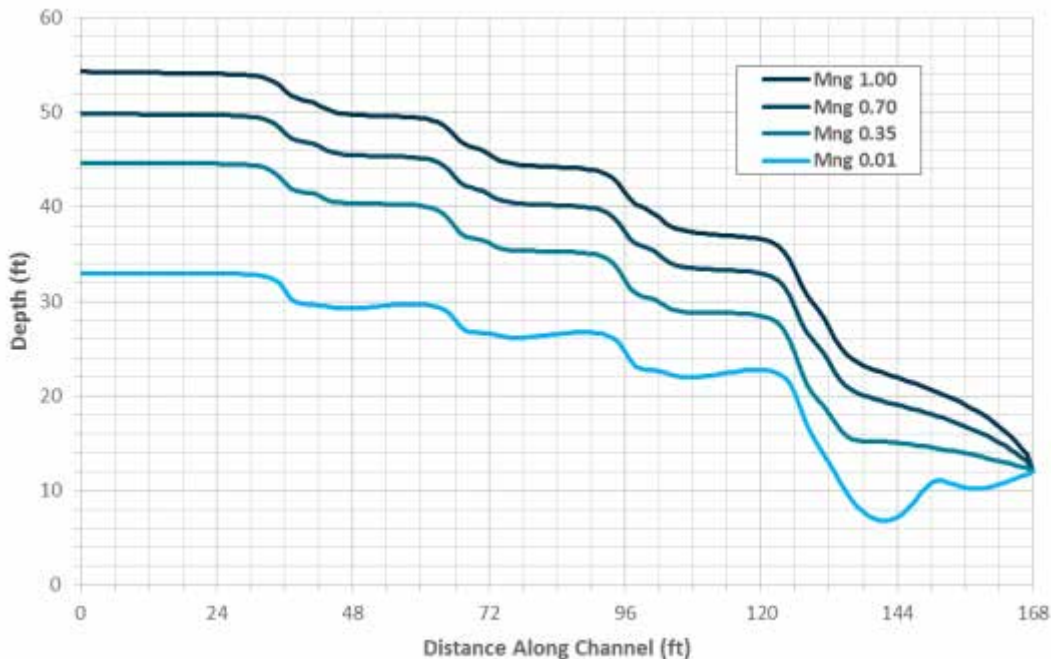


Figure 4.6: SRH-2D Roughness Coefficient Tests with Parabolic Turbulence Equal to 0.7 for all Trials

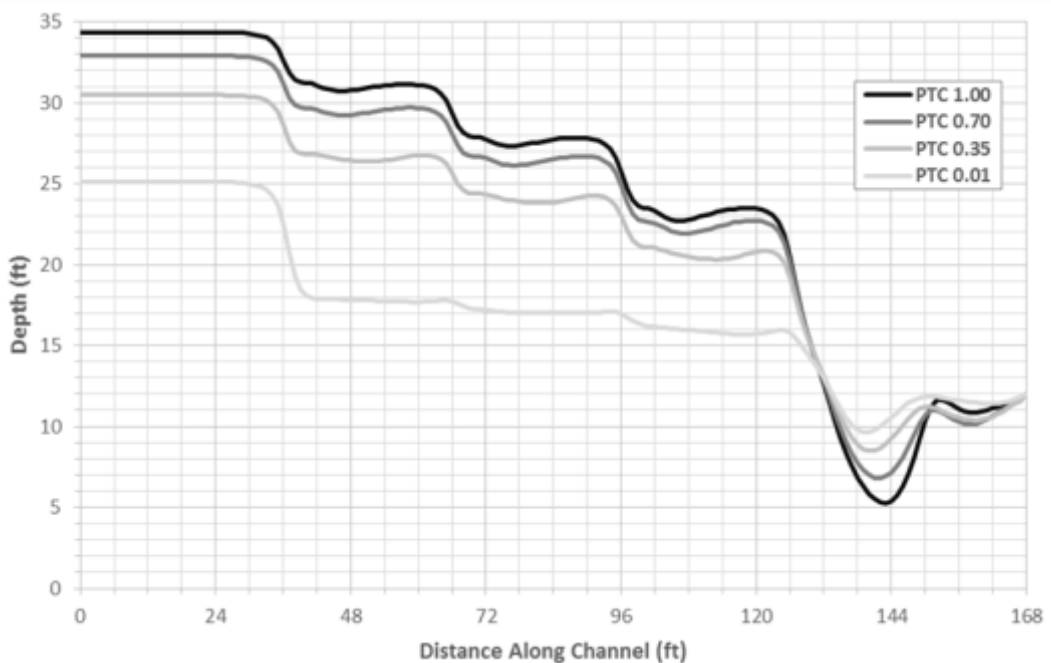


Figure 4.7: SRH-2D Parabolic Turbulence Constant Tests with Manning's Roughness Coefficient Equal to 0.01 for all Tests

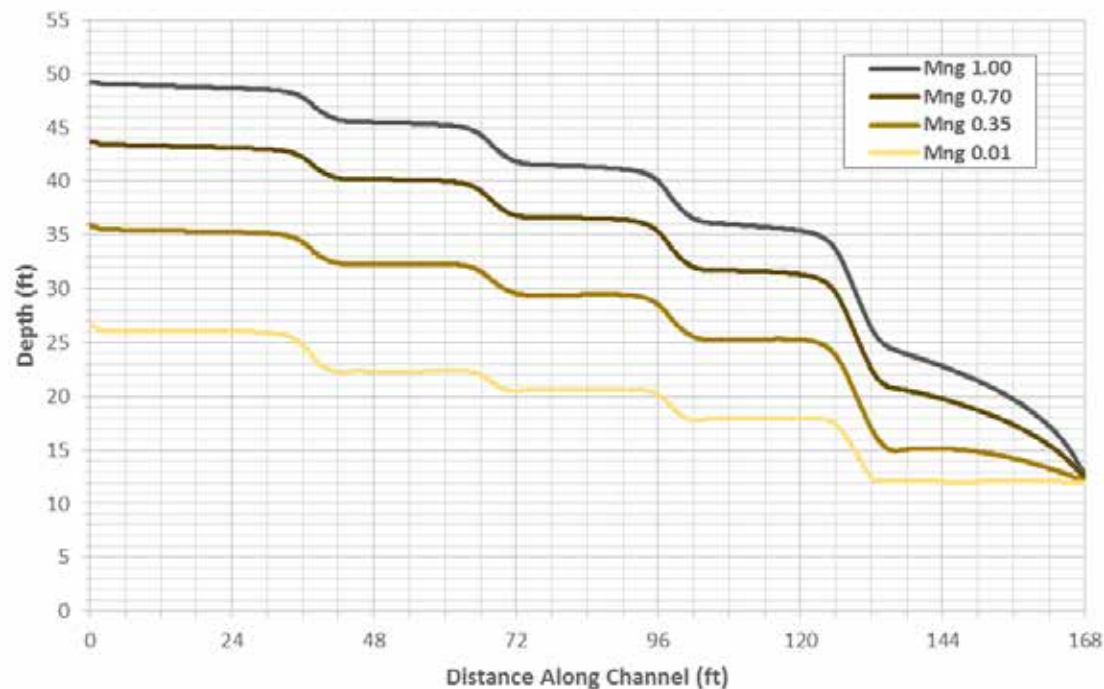


Figure 4.8: HEC-RAS 2D Roughness Coefficient Tests

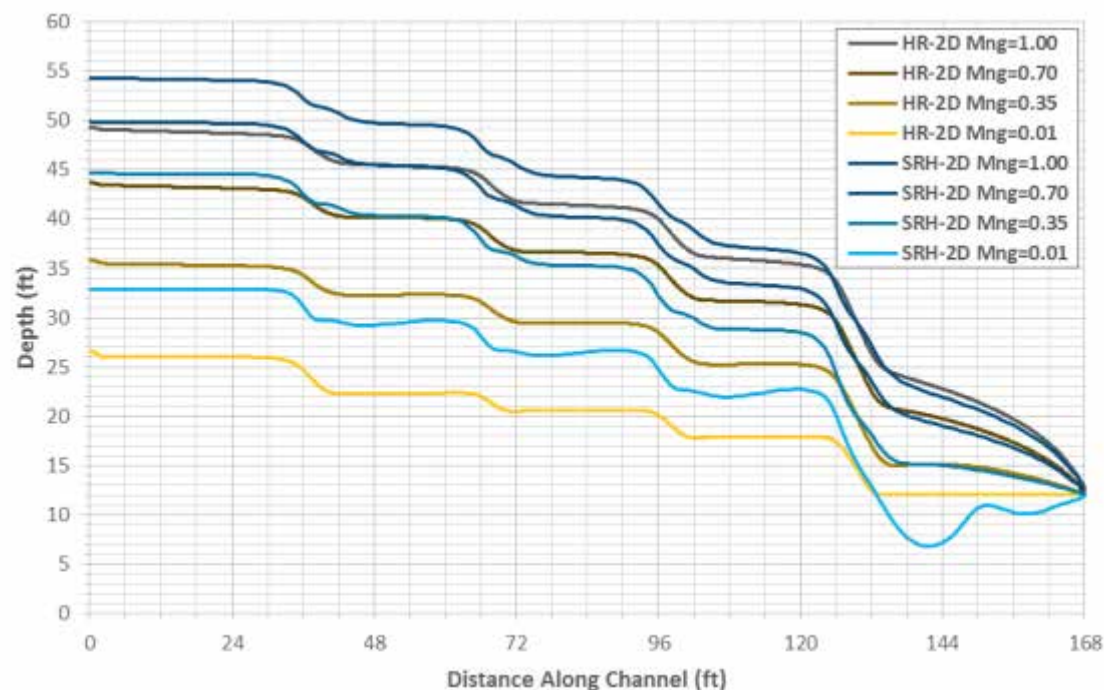


Figure 4.9: Comparison between Roughness Coefficient Test Results for SRH-2D and HEC-RAS 2D

Table 4.1: Change in Depth from Upstream to Downstream Normalized by the Channel Length

| Test Parameter Value | 0.01 | 0.35 | 0.70 | 1.00 |
|------------------------|------|------|------|------|
| $-\Delta y/L$ | | | | |
| SRH-2D PTC* | 0.08 | 0.11 | 0.12 | 0.13 |
| SRH-2D Manning's n* | 0.12 | 0.19 | 0.23 | 0.25 |
| HEC-RAS 2D Manning's n | 0.09 | 0.14 | 0.19 | 0.22 |

*Manning's Roughness Coefficient, $n=0.01$ for all SRH-2D PTC Tests.

**PTC=0.70 (default) for all SRH-2D Manning's n Tests.

For the SRH-2D Turbulence Test with PTC = 0.01,

$$\frac{-(\text{change in depth from } x = 0 \text{ ft to } x = 168 \text{ ft})}{\text{length of channel}} = \frac{-\Delta y}{L} = \frac{-(12.00 \text{ ft} - 25.13 \text{ ft})}{168 \text{ ft}} = \boxed{0.08}$$

Equation 4.1

Chapter 5: Mixed Flow Regime Test

5.1 Overview of the Mixed Flow Regime Test

This chapter evaluates the mixed flow regime capability of SRH-2D by addressing a two-lake problem where water flows between two lakes through a channel with two slope breaks. The objective was to conduct a simple test to assess how well the 2D models simulate well-established 1D principles. This was done by analyzing the problem within an Excel spreadsheet, applying the standard Depth Step Method and then using SRH-2D and both 1D and 2D HEC-RAS 5.0. The water surface profiles extracted from the channel centerline served as a major basis of comparison between these methods.

The channel connecting the two bodies of water is a straight reach that possesses a prismatic, trapezoidal cross section. The base width is 20 ft and the side slopes are 1:1 (H:V). Within the channel there are two breaks in grade. The first break is a transition from a grade of 0.2% to 2%, and the next returned to 0.2%. The first and third sections are hydraulically mild and the middle section is steep. The Manning's roughness coefficient, n , is a uniform 0.025 everywhere. The discharge is 1000 cfs. This channel is represented in Figures 5.1 and 5.2 (channel elevations provided are representative of the channel's centerline). A hydraulic jump was expected to occur somewhere in the channel.

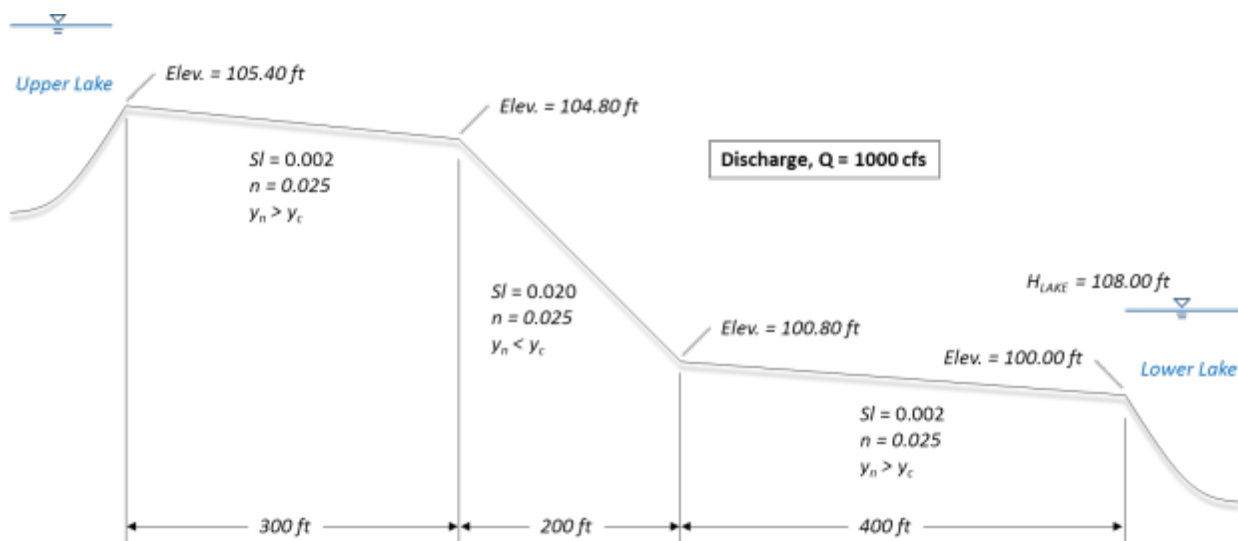


Figure 5.1: Elevation View of Reach with Exaggerated Z-Scale

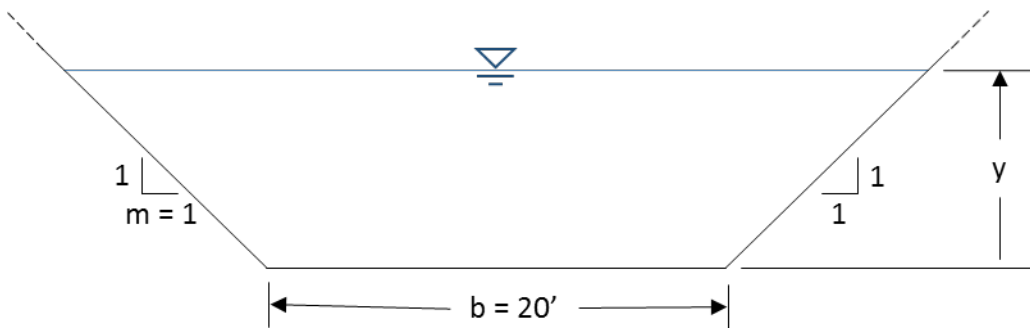


Figure 5.2: Representative Cross Section for Channel

5.2 Direct Step Method and Solution Procedure for Test Reach

The Depth Step Method is an explicit scheme for computing gradually varied flow profiles. A starting depth must be known at a location in the reach. Generally, this is a control section such as a free overfall with the resultant critical depth, or a lake with a known water surface elevation, uniform depth upstream or downstream, or some other such control section. A change in depth is then specified and a new horizontal position within the reach is directly calculated; then the process is repeated. A change in depth can be either positive or negative depending upon the situation. Supercritical profiles are calculated from upstream to downstream while the opposite is done for subcritical profiles. Friction losses between horizontal stations are calculated using Manning's equation (all equations used in this spreadsheet are presented in Section 5.4).

The Excel add-in Solver was used extensively to quickly arrive at solutions satisfying user-specified criteria. When using Solver, the user must specify an objective cell. This cell must contain a formula. The user must also specify what cell or cells contain the variable that should be changed to satisfy the requirements placed on the objective cell. Variable cells must contain an initial value; they cannot be empty cells. A good initial guess at these variables by the user will aid Solver in converging on a solution. Solver is not guaranteed to find an answer, even if one exists. This can be a problem if the initial guess is a poor one. Often further constraints are required for Solver to find a solution. This was the case when applying the Depth Step Method to this problem. Tables 5.1 and 5.2 show results of the solver method.

Table 5.1: Depth Step Method Spreadsheet with Incorrect Solution

| | |
|-------------------------------------------|----------|
| Bottom Width, b (ft) | 20 |
| Side Slope, m (H:V) | 1 |
| Bottom Slope, S_0 (ft/ft) | 0.002 |
| Manning's n | 0.025 |
| Discharge, Q (cfs) | 1000 |
| Initial Station for Profile (ft) | 500 |
| Final Station for Profile (ft) | 900 |
| Initial Bottom Elevation for Profile (ft) | 100.80 |
| Final Bottom Elevation for Profile (ft) | 100.00 |
| Initial Depth for Profile (ft) | 8.00 |
| Depth Step, Δy (ft) | 0.100000 |

Changing
Constraint
Objective

| Step n | y (ft) | A (sq.ft) | V (fps) | E (ft) | P _w (ft) | R (ft) | Fr | Avg. V (fps) | Avg. R (ft) | Avg. Sf (ft/ft) | Avg. Fr | Δx (ft) | x (ft) | z (ft) | y+z (ft) | M (cu.ft) |
|-----------|-----------|--------------|------------|-----------|------------------------|-----------|-------|-----------------|----------------|--------------------|---------|--------------------|-----------|-----------|-------------|--------------|
| 0 | 8.00 | 224.00 | 4.464 | 8.309 | 42.627 | 5.255 | 0.315 | - | - | - | - | - | 900.000 | 100.00 | 108.00 | 949.309 |
| 1 | 8.10 | 227.61 | 4.393 | 8.400 | 42.910 | 5.304 | 0.309 | 4.429 | 5.280 | 0.000601 | 0.312 | 64.502 | 964.502 | 99.87 | 107.97 | 969.690 |
| 2 | 8.20 | 231.24 | 4.325 | 8.490 | 43.193 | 5.354 | 0.302 | 4.359 | 5.329 | 0.000575 | 0.306 | 63.608 | 1028.111 | 99.74 | 107.94 | 990.491 |
| 3 | 8.30 | 234.89 | 4.257 | 8.581 | 43.476 | 5.403 | 0.296 | 4.291 | 5.378 | 0.000550 | 0.299 | 62.793 | 1090.903 | 99.62 | 107.92 | 1011.710 |
| 4 | 8.40 | 238.56 | 4.192 | 8.673 | 43.759 | 5.452 | 0.290 | 4.225 | 5.427 | 0.000527 | 0.293 | 62.046 | 1152.949 | 99.49 | 107.89 | 1033.349 |
| 5 | 8.50 | 242.25 | 4.128 | 8.765 | 44.042 | 5.500 | 0.284 | 4.160 | 5.476 | 0.000505 | 0.287 | 61.360 | 1214.309 | 99.37 | 107.87 | 1055.406 |
| 6 | 8.60 | 245.96 | 4.066 | 8.857 | 44.324 | 5.549 | 0.279 | 4.097 | 5.525 | 0.000484 | 0.281 | 60.728 | 1275.037 | 99.25 | 107.85 | 1077.883 |
| 7 | 8.70 | 249.69 | 4.005 | 8.949 | 44.607 | 5.598 | 0.273 | 4.035 | 5.573 | 0.000464 | 0.276 | 60.146 | 1335.183 | 99.13 | 107.83 | 1100.779 |
| 8 | 8.80 | 253.44 | 3.946 | 9.042 | 44.890 | 5.646 | 0.268 | 3.975 | 5.622 | 0.000445 | 0.270 | 59.607 | 1394.790 | 99.01 | 107.81 | 1124.095 |
| 9 | 8.90 | 257.21 | 3.888 | 9.135 | 45.173 | 5.694 | 0.263 | 3.917 | 5.670 | 0.000427 | 0.265 | 59.107 | 1453.897 | 98.89 | 107.79 | 1147.831 |
| 10 | 9.00 | 261.00 | 3.831 | 9.228 | 45.456 | 5.742 | 0.258 | 3.860 | 5.718 | 0.000410 | 0.260 | 58.643 | 1512.539 | 98.77 | 107.77 | 1171.988 |
| 49 | 12.90 | 424.41 | 2.356 | 12.986 | 56.487 | 7.513 | 0.136 | 2.369 | 7.492 | 0.000108 | 0.137 | 51.851 | 3620.873 | 94.56 | 107.46 | 2452.837 |
| 50 | 13.00 | 429.00 | 2.331 | 13.084 | 56.770 | 7.557 | 0.135 | 2.344 | 7.535 | 0.000105 | 0.135 | 51.793 | 3672.666 | 94.45 | 107.45 | 2494.725 |

Table 5.2: Depth Step Method Spreadsheet with Correct Solution

| | |
|-------------------------------------------|-----------|
| Bottom Width, b (ft) | 20 |
| Side Slope, m (H:V) | 1 |
| Bottom Slope, S_0 (ft/ft) | 0.002 |
| Manning's n | 0.025 |
| Discharge, Q (cfs) | 1000 |
| Initial Station for Profile (ft) | 500 |
| Final Station for Profile (ft) | 900 |
| Initial Bottom Elevation for Profile (ft) | 100.80 |
| Final Bottom Elevation for Profile (ft) | 100.00 |
| Initial Depth for Profile (ft) | 8.00 |
| Depth Step, Δy (ft) | -0.011676 |

Changing
Constraint
Objective

| Step n | y (ft) | A (sq.ft) | V (fps) | E (ft) | P _w (ft) | R (ft) | Fr | Avg. V (fps) | Avg. R (ft) | Avg. Sf (ft/ft) | Avg. Fr | Δx (ft) | x (ft) | z (ft) | y+z (ft) | M (cu.ft) |
|-----------|-----------|--------------|------------|-----------|------------------------|-----------|-------|-----------------|----------------|--------------------|---------|--------------------|-----------|-----------|-------------|--------------|
| 0 | 8.00 | 224.00 | 4.464 | 8.309 | 42.627 | 5.255 | 0.315 | - | - | - | - | - | 900.000 | 100.00 | 108.00 | 949.309 |
| 1 | 7.99 | 223.58 | 4.473 | 8.299 | 42.594 | 5.249 | 0.316 | 4.468 | 5.252 | 0.000616 | 0.316 | -7.594 | 892.406 | 100.02 | 108.00 | 946.957 |
| 2 | 7.98 | 223.16 | 4.481 | 8.288 | 42.561 | 5.243 | 0.317 | 4.477 | 5.246 | 0.000619 | 0.317 | -7.607 | 884.799 | 100.03 | 108.01 | 944.610 |
| 3 | 7.96 | 222.74 | 4.490 | 8.278 | 42.528 | 5.237 | 0.318 | 4.485 | 5.240 | 0.000622 | 0.317 | -7.621 | 877.178 | 100.05 | 108.01 | 942.269 |
| 4 | 7.95 | 222.32 | 4.498 | 8.267 | 42.495 | 5.232 | 0.319 | 4.494 | 5.235 | 0.000625 | 0.318 | -7.635 | 869.543 | 100.06 | 108.01 | 939.934 |
| 5 | 7.94 | 221.90 | 4.507 | 8.257 | 42.462 | 5.226 | 0.319 | 4.502 | 5.229 | 0.000629 | 0.319 | -7.649 | 861.894 | 100.08 | 108.02 | 937.604 |
| 6 | 7.93 | 221.48 | 4.515 | 8.246 | 42.429 | 5.220 | 0.320 | 4.511 | 5.223 | 0.000632 | 0.320 | -7.663 | 854.231 | 100.09 | 108.02 | 935.280 |
| 7 | 7.92 | 221.06 | 4.524 | 8.236 | 42.396 | 5.214 | 0.321 | 4.519 | 5.217 | 0.000635 | 0.321 | -7.677 | 846.553 | 100.11 | 108.03 | 932.962 |
| 8 | 7.91 | 220.65 | 4.532 | 8.226 | 42.363 | 5.208 | 0.322 | 4.528 | 5.211 | 0.000639 | 0.321 | -7.692 | 838.861 | 100.12 | 108.03 | 930.650 |
| 9 | 7.89 | 220.23 | 4.541 | 8.215 | 42.330 | 5.203 | 0.323 | 4.536 | 5.206 | 0.000642 | 0.322 | -7.707 | 831.154 | 100.14 | 108.03 | 928.343 |
| 10 | 7.88 | 219.81 | 4.549 | 8.205 | 42.297 | 5.197 | 0.323 | 4.545 | 5.200 | 0.000646 | 0.323 | -7.721 | 823.433 | 100.15 | 108.04 | 926.042 |
| 49 | 7.43 | 203.73 | 4.908 | 7.802 | 41.009 | 4.968 | 0.358 | 4.904 | 4.971 | 0.000798 | 0.357 | -8.473 | 508.498 | 100.78 | 108.21 | 840.774 |
| 50 | 7.42 | 203.32 | 4.918 | 7.792 | 40.976 | 4.962 | 0.359 | 4.913 | 4.965 | 0.000802 | 0.358 | -8.498 | 500.000 | 100.80 | 108.22 | 838.703 |

The solution procedure for this reach was first to determine the gradually varied flow (GVF) profile backward from the lower lake to the horizontal station where the channel transitions from a steep grade to a mild grade (Table 5.3). The next step was to solve simultaneously two GVF profiles in the steep section (Table 5.4). The upstream boundary

condition was located at the upstream end of the third section and was the depth determined from the previous GVF profile. The main constraint for the solution here was that the horizontal stations and the specific forces between the super- and subcritical profiles were equal. Lastly, the GVF profile for the uppermost section of the reach was back-calculated to the upper lake using critical depth as the downstream boundary condition (Table 5.5).

Table 5.3: Depth Step Method Results for M1 Profile from Station 500 to 900

| Depth Step, Δy (ft) | | -0.0117 | | | | | | | | | | | | | | |
|-----------------------------|--------|-----------|---------|--------|---------------------|--------|-------|--------------|-------------|-----------------|---------|-----------------|---------|---------|----------|-----------|
| Step n | y (ft) | A (sq.ft) | V (fps) | E (ft) | P _w (ft) | R (ft) | Fr | Avg. V (fps) | Avg. R (ft) | Avg. Sf (ft/ft) | Avg. Fr | Δx (ft) | x (ft) | z (ft) | y+z (ft) | M (cu.ft) |
| 0 | 8.000 | 224.000 | 4.464 | 8.309 | 42.627 | 5.255 | 0.315 | - | - | - | - | - | 900.000 | 100.000 | 108.000 | 949.309 |
| 1 | 7.988 | 223.580 | 4.473 | 8.299 | 42.594 | 5.249 | 0.316 | 4.468 | 5.252 | 0.00062 | 0.316 | -7.594 | 892.406 | 100.015 | 108.004 | 946.957 |
| 2 | 7.977 | 223.160 | 4.481 | 8.288 | 42.561 | 5.243 | 0.317 | 4.477 | 5.246 | 0.00062 | 0.317 | -7.607 | 884.799 | 100.030 | 108.007 | 944.610 |
| 3 | 7.965 | 222.740 | 4.490 | 8.278 | 42.528 | 5.237 | 0.318 | 4.485 | 5.240 | 0.00062 | 0.317 | -7.621 | 877.178 | 100.046 | 108.011 | 942.269 |
| 4 | 7.953 | 222.321 | 4.498 | 8.267 | 42.495 | 5.232 | 0.319 | 4.494 | 5.235 | 0.00063 | 0.318 | -7.635 | 869.543 | 100.061 | 108.014 | 939.934 |
| ... | ... | ... | ... | ... | ... | ... | ... | ... | ... | ... | ... | ... | ... | ... | ... | |
| 47 | 7.451 | 204.545 | 4.889 | 7.822 | 41.075 | 4.980 | 0.356 | 4.884 | 4.983 | 0.00079 | 0.355 | -8.424 | 525.420 | 100.749 | 108.200 | 844.934 |
| 48 | 7.440 | 204.138 | 4.899 | 7.812 | 41.042 | 4.974 | 0.357 | 4.894 | 4.977 | 0.00079 | 0.356 | -8.449 | 516.971 | 100.766 | 108.206 | 842.851 |
| 49 | 7.428 | 203.730 | 4.908 | 7.802 | 41.009 | 4.968 | 0.358 | 4.904 | 4.971 | 0.00080 | 0.357 | -8.473 | 508.498 | 100.783 | 108.211 | 840.774 |
| 50 | 7.416 | 203.324 | 4.918 | 7.792 | 40.976 | 4.962 | 0.359 | 4.913 | 4.965 | 0.00080 | 0.358 | -8.498 | 500.000 | 100.800 | 108.216 | 838.703 |

Table 5.4: Combined Depth Step Method Results for S2 and S1 Profiles from Station 300 to 500

| Depth Step, Δy (ft) | | -0.0193 | | | | | | | | | | | | | | |
|-----------------------------|--------|-----------|---------|--------|---------------------|--------|-------|--------------|-------------|-----------------|---------|-----------------|---------|---------|----------|-----------|
| Step n | y (ft) | A (sq.ft) | V (fps) | E (ft) | P _w (ft) | R (ft) | Fr | Avg. V (fps) | Avg. R (ft) | Avg. Sf (ft/ft) | Avg. Fr | Δx (ft) | x (ft) | z (ft) | y+z (ft) | M (cu.ft) |
| 0 | 3.979 | 95.399 | 10.482 | 5.685 | 31.253 | 3.052 | 1.000 | - | - | - | - | - | 300.000 | 104.800 | 108.779 | 504.815 |
| 1 | 3.959 | 94.861 | 10.542 | 5.685 | 31.198 | 3.041 | 1.008 | 10.512 | 3.047 | 0.00704 | 1.004 | 0.012 | 300.012 | 104.800 | 108.759 | 504.829 |
| 2 | 3.940 | 94.323 | 10.602 | 5.685 | 31.144 | 3.029 | 1.016 | 10.572 | 3.035 | 0.00716 | 1.012 | 0.036 | 300.047 | 104.799 | 108.739 | 504.872 |
| 3 | 3.921 | 93.787 | 10.663 | 5.686 | 31.089 | 3.017 | 1.024 | 10.632 | 3.023 | 0.00728 | 1.020 | 0.060 | 300.108 | 104.798 | 108.719 | 504.944 |
| 4 | 3.901 | 93.251 | 10.724 | 5.687 | 31.035 | 3.005 | 1.032 | 10.693 | 3.011 | 0.00740 | 1.028 | 0.086 | 300.194 | 104.796 | 108.698 | 505.046 |
| ... | ... | ... | ... | ... | ... | ... | ... | ... | ... | ... | ... | ... | ... | ... | ... | |
| 47 | 3.073 | 70.902 | 14.104 | 6.162 | 28.692 | 2.471 | 1.509 | 14.054 | 2.478 | 0.01659 | 1.502 | 7.086 | 376.369 | 103.273 | 106.346 | 542.113 |
| 48 | 3.054 | 70.399 | 14.205 | 6.187 | 28.637 | 2.458 | 1.524 | 14.154 | 2.465 | 0.01694 | 1.517 | 8.192 | 384.561 | 103.109 | 106.162 | 543.884 |
| 49 | 3.034 | 69.896 | 14.307 | 6.213 | 28.583 | 2.445 | 1.540 | 14.256 | 2.452 | 0.01730 | 1.532 | 9.631 | 394.191 | 102.916 | 105.951 | 545.704 |
| 50 | 3.015 | 69.395 | 14.410 | 6.240 | 28.528 | 2.432 | 1.555 | 14.359 | 2.439 | 0.01768 | 1.548 | 11.580 | 405.772 | 102.685 | 105.700 | 547.576 |
| Depth Step, Δy (ft) | | -0.0461 | | | | | | | | | | | | | | |
| Step n | y (ft) | A (sq.ft) | V (fps) | E (ft) | P _w (ft) | R (ft) | Fr | Avg. V (fps) | Avg. R (ft) | Avg. Sf (ft/ft) | Avg. Fr | Δx (ft) | x (ft) | z (ft) | y+z (ft) | M (cu.ft) |
| 0 | 7.416 | 203.324 | 4.918 | 7.792 | 40.976 | 4.962 | 0.359 | - | - | - | - | - | 500.000 | 100.800 | 108.216 | 838.703 |
| 1 | 7.370 | 201.719 | 4.957 | 7.752 | 40.846 | 4.939 | 0.363 | 4.938 | 4.950 | 0.00081 | 0.361 | -2.092 | 497.908 | 100.842 | 108.212 | 830.574 |
| 2 | 7.324 | 200.118 | 4.997 | 7.712 | 40.715 | 4.915 | 0.366 | 4.977 | 4.927 | 0.00083 | 0.364 | -2.087 | 495.821 | 100.884 | 108.207 | 822.535 |
| 3 | 7.278 | 198.521 | 5.037 | 7.672 | 40.585 | 4.892 | 0.370 | 5.017 | 4.903 | 0.00085 | 0.368 | -2.082 | 493.738 | 100.925 | 108.203 | 814.587 |
| 4 | 7.232 | 196.929 | 5.078 | 7.632 | 40.454 | 4.868 | 0.374 | 5.058 | 4.880 | 0.00087 | 0.372 | -2.077 | 491.661 | 100.967 | 108.198 | 806.729 |
| ... | ... | ... | ... | ... | ... | ... | ... | ... | ... | ... | ... | ... | ... | ... | ... | |
| 47 | 5.248 | 132.490 | 7.548 | 6.132 | 34.843 | 3.803 | 0.638 | 7.508 | 3.816 | 0.00266 | 0.634 | -1.593 | 410.403 | 102.592 | 107.840 | 557.946 |
| 48 | 5.201 | 131.085 | 7.629 | 6.105 | 34.712 | 3.776 | 0.647 | 7.588 | 3.789 | 0.00274 | 0.643 | -1.569 | 408.834 | 102.623 | 107.825 | 554.378 |
| 49 | 5.155 | 129.685 | 7.711 | 6.079 | 34.582 | 3.750 | 0.657 | 7.670 | 3.763 | 0.00283 | 0.652 | -1.544 | 407.290 | 102.654 | 107.810 | 550.921 |
| 50 | 5.109 | 128.288 | 7.795 | 6.053 | 34.451 | 3.724 | 0.667 | 7.753 | 3.737 | 0.00292 | 0.662 | -1.518 | 405.772 | 102.685 | 107.794 | 547.576 |

Table 5.5: Depth Step Method Results for M2 Profile from Station 0 to 300

| Depth Step, Δy (ft) 0.0252 | | | | | | | | | | | | | | | | |
|------------------------------------|--------|-----------|---------|--------|---------------------|--------|-------|--------------|-------------|-----------------|---------|-----------------|---------|---------|----------|-----------|
| Step n | y (ft) | A (sq.ft) | V (fps) | E (ft) | P _w (ft) | R (ft) | Fr | Avg. V (fps) | Avg. R (ft) | Avg. Sf (ft/ft) | Avg. Fr | Δx (ft) | x (ft) | z (ft) | y+z (ft) | M (cu.ft) |
| 0 | 3.979 | 95.399 | 10.482 | 5.685 | 31.253 | 3.052 | 1.000 | - | - | - | - | - | 300.000 | 104.800 | 108.779 | 504.815 |
| 1 | 4.004 | 96.104 | 10.405 | 5.685 | 31.324 | 3.068 | 0.990 | 10.444 | 3.060 | 0.00691 | 0.995 | -0.052 | 299.948 | 104.800 | 108.804 | 504.839 |
| 2 | 4.029 | 96.811 | 10.329 | 5.686 | 31.396 | 3.084 | 0.980 | 10.367 | 3.076 | 0.00676 | 0.985 | -0.158 | 299.790 | 104.800 | 108.829 | 504.912 |
| 3 | 4.054 | 97.518 | 10.254 | 5.687 | 31.467 | 3.099 | 0.970 | 10.292 | 3.091 | 0.00662 | 0.975 | -0.268 | 299.522 | 104.801 | 108.855 | 505.032 |
| 4 | 4.079 | 98.227 | 10.180 | 5.689 | 31.538 | 3.115 | 0.961 | 10.217 | 3.107 | 0.00648 | 0.965 | -0.382 | 299.139 | 104.802 | 108.881 | 505.200 |
| ... | ... | ... | ... | ... | ... | ... | ... | ... | ... | ... | ... | ... | ... | ... | ... | |
| 47 | 5.163 | 129.913 | 7.697 | 6.083 | 34.603 | 3.754 | 0.655 | 7.720 | 3.747 | 0.00288 | 0.658 | -16.184 | 55.866 | 105.288 | 110.451 | 551.478 |
| 48 | 5.188 | 130.678 | 7.652 | 6.097 | 34.674 | 3.769 | 0.650 | 7.675 | 3.762 | 0.00283 | 0.653 | -17.326 | 38.540 | 105.323 | 110.511 | 553.362 |
| 49 | 5.213 | 131.444 | 7.608 | 6.112 | 34.745 | 3.783 | 0.645 | 7.630 | 3.776 | 0.00279 | 0.648 | -18.579 | 19.961 | 105.360 | 110.573 | 555.280 |
| 50 | 5.238 | 132.211 | 7.564 | 6.127 | 34.817 | 3.797 | 0.640 | 7.586 | 3.790 | 0.00274 | 0.643 | -19.961 | 0.000 | 105.400 | 110.638 | 557.230 |

5.3 Direct Step Method Results

The profile characteristics found through the channel from upstream to downstream were M2, S2, the occurrence of a hydraulic jump at a horizontal station of 405.77 ft, S1, and then M1. Since each step involved averaging properties between horizontal locations, the large number of depth steps used in calculating each profile was to ensure the greatest and most reasonable accuracy for this method. An even greater number of steps could have been used, but this would not have had any significant impact on the results.

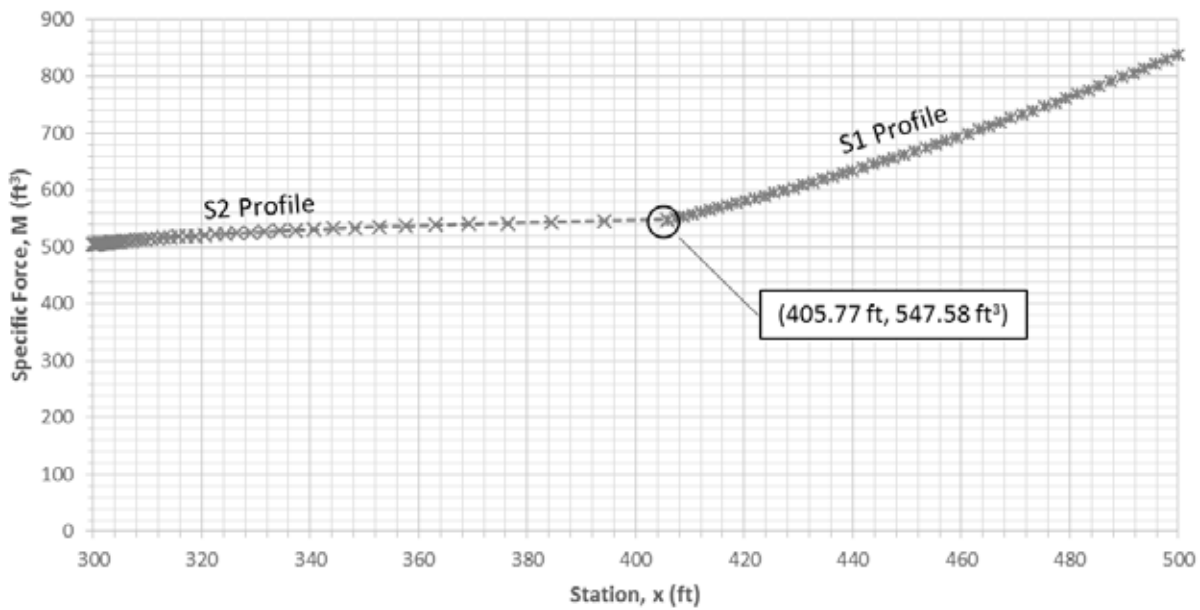


Figure 5.3: Locating Hydraulic Jump on the Hydraulically Steep Section

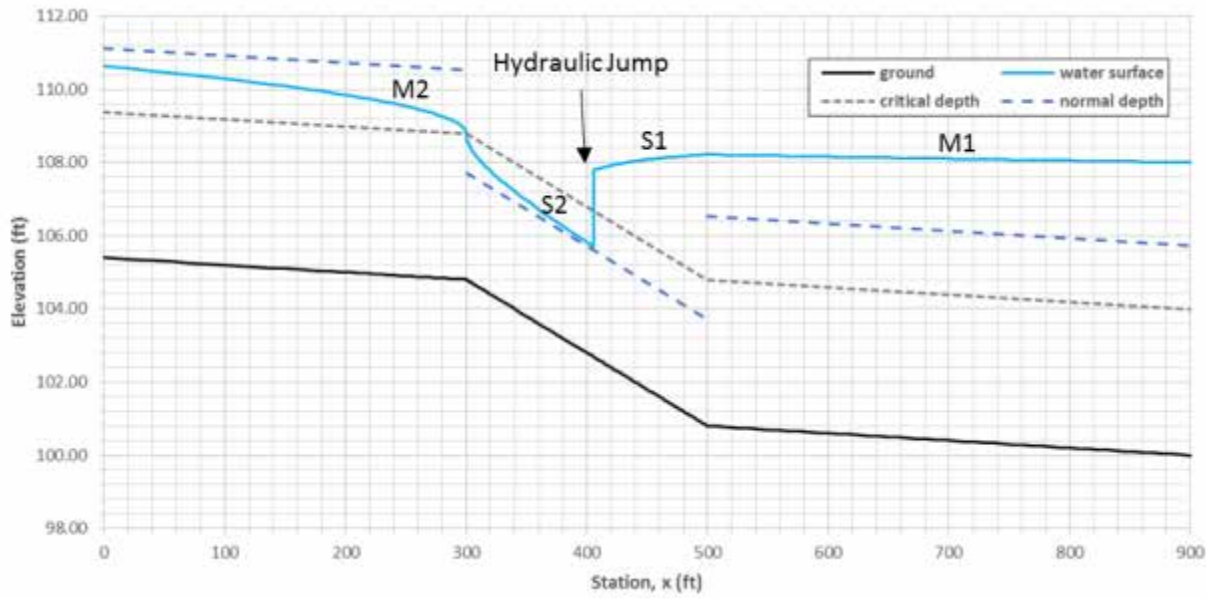


Figure 5.4: Composite Water Surface Profile from the Depth Step Method

5.4 Equations Used for Depth Step Method

$$A = y(b + my) \quad \text{Equation 5.1}$$

$$V = Q/A \quad \text{Equation 5.2}$$

$$E = y + \frac{Q^2}{2gA^2} \quad \text{Equation 5.3}$$

$$P = b + 2y\sqrt{1 + m^2} \quad \text{Equation 5.4}$$

$$R = A/P \quad \text{Equation 5.5}$$

$$Fr = \frac{V}{\sqrt{gD}} = \frac{V}{\sqrt{g\frac{A}{T}}} = \frac{V}{\sqrt{g \frac{A}{b + 2my}}} \quad \text{Equation 5.6}$$

$$\bar{V} = \frac{V_n + V_{n+1}}{2} \quad \text{Equation 5.7}$$

$$\bar{R} = \frac{R_n + R_{n+1}}{2} \quad \text{Equation 5.8}$$

$$\bar{S_f} = \left(\frac{\bar{V} \cdot n}{c \cdot \bar{R}^{2/3}} \right) \quad \text{Equation 5.9}$$

$$\bar{Fr} = \frac{Fr_n + Fr_{n+1}}{2} \quad \text{Equation 5.10}$$

$$\Delta x = \frac{\Delta E}{S_o - \bar{S_f}} \quad \text{Equation 5.11}$$

$$x_{n+1} = x_n + \Delta x \quad \text{Equation 5.12}$$

$$z_{n+1} = z_n + \Delta x \cdot S_o \quad \text{Equation 5.13}$$

$$M = \frac{Q^2}{gA} + A\bar{y} \rightarrow M_{TRAP.} = \frac{Q^2}{gy(b + my)} + \frac{by^2}{2} + \frac{my^3}{3} \quad \text{Equation 5.14}$$

5.5 SRH-2D Hydraulic Jump Test Terrain Setup and Determining Results for Comparison

One major capability of SRH-2D is that “all flow regimes, i.e., subcritical, transcritical, and supercritical flows, may be simulated simultaneously without the need for special treatments” (Lai, 2008). So, locating the hydraulic jump should be as straightforward as inputting the channel geometry, roughness, and appropriate boundary conditions, and then running the simulation for an appropriate length of time in order to reach steady state conditions. The files used to define the site in SMS 12.1 were prepared in ArcMap 10.2. The elevations for the channel were defined by scatter points arranged in a 1×1 -ft grid pattern. These scatter points were calculated in Excel, imported into ArcMap, and then converted into a shapefile. This shapefile was used to generate a DEM raster (not used with the SRH-2D, but used with HEC-

RAS 2D) as well as a text file with XYZ data for easy importation into SMS. The scatter points were used to define an area slightly larger than the Manning's n coverage that would become the extent of the model space. This was done to ensure SMS would not extrapolate elevations at the outermost limits of the mesh. The dimensions of the coverage were selected as 900 ft by 48 ft to include the entire length of the channel and to accommodate the maximum top width of the water surface, 36 ft, located at the downstream lake. The dimensions were also chosen to gain some additional space in case of unforeseen differences in the 2D model without being unnecessarily large.



Figure 5.5: Raster and Lines Denoting Channel Slope Changes

In order to locate the hydraulic jump using SRH-2D, three different meshes were created, each composed of perfectly square elements. The second two meshes each possessed smaller elements than the preceding one. First, 4-ft elements were used, then 2-ft, and then 1-ft. Images of these meshes, along with the hydraulic jumps from each simulation, are shown in Figures 5.6, 5.7, and 5.8.

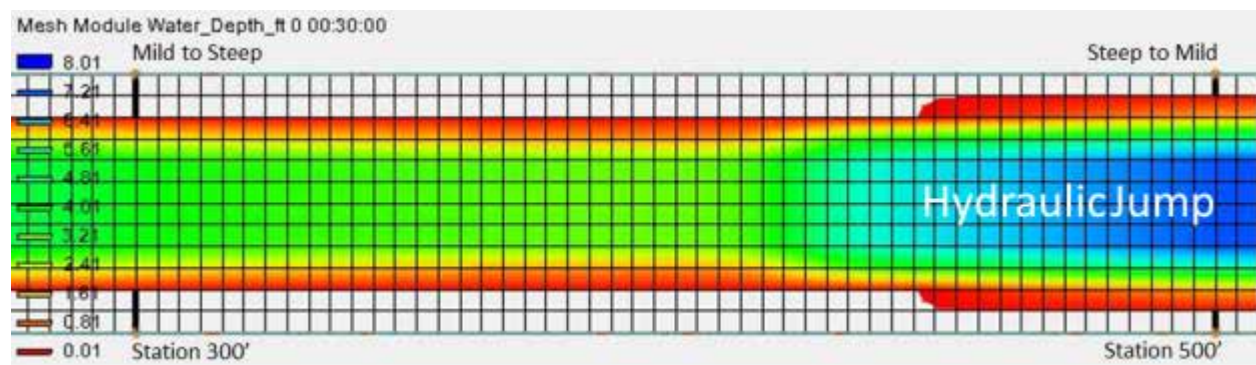


Figure 5.6: Plan View in SMS 12.1 with Color Fill Contours of SRH-2D Hydraulic Jump Trial Results Using Square 4-Foot Elements

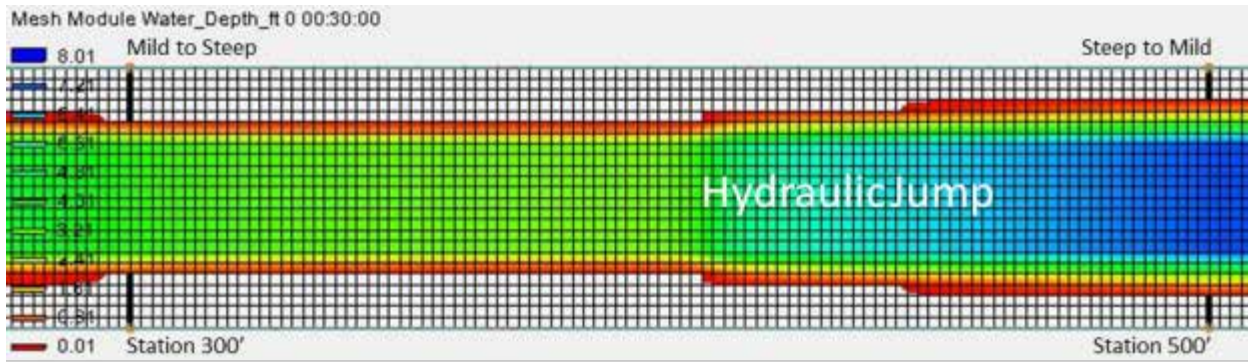


Figure 5.7: Plan View in SMS 12.1 with Color Fill Contours of SRH-2D Hydraulic Jump Trial Results Using Square 2-Foot Elements

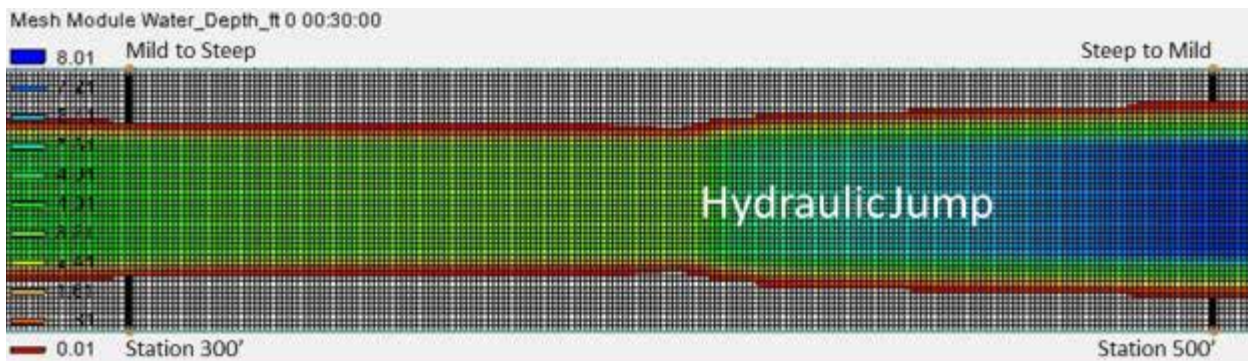


Figure 5.8: Plan View in SMS 12.1 with Color Fill Contours of SRH-2D Hydraulic Jump Trial Results Using Square 1-Foot Elements

As comparison of Figures 5.7 and 5.8 shows, each simulation placed the hydraulic jump similarly in the channel; therefore, it was deemed unnecessary to use a tighter mesh size with the necessarily smaller computational timestep. The model that employed the mesh with 4-ft square elements simulated 1 full hour of flow. From this run, it was determined that the model reached steady state conditions long before the full hour had elapsed. For the models that used the 2-ft and the 1-ft mesh elements, the simulated time span was half an hour; further inspection of the results determined that 10 minutes would have been adequate. Results from the simulation using the 1-ft mesh elements were used for comparisons between methods.

5.6 SRH-2D Hydraulic Jump Test Results from Simulation with Square 1-Foot Elements

Figure 5.9 shows the final steady state output from this simulation. This information was extracted from SMS using the Plot Wizard display tool to graph the results for an Observation

Profile drawn along the channel's centerline. The data was then taken from the plot by right-clicking it, selecting “view values,” and then copying and pasting these values into an Excel spreadsheet.

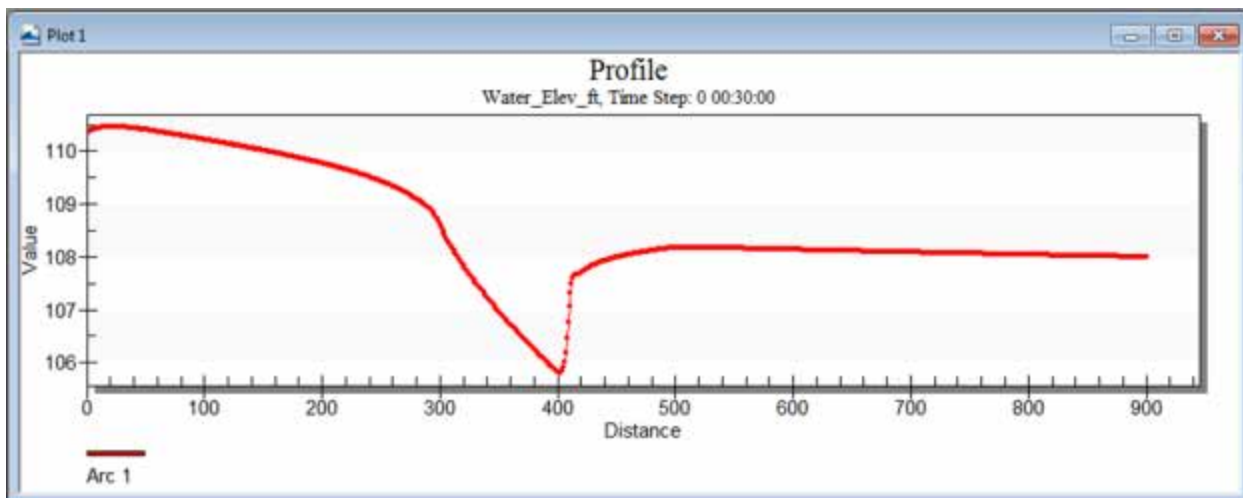


Figure 5.9: SMS 12.1 Output for Centerline Water Surface Elevation Data from Hydraulic Jump Test with 1-Foot Square Mesh Elements

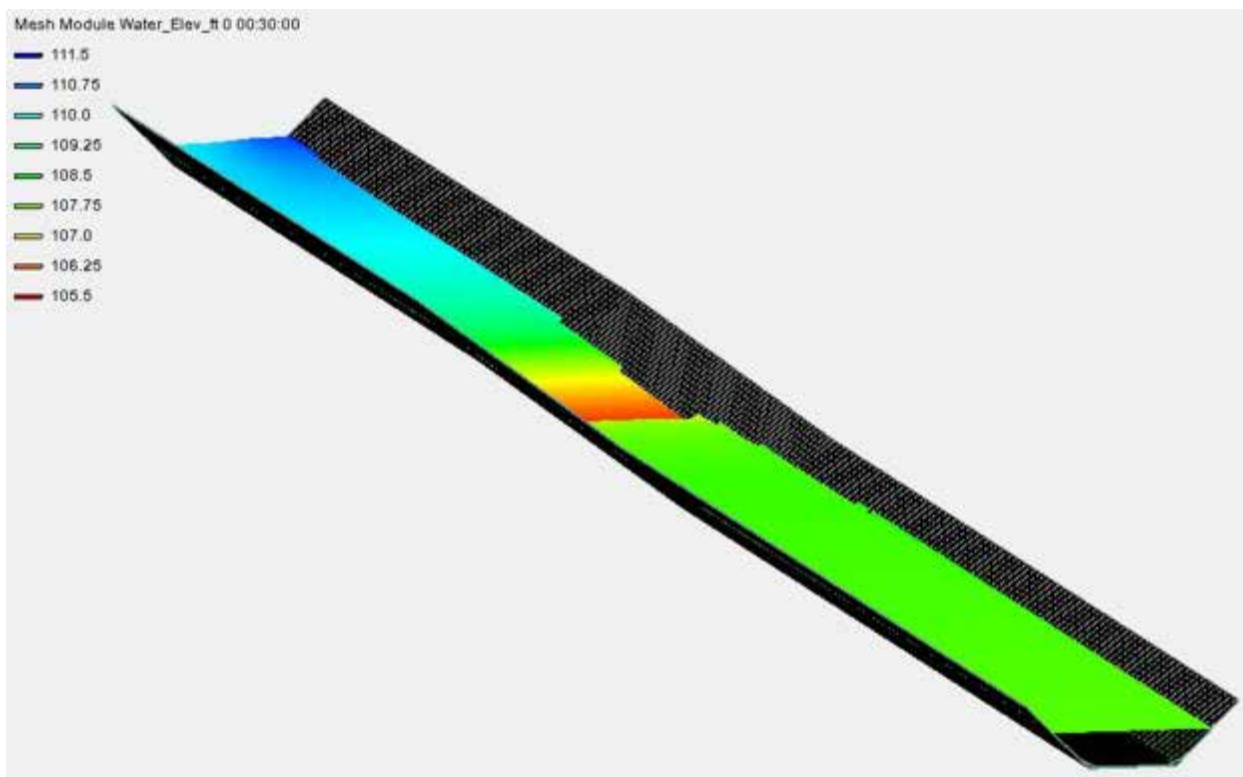


Figure 5.10: Oblique View of Simulation Output without Exaggerated Z-Scale

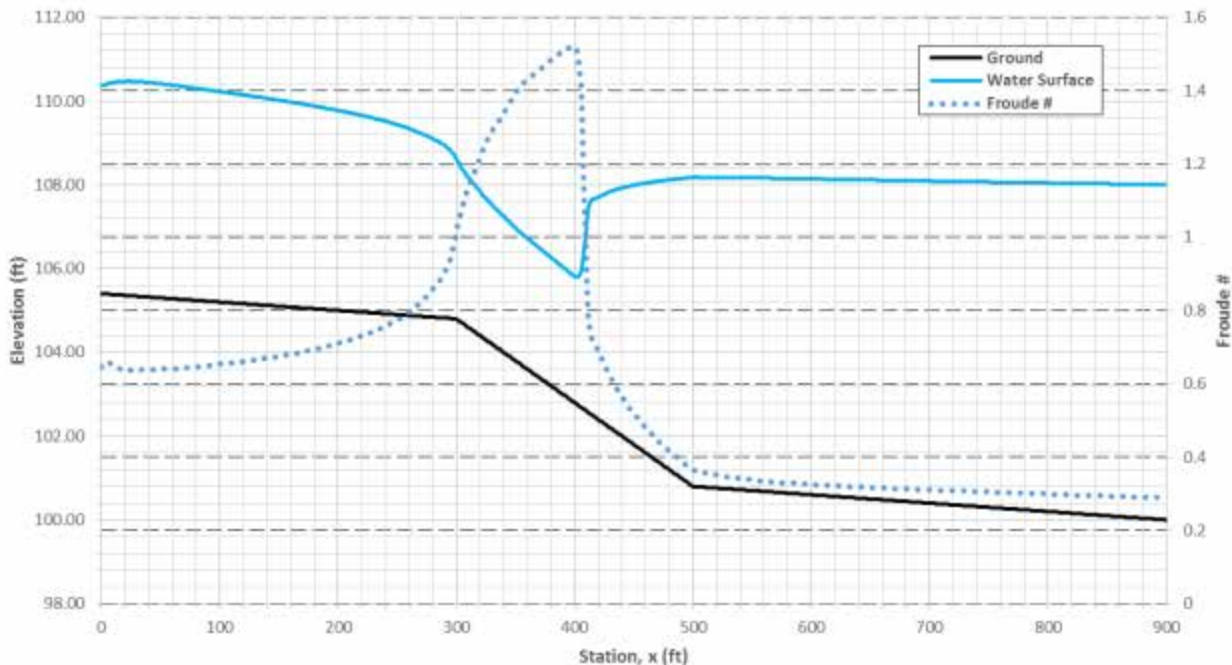


Figure 5.11: Complete Water Surface Profile along Channel Centerline for SRH-2D Hydraulic Jump Test

Figure 5.11 clearly shows that the hydraulic jump occurs in roughly the same location as calculated using the step method, at Station 405.77. The result of the 2D model also shows the hydraulic jump occurring over some horizontal distance, unlike the result of the step method, which places the jump at a single location. While the 2D result is more physically realistic, it creates difficulty for comparing methods and for determining a specific station where the hydraulic jump occurs. However, if the definition of a hydraulic jump as an abrupt transition from supercritical to subcritical flow is strictly applied, then the position where this change occurs is between Stations 409.00 and 410.00 with Froude numbers of 1.004 and 0.895 respectively. This does not seem satisfactory, however, as the maximum Froude number found along the channel centerline occurs at Station 399.00 and has a value of 1.520, and the Froude number at Station 417.00, where the rollers on the surface of the hydraulic jump have dissipated and something resembling the typical S1 type curve begins, has a value of 0.708. Thus, the jump could be said to occur over a horizontal distance of 18 ft, which, relative to the 200-ft length of the steep section, may be deemed “abrupt.” It is worth noting that the two stations, Stations

399.00 and 417.00, do properly bracket the hydraulic jump's location as predicted using the Direct Step Method.

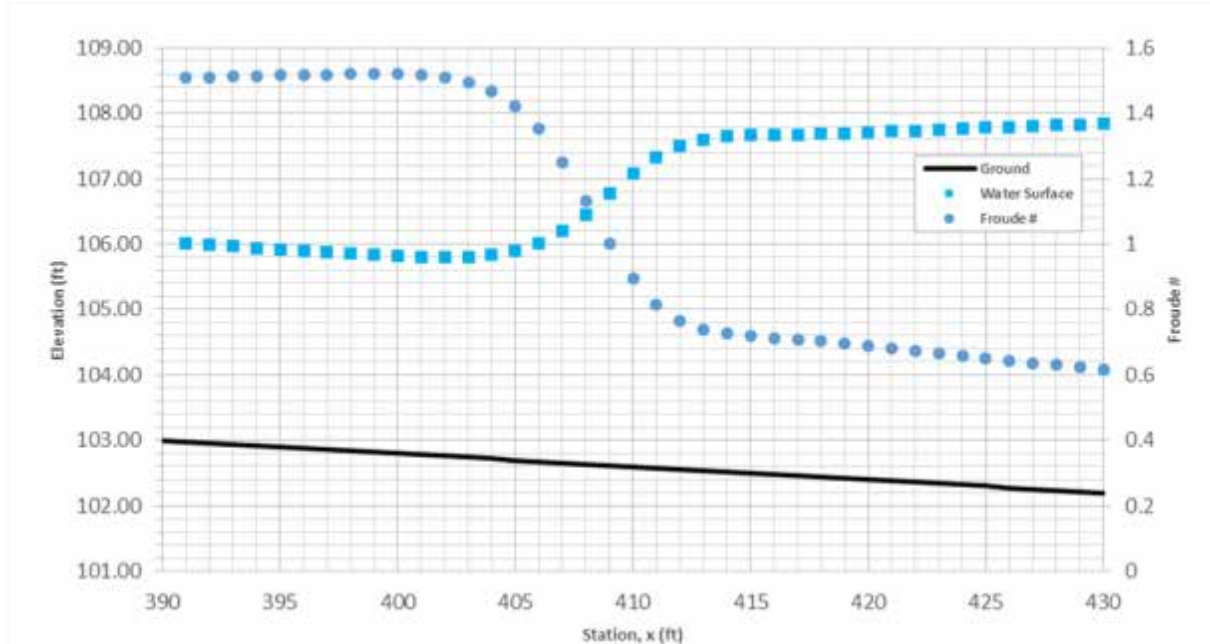


Figure 5.12: Data from Figure 5.11 near the Location of the Hydraulic Jump

An approximate length for the hydraulic jump, then, is 18 ft. To assess this value, the eminent resource *Open-Channel Hydraulics* (Chow, 1959) was consulted. Chapter 15, “Hydraulic Jump and Its Use as an Energy Dissipater,” contains a chart relating upstream Froude number to the ratio of the length of the hydraulic jump to the downstream depth. While this chart “was developed primarily for jumps occurring in rectangular channels,” the author also states, “In the absence of adequate data, this curve may also be applied approximately to jumps formed in trapezoidal channels.” Since the horizontal to vertical side slope of this test reach is relatively steep (1:1), application of the curve was considered appropriate. After the maximum Froude number found upstream was rounded to 1.5 for simplicity’s sake, and after the chart mentioned above was entered, the curve yielded a value of approximately 3.75 for the ratio of the hydraulic jump’s length to the downstream depth. Using the depth at Station 417.00, equal to 5.214 ft, a length of 19.55 ft was calculated. Subtracting this length from Station 417.00 placed the beginning of the hydraulic jump at Station 397.45. This estimate is near Station 399.00,

previously suggested as the initial station of the hydraulic jump. It seems reasonable that for a trapezoidal channel, the hydraulic jump could occur over a shorter distance than for a rectangular one, since in the case of the trapezoidal channel, the flow can move up the side slopes to match the downstream depth. Another source of discrepancy may be precision errors in rounding or reading the chart, or resulting from the fact that the chart in Chow was also intended for horizontal channels, while this channel was sloped. However, over a horizontal distance of 18 ft (the first estimate for the hydraulic jump's length) the drop in bed elevation for this steep section is 0.36 ft and thus probably not an enormous source of error. It is not negligible, however, considering the depths involved (3.016 ft at Station 399.00 and 5.214 ft at Station 417.00).

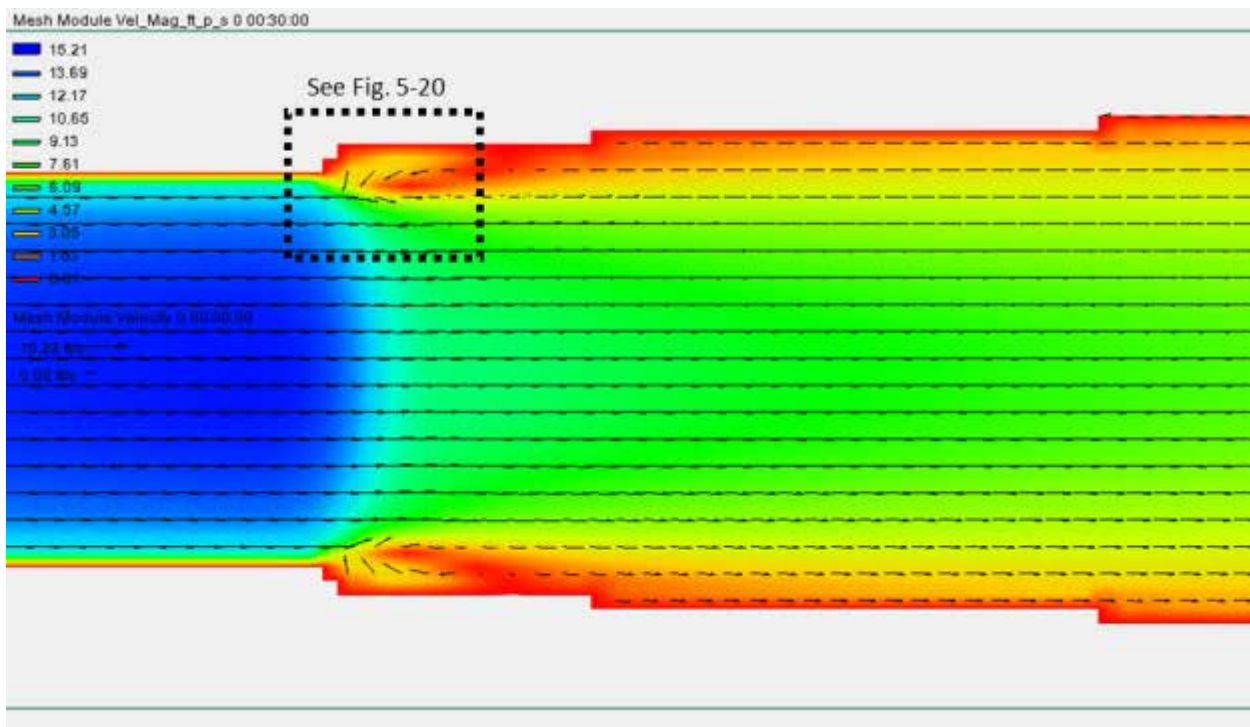


Figure 5.13: Velocity Details near Hydraulic Jump from SRH-2D Viewed in SMS

Furthermore, discrepancies arise from the fact that a hydraulic jump in a trapezoidal channel is simply not a 1D problem. As Figure 5.13 shows, the velocity is far from uniform for any given cross section perpendicular to the channel centerline. This, and the fact that the depth varies across the cross section, means that the Froude number varies laterally. So, a single cross section may be at once super- and subcritical simultaneously (Figure 5.15). Also, there is some

recirculating flow on this trapezoidal channel's side slopes that is actually traveling upstream. Clearly, a hydraulic jump in a trapezoidal channel is at least a 2D problem. Even more accurately, though, it is a 3D problem. This is due to the recirculating flow that exists on the surface of a hydraulic jump known as *rollers*. While these rollers cannot be directly modeled by SRH-2D, it is unknown if the program makes an attempt to account for them. Despite all of this, as Figure 5.16 shows, the water surface profiles from the direct step method spreadsheet and that from the channel centerline for the SRH-2D simulation closely resemble one another.

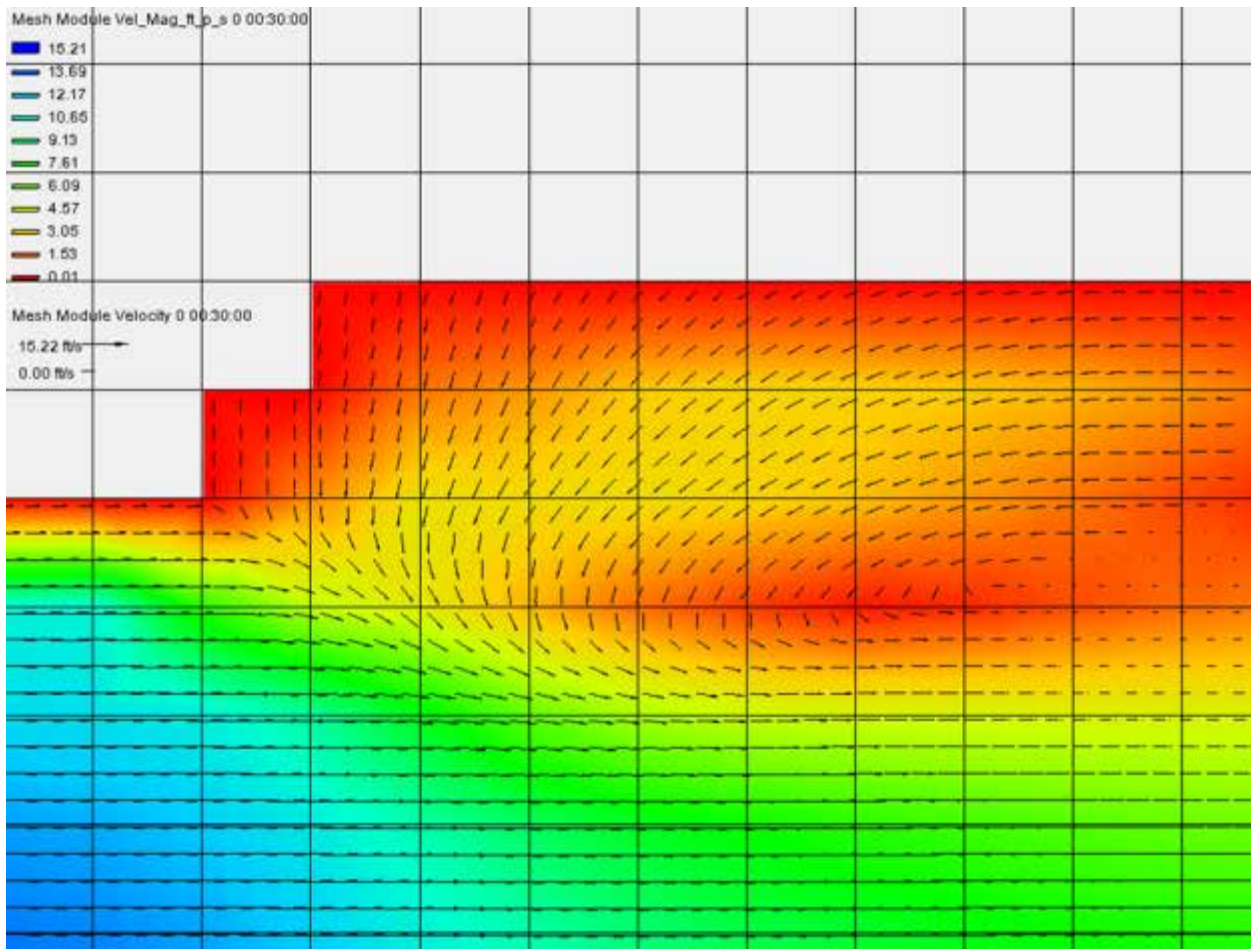


Figure 5.14: Close-Up of Recirculating Flow Where Extents Are Defined in Figure 5.13

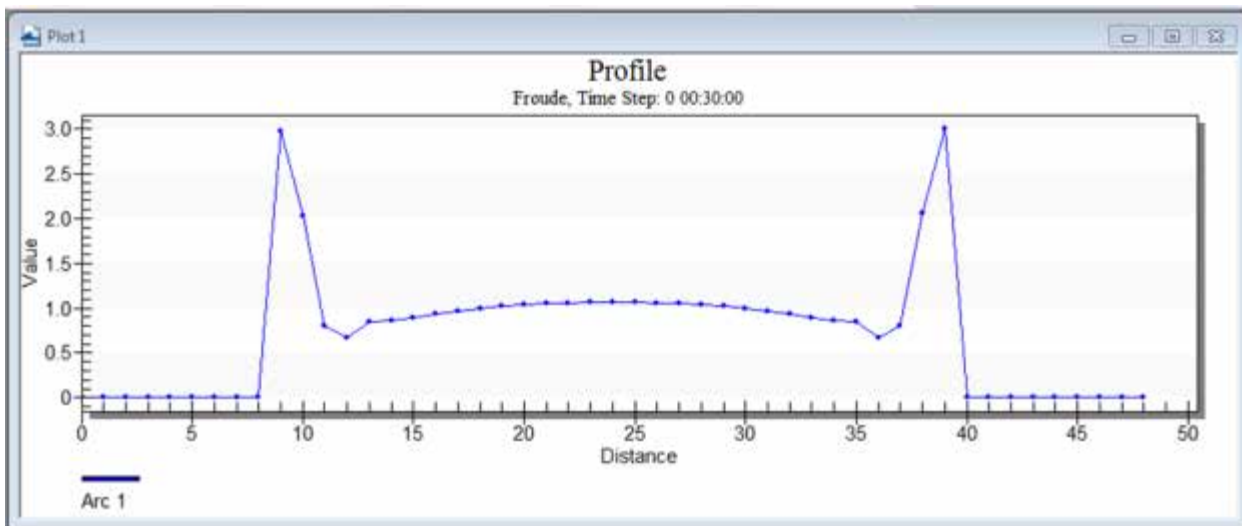


Figure 5.15: Froude Number Data across Cross Section at Station 408.50

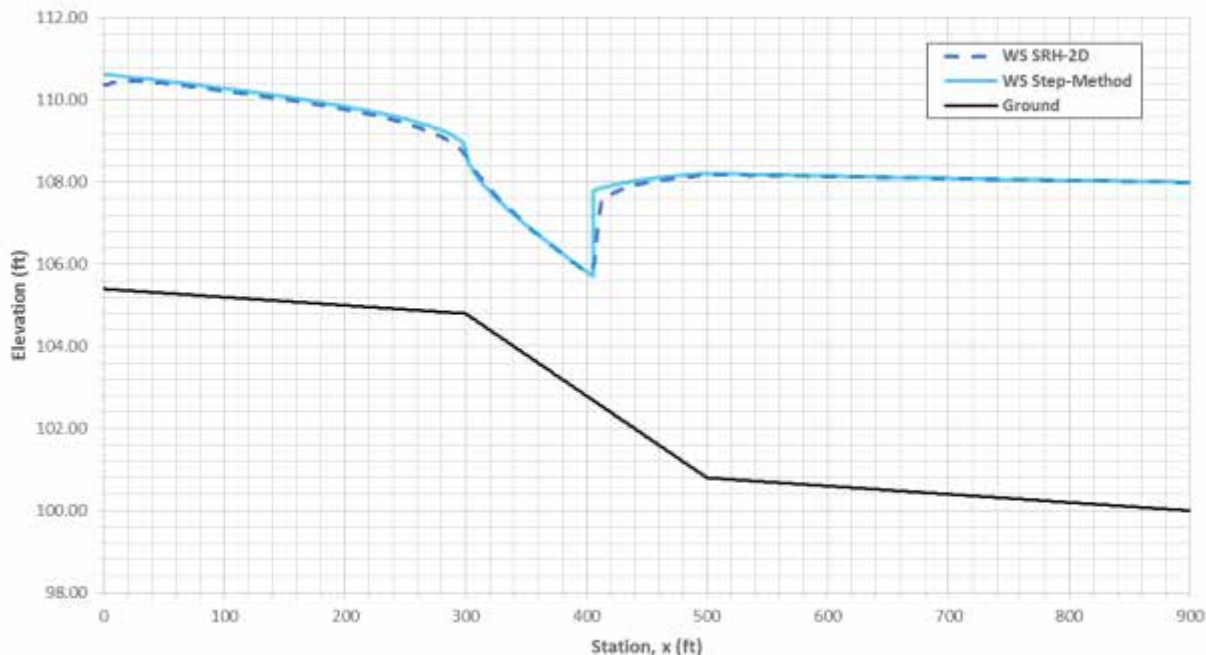


Figure 5.16: Gradually Varied Flow Profiles for Hydraulic Jump Test Reach from Step Method and SRH-2D

One interesting detail noticeable in Figure 5.16 is that the depth of flow at the transition from mild to steep, located at Station 300, predicted by SRH-2D is below that calculated within the spreadsheet following standard hydraulic engineering assumptions. It is ordinary practice to assume critical depth exists right at the station where such a slope transition occurs, although in

reality this is generally not true. Chapter 6 of Henderson (1966), “Channel Controls,” contains a discussion of the free overfall. At this location, Henderson states, for subcritical flow travelling off the brink, the critical section will be upstream from the drop-off point by a distance equal to about 3 to 4 times the critical depth, and downstream of that point the pressure within the flow is not hydrostatic. Further, if a mild slope transitions into a very steep slope, “the flow would have some of the character of flow over an overfall—in which...the critical section retreats upstream to some ill-defined location.” To determine whether this was indeed the case, Figure 5.17 was created using the output of the simulation.

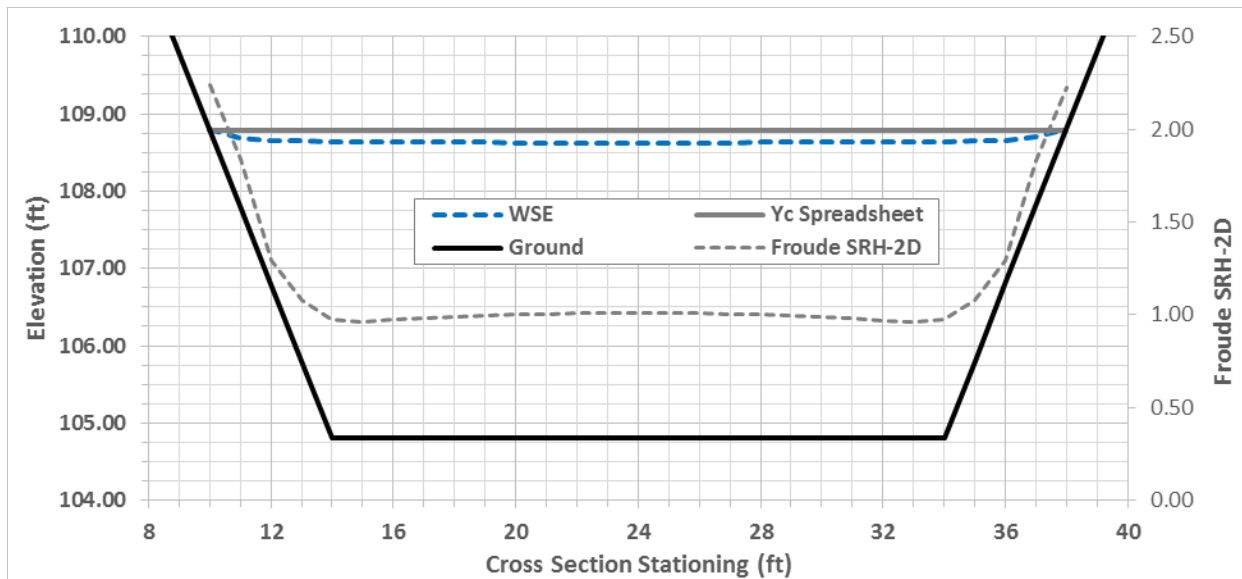


Figure 5.17: Detailed Summary of Cross Section at Station 300

At the cross section at Station 300, all types of flow exist—subcritical, critical, and supercritical. On both side slopes, all flow is supercritical, but within the central part of the channel things are more complex. The flow near the center of the channel is very slightly supercritical, while within several feet on each side of the supercritical flow is critical flow. Between the side slopes and this critical flow, very slightly subcritical conditions exist. Table 5.6 concisely displays this information.

Table 5.6: SRH-2D Froude Numbers at Station 300 for Hydraulic Jump Test

| XS Station | 10 | 11 | 12 | 13 | 14 | 15 | 16 | 17 | 18 | 19 | 20 | 21 | 22 | 23 | 24 |
|------------|-------|-------|-------|-------|-------|-------|-------|-------|-------|-------|-------|-------|-------|-------|-------|
| Froude # | 2.236 | 1.836 | 1.295 | 1.078 | 0.977 | 0.960 | 0.972 | 0.982 | 0.990 | 0.997 | 1.002 | 1.006 | 1.008 | 1.010 | 1.011 |
| XS Station | 25 | 26 | 27 | 28 | 29 | 30 | 31 | 32 | 33 | 34 | 35 | 36 | 37 | 38 | |
| Froude # | 1.010 | 1.008 | 1.006 | 1.002 | 0.997 | 0.990 | 0.982 | 0.972 | 0.959 | 0.976 | 1.077 | 1.293 | 1.831 | 2.228 | |

In light of Table 5.6, it is possible to say that something resembling the conditions which exist at a free overfall are present in the SRH-2D results. However, the extent to which SRH-2D could model this phenomenon is not known. If the channel were to transition from a mild to a very extreme steep slope, the drawdown that occurs upstream of the break in grade would involve a non-negligible vertical velocity component, thus turning the problem into a 3D one.

5.7 One-Dimensional HEC-RAS Hydraulic Jump Test

In order to determine depths at various cross sections, HEC-RAS employs a form of the step method that differs from the one used above. Rather than specifying the change in depth and directly calculating a station, HEC-RAS begins with a known station and must determine the change in depth. Since head losses due to friction depend on several factors, depth chief among them, and because in order to apply the step method the friction slope must be averaged between cross sections, the solution to this form of the step method requires an implicit solution, whereas the form of the step method used in Section 5.2 can be solved explicitly (see Henderson, 1966, 5.4, “Step Method – Depth Calculated from Distance” for an in-depth discussion).

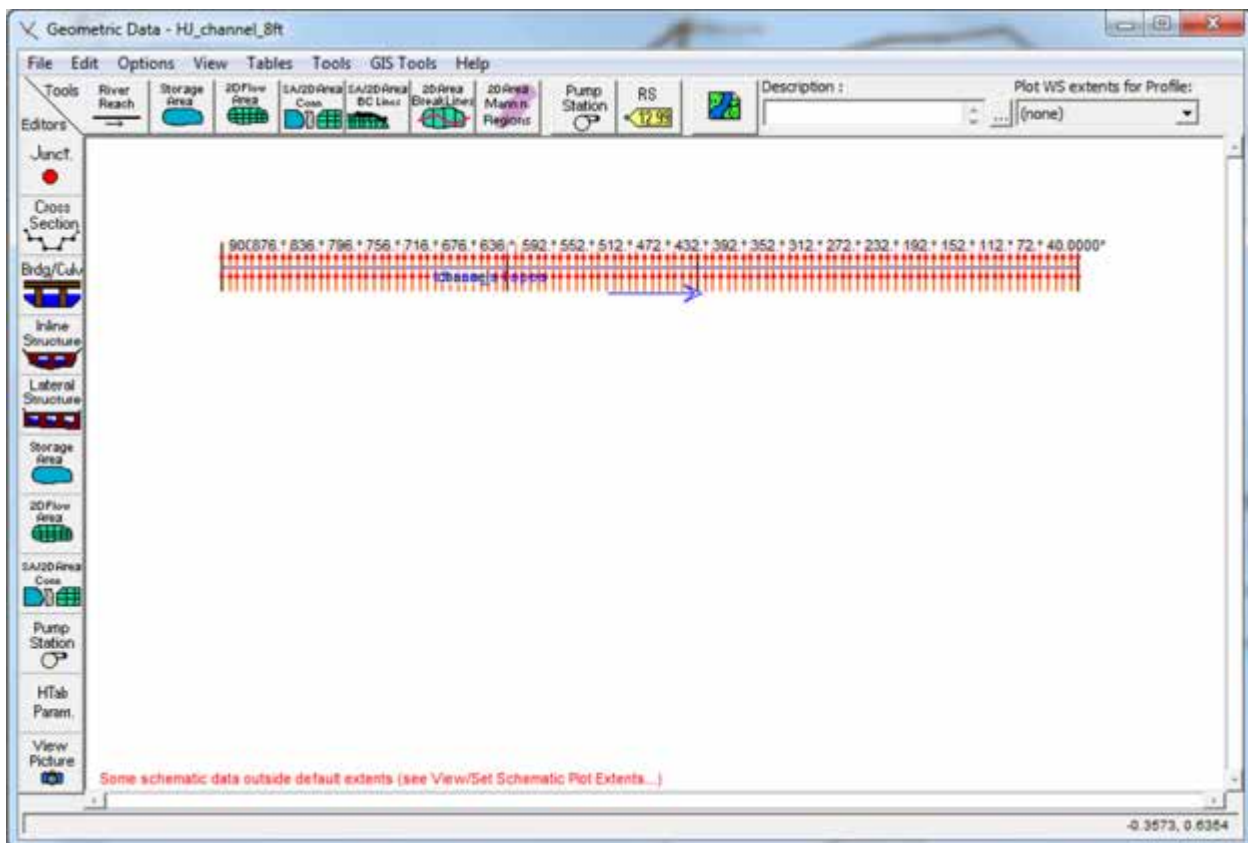


Figure 5.18: Graphical Representation of HEC-RAS 5.0 1D Cross Sections for Hydraulic Jump Test at 8-Foot Spacing

For the 1D HEC-RAS model shown in Figure 5.18, the primary cross sections were created at four stations: the upstream lake, the downstream lake, and at each break in grade. All other cross sections were generated using the Cross Section Interpolation tool within HEC-RAS. The interpolated cross sections are those labeled with an asterisk in Figure 5.18. Generating these interpolated cross sections brought the total number of cross sections to 114, as opposed to the 203 locations used for the depth step method above.

The upstream and downstream boundary conditions for the 1D HEC-RAS model were both set to “known water surface elevations”—108.00 feet for the lower lake, and 110.64 feet for the upper lake. The value for the top lake was obtained from the GVF profile in the Depth Step Method spreadsheet. The flow for the profile was set to 1000 cfs at Station 900. In order for HEC-RAS to calculate a hydraulic jump in 1D, the option for a “Mixed” flow regime must be selected before running the steady simulation. Typically, for floodplain mapping the flow regime

is left as “Subcritical” to force the results to have the greatest depths, and thus for the floodplain to be as large as possible. This is considered to be conservative. Also, realistically, in most natural channels subcritical flow is by far the most common. Figures 5.19 and 5.20 show the results of a subcritical run, the menu containing the option for changing the flow regime, and the results of a mixed run.

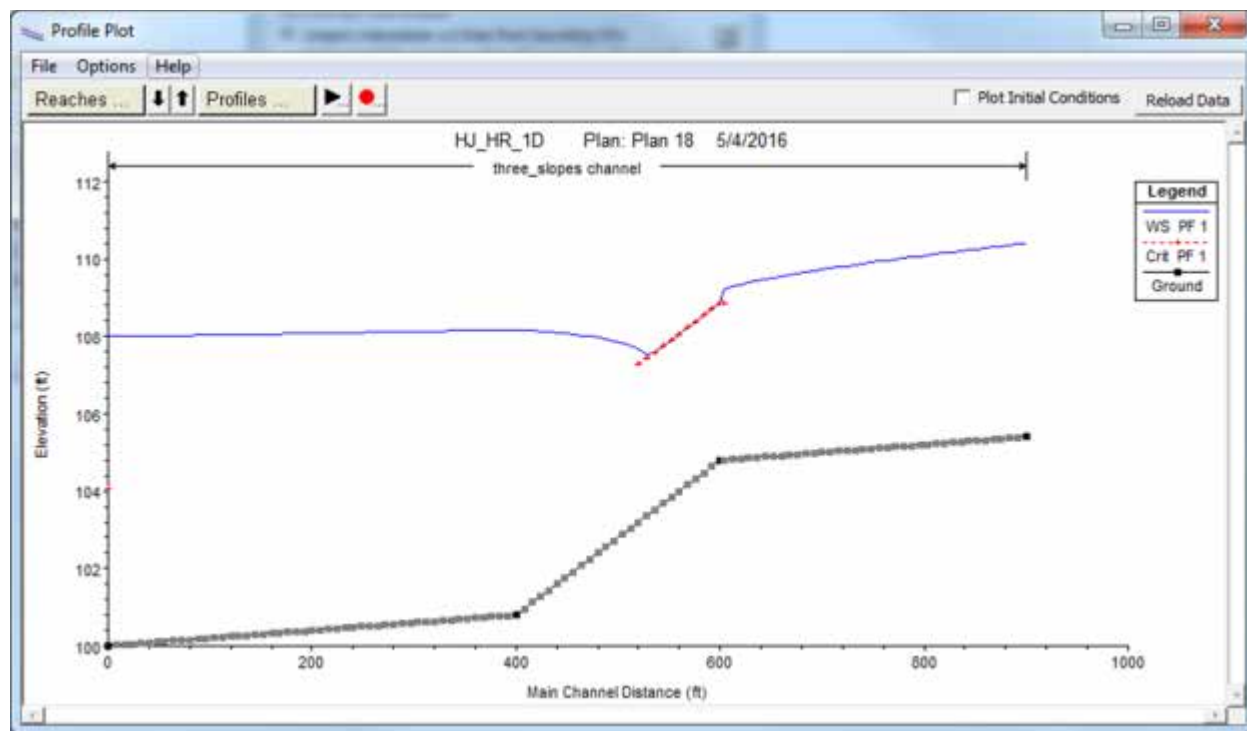


Figure 5.19: Poor Results of Hydraulic Jump Test for 1D HEC-RAS Simulation Using Subcritical Flow Regime Option

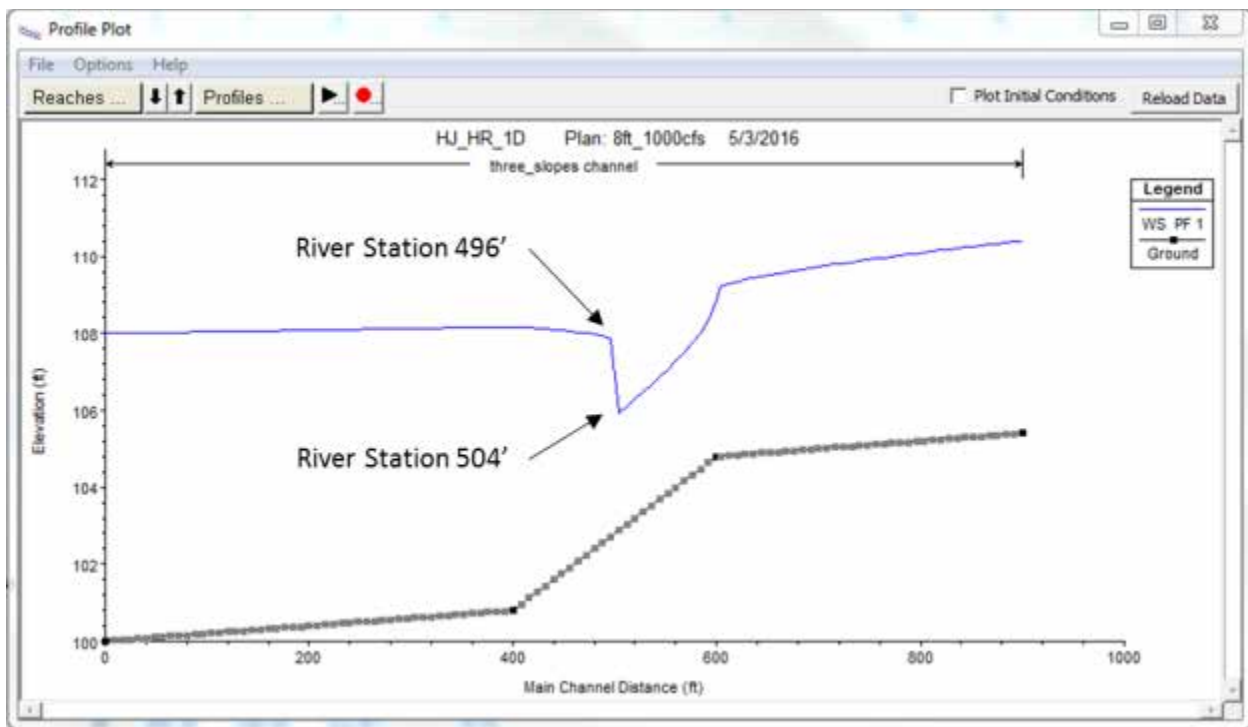


Figure 5.20: Initial HEC-RAS 1D Simulation to Locate Hydraulic Jump Using 8-Foot Spacing for Cross Sections

The results of the first test, shown in Figure 5.20, appear to capture the correct location of the hydraulic jump. Note that the stationing in the HEC-RAS profile plots is reversed from spreadsheets, SRH-2D simulations, and the direction generally presented throughout this report. This is due to the HEC-RAS convention of displaying flows from right to left, with cross sections increasing from downstream to upstream. Thus this profile plot is backwards from the cross section display in Figure 5.18, but River Stations 496 and 504 correspond with spreadsheet and SRH-2D Stations 404 and 396, respectively (subsequent profile plots were adjusted in Excel to resemble other plots with flow from left to right). Thus, HEC-RAS 1D determined that a hydraulic jump should occur between those two stations. This estimate was close to the value of 405.77 ft obtained from the spreadsheet, and partially falls within the range of 399.00 ft to 417.00 ft for the hydraulic jump obtained from SRH-2D. The HEC-RAS estimate, however, is upstream of the value from the spreadsheet. Originally, it was expected that the hydraulic jump would occur between Stations 404 and 412, properly bracketing the solution obtained from the spreadsheet. It was assumed that reducing the spacing of the cross sections within the HEC-RAS

model would cause the similarity to the value obtained from the spreadsheet to increase; this, however, was not the case. Figure 5.21 shows the results of the subsequent test.

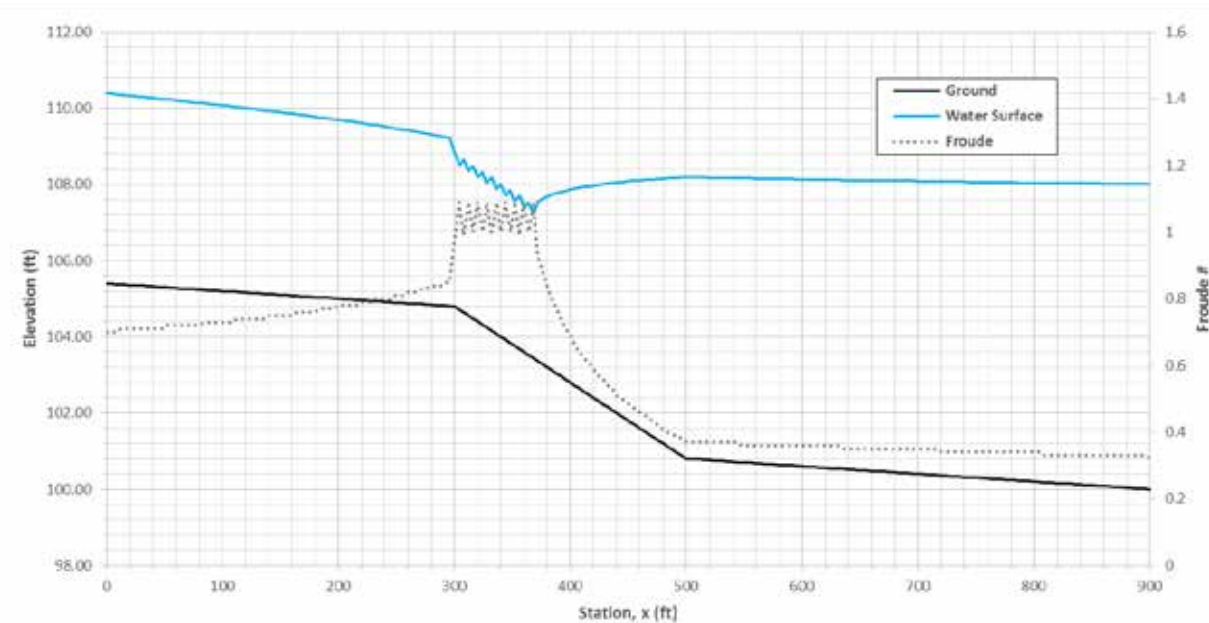


Figure 5.21: HEC-RAS 1D Simulation to Locate Hydraulic Jump Using 4-Foot Spacing for Cross Sections

Clearly, merely doubling the number of cross sections did not increase the accuracy of the results. In fact, they are quite dubious. From the first break in grade, at Station 300, until about a third of the way down the steep section, at Station 368, the depth oscillates weirdly around critical depth. From Station 372 until the end of the channel, the depth remains subcritical. The reason why these HEC-RAS simulations are behaving thus is twofold. First, the bank points are in the wrong places. The second reason has to do with expansion and contraction losses included in the Energy Equation used by HEC-RAS. The bank points were dealt with first, and an explanation of this problem follows below.

Chapter 2 explained that HEC-RAS uses Manning's equation to compute a depth from discharge that satisfies the energy equation. However, each cross section is subdivided into smaller parts and the conveyance is calculated separately for each section. In the present case, the conveyance sections for the channel include each side slope and the central part of the channel. The example given in Figure 5.22 seeks to illustrate the impact of this approach by

analyzing the channel using the HEC-RAS conveyance equations and the normal depth calculated in the depth step spreadsheet for the mild sections of this channel using the given discharge of 1000 cfs.

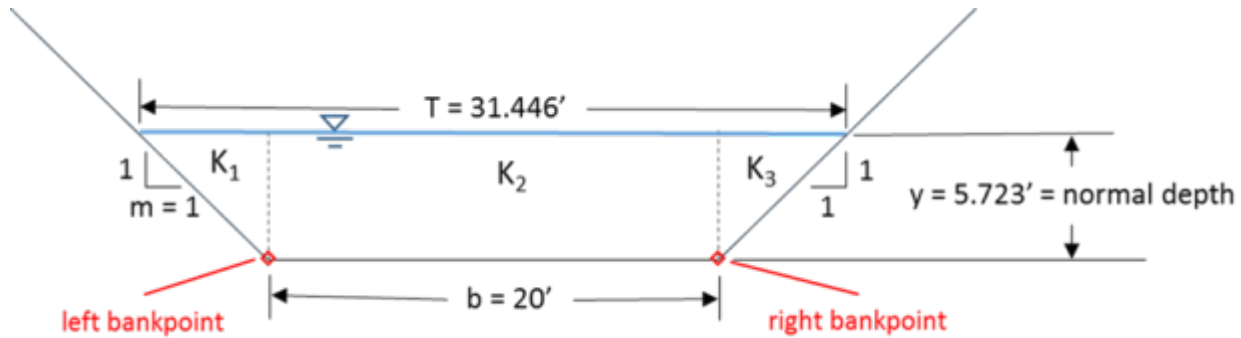


Figure 5.22: Conveyance Sections for Normal Depth on the Hydraulically Mild Portion of the Hydraulic Jump Test Reach with Incorrect Placement of Bank Points

$$Q = (K_1 + K_2 + K_3)S_f^{1/2} = \left(\frac{1.486}{n_1} \cdot \frac{A_1^{5/3}}{P_{w1}^{2/3}} + \frac{1.486}{n_2} \cdot \frac{A_2^{5/3}}{P_{w2}^{2/3}} + \frac{1.486}{n_3} \cdot \frac{A_3^{5/3}}{P_{w3}^{2/3}} \right) S_o^{1/2}$$

Equation 5.15

Where:

$n_1 = n_2 = n_3 = n$ and 1.486 (= 1.49 to match spreadsheet's value for English units)

$$\begin{aligned} &= \frac{1.49}{n} \left(\frac{A_1^{5/3}}{P_{w1}^{2/3}} + \frac{A_2^{5/3}}{P_{w2}^{2/3}} + \frac{A_3^{5/3}}{P_{w3}^{2/3}} \right) S_o^{1/2} \\ &= \frac{1.49}{n} \left(\frac{\left(\frac{1}{2} \cdot y_n^2 m\right)^{5/3}}{(y_n \sqrt{1+m^2})^{2/3}} + \frac{(b y_n)^{5/3}}{(b)^{2/3}} + \frac{\left(\frac{1}{2} \cdot y_n^2 m\right)^{5/3}}{(y_n \sqrt{1+m^2})^{2/3}} \right) \\ &= \frac{1.49}{0.025} \left(\frac{\left(\frac{1}{2} \cdot (5.72 ft)^2\right)^{5/3}}{(5.72 ft \sqrt{1+1^2})^{2/3}} + \frac{(20 ft \cdot 5.72 ft)^{5/3}}{(20 ft)^{2/3}} + \frac{\left(\frac{1}{2} \cdot (5.72 ft)^2\right)^{5/3}}{(5.72 ft \sqrt{1+1^2})^{2/3}} \right) \\ &= Q_1 + Q_2 + Q_3 = 69.8 cfs + 976 cfs + 69.8 cfs = 1116 cfs = Q. \end{aligned}$$

Equation 5.16

The analysis detailed in Figure 5.22 shows that it would take a discharge 11.6% higher than used for direct step method calculations to have the same normal depth, where the entire cross section was used as a single conveyance section. Figure 5.23 shows the cross section editor within HEC-RAS with adjusted bank points. This editor was applied to every cross section: the interpolated cross sections were deleted, the bank points for the four primary cross sections were manually fixed, and the cross sections were then re-interpolated.

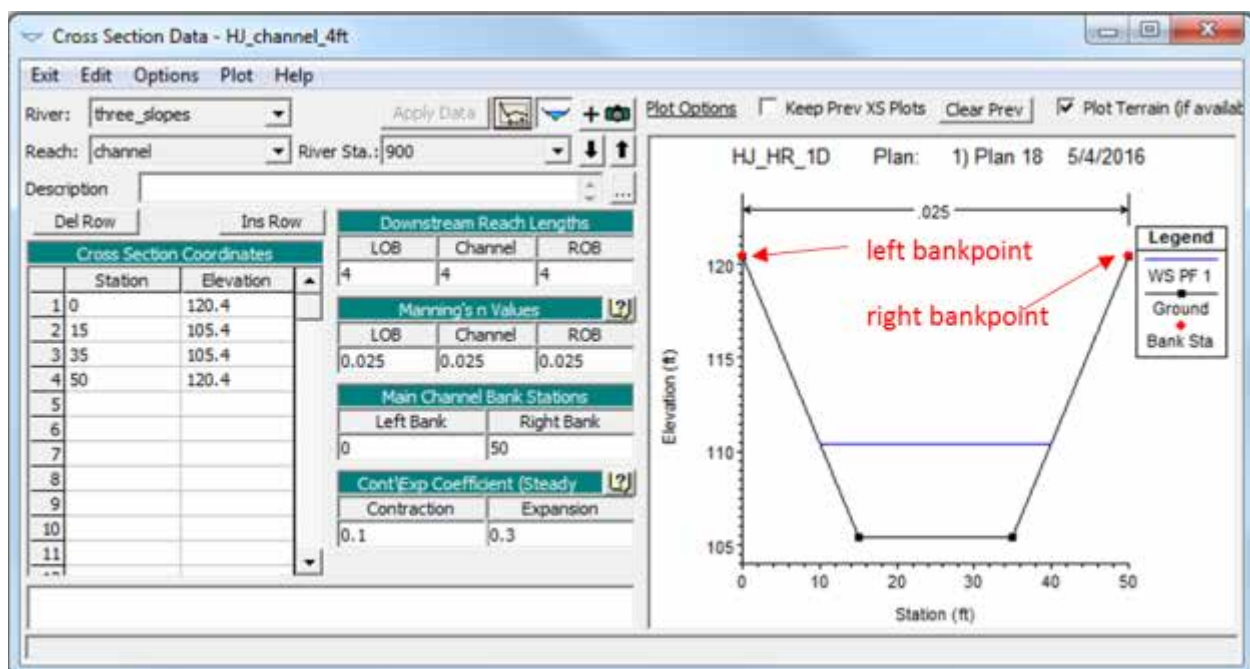


Figure 5.23: Proper Placement of HEC-RAS Bank Points on the Trapezoidal Channel

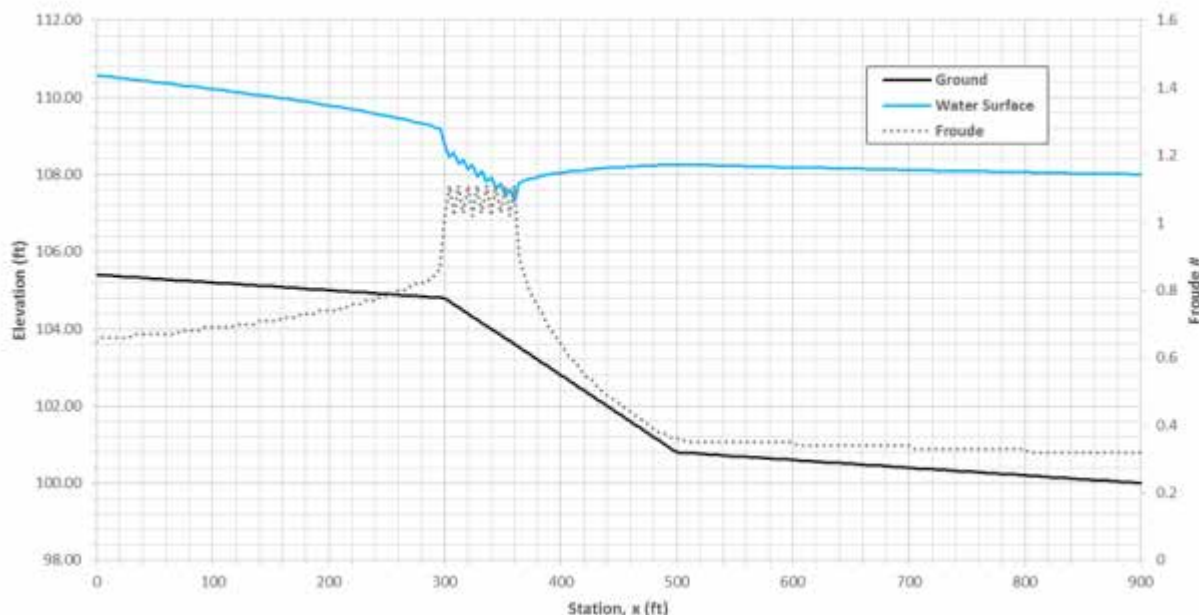


Figure 5.24: HEC-RAS 1D Simulation to Locate Hydraulic Jump Using 4-Foot Spacing for Cross Sections and Proper Placement of Bank Points

Obviously, the results shown in Figure 5.24 are not correct. A strange oscillation around critical depth is still evident in the water surface profile. Fixing the bank points for the HEC-RAS model that used 8-ft spacing for the cross sections still failed to properly bracket the solution. The upstream and downstream stations of the hydraulic jump actually moved farther upstream, to Stations 388 and 396, when the jump was already located upstream of where it was predicted using the depth step method, although for that model the flow managed to properly achieve supercritical depths leading up to the hydraulic jump. The discrepancy between the HEC-RAS 1D and direct step method solutions must be attributable to some other factor. The only type of losses accounted for when applying the depth step method in the spreadsheet were friction losses. To make possible comparison between the HEC-RAS 1D and spreadsheet solutions, expansion and contraction losses must be removed from the HEC-RAS simulation. Using HEC-RAS editing tools, the contraction and expansion coefficients for all cross sections were set to zero.

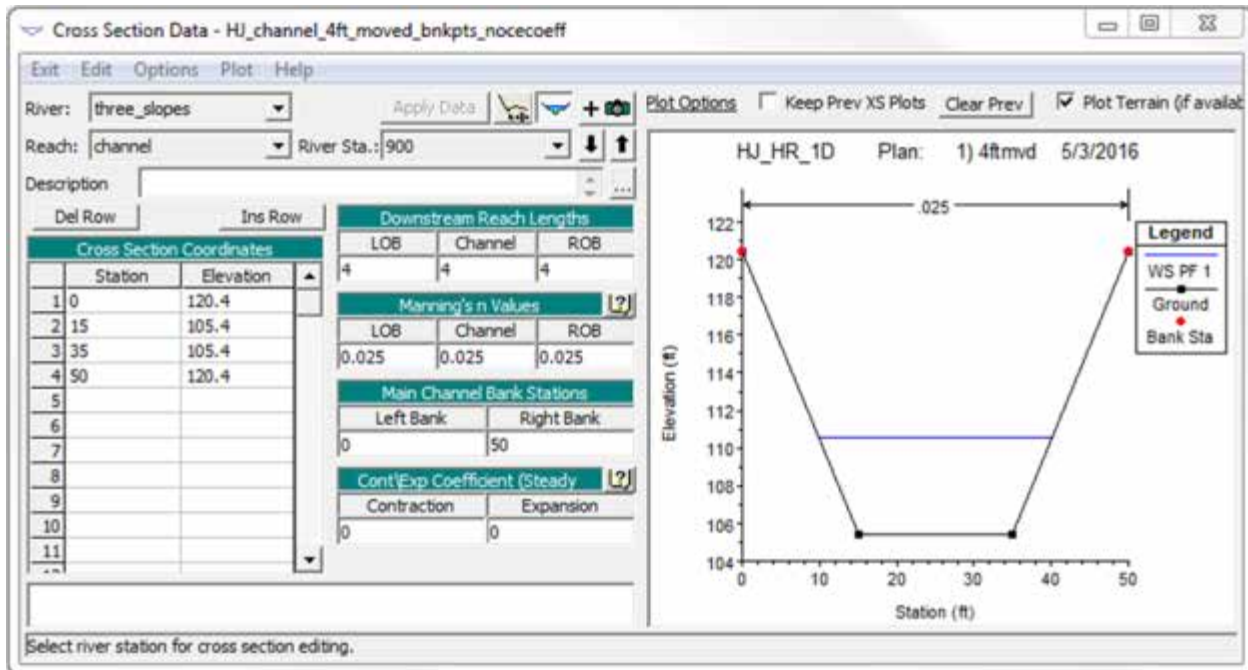


Figure 5.25: Cross Section Data Showing Adjusted Bank Points and No Contraction or Expansion Loss Coefficients

One last simulation was performed using the 1D HEC-RAS model for this hydraulic jump test. It finally provided results in close agreement with both the depth step method and with SRH-2D. The location of the hydraulic jump was properly bracketed by Stations 404 and 408. The model contained a total of 226 cross sections. It is expected that if the number of cross sections were further increased, at the very least in the sections where depth changes rapidly, such as near the hydraulic jump itself, the solution would converge on the same location as determined within the depth step method spreadsheet.

It is possible that HEC-RAS 1D could provide better results than were achievable within the spreadsheet, since HEC-RAS accounts for expansion and contraction losses of the flow. Clearly, however, problems arise with the results when a large number of cross sections are included in the model. The oscillation around critical depth is simply not physically realistic. While that result is certainly not desirable, perhaps some manual fine-tuning of the contraction and expansion loss coefficients may produce superior results. This fine-tuning was not conducted as part of this research.

5.8 Two-Dimensional HEC-RAS Hydraulic Jump Test

Lastly, the hydraulic jump test was performed using the 2D capabilities of HEC-RAS 5.0. Both sets of equations offered within the application were employed: the diffusion wave equation and the full momentum equation. The setup was identical for each model, although before each simulation was run the desired equation had to be selected. The upstream boundary condition was a ramped-up hydrograph that used an energy grade line (EGL) of 0.00274 to distribute flow at the inlet. The downstream boundary condition was normal depth with an EGL of 0.00062. Both EGLs for the boundary conditions were approximated using the nearest average friction slope obtained from the depth step method spreadsheet (these could have also been obtained, probably more precisely, from the first and last cross sections from the 1D model). The flow area was composed of 2×2 -ft square elements. The computational timestep used was 0.2 seconds. The model ran for a simulated time of 1 hour (hr). It is possible to allow the model to warm up before the simulation begins, but this step was skipped, and the model was allowed to start with all cells dry and simply to use the boundary conditions to begin the analysis. It was thought necessary to check the option for mixed flow regime profiles, although this may only be required for 1D sections that are connected to a 2D model. The results of each test were saved as maps in the form of rasters within HEC-RAS. These rasters were then opened in ArcMap, and the Interpolate Line tool on the 3D Analyst toolbar was used to extract the water surface elevation data from the channel centerline. Figures 5.26 through 5.36 describe the details above and the results of the simulations.



Figure 5.26: 2D Flow Area for HEC-RAS Hydraulic Jump Test Model



Figure 5.27: Default Manning's Roughness Coefficient and Grid Spacing for 2D Flow Area

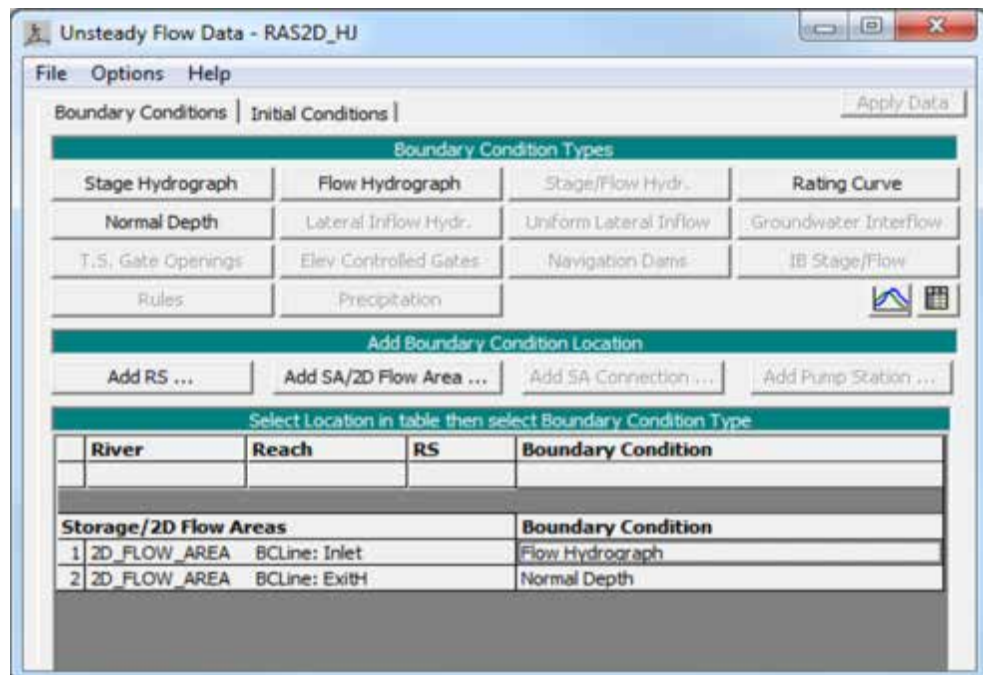


Figure 5.28: Boundary Conditions for the HEC-RAS 2D Hydraulic Jump Test

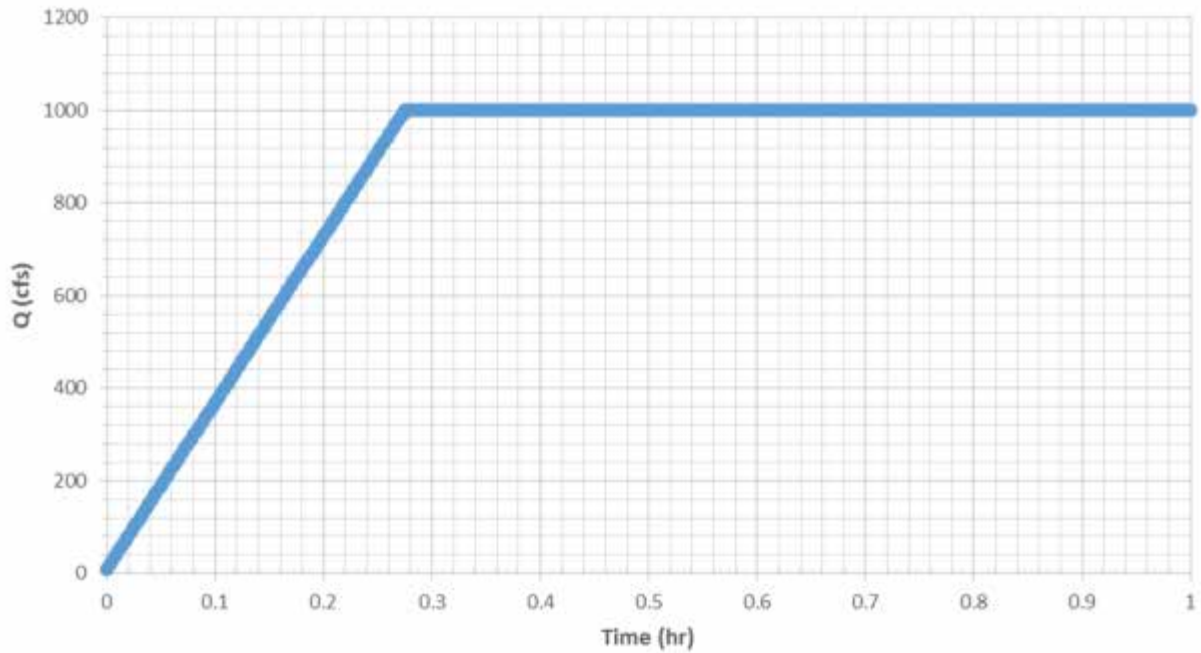


Figure 5.29: Hydrograph Used for the HEC-RAS 2D Hydraulic Jump Test

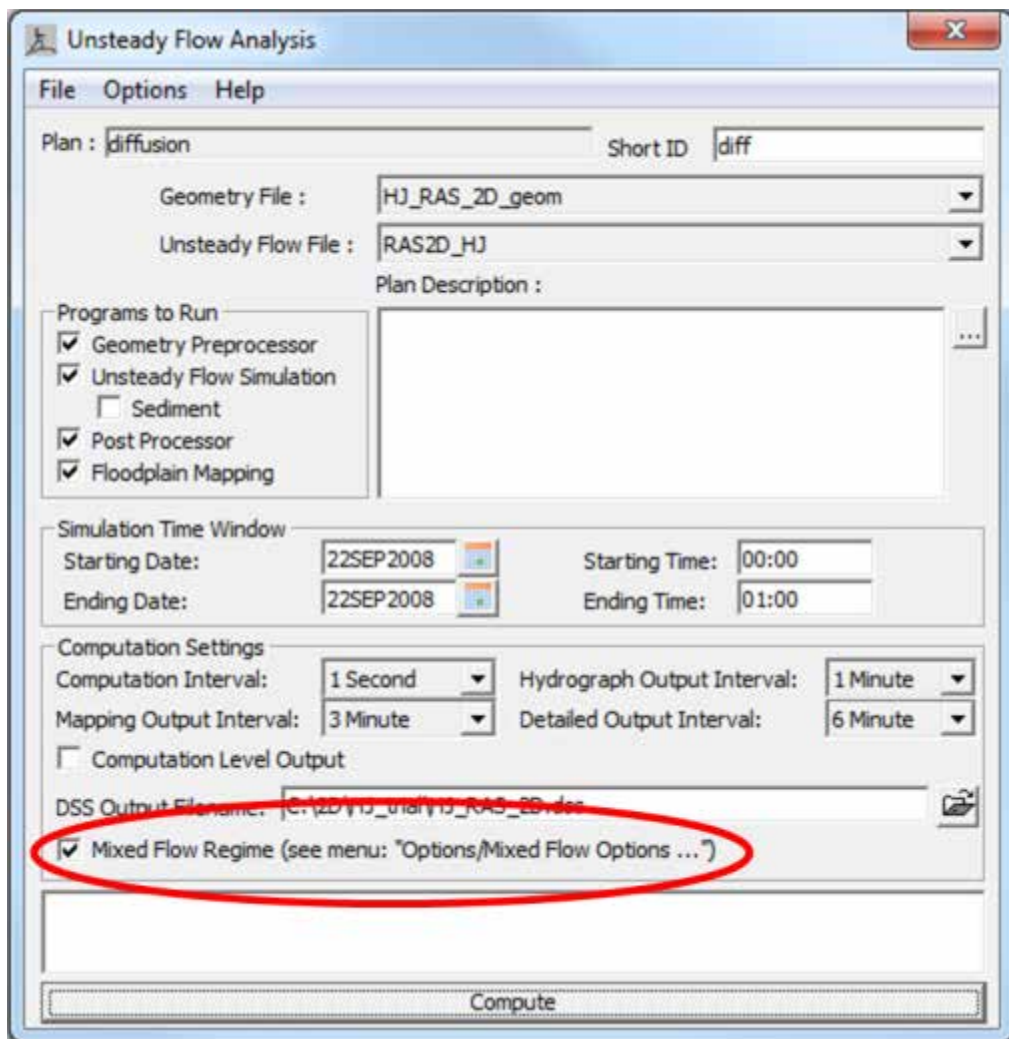


Figure 5.30: Option for Sub- and Supercritical Flow in the Unsteady Flow Analysis Menu

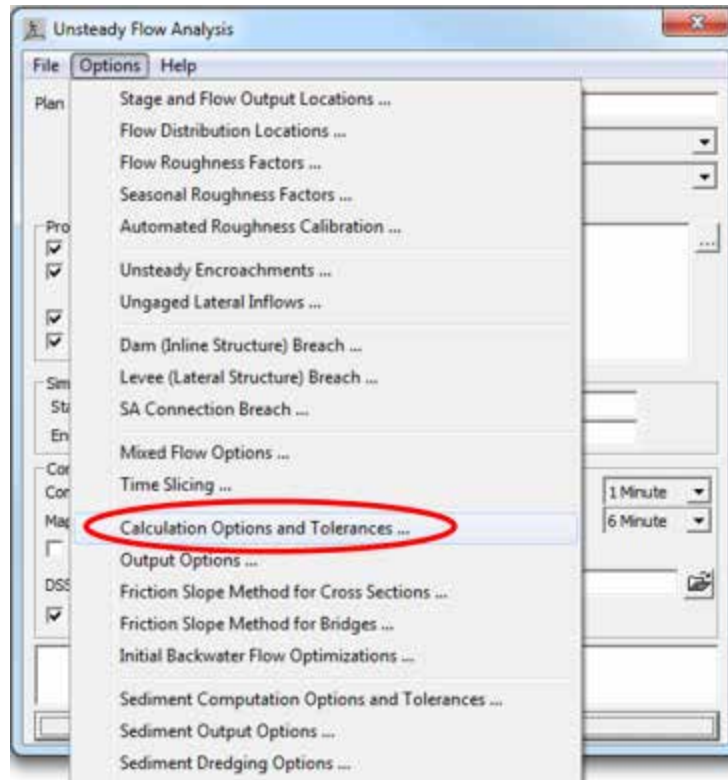


Figure 5.31: Options Leading to the Governing Equations Used for 2D Simulation

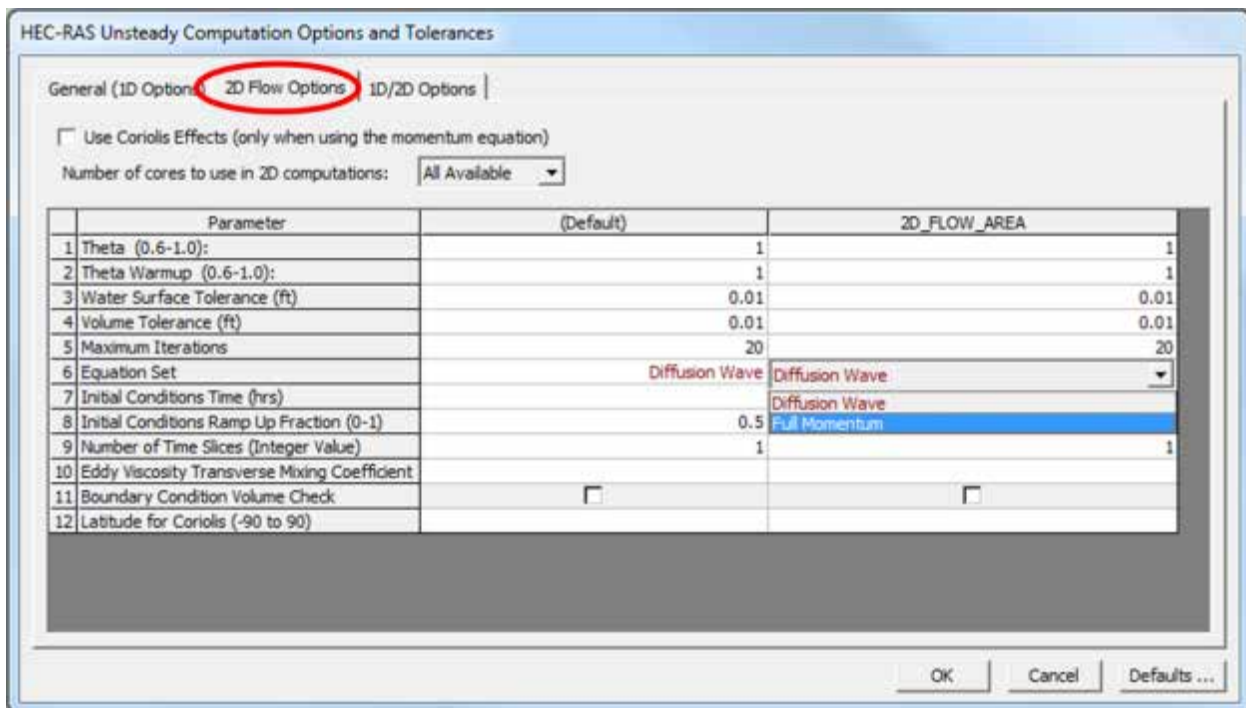


Figure 5.32: Tab Including Options for Selecting Equations of Fluid Motion

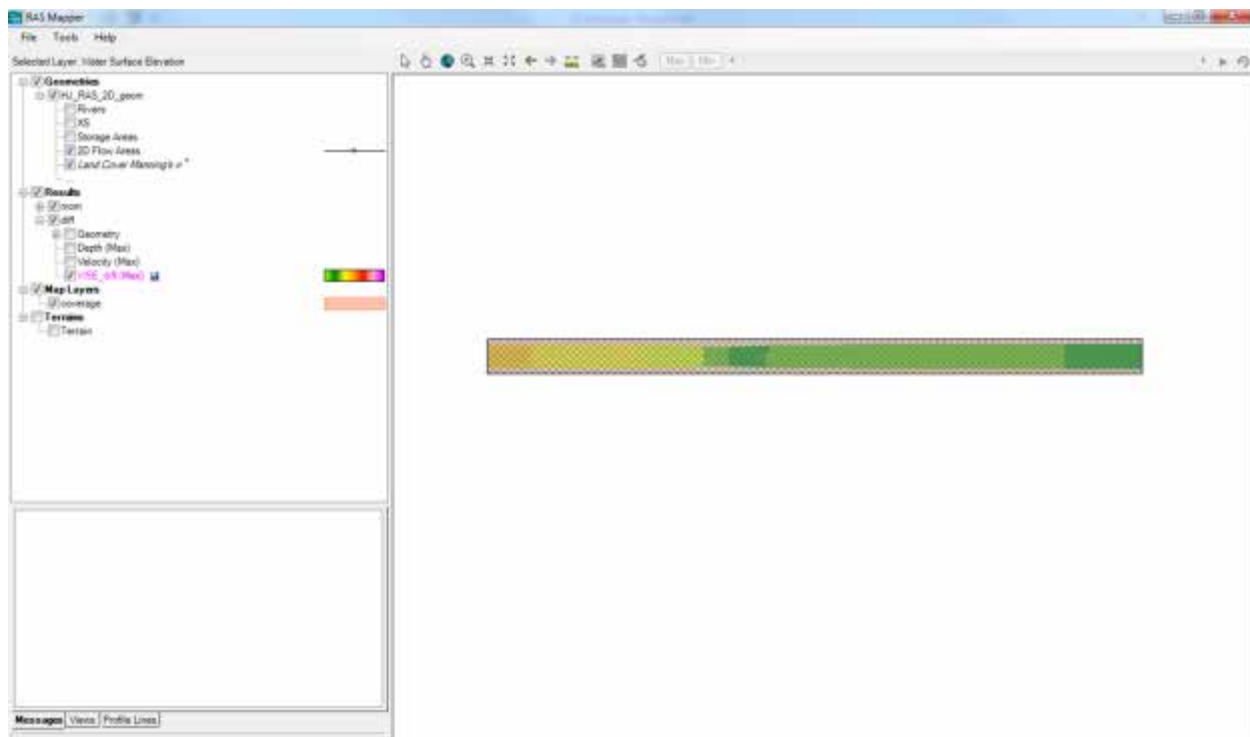


Figure 5.33: RAS Mapper Window Showing Results of the Simulation Using the Diffusion Wave Equation

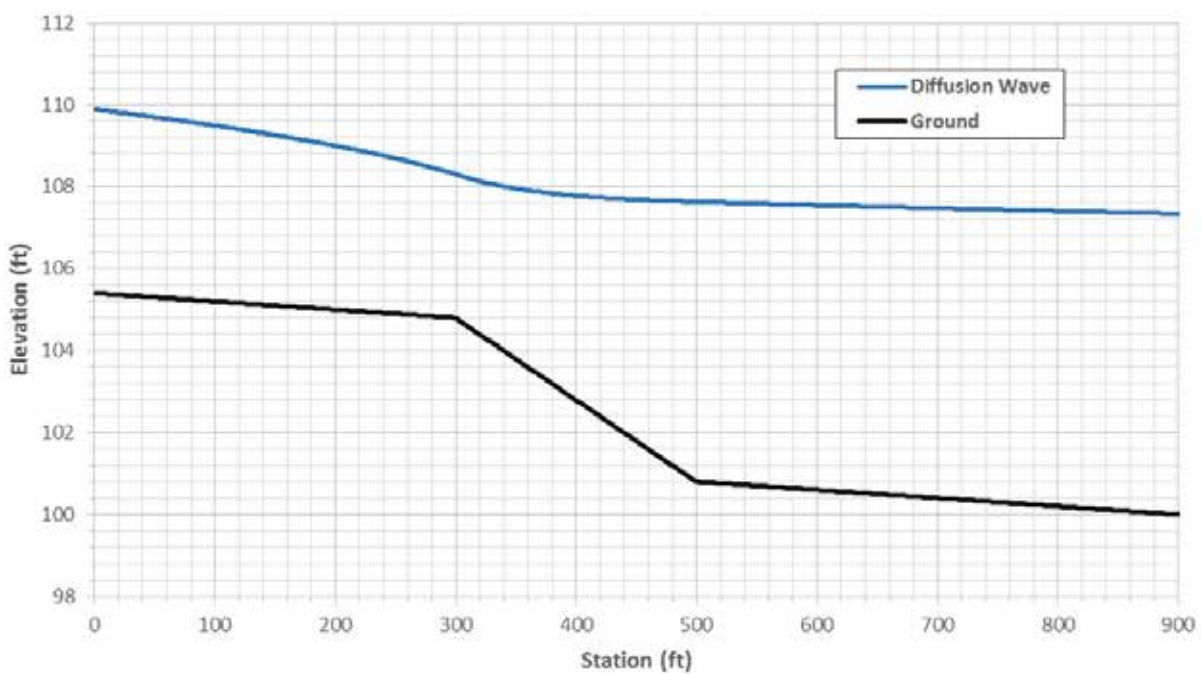


Figure 5.34: Water Surface Profile for HEC-RAS 2D Hydraulic Jump Test Using Simplified Equation of Fluid Motion

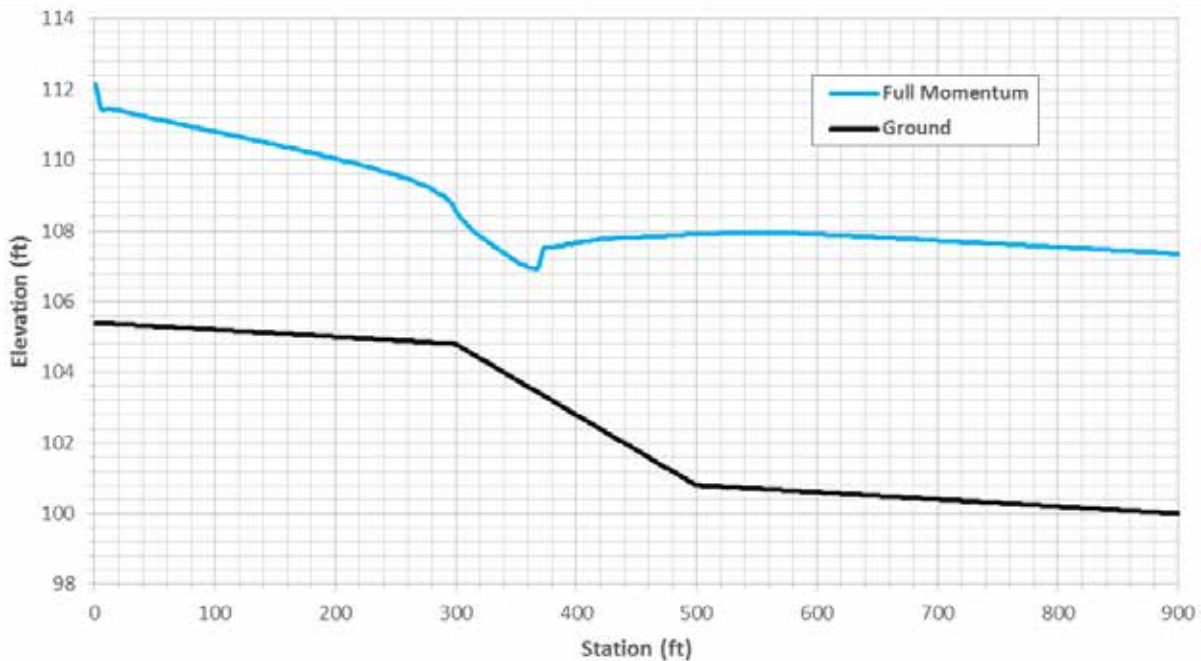


Figure 5.35: Water Surface Profile for HEC-RAS 2D Hydraulic Jump Test Using St. Venant Equation

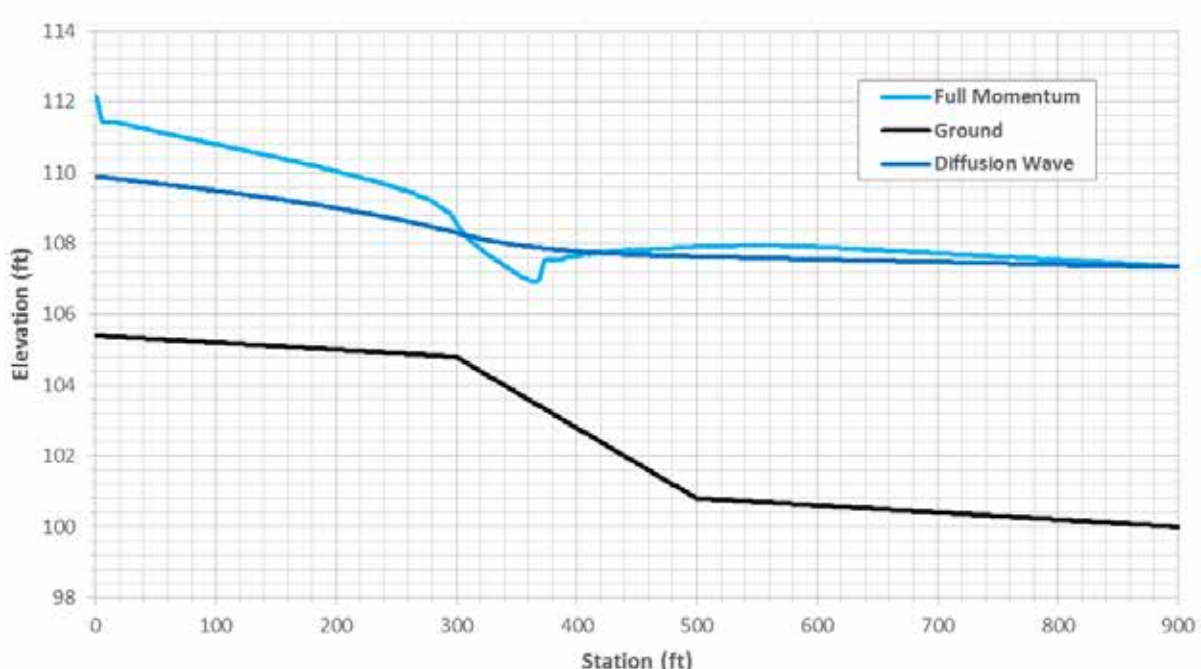


Figure 5.36: Both Water Surface Profiles from HEC-RAS 2D Simulations for Hydraulic Jump Test

Figure 5.34 shows that the Diffusion Wave equation completely missed the hydraulic jump and thus shows subcritical flow throughout the entire reach. Figure 5.35 shows some strange behavior at the section farthest upstream, where the water starts out very deep, drops rapidly, and then progresses in a more coherent manner. However, the full momentum simulation does show a hydraulic jump in the steep section of the channel, and, realistically, it shows it occurring over some difficult-to-determine distance. The depth increases rapidly from Station 366 to 372, progresses with very marked waves from Station 372 to about Station 410, and then continues with smaller waves for the rest of the length of the steep reach. The hydraulic jump occurs well before the predictions from the depth step method spreadsheet, SRH-2D, and HEC-RAS 1D. Figure 5.37 shows all final profiles determined.

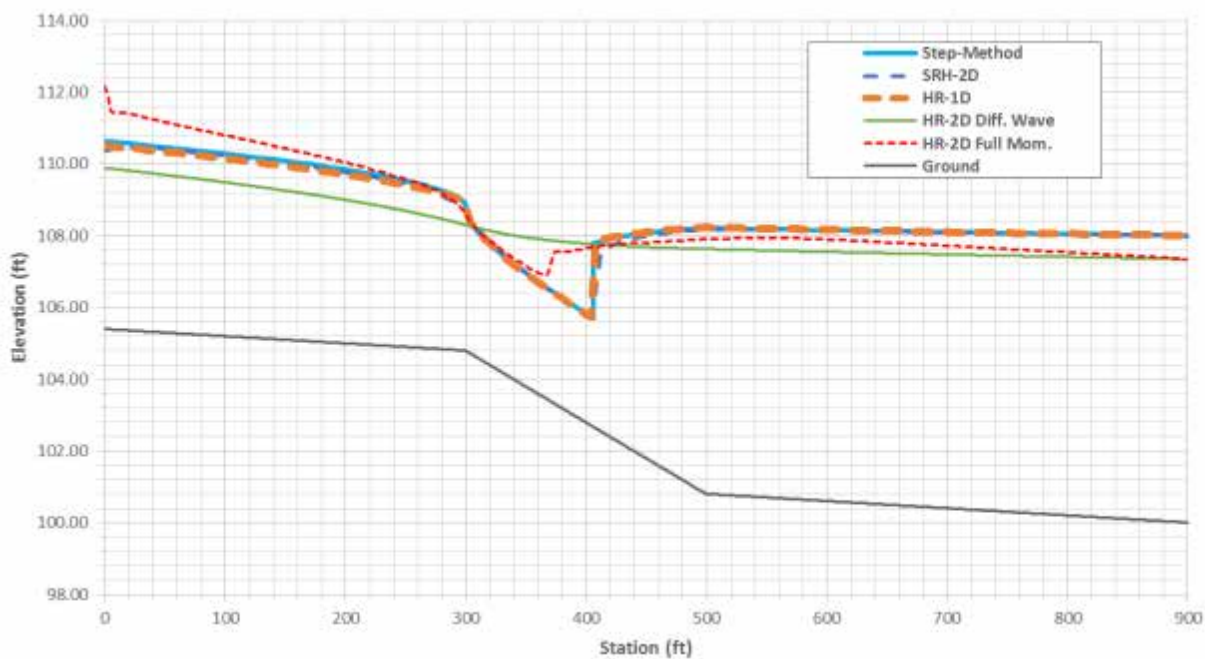


Figure 5.37: Summary of Profiles from Hydraulic Jump Tests

Chapter 6: Bridge Flume Modeling Study

6.1 Background for the Bridge Flume Modeling Study

This chapter seeks to compare computer model results with observed measurements from a physical model study presented in the report “A Model Study of Bridge Hydraulics, Edition 2” (Parr, Milburn, Malone, & Bender, 2010). The original study, performed at the University of Kansas in cooperation with the Kansas Department of Transportation, was intended to add some insight into the effect of bridge hydraulic features such as ineffective flow regions, weir overflow, tailwater conditions, and flow through skewed bridges. To achieve this goal, a laboratory flume was constructed. The flume shown below in Figure 6.1 has a 24-ft-long test region with the middle 7.5 ft containing the piezometers. The piezometer locations are shown in Figure 6.2, which includes both lab stations and 20-scale prototype stations.

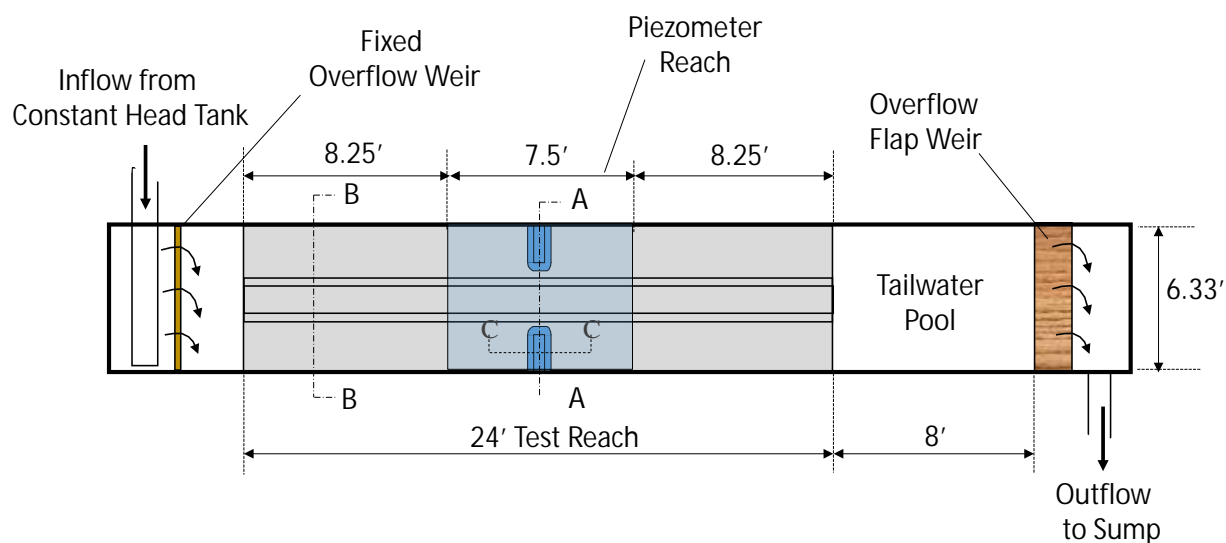


Figure 6.1: Plan View of Laboratory Model

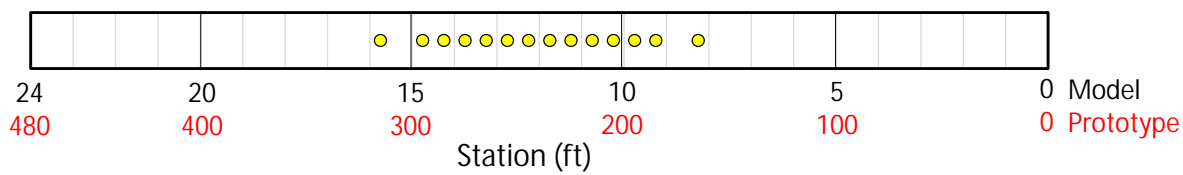


Figure 6.2: Location of Piezometers in Lab and Prototype Stations

Figure 6.3 shows an example of an experimental water surface profile obtained from the piezometer readings.

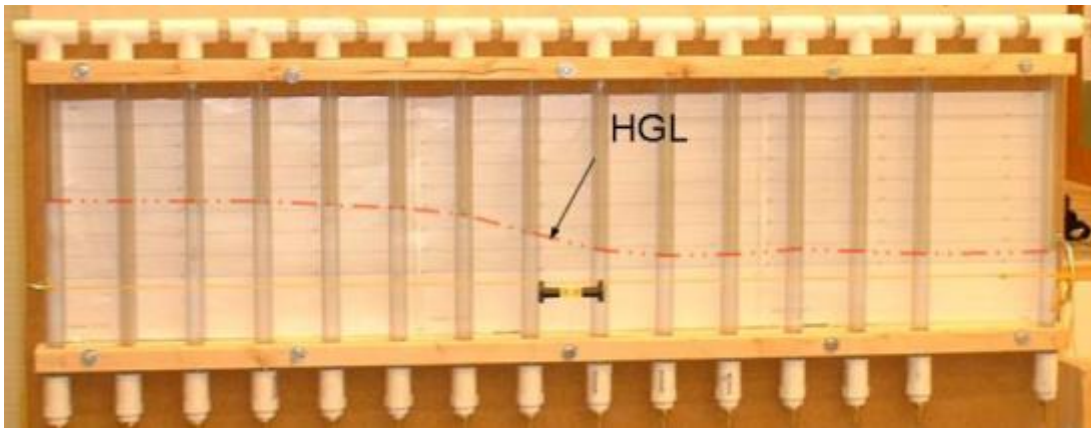


Figure 6.3: Piezometric Surface for Flume Experiment

This chapter discusses both *short models*, which model only the 7.5-ft-long section of the flume equipped with piezometers and *long models*, which simulate the entire 24-ft-long test reach. Both lab and prototype stations for the short and long models are given in Table 6.1. Note that Piezometer 2 did not function and there was no Piezometer 15. Also, the short and long models used HEC-RAS 2D versions 5.0.1 and 5.0.3, respectively. The long models were created to give better agreement with the laboratory data.

Section C–C (a cross section of the bridge abutment) of Figure 6.1 is shown in Figure 6.4, and Sections A–A and B–B (cross sections of the channel) are shown in Figure 6.5. Table 6.2 shows the station-elevation data for Sections A–A and B–B of Figure 6.1, respectively. The 1D HEC-RAS model bridge geometry was taken from Figure 6.1 since it included bridge deck parameters and pier caps.

Table 6.1: Stations for Short and Long Lab and Prototype Piezometer Locations

| Piezometer Number | Lab Short Sta (ft) | Prototype Short Station (ft) | Lab Long Sta (ft) | Prototype Long Station (ft) |
|-------------------|--------------------|------------------------------|-------------------|-----------------------------|
| 1 | 2 | 3 | 4 | 5 |
| 1 | 0 | 0 | 8.25 | 165 |
| 3 | 1 | 20 | 9.25 | 185 |
| 4 | 1.5 | 30 | 9.75 | 195 |
| 5 | 2 | 40 | 10.25 | 205 |
| 6 | 2.5 | 50 | 10.75 | 215 |
| 7 | 3 | 60 | 11.25 | 225 |
| 8 | 3.5 | 70 | 11.75 | 235 |
| 9 | 4 | 80 | 12.25 | 245 |
| 10 | 4.5 | 90 | 12.75 | 255 |
| 11 | 5 | 100 | 13.25 | 265 |
| 12 | 5.5 | 110 | 13.75 | 275 |
| 13 | 6 | 120 | 14.25 | 285 |
| 14 | 6.5 | 130 | 14.75 | 295 |
| 16 | 7.5 | 150 | 15.75 | 315 |

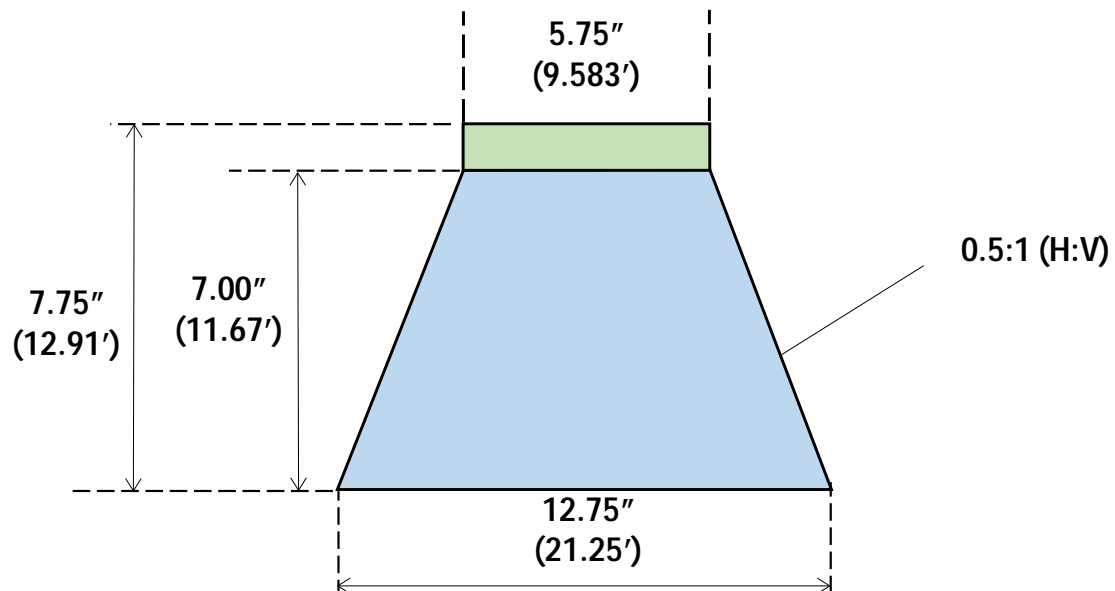


Figure 6.4: Section C-C (Figure 6.1) through Bridge Abutment

Table 6.2: Lab and Prototype Station–Elevation Points for Figure 6.1

Section A-A

Bounding Cross Sections

| Lab Model | | Prototype | |
|-----------|------------|-----------|-----------|
| Sta (in.) | Elev (in.) | Sta (ft) | Elev (ft) |
| 0.00 | 20.00 | 0.00 | 33.33 |
| 0.00 | 8.09 | 0.00 | 13.48 |
| 30.90 | 8.09 | 51.50 | 13.48 |
| 33.10 | 0.00 | 55.17 | 0.00 |
| 42.91 | 0.00 | 71.52 | 0.00 |
| 45.11 | 8.09 | 75.18 | 13.48 |
| 76.01 | 8.09 | 126.68 | 13.48 |
| 76.01 | 20.00 | 126.68 | 33.33 |

Abutments

| Lab Model | | | |
|-----------|-----------|----------|-----------|
| Left | | Right | |
| Sta (ft) | Elev (ft) | Sta (ft) | Elev (ft) |
| 0.00 | 15.09 | 49.01 | 8.09 |
| 23.24 | 15.09 | 52.77 | 15.09 |
| 27.00 | 8.09 | 76.01 | 15.09 |

Abutments

| Prototype | | | |
|-----------|-----------|----------|-----------|
| Left | | Right | |
| Sta (ft) | Elev (ft) | Sta (ft) | Elev (ft) |
| 0.00 | 25.15 | 81.68 | 13.48 |
| 38.73 | 25.15 | 87.95 | 25.15 |
| 45.00 | 13.48 | 126.68 | 25.15 |

Section B-B

Channel Cross Sections

| Lab Model | | Prototype | |
|-----------|------------|-----------|-----------|
| Sta (in.) | Elev (in.) | Sta (ft) | Elev (ft) |
| 0.00 | 20.00 | 0 | 33.33 |
| 0.00 | 8.09 | 0 | 13.48 |
| 30.90 | 8.09 | 51.5 | 13.48 |
| 33.10 | 0.00 | 55.17 | 0 |
| 42.91 | 0.00 | 71.52 | 0 |
| 45.11 | 8.09 | 75.18 | 13.48 |
| 76.01 | 8.09 | 126.68 | 13.48 |
| 76.01 | 20.00 | 126.68 | 33.33 |

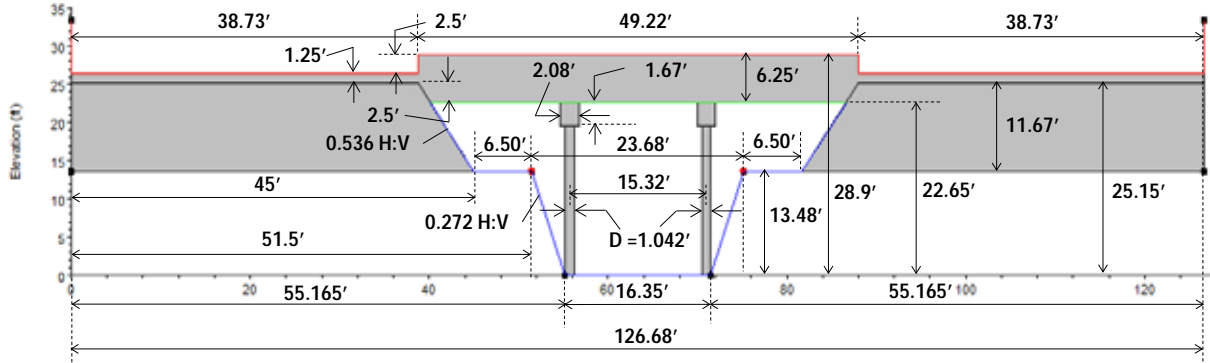
Bridge Deck

| Lab Model | | | Prototype | | |
|-----------|----------|---------|-----------|---------|---------|
| Sta (in.) | HS (in.) | L (in.) | Sta (ft) | HS (ft) | LS (ft) |
| 0.00 | 15.84 | 0 | 0.00 | 26.40 | |
| 23.24 | 15.84 | 0 | 38.73 | 26.40 | |
| 23.24 | 17.34 | 13.59 | 38.73 | 28.90 | 22.65 |
| 52.77 | 17.34 | 13.59 | 87.95 | 28.90 | 22.65 |
| 52.77 | 15.84 | 0 | 87.95 | 26.40 | |
| 76.01 | 15.84 | 0 | 126.68 | 26.40 | |

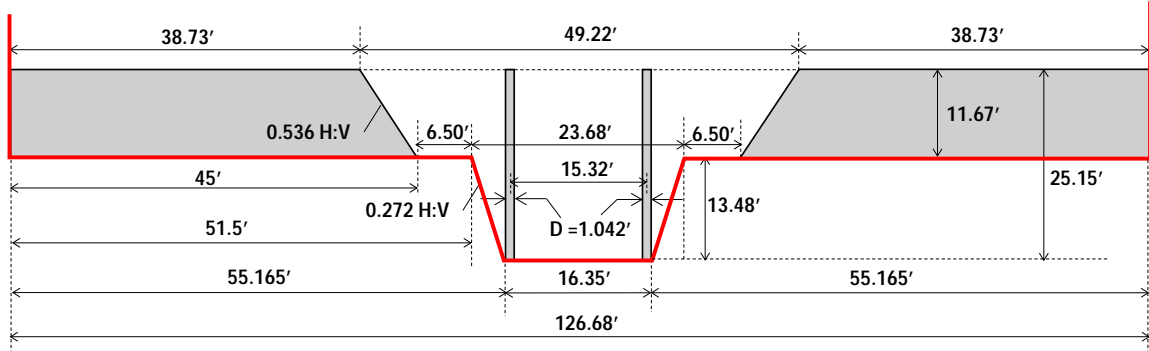
Pier Locations and Size

| | Model | | Prototype | |
|-----------|-----------|------------|-----------|-----------|
| D | 0.625 in. | | 1.042 ft | |
| Cap (b,h) | 1.25 in. | 1 in. | 2.08 ft | 1.67 ft |
| Pier | Sta (in.) | Elev (in.) | Sta (ft) | Elev (ft) |
| Left | 33.41 | 15.09 | 55.69 | 25.15 |
| Right | 75.70 | 15.09 | 126.16 | 25.15 |

(a) Section A-A (Lab Model and 1D HEC-RAS with Prototype Dimensions at 20-scale)



(b) Section A-A (2D HEC-RAS Model)



(c) Section B-B (Lab, 1D and 2D HEC-RAS Models)

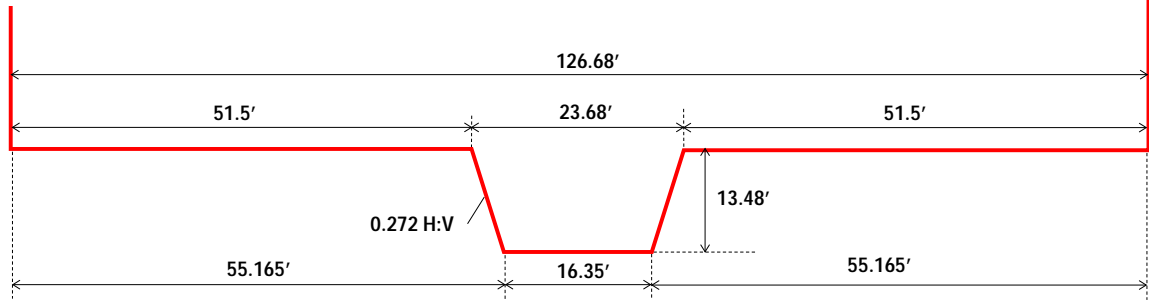


Figure 6.5: Cross Section Data for Sections A-A and B-B of Figure 6.1

Three types of configurations were examined in the flume for the 2010 report: Type One was a regular bridge with abutments, bridge piers, and roadway as represented in Figures 6.1 and 6.5; Type Two was a simple bridge opening with weir flow in one overbank; and Type Three was a simple skewed bridge. All configurations were tested using a range of flow and tailwater conditions. Only Type One experimental data are considered in this report. The Parr et al. (2010) study compared laboratory results to 1D HEC-RAS models. The second version of the report contained improvements to the HEC-RAS 1D models based on input provided by Gary W.

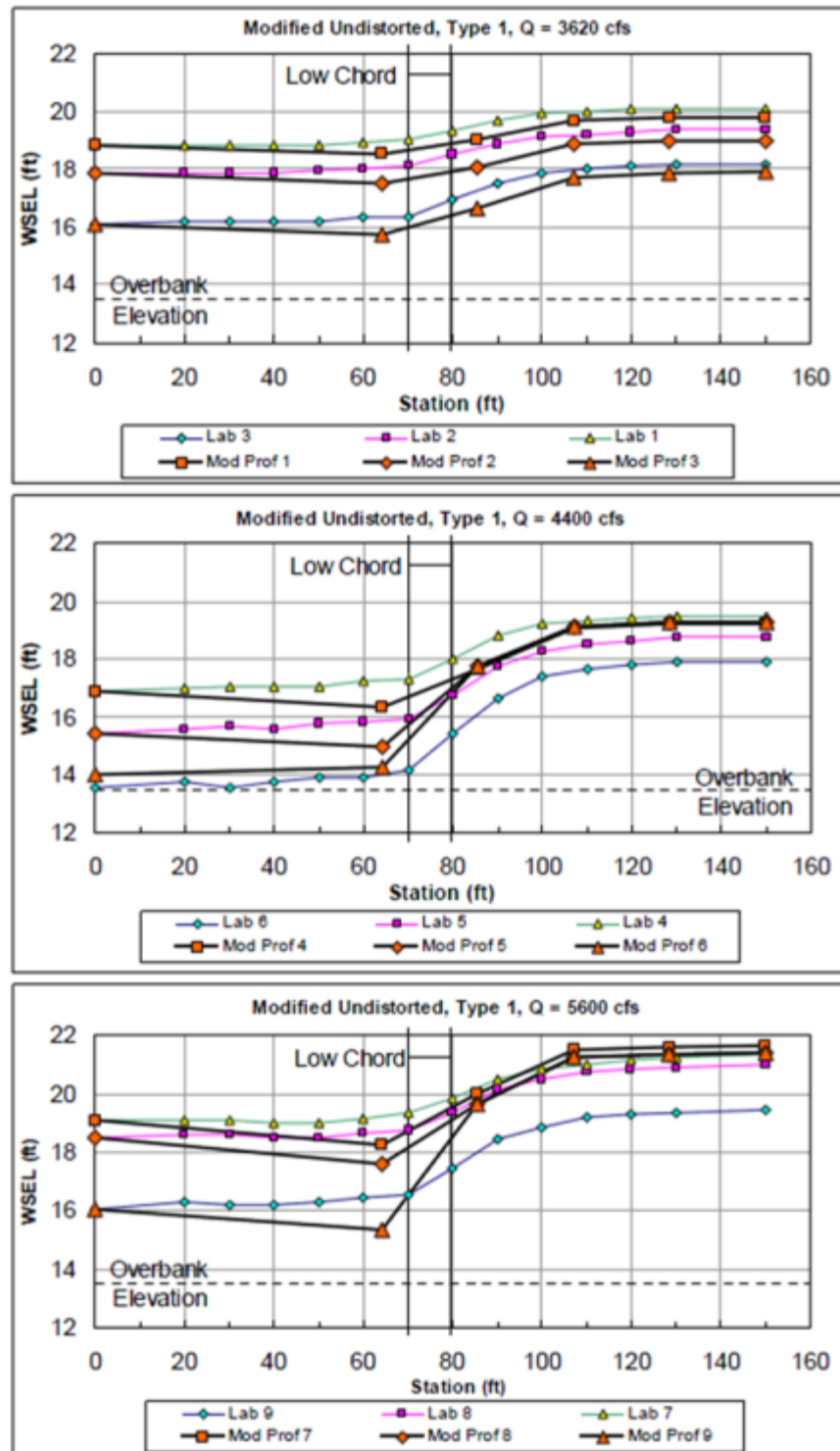
Brunner, Senior Technical Hydraulic Engineer at the Hydrologic Engineering Center (developer of the HEC-RAS software). His recommendations improved agreement between the HEC-RAS 1D models and the laboratory results. However, the improved models did not overturn a particular result presented in the initial report: for cases where the Froude number at the downstream bridge face cross section exceeded a Froude number of about 0.7, the water surface profiles upstream of the bridge were essentially unaffected by the tailwater conditions (this was especially true for the middle-range discharge). For these conditions, the HEC-RAS models appear to assume inlet control at the bridge section, and the subcritical flow upstream could not sense what was happening downstream of this critical section. This was the case despite the fact that the laboratory models showed a very definite change in the headwater depth, corresponding to a change in the tailwater depth for all cases.

The results for the Type One Laboratory experiments are shown in Table 6.3. The values are given in 20-scale prototype dimensions. Also, note the discharges for the lab, the 20-scale undistorted model (considered herein), and the distorted model, which used 20-scale in the vertical and 50-scale in the horizontal.

Table 6.3: WSE Values from Lab Experiments Expressed in 20-Scale Prototype Dimensions (Q in cfs)

| | | Q _{lab} (cfs) | | 2.02 | Q _{lab} (cfs) | | 2.46 | Q _{lab} (cfs) | | 3.13 |
|----------|------------|--------------------------|--------------|--------------|--------------------------|--------------|--------------|--------------------------|--------------|--------------|
| | | Q _{model} (cfs) | | 3620 | Q _{model} (cfs) | | 4400 | Q _{model} (cfs) | | 5600 |
| 1D model | 2D model | Laboratory Results | | | | | | Laboratory Results | | |
| | | Station | Station | Run 1 | Run 2 | Run 3 | Run 4 | Run 5 | Run 6* | Run 7 |
| (ft) | (ft) | (ft) | (ft) | (ft) | (ft) | (ft) | (ft) | (ft) | (ft) | (ft) |
| 1 | 2 | 3 | 4 | 5 | 6 | 7 | 8 | 9 | 10 | 11 |
| 150 | 315 | 20.08 | 19.36 | 18.18 | 19.49 | 18.77 | 17.91 | 21.33 | 21.00 | 19.45 |
| 130 | 295 | 20.08 | 19.36 | 18.18 | 19.49 | 18.77 | 17.91 | 21.24 | 20.91 | 19.37 |
| 120 | 285 | 20.08 | 19.27 | 18.09 | 19.40 | 18.60 | 17.83 | 21.16 | 20.83 | 19.28 |
| 110 | 275 | 20.00 | 19.19 | 18.01 | 19.32 | 18.52 | 17.66 | 20.99 | 20.75 | 19.20 |
| 100 | 265 | 19.91 | 19.11 | 17.84 | 19.24 | 18.27 | 17.41 | 20.83 | 20.50 | 18.87 |
| 90 | 255 | 19.66 | 18.86 | 17.51 | 18.82 | 17.77 | 16.66 | 20.49 | 20.16 | 18.45 |
| 80 | 245 | 19.33 | 18.52 | 16.93 | 17.99 | 16.77 | 15.41 | 19.83 | 19.33 | 17.45 |
| 70 | 235 | 19.00 | 18.11 | 16.34 | 17.32 | 15.93 | 14.16 | 19.33 | 18.75 | 16.53 |
| 60 | 225 | 18.91 | 18.02 | 16.34 | 17.24 | 15.85 | 13.91 | 19.16 | 18.66 | 16.45 |
| 50 | 215 | 18.83 | 17.94 | 16.18 | 17.07 | 15.77 | 13.91 | 18.99 | 18.50 | 16.28 |
| 40 | 205 | 18.83 | 17.86 | 16.18 | 17.07 | 15.60 | 13.75 | 18.99 | 18.50 | 16.20 |
| 30 | 195 | 18.83 | 17.86 | 16.18 | 17.07 | 15.68 | 13.58 | 19.08 | 18.58 | 16.20 |
| 20 | 185 | 18.83 | 17.86 | 16.18 | 17.02 | 15.60 | 13.75 | 19.08 | 18.58 | 16.28 |
| 0 | 165 | 18.83 | 17.86 | 16.09 | 16.90 | 15.43 | 13.58 | 19.08 | 18.50 | 16.03 |

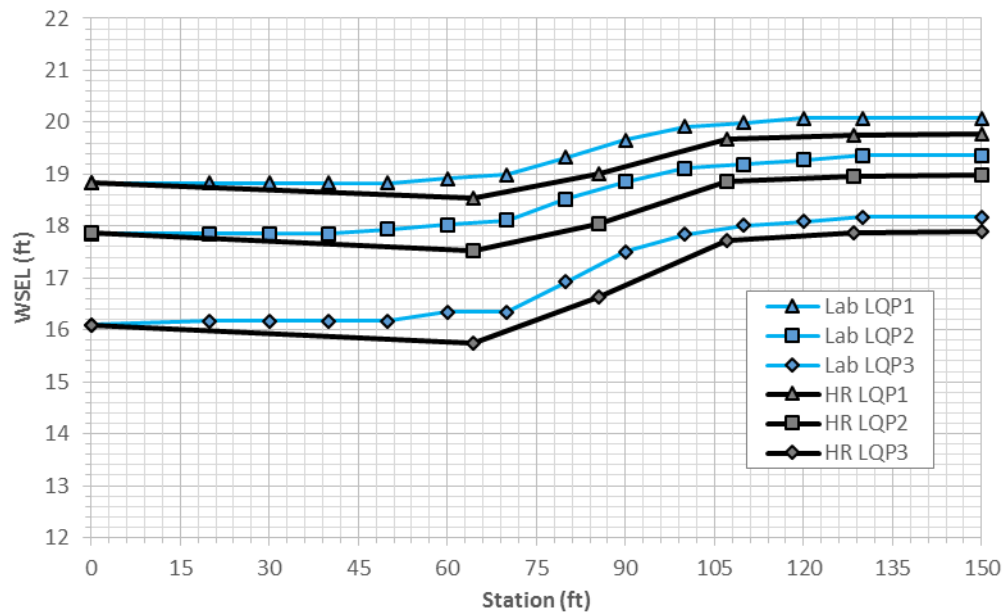
*DS piezometer reading too low at just 0.1 ft above overbank elevation in Model dimensions



Note: Lab numbers refer to observed water surface profiles from the corresponding Runs. Mod Prof refers to the modeled water surface profile using HEC-RAS 1D.

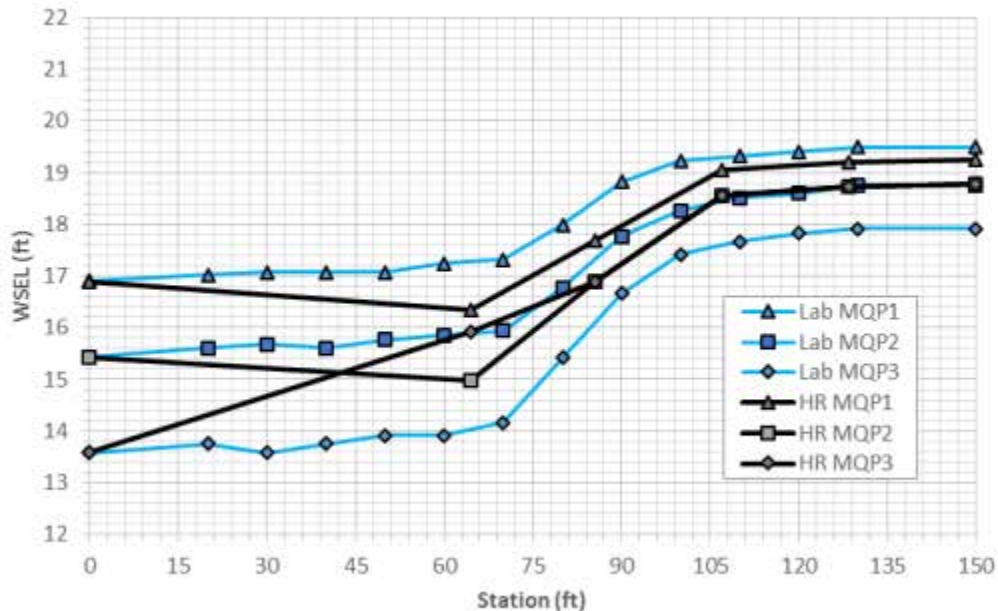
Figure 6.6: Results from Previous Study for the Type One Bridge Configuration Using HEC-RAS 4.1

It should be noted that, unless stated otherwise, all water surface profiles shown in this chapter are representative of the channel centerline. As can be seen from the plots in the Figure 6.6 above, the results from the Type One experiments showed that for the middle and high discharges, the undistorted HEC-RAS models (the analyses in the previous report used distorted x and y scales in some places) were only slightly responsive to the tailwater depth. These simulations were run using 2D HEC-RAS 5.0.1; Figures 6.7 to 6.9 show the subsequent results. They show a slight sensitivity to the tailwater depth, but one not nearly as distinct as was exhibited by the flume data.



Note: LAB LQP# refers to the run number for the laboratory data for the low discharge lab sets. HR LQP# refers to the run number for the HEC-RAS 1D simulations using the low discharge.

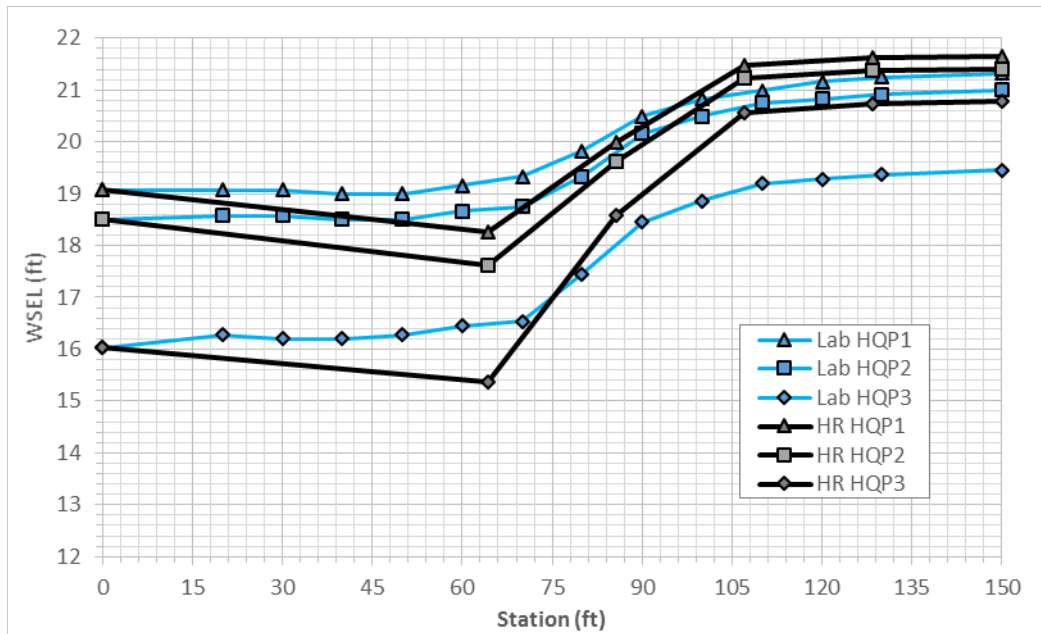
Figure 6.7: Comparison of Lab and Modified, Undistorted 1D HEC-RAS 5.0.1 Models from Previous Study for 3620 cfs



Note: LAB MQP# refers to the run number for the laboratory data for the medium discharge lab sets. HR MQP# refers to the run number for the HEC-RAS 1D simulations using the medium discharge.

Figure 6.8: Comparison of Lab and Modified, Undistorted 1D HEC-RAS 5.0.1 Models from Previous Study for 4400 cfs

The Type One bridge experiments for the undistorted case were rerun using HEC-RAS 2D with the full momentum equations and SRH-2D to see if these models, which preserve more of the physics of the flow, would exhibit behavior more like that seen in the flume. The diffusion equation was not adopted for these tests, since so many of the losses that occurred through this section were due to the rapid contraction and subsequent expansion of the flow. A preliminary run using the diffusion equation set in HEC-RAS 2D showed a total lack of ineffective flow upstream and downstream of the bridge, a result that is far from realistic.



Note: LAB HQP# refers to the run number for the laboratory data for the high discharge lab sets. HR HQP# refers to the run number for the HEC-RAS 1D simulations using the high discharge.

Figure 6.9: Comparison of Lab and Modified, Undistorted 1D HEC-RAS 5.0.1 Models from Previous Study for 5600 cfs

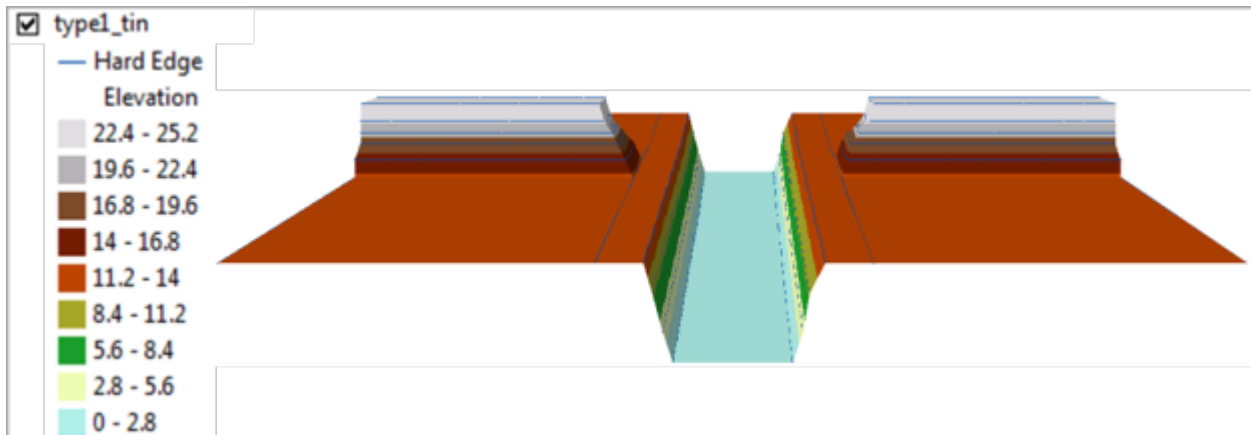


Figure 6.10: View from ArcScene of TIN for Type One Bridge Experiments with Elevations Given in Feet

The terrain used in both the HEC-RAS 2D and SRH-2D models was prepared in ArcMap using the details given in the previous report and presented in Figure 6.10 above. This was easily accomplished for the horizontal channel by first drawing lines along key features—such as the

upper limits of the main channel and toes of the embankments—and assigning the proper elevations to each line; the Feature to 3D by Attribute tool was then used to produce a shapefile, which in turn was used to generate a TIN. Figure 6.10 shows the results of this process. The four circular piers (not shown in Figure 6.10) were also defined in ArcMap. Both models used the same Manning's n value of 0.0233 as in the previous study, except at the locations of the piers in the HEC-RAS 2D model where a Manning's n of 1,000,000 was used to block flow through the piers. The SRH-2D model did not need to use this extraordinarily high roughness coefficient as the model is capable of simply generating a "wall" boundary condition line around each pier that does not allow water to cross it. The hydrographs used for each test were the same for both models and are shown in Table 6.4 and Figure 6.11. Details specific to each model are discussed in Sections 6.2 (HEC-RAS 2D) and 6.3 (SRH-2D).

Table 6.4: Ordinates of Hydrographs Used for Type One Bridge Study 2D Simulations

| Time (min.) | Discharge | | |
|----------------|-----------|------|------|
| | Low | Mid. | High |
| 0 | 360 | 400 | 500 |
| 15 | 3620 | 4400 | 5600 |
| 30 | 3620 | 4400 | 5600 |

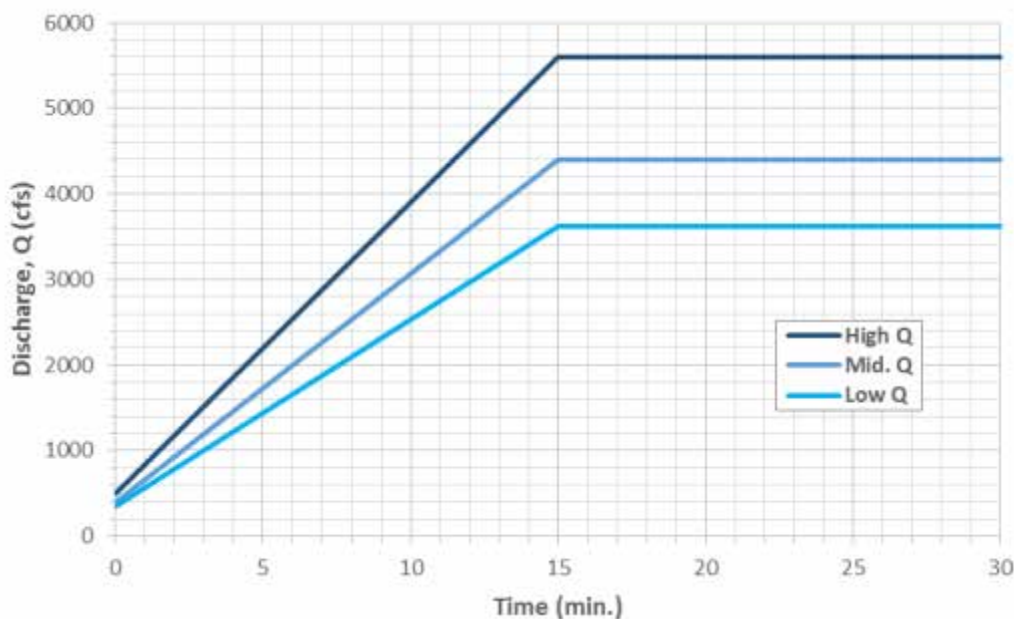


Figure 6.11: Hydrographs Used for Type One Bridge Study 2D Simulations

6.2 HEC-RAS 2D Model of Type One Bridge from Flume Study (Short Model)

The 2D flow area used for the HEC-RAS 2D full momentum model contained elements generated as 2-ft squares. The piers were then defined by breaklines with 1-ft spacing for cell centers around them, which is currently the closest they are allowed to be in HEC-RAS. Some manual editing of cell centers was necessary to actually satisfy the 1-ft spacing criterion, but also to ensure that the cell faces near the piers correctly gained the exceptionally high Manning's roughness coefficient of 1,000,000 corresponding to the piers (see Figure 6.12).

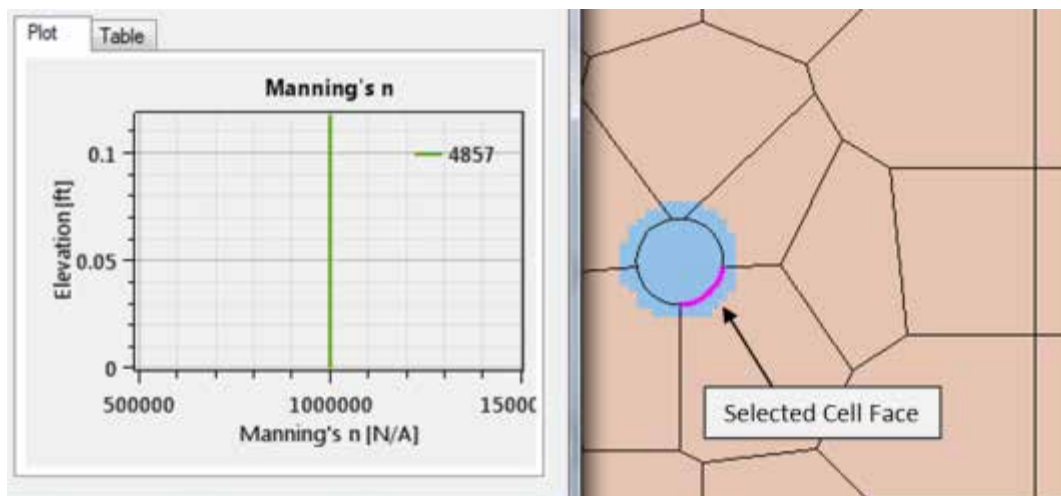


Figure 6.12: HEC-RAS 2D Cell Face on Bridge Piers for Flume Study

To ensure that the 2D elements of HEC-RAS captured the Manning's n for the 1.04-ft diameter piers, the shapefiles that represented them in the land use coverage within ArcMap were buffered by 0.2 ft, and when the coverage was brought into HEC-RAS via the RAS Mapper, the coverage polygons were specified to have a grid spacing of 0.1 ft so that the pier polygons would be approximately circular. All of this needed to be done because through practice it has been found that for a cell face to have a given roughness coefficient, at least 50% of its length needs to coincide with the coverage type that has that coefficient. Also for this reason, care was taken not to buffer the pier polygons too much.

The EGL for determining the conveyance at the upstream boundary was estimated by comparing the depths recorded in the lab for the two most upstream cross sections. Where the difference in depths between the two sections was equal to zero, the EGL was estimated as

0.0001—a value considered sufficiently small so as not to have a significant impact on the results. Table 6.5 contains the values used for all HEC-RAS 2D simulations.

Table 6.5: Determination of Upstream EGL from Flume Data for HEC-RAS 2D Simulations

| Q (cfs) | Profile - | Y_{@x=150} (ft) | Y_{@x=130} (ft) | Δy/L (ft/ft) | U/S EGL (ft/ft) |
|-------------------|---------------------|-----------------------------------|-----------------------------------|------------------------|---------------------------|
| 3620 | 1 | 20.08 | 20.08 | 0.00000 | 0.00010 |
| 3620 | 2 | 19.36 | 19.36 | 0.00000 | 0.00010 |
| 3620 | 3 | 18.18 | 18.18 | 0.00000 | 0.00010 |
| 4400 | 1 | 19.49 | 19.49 | 0.00000 | 0.00010 |
| 4400 | 2 | 18.77 | 18.77 | 0.00000 | 0.00010 |
| 4400 | 3 | 17.91 | 17.91 | 0.00000 | 0.00010 |
| 5600 | 1 | 21.33 | 21.24 | 0.00417 | 0.00417 |
| 5600 | 2 | 21.00 | 20.91 | 0.00417 | 0.00417 |
| 5600 | 3 | 19.45 | 19.37 | 0.00417 | 0.00417 |

The 2D flow area used contained 5,163 cells with a maximum size of 6.00 square ft, an average of 4.02 square ft, and a minimum of 0.78 square ft. All HEC-RAS 2D simulations were executed with a computational timestep of 0.1 second and with a warmup period of 1 hour during which the model was allowed to run with the minimum discharge for a given hydrograph. The results at the end of this period would become the initial condition of the simulation proper. While this warmup feature can be very useful for large and complicated sites, it was likely unnecessary here, and almost certainly not for an entire hour. Nevertheless, the HEC-RAS 2D models each took about 20 minutes to run, with the warmup period taking about 7 minutes of the total. The HEC-RAS 2D runs were much faster than the SRH-2D simulations (see Section 6.3). The results of the HEC-RAS 2D simulations (output from the final timestep at $t = 30$ minutes) are displayed alongside the flume data in Figures 6.13 to 6.15.

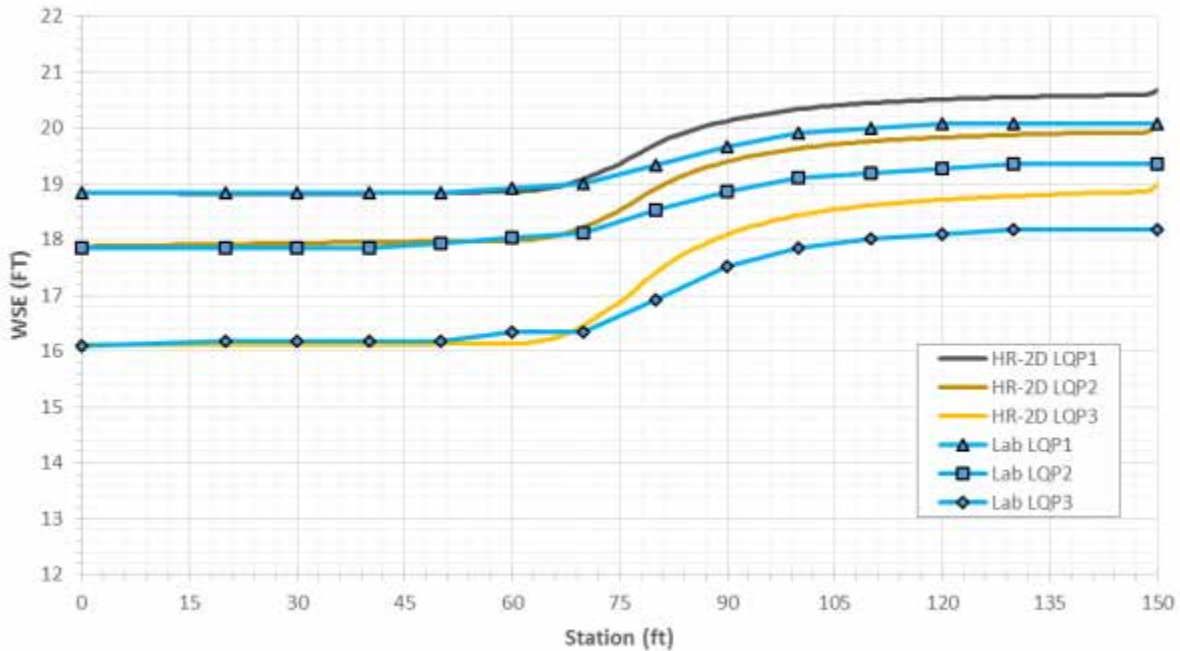


Figure 6.13: Lab and HEC-RAS 2D Full Momentum Equation Model Results for Type One Bridge Configuration and 3620 cfs

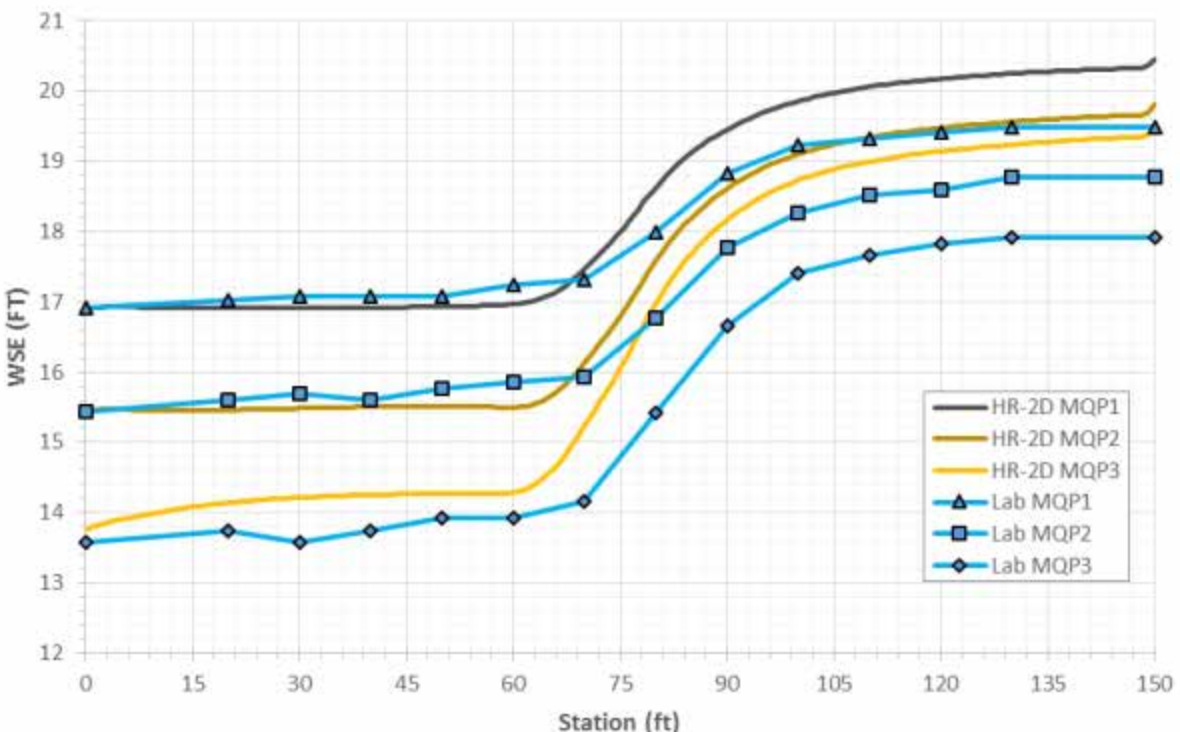


Figure 6.14: Lab and HEC-RAS 2D Full Momentum Equation Model Results for Type One Bridge Configuration and 4400 cfs

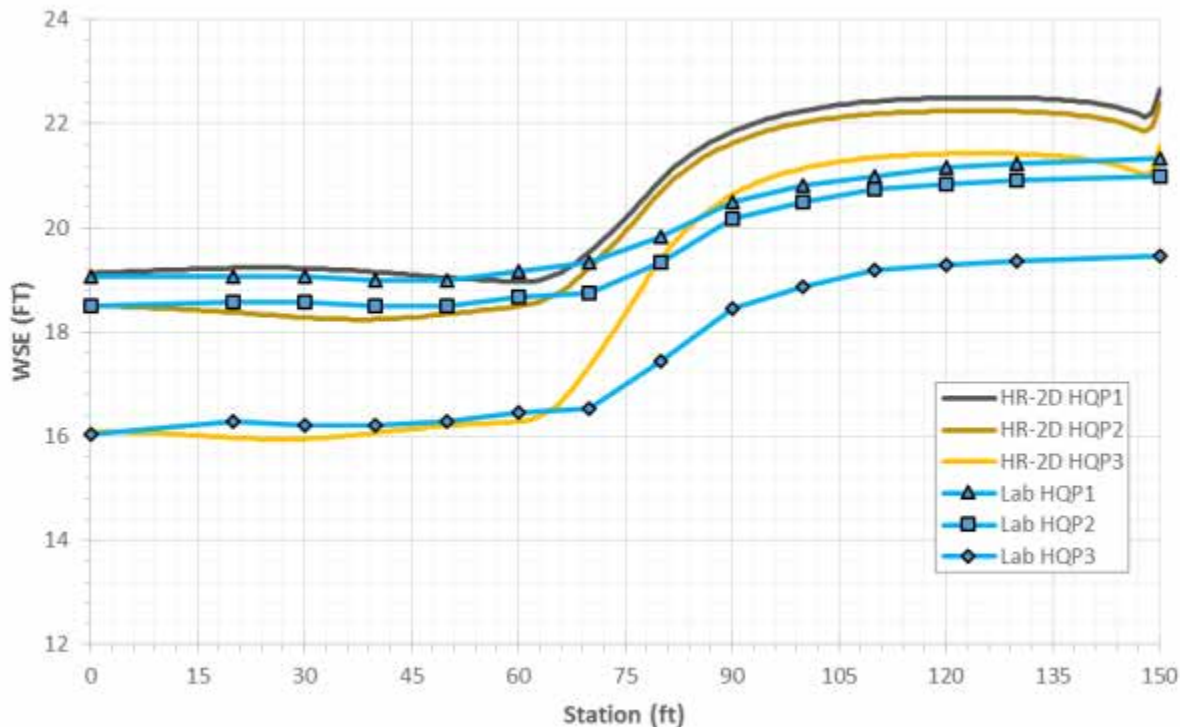


Figure 6.15: Lab and HEC-RAS 2D Full Momentum Equation Model Results for Type One Bridge Configuration and 5600 cfs

The profiles in Figures 6.13 to 6.15 show that the HEC-RAS 2D models, when solving the full momentum equations, display the relationship observed in the lab—that, for a given discharge, an increase in the tailwater should result in a higher depth upstream of the bridge. However, while the HEC-RAS 2D models show this trend, the actual values generated do not agree with those observed in the flume. In fact, HEC-RAS 2D overestimates the headwater in every single case. For the lowest discharge (Figure 6.13), the simulated profiles show almost the same sensitivity to tailwater depth as the physical flume model, yet the actual values for the headwater depths are much higher than seen in the flume; the middle HEC-RAS-2D profile has approximately the same headwater depth as the highest seen in the lab. For the middle discharge (Figure 6.9), the steps upwards in headwater depth from the HEC-RAS 2D simulations are somewhat similar to those from the lab, but the lowest headwater depth from the simulations is almost the same as the highest from the lab. For the highest discharge (Figure 6.15), the same pattern between profiles exists: the headwater depths between the profiles that correspond to the highest and the middle tailwater depths are much more similar than those between profiles for

the middle and lowest tailwater depths. Again, however, the lowest headwater depth seen in the HEC-RAS 2D results is nearly the same as the highest value from the flume (only slightly lower).

It was considered that increasing the EGL at the inlet would work to reduce the discrepancy between the HEC-RAS 2D and the lab values, allowing the flow to enter the model at a lower depth and a higher velocity. This adjustment was not expected to solve the problem, as it would likely only introduce new problems; an initial test revealed that this was indeed true. Figure 6.16 shows the results for the final timestep of one test case.

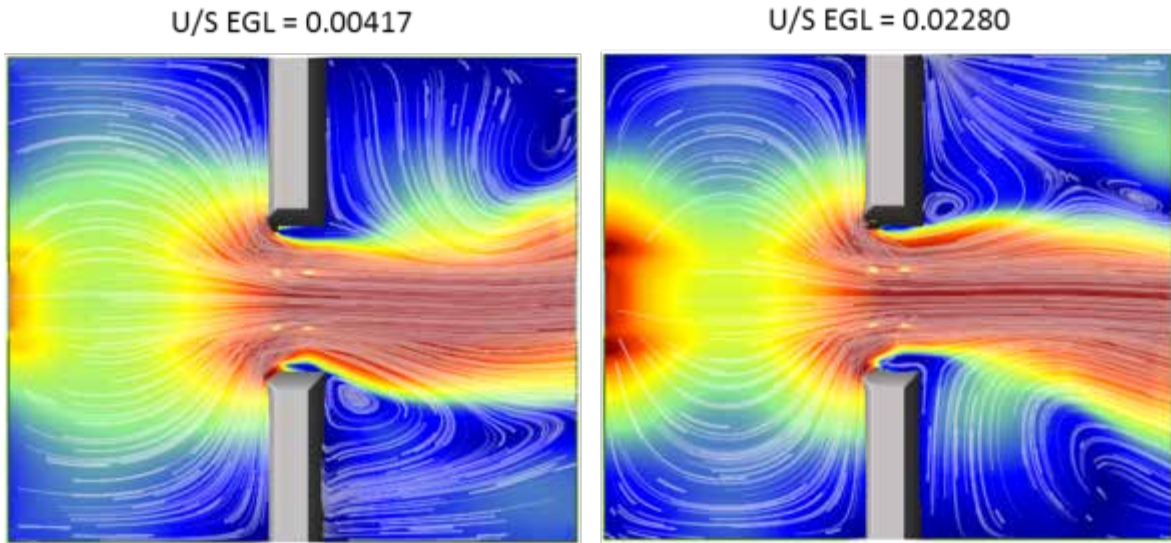


Figure 6.16: Velocity Contour Maps Ranging for 0 to 15 fps with Tracers for the Third High Discharge Profile Using Two Different Upstream EGLs

The image on the left side of Figure 6.16 shows the results from the simulation included as the “HR-2D HQP3” series in Figure 6.15. The image on the right shows a test case using a much higher upstream EGL, obtained by dividing the change in depth across the entire reach by the length of the reach. The lowest velocities are represented by dark blue and the highest by dark red. The tracers for the simulation represented in the image on the right show a very unusual and unrealistic flow pattern that spreads rapidly out from the main channel near the inlet and then converges again to pass through the bridge opening. This flow pattern resulted in a lower depth

at the inlet, but only in the main channel; in the corners of the model at the inlet, the depths were actually higher for the test case with the EGL equal to 0.02280.

The HEC-RAS 2D full momentum simulations represented in Figures 6.13 to 6.15 all gave very realistic flow patterns downstream of the bridge, where once steady state conditions had been reached at the maximum discharge for a given profile, the flow instability known as vortex shedding began to occur. This was evidenced by the oscillation of the downstream flow from side to side. The higher the discharge, the more pronounced the oscillation of this downstream flow became, and it increased even more for the same discharge when the tailwater was lower.

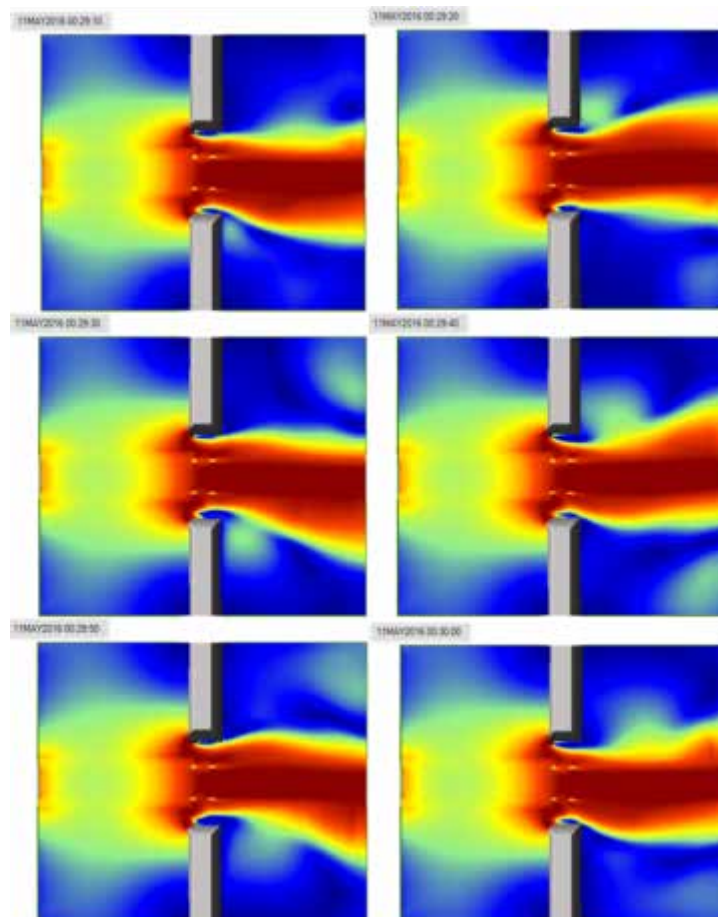


Figure 6.17: Time Series of Velocity Contour Maps Ranging from 0 to 15 fps for the Second Middle Discharge Profile

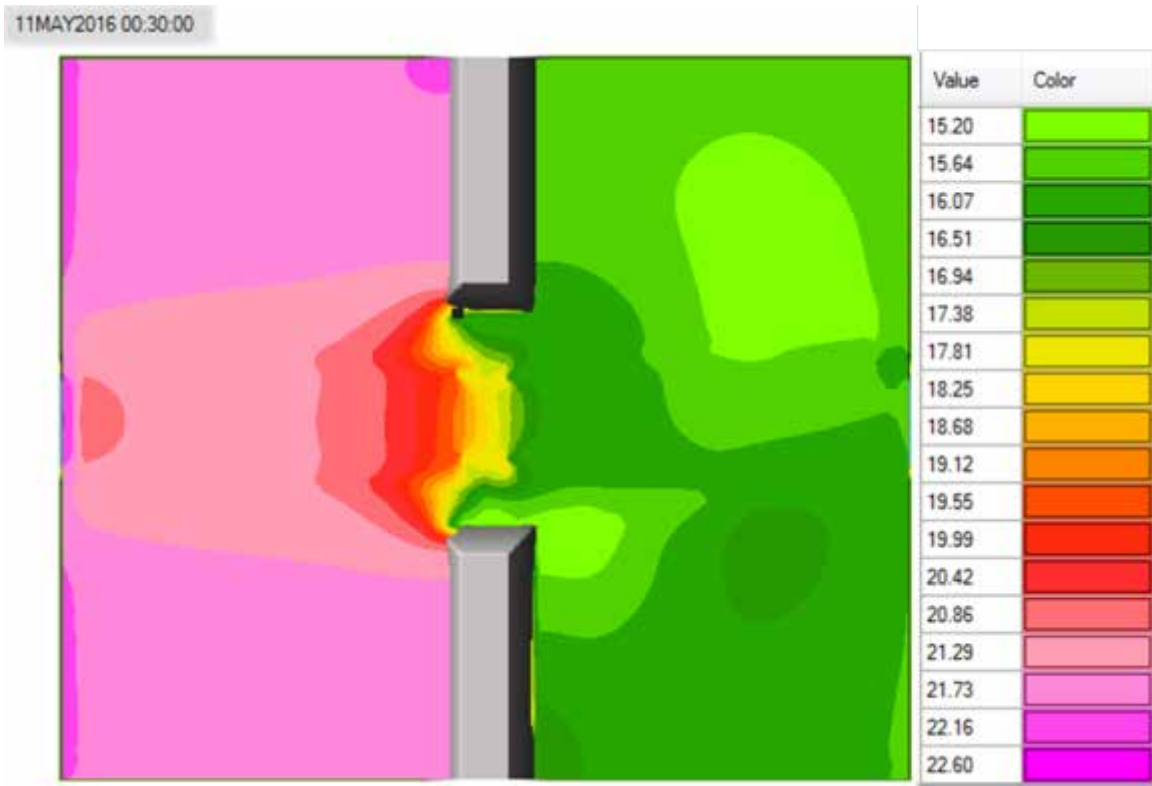


Figure 6.18: Water Surface Elevation Contour Map for the Final Timestep of the Second Middle Discharge Profile

One of the most challenging parts of using HEC-RAS 1D to model bridge openings is the placement of ineffective flow areas. The *HEC-RAS River Analysis System Hydraulic Reference Manual* (Brunner, 2016a) contains some guidance for establishing where these should be placed, depending on the expansion and contraction ratios assumed for the incoming and outgoing flow at the bridge. In the manual, the guidelines for selecting an acceptable range within which the actual ratios might fall suggests that these values are a function of the ratio of the Manning's roughness coefficient of the overbank to that of the main channel, the ratio of the bridge opening width to the total floodplain width, and the longitudinal slope of the channel. Some difficulty arises in that the total width of the floodplain can depend on the contraction and expansion ratios used in the model. Due to this difficulty, the values for the contraction and expansion ratios are often approximated as 1 and 2, respectively. Figure 6.19 shows the results of one simulation for these bridge tests that demonstrates these ratios. This profile, however, was the only one with these typical values.

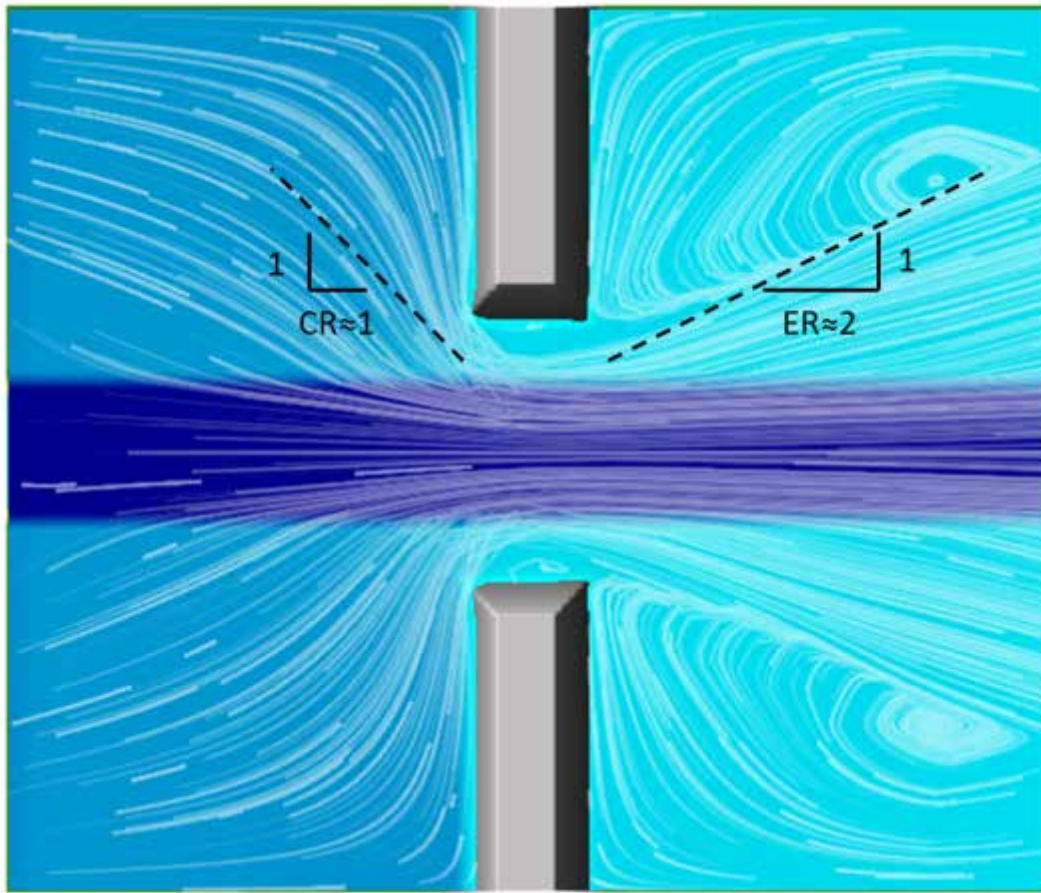


Figure 6.19: Depth Map with Tracers for the Second Middle Discharge Profile Showing Typical Expansion and Contraction Ratios

While the behavior upstream of the bridge was very similar for all profiles, the flow expansion witnessed for the lower discharge profiles was much less pronounced (with almost no expansion occurring) than shown in Figure 6.19. For the highest discharge profiles, though, the expansion was quite drastic. Thus, this shows a case where a simple 2D model may be used to inform a 1D one, if such a thing were desirable.

6.3 SRH-2D Model of Type One Bridge from Flume Study (Short Model)

The SRH-2D mesh generated in SMS (visible in Figure 6.20) contained elements of various size and shape. The number of elements was densest near the piers and wherever else flow velocities were expected to be highest. There was a combination of both triangles and quadrilaterals. The total quantity of elements was 16,183, with an average cell size of 1.13 square

ft, a maximum of 8.84 square ft (found in one of the corners of the model space), and a minimum of 0.02 square ft (found adjacent to one of the piers). It was necessary to draw and enforce breaklines with the correct elevations after mesh generation to properly define the high and low points of the sidewalls of the main channel and to force mesh elements to have the proper elevations near the piers.

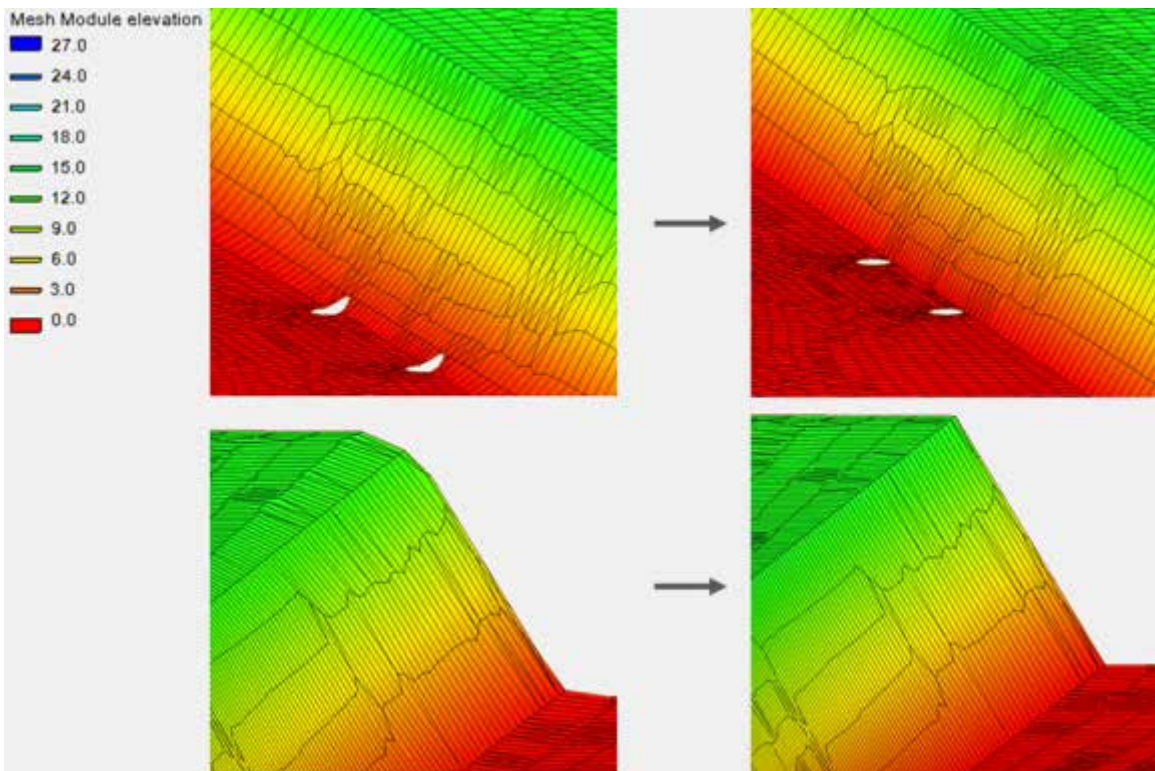


Figure 6.20: Before and After Manual Mesh Adjustment for SRH-2D Bridge Flume Model

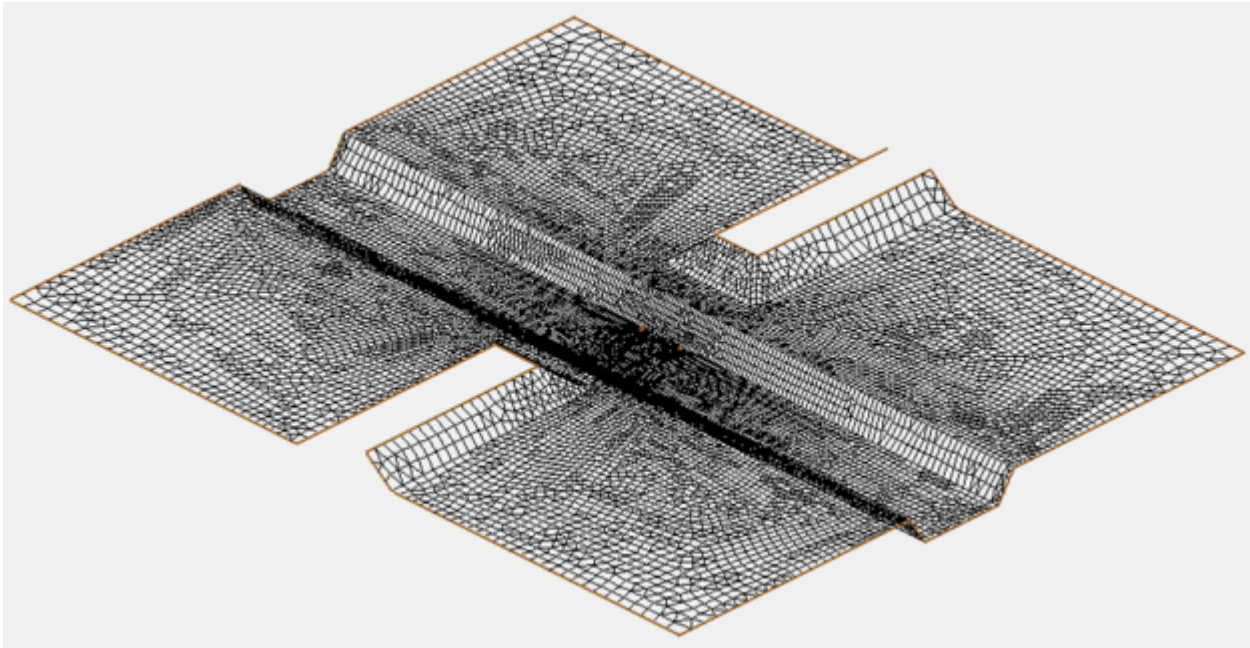


Figure 6.21: Oblique View from SMS 12.1 of the SRH-2D Computational Mesh Used for Type One Bridge Flume Simulations

Once the mesh was suitably defined, it was simple to set up the boundary conditions and simulation parameters for each discharge (distributed at the inlet using the conveyance method) and their respective tailwater depths. Every simulation used a timestep of 0.05 seconds and required approximately 2 hours to run to completion. Figures 6.22 to 6.24 show the results of these tests using the output from the final timestep at 30 minutes of simulation time.

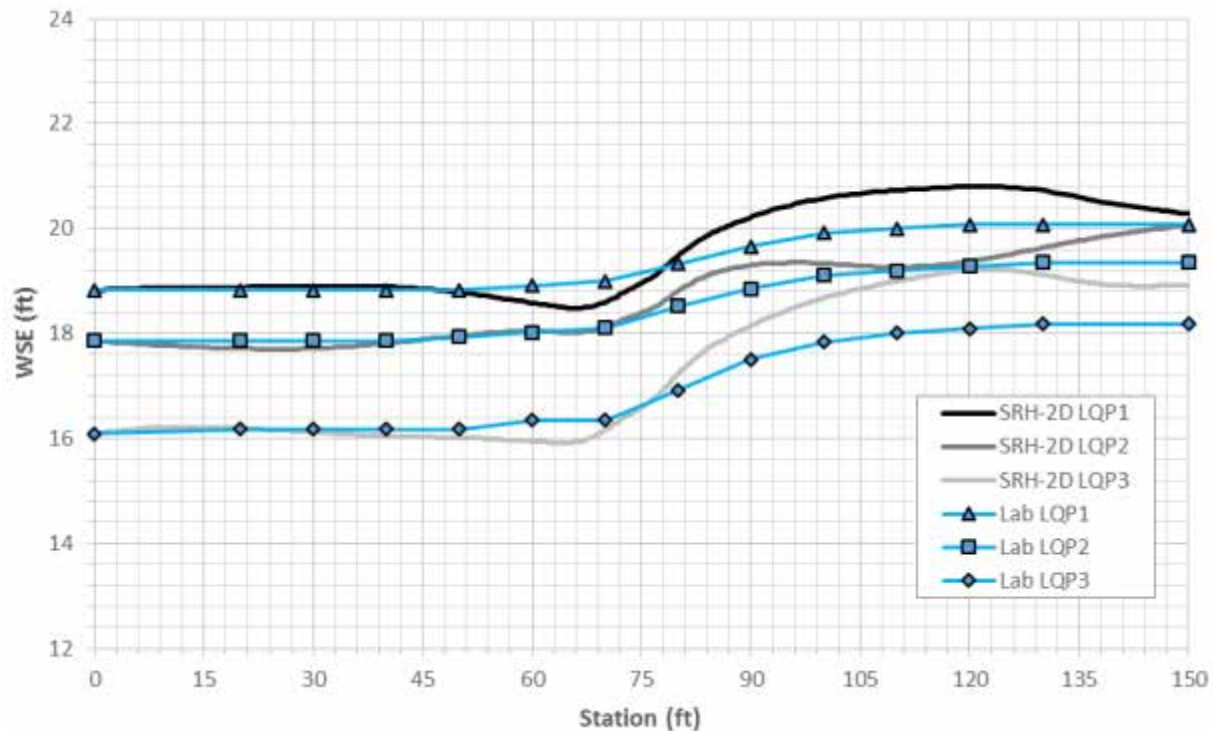


Figure 6.22: Lab and SRH-2D Model Results for Type One Bridge Configuration and 3620 cfs

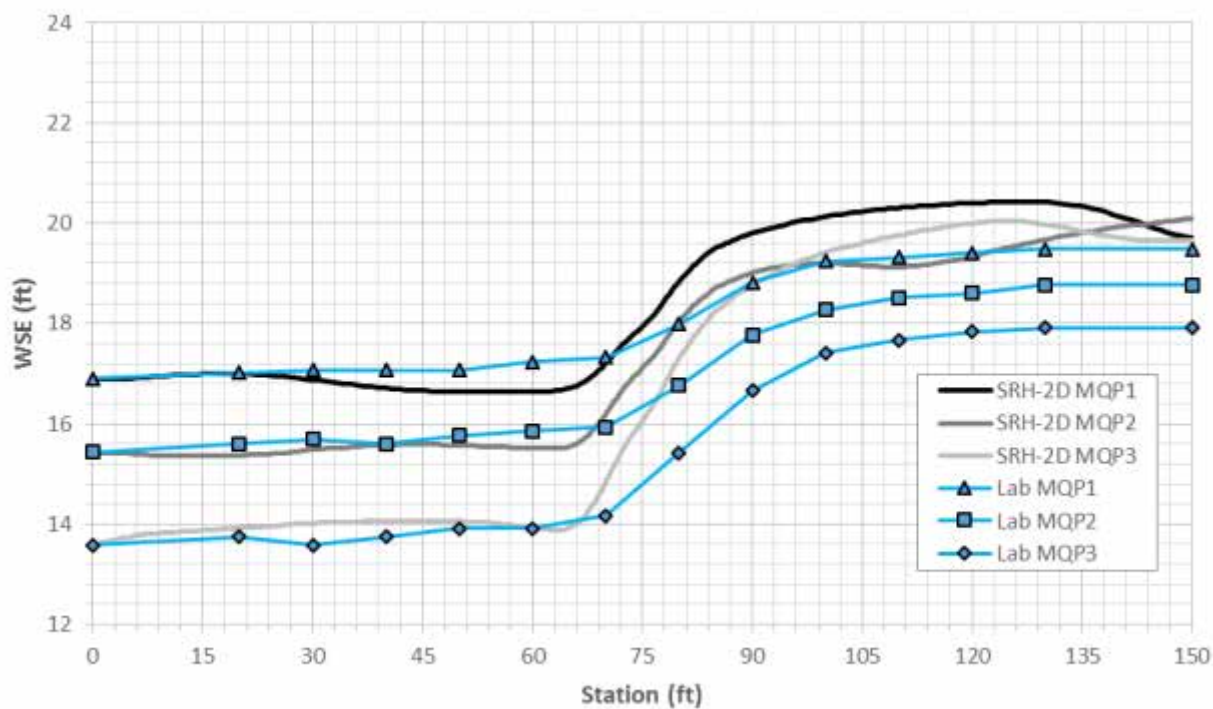


Figure 6.23: Lab and SRH-2D Model Results for Type One Bridge Configuration and 4400 cfs

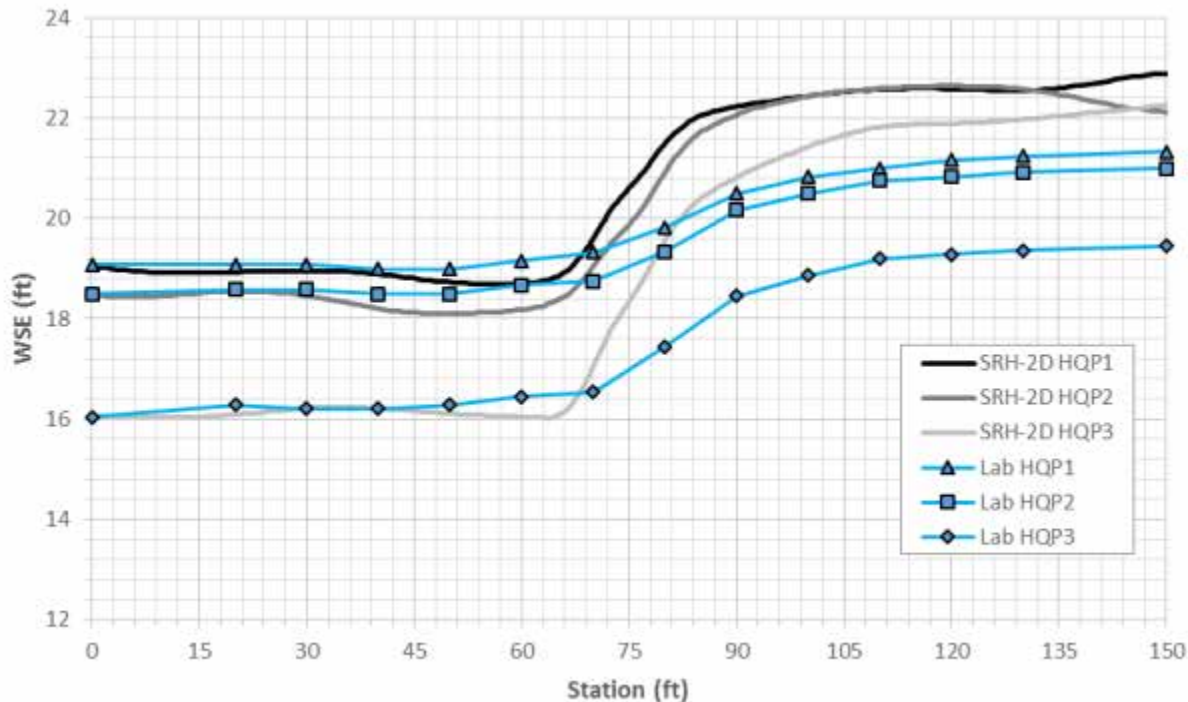


Figure 6.24: Lab and SRH-2D Model Results for Type One Bridge Configuration and 5600 cfs

It is difficult to determine from Figures 6.22 to 6.24 whether the SRH-2D results show any clear relationship between headwater and tailwater depth for a given discharge. Only the results from the lowest discharge trials (Figure 6.22) appear to adhere to the pattern that a higher tailwater depth for the same discharge results in a greater headwater depth. The results from the middle and highest discharge trials (Figures 6.23 and 6.24) suggest that both the expected result and its opposite might be possible—indicating that no pattern exists at all.

The reason for this outcome is a peculiar flow pattern witnessed for every trial with SRH-2D. Whereas one would expect the flow upstream of the bridge to be relatively stable over time and the downstream flow to oscillate due to vortex shedding (a result seen in the HEC-RAS 2D simulations), strangely, for the SRH-2D simulations, the upstream flow oscillated back and forth.

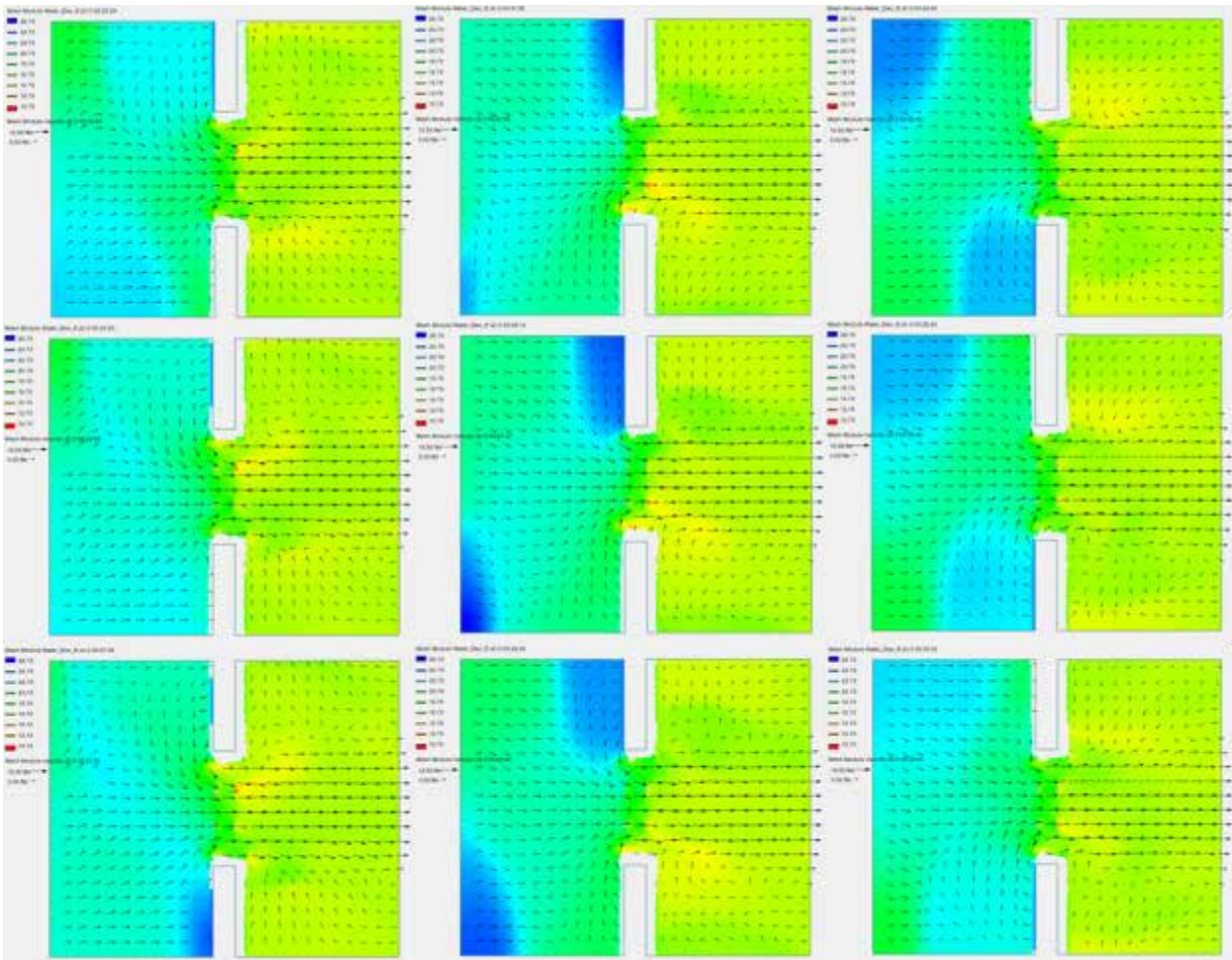


Figure 6.25: Time Series Showing Water Surface Elevation for the Third High Discharge Profile SRH-2D Simulation

The oscillating flow shown in Figure 6.25 had a period approximately equal to the output mapping interval of 0.02 hours (1 minute 12 seconds) or possibly some smaller multiple of this time. For this reason, the depth was averaged for the duration ranging from 15 minutes 36 seconds to the end of the simulation at 30 minutes. The flows were considered to have reached steady state after reaching their peak discharges at 15 minutes; this was confirmed by visual inspection of the model results, and by considering that in the 36 seconds that elapsed between when the discharges peaked and the timestep when the data for this averaging process began, the flow in the main channel would need to be travelling at about 4.17 fps to traverse the entire 150-ft length from inlet to exit. This criteria was easily satisfied by the model results.

Table 6.6: Results for Averaging Process at the Most Upstream Point for SRH-2D Bridge Flume Simulations

| Time (min:sec) | Depth (ft) | | | | | | | | |
|-------------------|---------------|-------|-------|-------|-------|-------|-------|-------|-------|
| | LQP1 | LQP2 | LQP3 | MQP1 | MQP2 | MQP3 | HQP1 | HQP2 | HQP3 |
| 15:36 | 20.27 | 19.39 | 18.61 | 20.56 | 19.75 | 19.73 | 23.14 | 22.23 | 21.12 |
| 16:48 | 20.69 | 19.99 | 18.91 | 20.58 | 19.98 | 19.63 | 23.03 | 22.53 | 22.42 |
| 18:00 | 20.25 | 19.82 | 18.71 | 20.60 | 20.02 | 19.32 | 22.91 | 22.68 | 22.05 |
| 19:12 | 20.70 | 19.84 | 18.87 | 20.60 | 19.16 | 18.91 | 22.42 | 22.75 | 21.92 |
| 20:24 | 20.55 | 20.00 | 18.98 | 20.58 | 20.09 | 19.26 | 22.24 | 22.81 | 22.26 |
| 21:36 | 20.23 | 19.43 | 18.44 | 20.54 | 19.95 | 19.57 | 22.99 | 22.87 | 21.50 |
| 22:48 | 20.70 | 19.95 | 18.91 | 20.47 | 19.68 | 19.77 | 23.33 | 22.94 | 22.41 |
| 24:00 | 20.27 | 19.99 | 18.86 | 20.38 | 20.02 | 19.83 | 23.22 | 23.03 | 22.17 |
| 25:12 | 20.69 | 19.64 | 18.76 | 20.28 | 19.63 | 19.81 | 23.07 | 23.09 | 21.32 |
| 26:24 | 20.56 | 19.97 | 18.97 | 20.16 | 20.03 | 19.76 | 22.96 | 23.04 | 22.41 |
| 27:36 | 20.20 | 19.68 | 18.31 | 20.02 | 19.99 | 19.77 | 22.60 | 22.85 | 22.01 |
| 28:48 | 20.70 | 19.89 | 18.92 | 19.85 | 19.27 | 19.76 | 22.17 | 22.53 | 22.11 |
| 30:00 | 20.29 | 20.06 | 18.93 | 19.71 | 20.09 | 19.65 | 22.88 | 22.12 | 22.26 |
| AVG (ft): | 20.47 | 19.82 | 18.78 | 20.33 | 19.82 | 19.60 | 22.84 | 22.73 | 22.00 |
| TW (ft) | 18.83 | 17.86 | 16.09 | 16.90 | 15.43 | 13.58 | 19.08 | 18.50 | 16.03 |

After accounting for the oscillating depth at the upstream point, it becomes clear that the relationship between the headwater and tailwater depths holds true for the SRH-2D simulations as well. Like HEC-RAS 2D, however, SRH-2D overestimates the depths of flow at the upstream cross section. The steps between profiles produced by SRH-2D also follow trends similar to those seen in the lab data: the steps are fairly uniform for the low and medium discharges, and then for the highest discharge, the difference between the highest and middle headwater depths are much more similar than the middle and the lowest values.

One detail of interest in the hydraulics of channel constrictions is the assumption, made in many 1D analyses, that inlet control exists at the entrance of bridges and culverts. This assumption was likely to blame for the dubious results given by the previous version of HEC-RAS and discussed in the previous report. The assumption does not, however, appear to be so unfounded in the latest 1D bridge routines employed by HEC-RAS. Inlet control depends on the existence of critical depth at the upstream bridge cross section, and while for simple geometries it is perfectly valid to assume inlet control, for complex geometries it will likely not completely apply. Currently the RAS Mapper portion of the HEC-RAS software is not capable of mapping the spatial variation of the Froude number for a given simulation. SMS 12.1, however, is capable

of mapping these results of an SRH-2D simulation. Figure 6.26 shows the Froude number in the vicinity of the bridge opening for one profile.

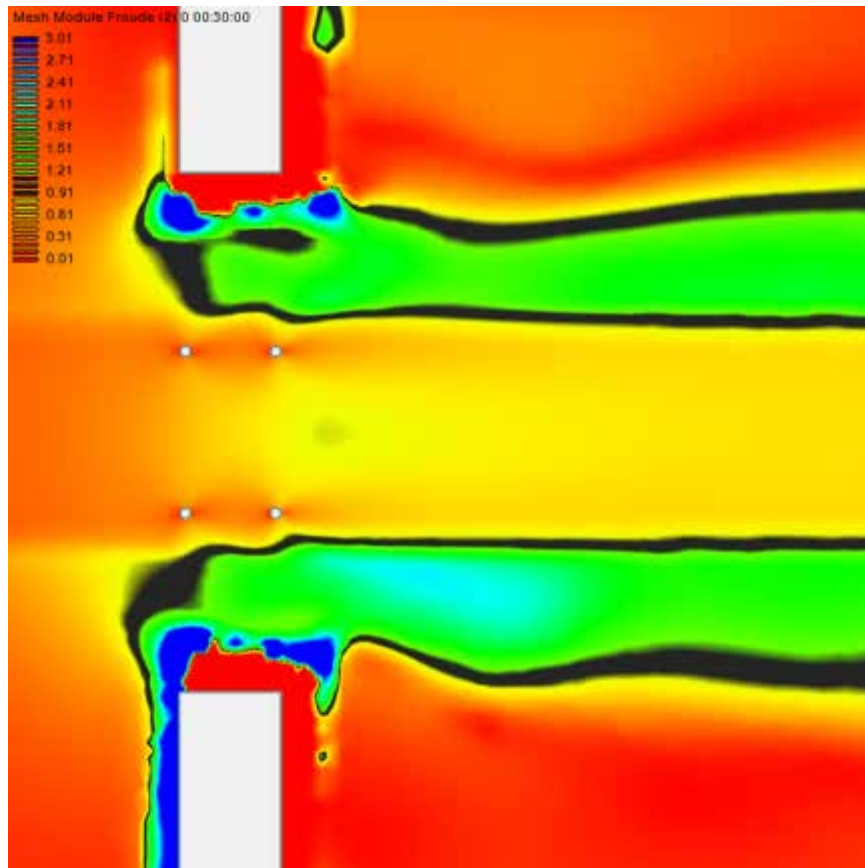


Figure 6.26: Froude Number Contour Map from SMS 12.1 for the Third High Discharge Profile SRH-2D Simulation

In Figure 6.26, Froude numbers greater than or equal to 0.91 yet less than or equal to 1.11 are represented by the color black, and thus are either critical or near critical depth; red to yellow hues represent subcritical flow; and green to blue represent supercritical flow. Therefore, given that subcritical flow is controlled from downstream and supercritical flow from upstream, it seems reasonable that for this section, which experiences both flow regimes, flow should be at least partially controlled from downstream.

6.4 Summary of Water Surface Profiles for the Type One Bridge Experiments

Table 6.7 shows that the HEC-RAS 2D full momentum results and the SRH-2D results differ only slightly from each other, but both models overestimated the headwater depth in every case. Remarkably, the HEC-RAS 1D model (which did take the greatest level of expertise to develop) gave answers most similar to those found in the lab. For the middle discharge, however, the 1D model still shows a slight insensitivity to the tailwater depth, as suggested by the total lack of change for the headwater depths between Profiles 2 and 3. While the HEC-RAS 1D results occasionally underestimate and other times overestimate, they are always rather close to the observed headwater depths; the 2D models, on the other hand, both always overestimate the values. The magnitude of their overestimation increases along with discharge. For a given discharge, the overestimation increases as tailwater decreases, and it is always comparable between HEC-RAS 2D and SRH-2D. Thus, the best agreement occurs at the lowest discharge for the highest tailwater depth, with a 3.0% and a 1.9% overestimation by the HEC-RAS 2D and SRH-2D models, respectively, and the greatest deviation from the lab data occurs at the highest discharge with the lowest tailwater depths, with an 11.0% and a 13.1% overestimate by each model. All models seem to agree fairly well at the low discharges, but their ability to accurately reproduce the lab results diminishes as discharge increases. This pattern is not as distinct for the 1D model, but for both 2D models, the pattern is completely supported by the results, with SRH-2D performing slightly better than HEC-RAS 2D at the lowest discharge and the opposite occurring at the highest discharge.

Based upon a measured Manning's roughness coefficient of 0.0141 from the flume tests, Froude number similarity was used to determine the prototype coefficient of 0.0233 that was used in all HEC-RAS 1D models in the previous study and subsequently in all 2D models discussed in this report. The dimensional scaling based on the Froude number similarity depends on the depth and velocity of the flow, and thus the Manning's roughness coefficient should vary with the discharge as well as from one profile to the next. The following section investigates the impact of varying the roughness coefficient for the 2D models using the same discharge and profile as corresponds to the 1D results that already agree with the laboratory value for the headwater depth in order to match the 2D results to the headwater depth observed in the lab.

Table 6.7: Summary of Water Surface Profiles for the Type One Bridge Experiments

| Flow | Profile | Tailwater | Headwater (ft) | | | HW-TW (ft) | | | (HW-TW)/L | | | | | | | | |
|------|---------|-----------|-------------------|-------|-------|---------------|----------------------|-------|-----------|------|----------------------|-------|--------|-------|----------------------|-------|--------|
| | | | (cfs) | - | (ft) | Lab | HR 5.0 - 1D (GWB) | HR-2D | SRH-2D* | Lab | HR 5.0 - 1D (GWB) | HR-2D | SRH-2D | Lab | HR 5.0 - 1D (GWB) | HR-2D | SRH-2D |
| 3620 | 1 | 18.83 | 20.08 | 19.78 | 20.68 | 20.47 | 1.25 | 0.95 | 1.85 | 1.64 | 0.008 | 0.006 | 0.012 | 0.011 | | | |
| 3620 | 2 | 17.86 | 19.36 | 18.99 | 20.03 | 19.82 | 1.50 | 1.13 | 2.17 | 1.96 | 0.010 | 0.008 | 0.014 | 0.013 | | | |
| 3620 | 3 | 16.09 | 18.18 | 17.89 | 18.98 | 18.78 | 2.09 | 1.80 | 2.89 | 2.69 | 0.014 | 0.012 | 0.019 | 0.018 | | | |
| 4400 | 1 | 16.90 | 19.49 | 19.24 | 20.46 | 20.33 | 2.59 | 2.34 | 3.56 | 3.43 | 0.017 | 0.016 | 0.024 | 0.023 | | | |
| 4400 | 2 | 15.43 | 18.77 | 18.77 | 19.81 | 19.82 | 3.34 | 3.34 | 4.38 | 4.39 | 0.022 | 0.022 | 0.029 | 0.029 | | | |
| 4400 | 3 | 13.58 | 17.91 | 18.77 | 19.50 | 19.60 | 4.33 | 5.19 | 5.92 | 6.02 | 0.029 | 0.035 | 0.039 | 0.040 | | | |
| 5600 | 1 | 19.08 | 21.33 | 21.65 | 22.65 | 22.84 | 2.25 | 2.57 | 3.57 | 3.76 | 0.015 | 0.017 | 0.024 | 0.025 | | | |
| 5600 | 2 | 18.50 | 21.00 | 21.41 | 22.39 | 22.73 | 2.50 | 2.91 | 3.89 | 4.23 | 0.017 | 0.019 | 0.026 | 0.028 | | | |
| 5600 | 3 | 16.03 | 19.45 | 20.78 | 21.59 | 22.00 | 3.42 | 4.75 | 5.56 | 5.97 | 0.023 | 0.032 | 0.037 | 0.040 | | | |

*Average overtime at steady state conditions

| Flow | Profile | Tailwater | (HW - Lab HW)/Lab HW * 100% | | | ΔHW | | | $\Delta HW/\Delta TW$ | | | | |
|-------|---------|-----------|-----------------------------|-------|--------|-------------|----------------------|-------|-----------------------|-------|----------------------|-------|--------|
| | | | (ft) | | | (ft) | | | (ft) | | | | |
| (cfs) | - | (ft) | HR 5.0 - 1D (GWB) | HR-2D | SRH-2D | Lab | HR 5.0 - 1D (GWB) | HR-2D | SRH-2D | Lab | HR 5.0 - 1D (GWB) | HR-2D | SRH-2D |
| 3620 | 1 | 18.83 | -1.5% | 3.0% | 1.9% | - | - | - | - | - | - | - | - |
| 3620 | 2 | 17.86 | -1.9% | 3.5% | 2.4% | 0.25 | 0.18 | 0.31 | 0.32 | -0.26 | -0.19 | -0.32 | -0.33 |
| 3620 | 3 | 16.09 | -1.6% | 4.4% | 3.3% | 0.59 | 0.67 | 0.72 | 0.73 | -0.33 | -0.38 | -0.41 | -0.41 |
| 4400 | 1 | 16.90 | -1.3% | 5.0% | 4.3% | - | - | - | - | - | - | - | - |
| 4400 | 2 | 15.43 | 0.0% | 5.5% | 5.6% | 0.75 | 1.00 | 0.82 | 0.96 | -0.51 | -0.68 | -0.56 | -0.65 |
| 4400 | 3 | 13.58 | 4.8% | 8.9% | 9.4% | 1.00 | 1.85 | 1.54 | 1.63 | -0.54 | -1.00 | -0.83 | -0.88 |
| 5600 | 1 | 19.08 | 1.5% | 6.2% | 7.1% | - | - | - | - | - | - | - | - |
| 5600 | 2 | 18.50 | 2.0% | 6.6% | 8.3% | 0.25 | 0.34 | 0.32 | 0.47 | -0.43 | -0.59 | -0.55 | -0.81 |
| 5600 | 3 | 16.03 | 6.8% | 11.0% | 13.1% | 0.92 | 1.84 | 1.67 | 1.74 | -0.37 | -0.74 | -0.68 | -0.70 |

6.5 Calibration of the Two-Dimensional Models to the Laboratory Results (Short Model)

The trial selected for calibration purposes was the second profile of the middle discharge, with a discharge of 4400 cfs and a tailwater depth of 15.43 ft. This profile was selected because the 1D results showed the same headwater depth as the laboratory model. Because of this and the fact that it used the middle tailwater depth with middle discharge, it was considered fairly representative of all trials. The point selected for comparison was one along the channel centerline 90 ft upstream from the downstream boundary, 4.4 ft upstream from the toe of the upstream embankment. The laboratory value for depth at this point was 17.77 ft.

The Manning's roughness coefficient was the main parameter adjusted throughout these calibration trials, but one trial using SRH-2D also reduced the parabolic turbulence constant, K , from the default value of 0.7 to 0.1. The eddy viscosity was not adjusted for the HEC-RAS 2D full momentum model because, as stated in Chapter 3, the feature for adjusting this variable currently does not work correctly in HEC-RAS 2D (simulations will fail to run and return an error message if viscosity is adjusted). The newest version of HEC-RAS 2D (v. 5.0.3) does allow the user to adjust the eddy viscosity. This model version was not available for testing at the time

of this report. Four roughness coefficients were examined in addition to the one used in the profile simulations. The five roughness coefficients used were 0.0233, 0.0141 (measured from the flume before dimensional scaling), 0.0050, 0.0010, and 0.0001.

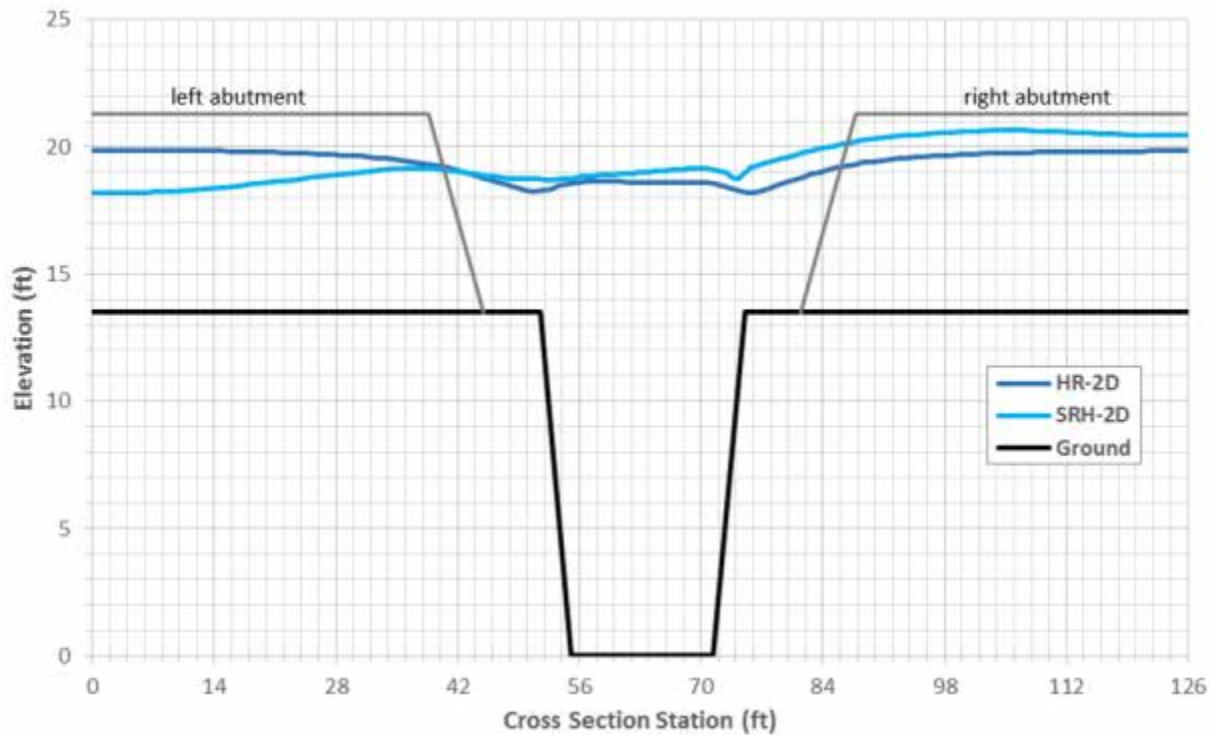


Figure 6.27: Water Surface Profiles at the Cross Section 90 feet Upstream for the Final Timestep of the Profile with a Discharge of 4400 cfs and a Tailwater Depth of 15.43 feet

The SRH-2D profile shown in Figure 6.27 demonstrates the oscillatory flow described for this model in Section 6.3. These results were taken from the final timestep of each simulation, but at the previous timestep (28 minutes and 48 seconds) the SRH-2D results showed that the deeper flow was on the left side of the cross section rather than the right. The HEC-RAS 2D profile is mostly symmetrical around the longitudinal axis along the stream centerline, but the water surface undulates up and down with respect to time, perhaps due to disturbances propagating upstream related to the vortex shedding downstream of the bridge. The conditions upstream of the bridge determined from the HEC-RAS 2D simulations were, however, much more stable than those determined from SRH-2D.

To account for the transient nature of the flow at steady state conditions, the water surfaces at the selected point were averaged over time using data points collected at discrete times, as was done for the upstream point in SRH-2D (Section 6.3). From the SRH-2D models data existed every 1 minute 12 seconds, and so every point available from 15 minutes 36 seconds to 30 minutes was used. The HEC-RAS 2D models had data available every 10 seconds, but values were only taken every 1 minute starting at 16 minutes and continuing until 30 minutes. This was regarded as appropriate because the depth of flow only varied slightly with time, and because of the rather manual process for retrieving the water depth at the desired point from RAS Mapper, the extra effort required to use all available data would not have been worthwhile. A point was created at the desired location upstream of the bridge in ArcMap, and this shapefile was imported into both SMS and RAS Mapper. In SMS an entire time series for the observation point could be easily extracted and then copied and pasted into Excel, while the data from HEC-RAS 2D had to be mapped to the point separately for each timestep and for all trials; then, that value had to be manually entered into Excel. Figure 6.28 shows an example of the depth written to this point in RAS Mapper for one trial. Tables 6.8 to 6.10 show the data collected including the average depth for each trial.

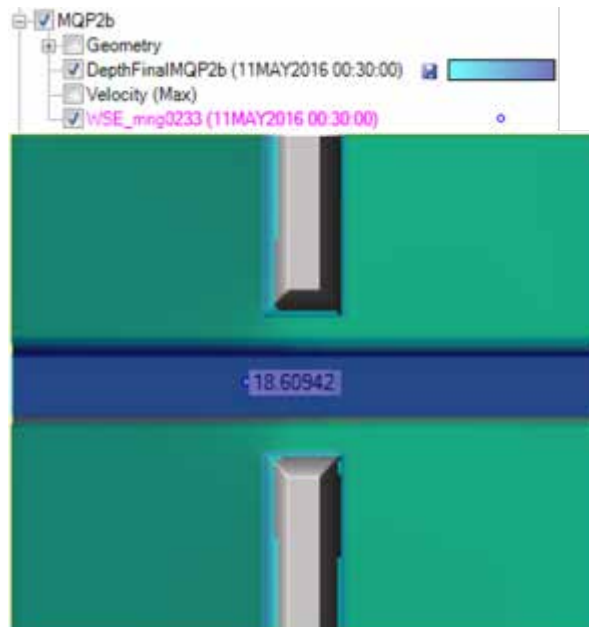


Figure 6.28: Example of Depth at a Discrete Time Mapped to an Observation Point in the RAS Mapper

Table 6.8: HEC-RAS 2D Results for Time-Averaged Depth at a Point Upstream of the Bridge

| Time (min:sec) | n | | | | |
|------------------------|-----------|--------|--------|--------|--------|
| | 0.0233 | 0.0141 | 0.0050 | 0.0010 | 0.0001 |
| | y (ft) | | | | |
| 16:00 | 18.60 | 18.61 | 18.58 | 18.56 | 18.60 |
| 17:00 | 18.60 | 18.60 | 18.56 | 18.56 | 18.55 |
| 18:00 | 18.60 | 18.59 | 18.58 | 18.68 | 18.54 |
| 19:00 | 18.60 | 18.63 | 18.78 | 18.70 | 18.69 |
| 20:00 | 18.61 | 18.67 | 18.57 | 18.57 | 18.64 |
| 21:00 | 18.61 | 18.68 | 18.56 | 18.55 | 18.58 |
| 22:00 | 18.61 | 18.68 | 18.75 | 18.80 | 18.60 |
| 23:00 | 18.61 | 18.68 | 18.66 | 18.58 | 18.63 |
| 24:00 | 18.62 | 18.68 | 18.57 | 18.57 | 18.63 |
| 25:00 | 18.63 | 18.67 | 18.56 | 18.73 | 18.63 |
| 26:00 | 18.64 | 18.66 | 18.78 | 18.67 | 18.62 |
| 27:00 | 18.63 | 18.65 | 18.57 | 18.57 | 18.61 |
| 28:00 | 18.62 | 18.63 | 18.56 | 18.57 | 18.61 |
| 29:00 | 18.61 | 18.62 | 18.75 | 18.78 | 18.61 |
| 30:00 | 18.61 | 18.62 | 18.66 | 18.57 | 18.61 |
| AVG. (ft): | 18.61 | 18.65 | 18.63 | 18.63 | 18.61 |
| Std. Dev. (ft): | 0.01 | 0.03 | 0.09 | 0.09 | 0.04 |

Table 6.9: SRH-2D Results for Time-Averaged Depth at a Point Upstream of the Bridge

| Time (min:sec) | n | | | | | |
|------------------------|-----------|--------|--------|--------|--------|--------|
| | 0.0233 | 0.0141 | 0.0050 | 0.0010 | 0.0001 | 0.0001 |
| | K | | | | | |
| | 0.7 | 0.7 | 0.7 | 0.7 | 0.7 | 0.1 |
| | y (ft) | | | | | |
| 15:36 | 18.74 | 18.06 | 17.89 | 18.10 | 18.10 | 17.89 |
| 16:48 | 18.71 | 18.27 | 17.91 | 18.01 | 18.01 | 18.07 |
| 18:00 | 18.66 | 18.39 | 18.02 | 17.64 | 17.64 | 18.10 |
| 19:12 | 18.69 | 18.27 | 18.06 | 18.24 | 18.24 | 18.18 |
| 20:24 | 18.49 | 18.34 | 17.67 | 17.93 | 17.93 | 17.98 |
| 21:36 | 18.42 | 18.27 | 18.22 | 17.68 | 17.68 | 17.85 |
| 22:48 | 18.50 | 18.10 | 18.03 | 18.11 | 18.11 | 17.76 |
| 24:00 | 18.67 | 18.03 | 17.82 | 17.84 | 17.84 | 17.82 |
| 25:12 | 18.79 | 18.23 | 17.99 | 17.87 | 17.87 | 17.91 |
| 26:24 | 18.74 | 18.41 | 17.99 | 17.92 | 17.92 | 18.00 |
| 27:36 | 18.68 | 18.25 | 18.11 | 17.94 | 17.94 | 18.02 |
| 28:48 | 18.64 | 18.35 | 17.75 | 17.95 | 17.95 | 18.00 |
| 30:00 | 18.69 | 18.29 | 18.27 | 17.82 | 17.82 | 17.90 |
| AVG. (ft): | 18.65 | 18.25 | 17.98 | 17.93 | 17.93 | 17.96 |
| Std. Dev. (ft): | 0.11 | 0.12 | 0.17 | 0.17 | 0.17 | 0.12 |

Table 6.10: Comparison of the Calibration Test Results from Both Two-Dimensional Models to the Laboratory Depth of 17.77 feet

| Model | n | K | y | Simul. y - Lab y |
|-----------------------------|--------|-----|-------|------------------|
| | - | - | (ft) | (ft) |
| HEC-RAS 2D Full Momentum | 0.0233 | - | 18.61 | 0.85 |
| | 0.0141 | - | 18.65 | 0.88 |
| | 0.0050 | - | 18.63 | 0.87 |
| | 0.0010 | - | 18.63 | 0.86 |
| | 0.0001 | - | 18.61 | 0.84 |
| SRH-2D | 0.0233 | 0.7 | 18.65 | 0.88 |
| | 0.0141 | 0.7 | 18.25 | 0.48 |
| | 0.0050 | 0.7 | 17.98 | 0.21 |
| | 0.0010 | 0.7 | 17.93 | 0.16 |
| | 0.0001 | 0.7 | 17.93 | 0.16 |
| | 0.0001 | 0.1 | 17.96 | 0.19 |

The HEC-RAS 2D model showed virtually no sensitivity to the Manning's roughness coefficient used. This is a surprising outcome considering the results discussed in Chapter 3 of this report: the geometry for the test reach discussed in that chapter involved a series of channel constrictions not totally unlike what was being modeled here, and where the model showed a strong sensitivity to the roughness coefficient. The SRH-2D models showed some sensitivity to the roughness coefficient, but even when the coefficient used was as low as 0.0010, the calculated depth still exceeded the laboratory value by 0.16 ft. Further reduction of the roughness coefficient to 0.0001 (10^{-4}) netted no corresponding decrease in the depth, suggesting a bottom limit for the decrease in depth achievable by reducing the Manning's n . An attempt was made to run an SRH-2D simulation using a roughness coefficient equal to 0.00001 (10^{-5}), but the code could not converge on a solution no matter how small the timestep. Since the bulk of the head losses through this reach were local effects associated with the bridge, it was expected that reducing the parabolic turbulence constant, and thus reducing energy dissipation in the eddies, would lead to a corresponding decrease in the depth. However, this was not the case. In fact, the depth increased slightly when a lower value for K was used, seemingly contradicting the results presented in Chapter 3. It is unknown if these results were particular to the discharge and the tailwater depth used, or if similar results would be found by doing this same analysis for one of

the other eight flow profiles discussed in this chapter. It is possible that if the eddy viscosity term could be adjusted in HEC-RAS when performing a 2D analysis with the full momentum equations, then that type of analysis could be an excellent match with the laboratory data. Further investigation may be warranted.

6.6 HEC-RAS 2D Modeling of Type One Bridge Experiments from Flume Study (Long Model)

The results of the short models presented above show impacts of the upstream and downstream boundaries and that the flow downstream from the bridge behaves much like a jet in a confined receiving water. Figure 6.16 in particular shows that the approach flow pattern at the upstream end of the modeled domain is not as straight as one would like to see. Also, downstream from the bridge there is a great deal of recirculation (reverse flow) in the overbanks where the flow is trying to meet the entrainment demand of the high velocity main channel jet. For this reason, the entire 24-ft length of the lab model was simulated by the HEC-RAS 2D version 5.0.3 and SRH-2D models to create models that were more consistent with the actual lab model and achieved better agreement with the laboratory data.

The long models represent the piers by creating a modified terrain in lieu of the high n -value approach used for the short models (both modified terrain and high n -value simulations were compared and results were found to be virtually identical). Figure 6.29 shows the plan view of the terrain created in HEC-RAS 2D and used to assign the pertinent ground characteristics to the grid cells. The terrain was created in HEC-RAS 2D by inputting two raster surfaces: one for the piers at a grid-cell size of 0.01 ft (pier raster) and the other for the model surface including the overbanks, channel, and abutments (land raster). The land raster had a 0.1-ft cell size and was created from the polyline Z shown in Figure 6.30. This was accomplished by first creating a TIN from the polyline Z lines, and then from the TIN, creating the 0.1-ft raster. The extent of the 0.1-ft cell raster was beyond the edges of the 126.7-ft \times 480-ft model area to avoid errors that can occur during grid development in HEC-RAS 2D. Figure 6.31 illustrates the merging of the two different grids within HEC-RAS 2D to create the requisite terrain.

The pier raster is created by using the Mosaic function in ArcGIS to combine a 0.01-ft pier top raster that has a diameter somewhat larger than the actual pier and a 0.01-ft land disk raster larger in diameter than the pier top raster. The pier top raster is greater in diameter than the actual pier to ensure that the HEC-RAS 2D grid cell sides (which align with the edges of the pier) are within the jagged portions of the pier top raster. In this case the diameter of the pier top raster is 1.082 ft, which is 0.04 ft greater than the 1.042-ft diameter pier. Creating the land disk raster entails first creating a rectangular 0.01-ft raster from the TIN in the area of the bridge opening and then using the Extract by Mask function in ArcGIS to obtain the disk raster using circular polygons slightly greater than the pier top raster. Here the diameter of the circular polygons was 1.122 ft, 0.08 ft greater than the pier diameter. The process is illustrated in Figure 6.32, where the size of the land disk raster is greatly exaggerated. Figure 6.33 shows the pier raster used in this study. The bright inner circle is the outline of the 1.042-ft diameter pier.

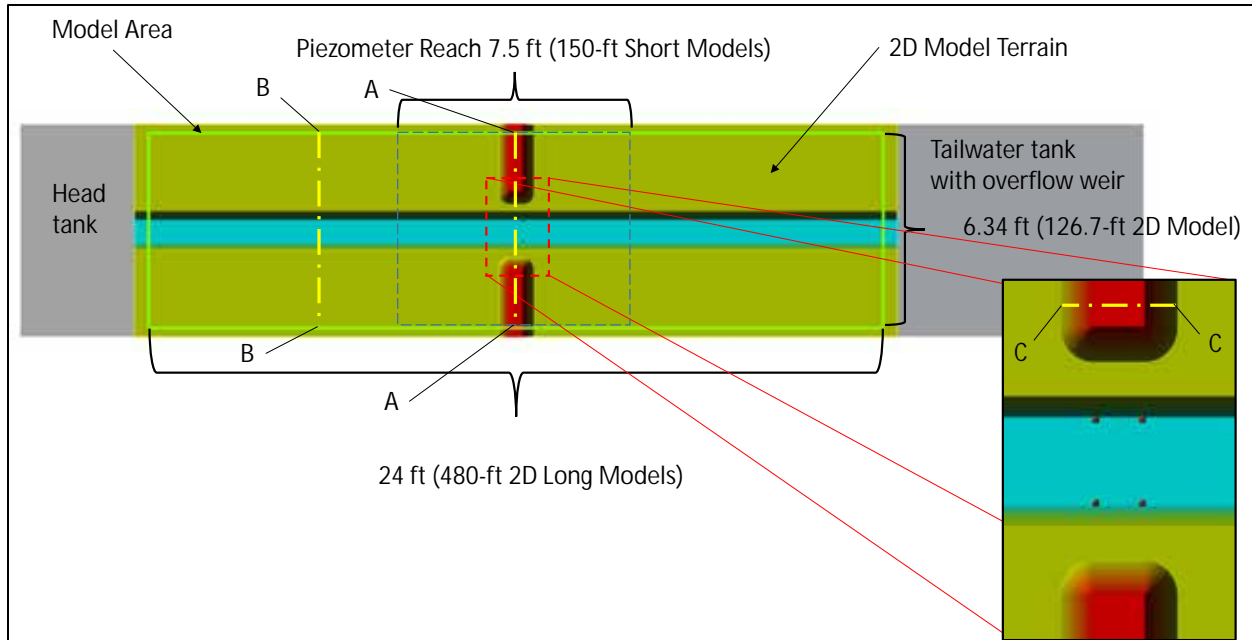


Figure 6.29: HEC-RAS 2D Terrain

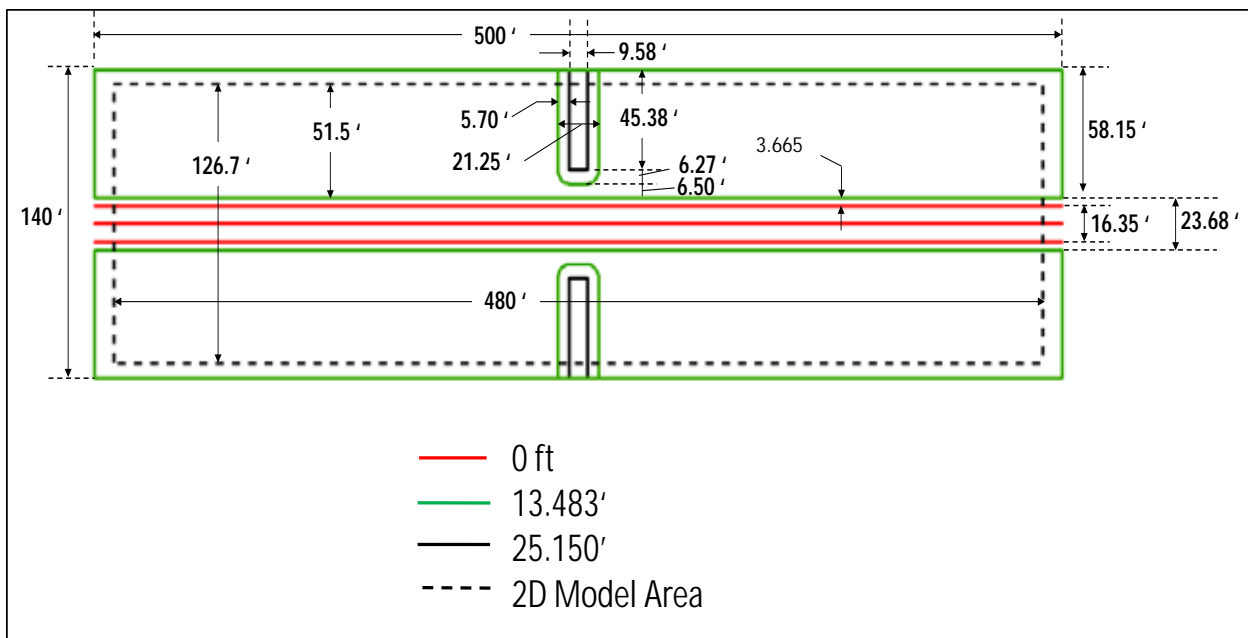


Figure 6.30: Polyline Z Lines in GIS Used to Create the Land Raster

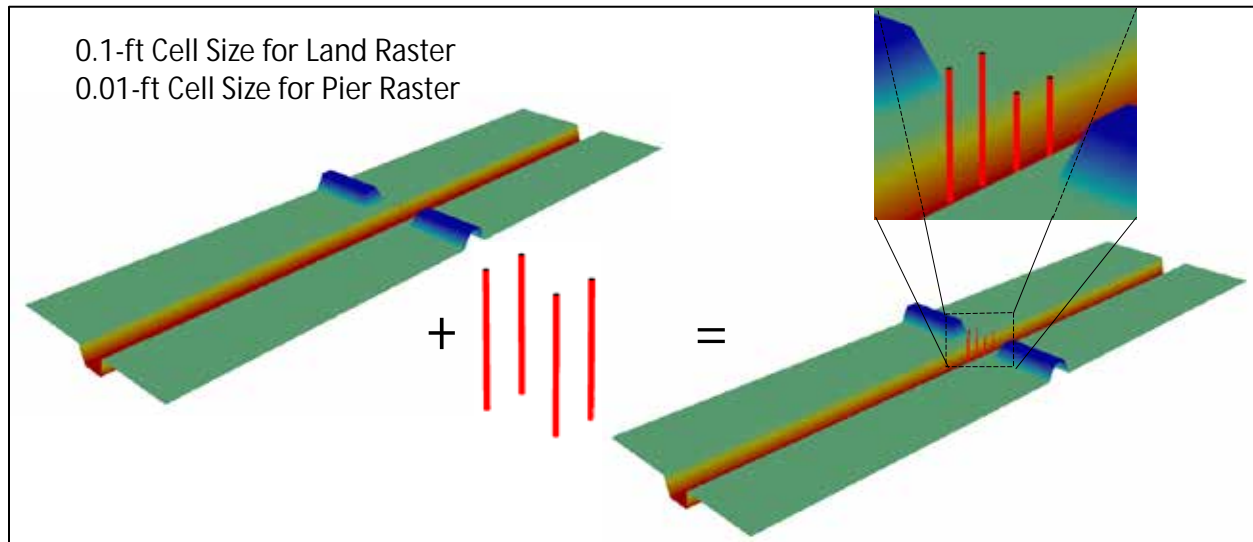


Figure 6.31: ArcScene Illustration of Combining Land and Pier Rasters to Create the HEC-RAS 2D Terrain

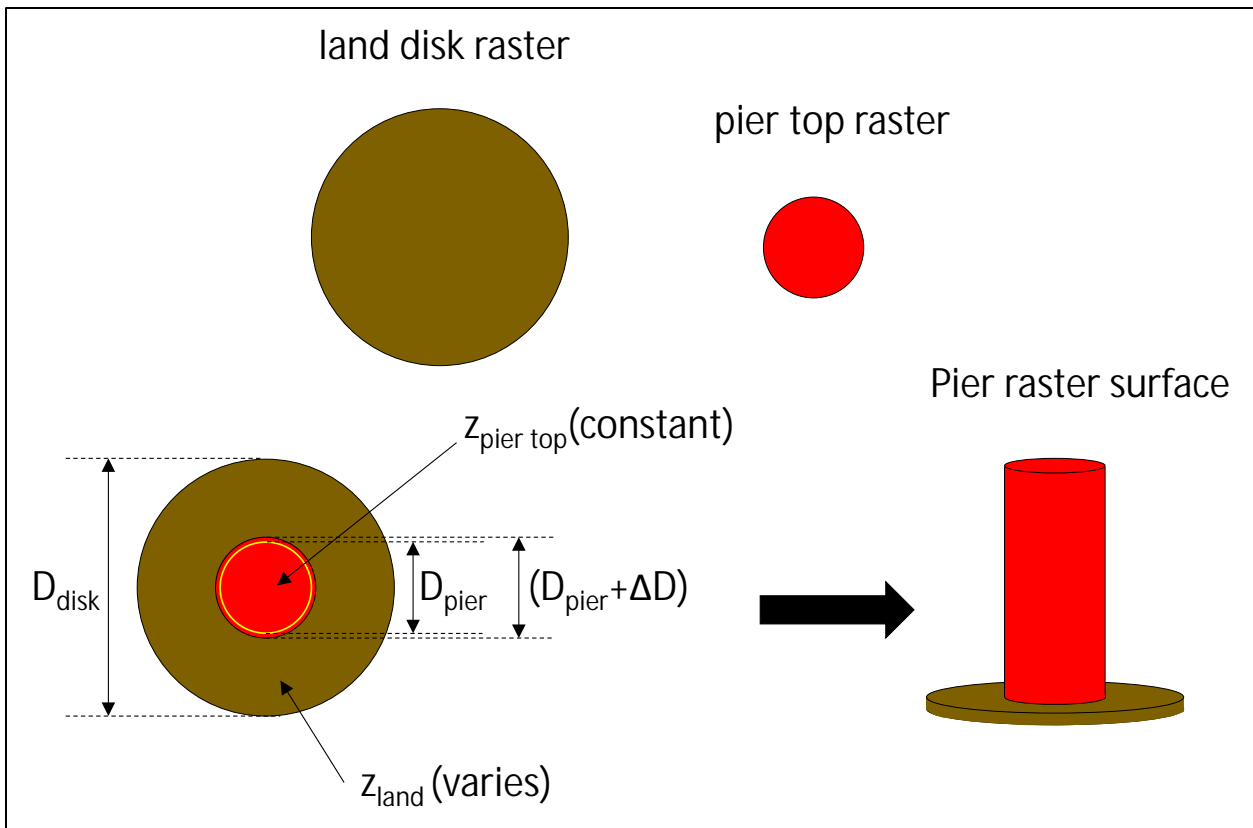


Figure 6.32: Creating the Pier Raster

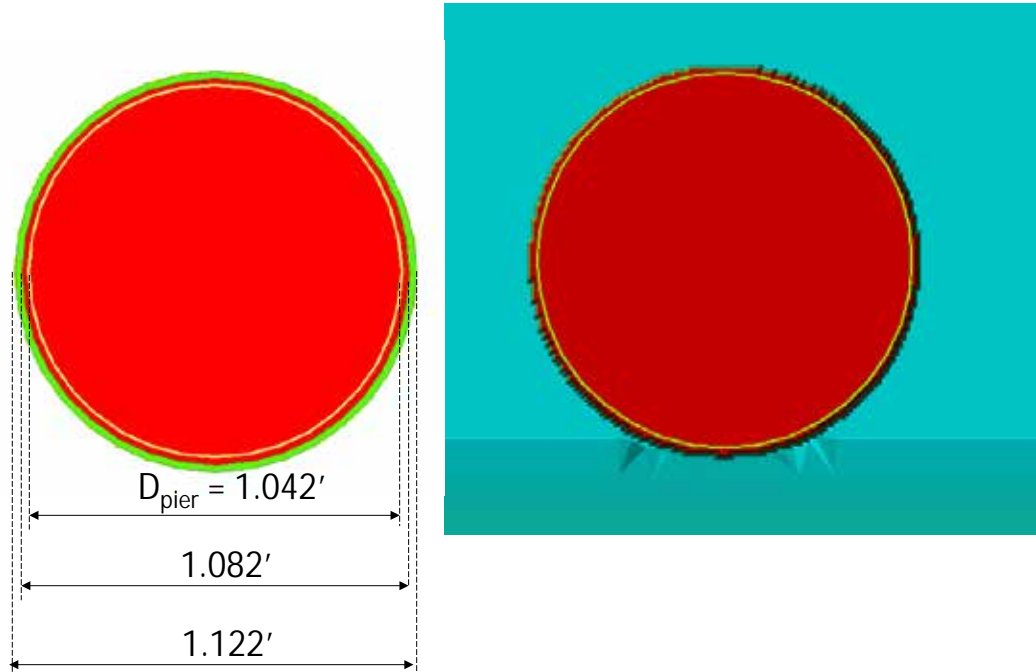


Figure 6.33: Pier Raster Used in this Study

HEC-RAS 5.0.1 and 5.0.3 (the two most recent versions at the time of this report) added the option to create breaklines. This feature greatly enhances the development of an effective grid cell network. The breaklines used for this model are shown in Figure 6.34 below. They each have a cell spacing of 1 ft. The general cell spacing was 2 feet. Figure 6.35 shows the grid network in the vicinity of the bridge.

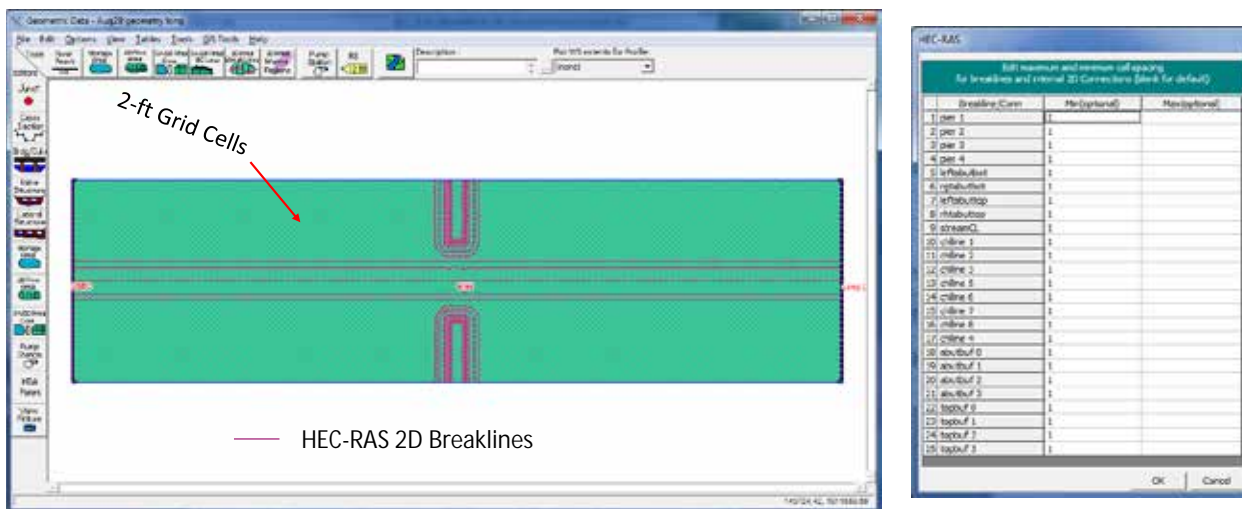


Figure 6.34: HEC-RAS 2D Breaklines

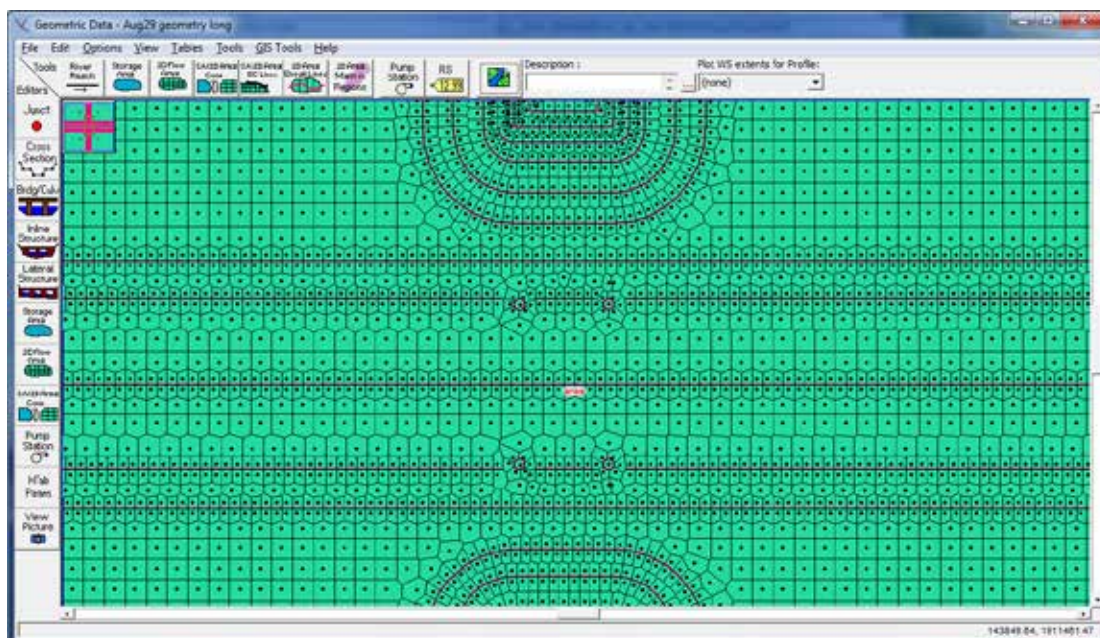


Figure 6.35: HEC-RAS 2D Grid Cells and Breaklines

Figure 6.36 shows that the average grid cell area is 2.96 ft². The total number of grid cells is 20,578. Table 6.11 shows the Ave, Min, and Max Cell size for HEC-RAS 2D and for SRH 2D. The Courant number is defined by the equation below.

$$C = \frac{V\Delta t}{\Delta x} \quad \text{Equation 6.1}$$

Where:

V = velocity,

Δt = timestep, and

Δx = cell size.

Therefore, the timestep can be expressed by the equation.

$$\Delta t = \frac{C\Delta x}{V} \quad \text{Equation 6.2}$$

An approximate average cell size is the square root of the area of the average cell area, which in this case is given by:

$$\Delta x \cong \sqrt{2.96} = 1.72 \text{ ft} \quad \text{Equation 6.3}$$

Table 6.11 below shows Δt -values for Courant number = 1 for the maximum velocities for Run 1 and Run 9 of 11.49 fps and 18.82 fps, respectively. These velocities were from runs using $\Delta t = 0.2$ seconds.

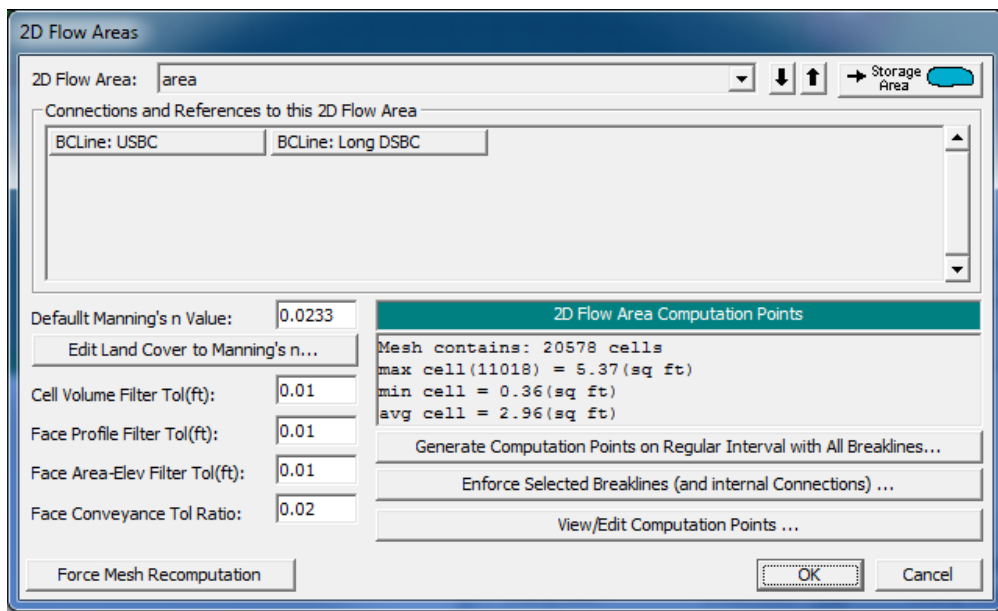


Figure 6.36: HEC-RAS Grid Cell Parameters

Table 6.11: HEC-RAS Grid Cell Parameters

| | HEC-RAS 2D | | SRH 2D | |
|-----------------|---------------------|----------------------------|---------------------|----------------------------|
| No. Cells | 20,578 | | 24,824 | |
| | A (ft^2) | $\Delta x \approx A^{1/2}$ | A (ft^2) | $\Delta x \approx A^{1/2}$ |
| Ave Cell | 5.37 | 2.32 | 0.413 | 0.64 |
| Min Cell | 0.36 | 0.60 | 0.0721 | 0.27 |
| Max Cell | 2.96 | 1.72 | 10.7 | 3.27 |
| Velocity (fps) | | 11.49 | | 11.49 |
| Δt sec* | | 0.20 | | 0.06 |
| Velocity (fps) | | 18.82 | | 18.82 |
| Δt sec* | | 0.12 | | 0.03 |

*Courant Number = 1

The timestep of 0.5 seconds was used for all runs except Run 6, which was abandoned because of extremely low tailwater overbank depths in the lab. The hydrographs were the same as those shown in Figure 6.11, but the run times were limited to 1.5 hours. The most difficult, or rather tedious, process was determining the downstream boundary conditions. For the short model runs, the downstream boundary condition was the depth at Piezometer 1 in Table 6.3. For the long model, the downstream limit of the model was 165 prototype feet downstream from the section corresponding to Piezometer 1. Thus, trial and error was used for each run to determine the downstream boundary condition (DSBC) at Station 0 that produced the correct WSE at

Station 165. Also, for different Δt values, this DSBC was not the same for the same run. Table 6.12 shows the DSBC values for Runs 1–9, excluding Run 6.

Table 6.12: DSBC for Long Model for $Dt = 0.2$ seconds

| Run No. | DSBC (ft) |
|---------|-----------|
| 1 | 18.4 |
| 2 | 17.55 |
| 3 | 16 |
| 4 | 16.8 |
| 5 | 15.36 |
| 6 | na |
| 7 | 18.1 |
| 8 | 17.75 |
| 9 | 15.74 |

Figure 6.37 shows the results of Max WSE for the HEC-RAS 2D runs for $Dt = 0.5$ seconds, together with the laboratory data. The results are extremely good for Runs 1, 2, 3, 4, and 5. Although Runs 7, 8, and 9 do not agree as well, they do show the same pattern as the lab data. Figure 6.38 shows the best-fit Dt -values were 2, 2, and 4 seconds for Runs 7, 8, and 9, respectively. Additional study is necessary to address the correct choice of the timestep.

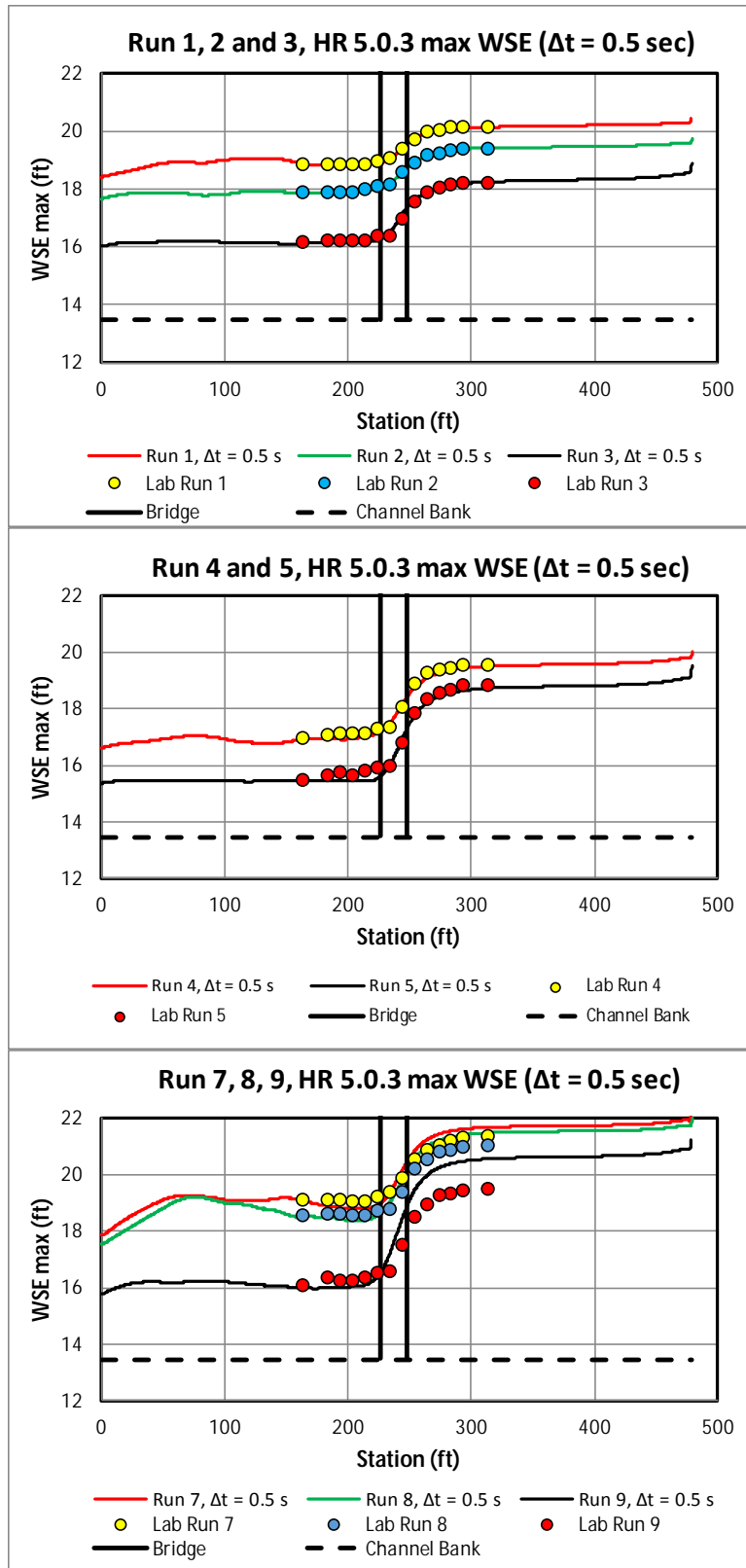


Figure 6.37: HEC-RAS 2D Long Model Results for $\Delta t = 0.5$ seconds

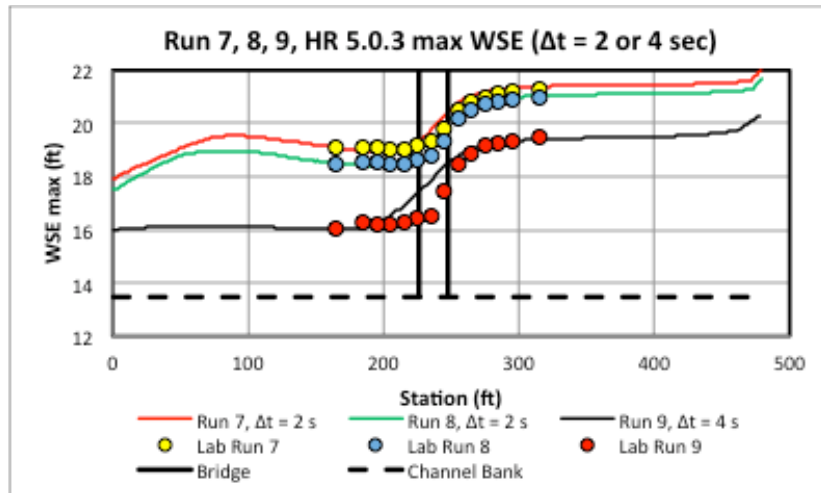


Figure 6.38: HEC-RAS 2D Long Model Best Fit Results for Runs 7, 8, and 9

Figure 6.39 shows the flow pattern at the end of the simulation for Run 1 for $\Delta t = 0.2$ seconds. The location of the upstream piezometer and the upstream end of the short model is shown as Station 150. The flow has pretty much straightened out by the time it gets to Station 150. Downstream from the bridge, the flow wags back and forth throughout the simulation as it does for all the runs, sometimes favoring the left overbank and sometimes the right.

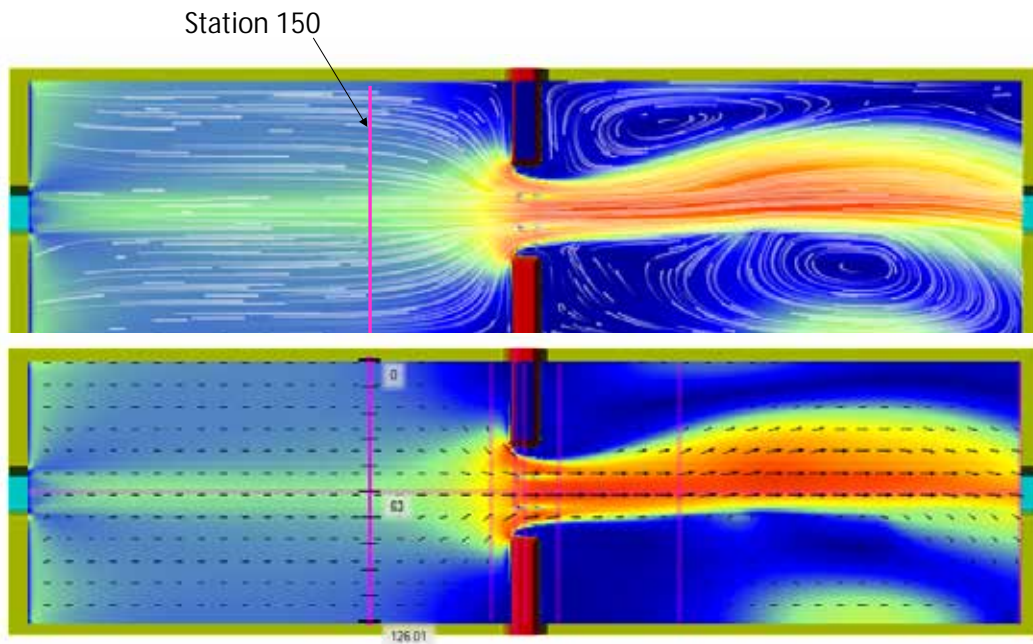


Figure 6.39: Velocity Patterns and Vectors at the End of Run 1 for $\Delta t = 0.2$ seconds

6.7 SRH-2D Modeling of Type One Bridge Experiments from Flume Study (Long Model)

The SRH-2D model was applied using the same boundary conditions determined by iteration with HEC-RAS 2D and shown in Table 6.12. A timestep of 0.1 second was needed to obtain meaningful results; larger timesteps resulted in erratic WSE profiles (as illustrated in Figure 6.40). This timestep of 0.1 second is in line with the value of 0.06 seconds in Table 6.11. Figure 6.41 shows the SRH-2D results for Runs 1–5 and 7–9. The SRH-2D results are shown together with the $\Delta t = 0.5$ seconds results from HEC-RAS 2D in Figures 6.41 to 6.44. Open lab data points were used to better view the 2D profiles. Overall, the SRH-2D results were similar to the HEC-RAS 2D results, though the fit was not quite as good for Runs 1–5. It must be noted, however, that the DSBC for the SRH-2D runs was not determined iteratively to match the downstream lab data point as was done in HEC-RAS 2D. Instead, the HEC-RAS DSBC values were used. While this worked well for SRH-2D Runs 3, 4, 5, and 9, the other SRH-2D profiles missed the data point at Station 165. If this were corrected by iteratively finding the DSBC for each SRH 2D run that would create a match at the lab data point at Station 165, the SRH 2D results would vary even further from the experimental lab data points for Runs 7 and 8.

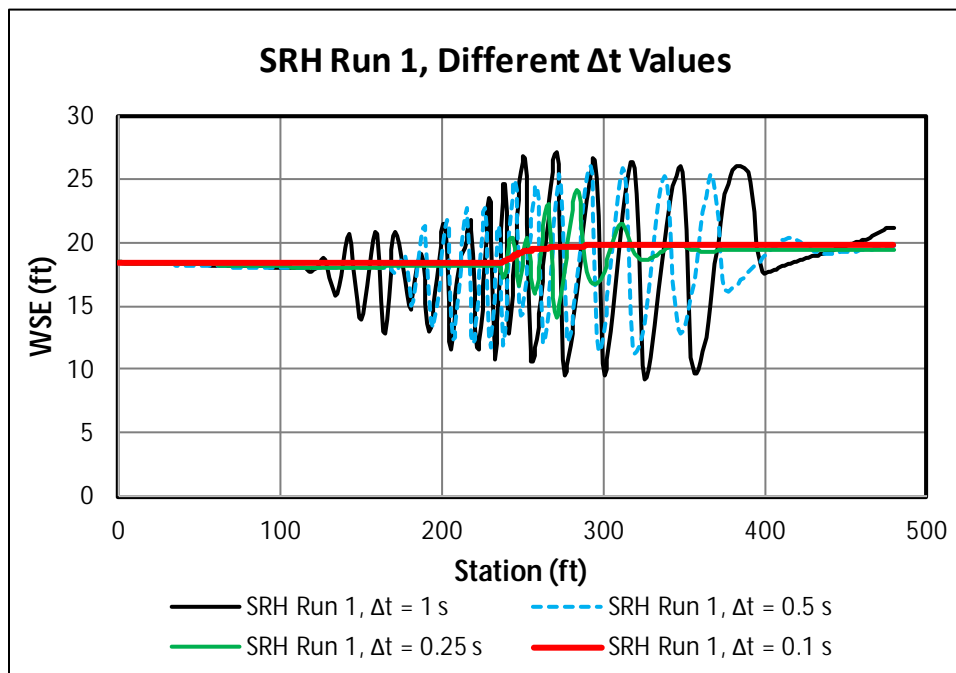


Figure 6.40: Selection of Δt for SRH-2D

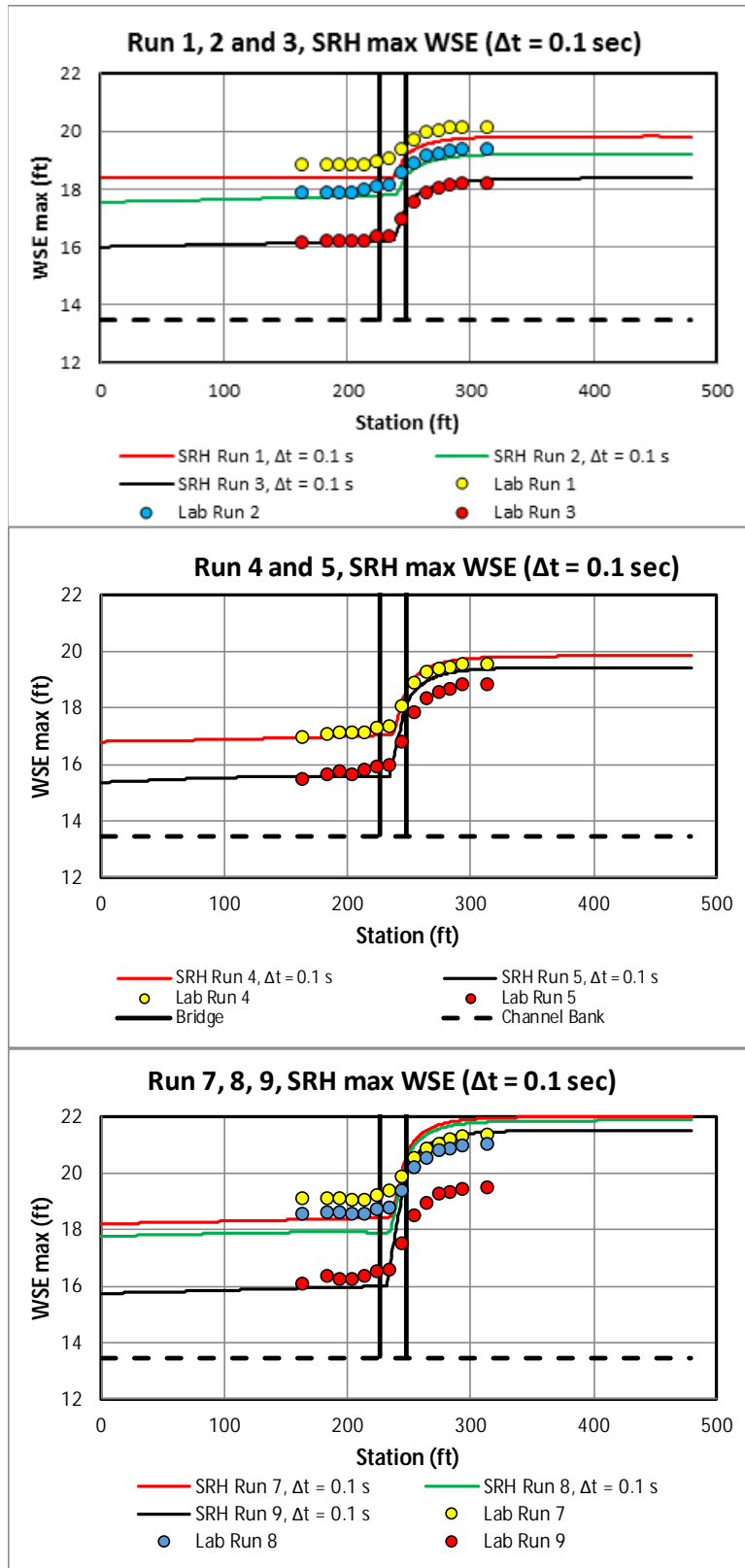


Figure 6.41: SRH-2D Long Model Results for $\Delta t = 0.1$ second

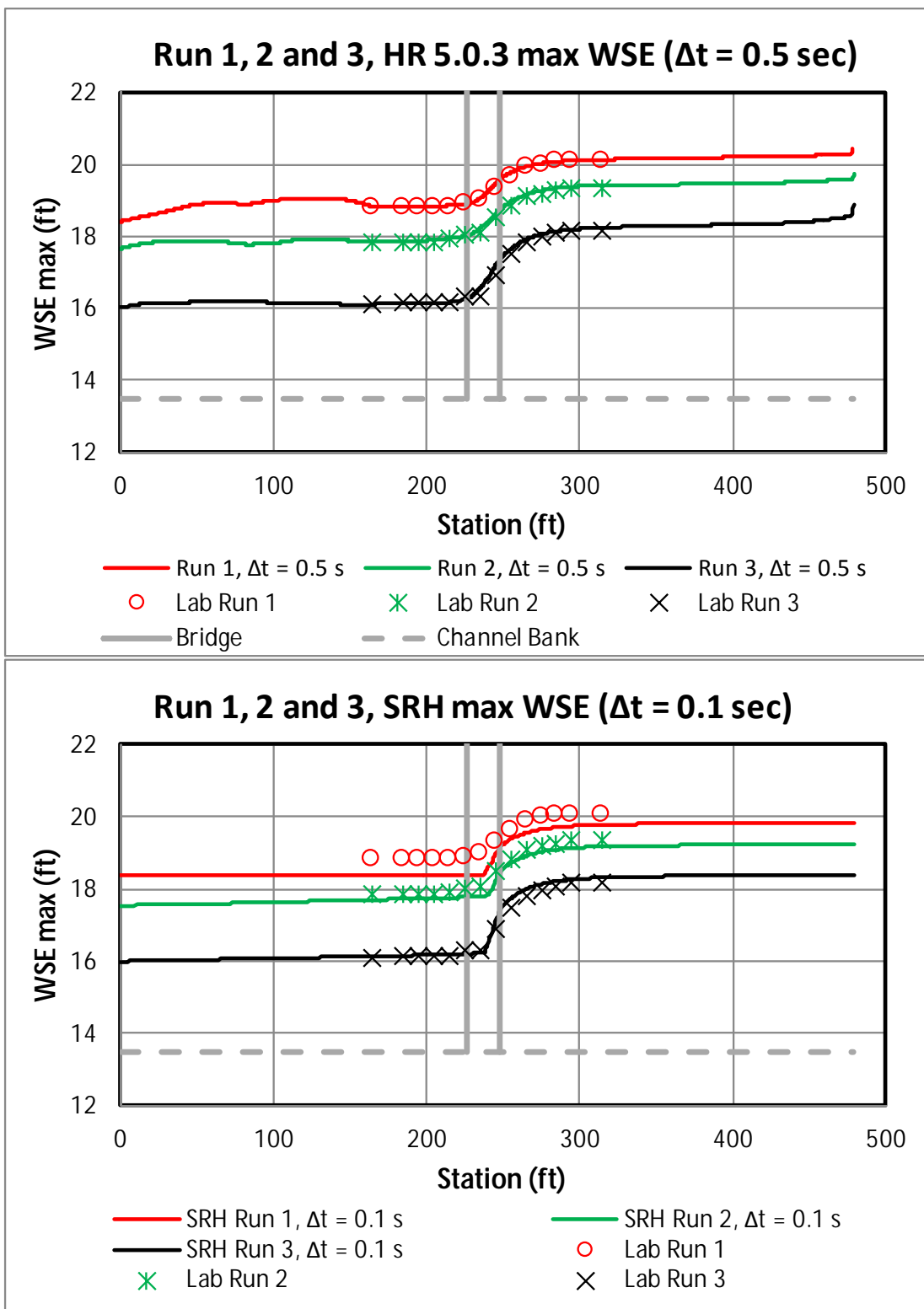


Figure 6.42: HEC-RAS 2D and SRH-2D Max WSE Profiles for Runs 1, 2, and 3

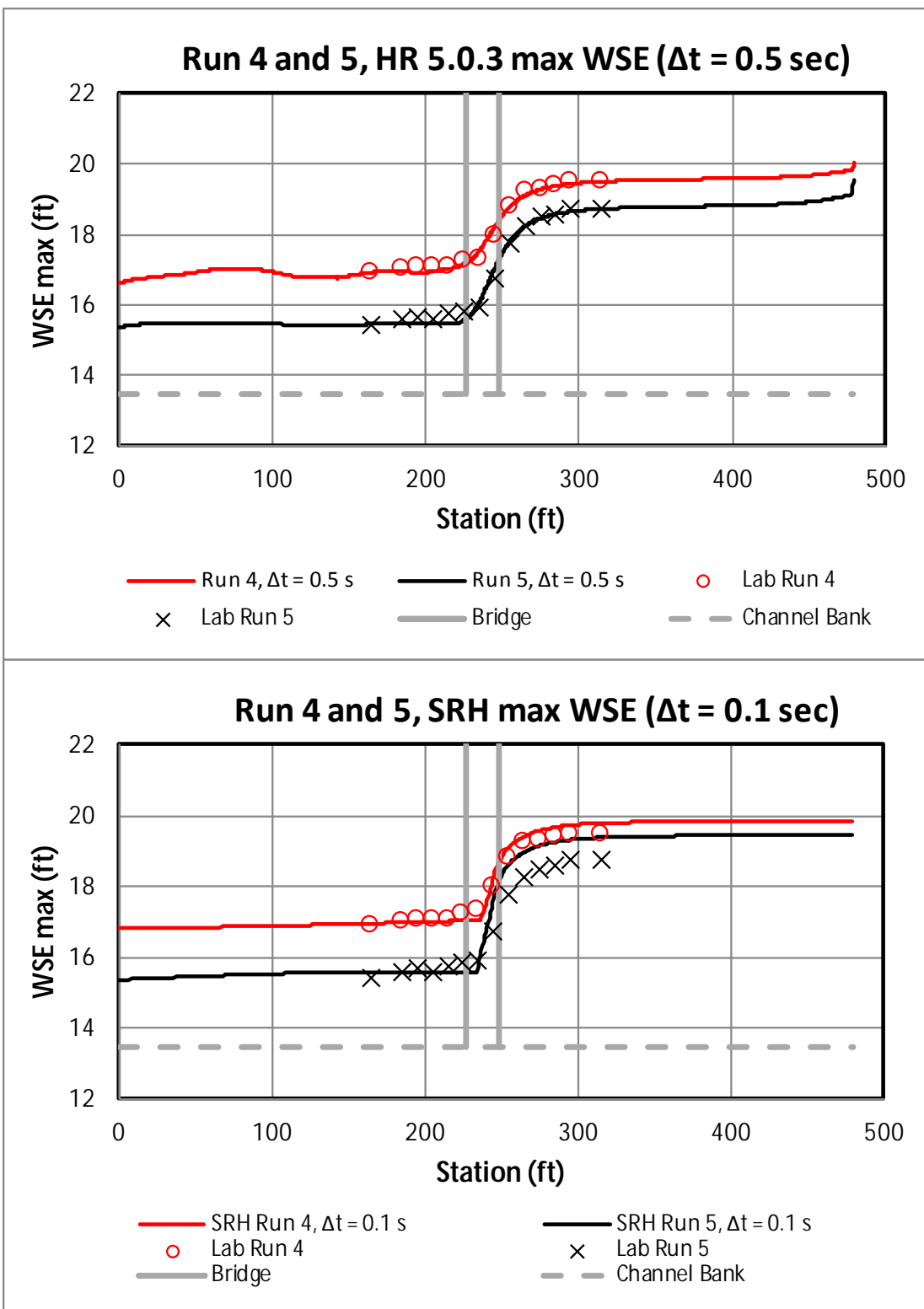


Figure 6.43: HEC-RAS 2D and SRH-2D Max WSE Profiles for Runs 4 and 5

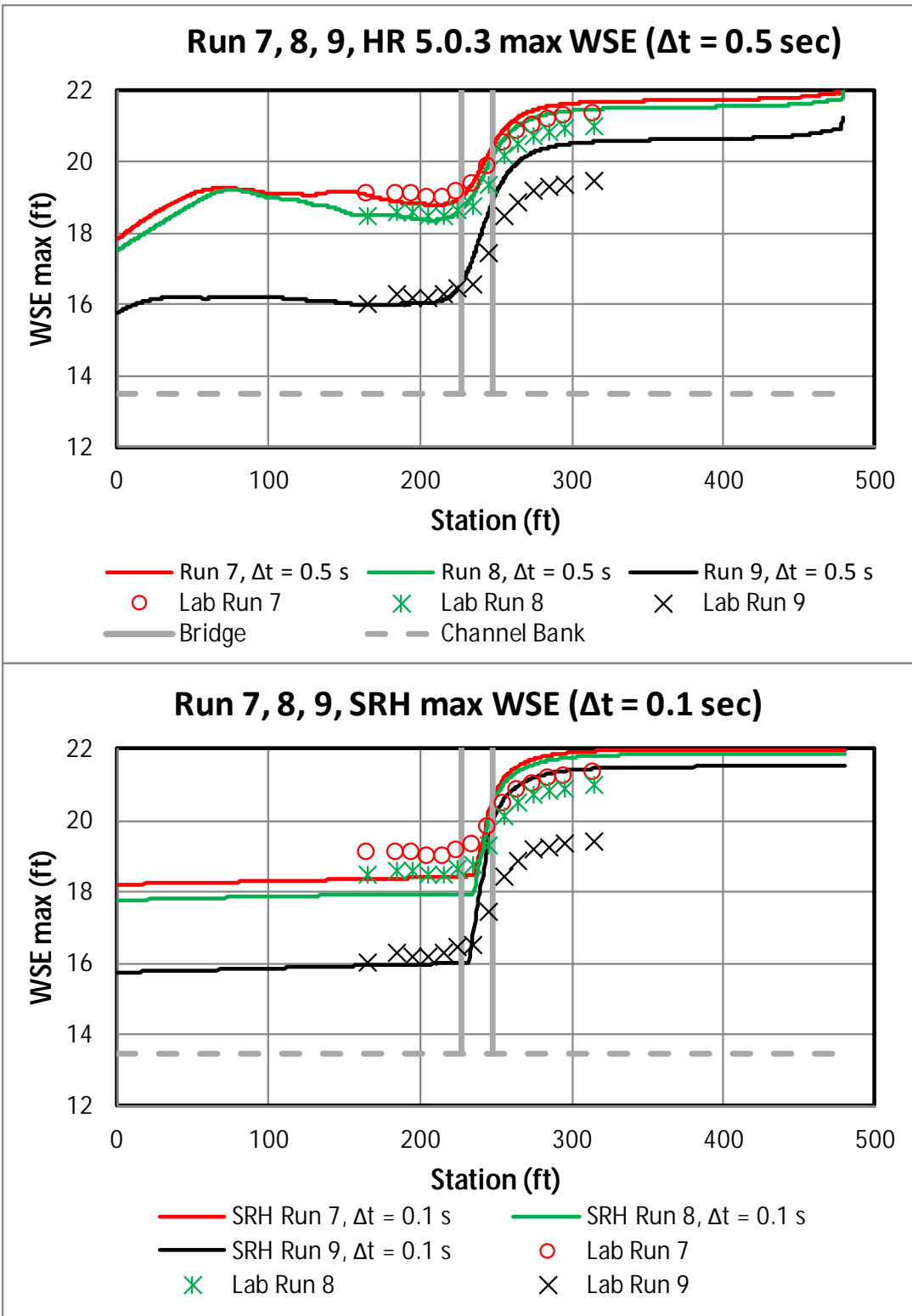


Figure 6.44: HEC-RAS 2D and SRH 2D Max WSE Profiles for Runs 7, 8, and 9

6.8 Runtime Comparison

Comparing runtimes for SRH-2D and HEC-RAS 2D is challenging. Mesh density, domain size, and time step all have a large influence on the total run time. Chapter 3 presents runtime comparisons for SRH-2D and HEC-RAS 2D for similar mesh densities, domain sizes, and time steps. Although this would seem to be the most direct way to compare model computational demands, it is misleading. Experience with the two models shows that HEC-RAS 2D can use a much larger cell size (due in part to the way HEC-RAS 2D preserves sub-grid cell variability) and a much larger time step than SRH-2D while still maintaining better results. Table 6.13 presents run times for simulations of the long model Runs 1 through 9 using a laptop with the parameters outlined in Figure 6.45. The SRH-2D model used 24,824 mesh elements while the HEC-RAS 2D model used 20,578. On average, the HEC-RAS 2D model with $dt = 0.5$ seconds ran 4.7 times faster than the SRH-2D model. The HEC-RAS 2D model with $dt = 4$ seconds (for Run 9) ran 23.8 times faster than SRH-2D. These differences in performance make HEC-RAS 2D attractive for design work, especially for designs requiring iterative solutions.

| | |
|-------------------------|--------------------------------------------------|
| Processor: | Intel(R) Core(TM) i7-6500U CPU @ 2.50GHz 2.60GHz |
| Installed memory (RAM): | 8.00 GB (7.86 GB usable) |
| System type: | 64-bit Operating System, x64-based processor |

Figure 6.45: Computer Specifications

Table 6.13: Comparison of Runtimes

RUN TIMES GIVEN IN MINUTES

| Lab Run No. | HR 2D (5.0.3) | | | SRH 2D |
|-------------|---------------|-------|-------|---------|
| | 0.5 sec | 2 sec | 4 sec | 0.1 sec |
| Run 1 | 21.9 | -- | -- | 88.2 |
| Run 2 | 17.4 | -- | -- | 81.3 |
| Run 3 | 18.1 | -- | -- | 80.3 |
| Run 4 | 16.5 | -- | -- | 109.5 |
| Run 5 | 19.7 | -- | -- | 101.7 |
| Run 7 | 22.8 | 6.2 | -- | 100.9 |
| Run 8 | 23.8 | 6.2 | -- | 98.3 |
| Run 9 | 24.6 | -- | 4.1 | 98.5 |

Chapter 7: Neodesha Floodplain Study

7.1 Background for the Neodesha Floodplain Study

The complexity of the Neodesha site is of particular interest to hydraulic modelers of river systems. HEC-RAS 1D, HEC-RAS 2D run with the full momentum equations, and SRH-2D were all used to model a section of the Fall River upstream of where it joins the Verdigris River. The city of Neodesha, Kansas (Wilson County), is at the confluence of these two rivers. The following image in Figure 7.1 delineates the boundary of the model space.

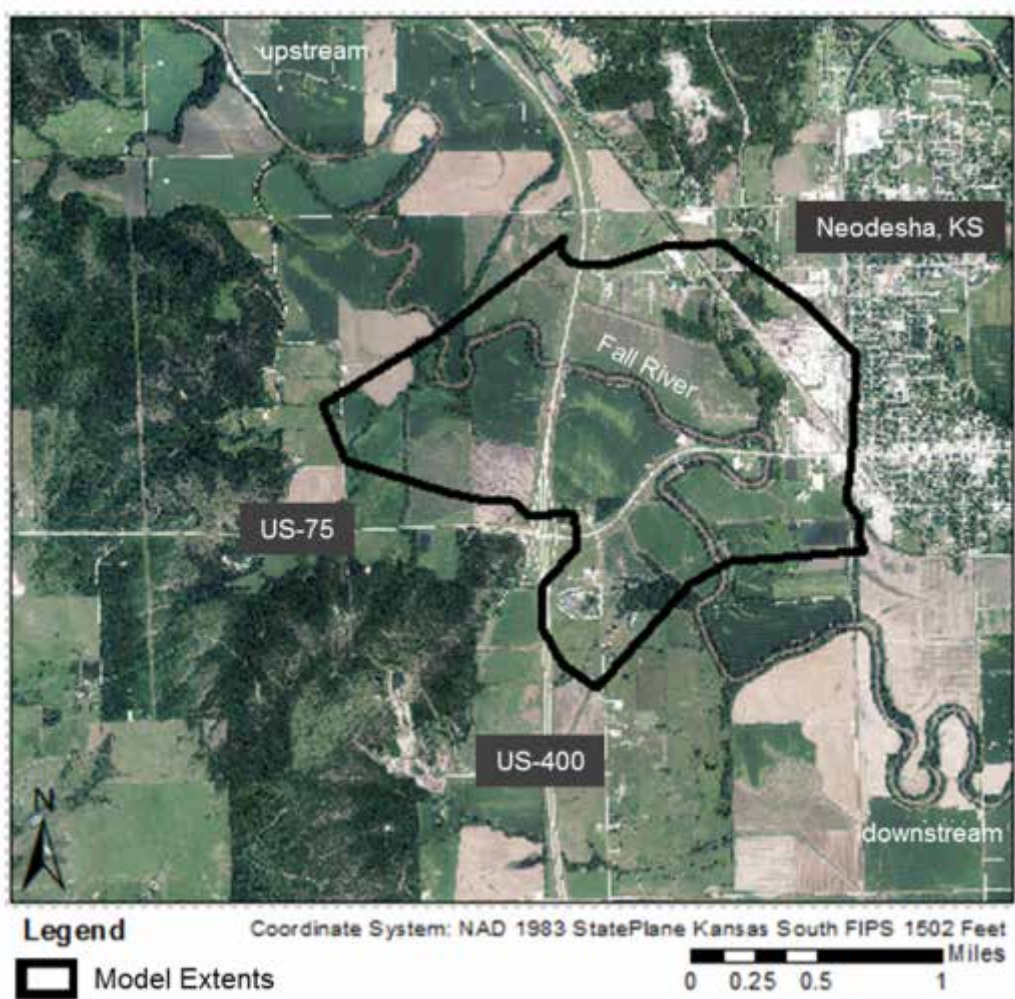


Figure 7.1: Neodesha Floodplain Study Site and Surrounding Area

The aerial photographs composing the image were obtained from the USGS online National Map Viewer. The total model area was 2.15 square miles (mi) and the reach length

15,907 ft. The major bases for comparison between models were the floodplain extents, the area inundated, the water surface profile along the main channel's centerline, and flow divisions through the bridge openings.

The section of this reach that is of interest possesses many features that make a standard 1D analysis difficult. On the upstream end the channel changes direction frequently, widely meandering as it progresses across the relatively flat floodplain. The flow then encounters Highway 400, where four hydraulic structures exist: a bridge over the main channel, a relief bridge and a relief culvert south of the main bridge, and a small culvert north of the main channel. The river then proceeds eastward to run nearly parallel to Highway 75 before it turns abruptly to pass through the main bridge under the road. In addition to the main bridge on Highway 75, there are two relief structures to the southwest. Once the flow has bypassed the main bridge under Highway 75, it curves back to the west, the opposite direction it was heading before, once again running parallel to the highway. The flow from the two relief bridges then recombines with the main channel flow as it heads by a water treatment plant whose ponds on the eastern side of the downstream extent of the model space are protected from flooding by levees. These details frustrate the task of defining cross sections that do not overlap and that suitably approximate the complicated flow patterns.

The space chosen was intended to include the notable features of the site, those that make it difficult to model, but it was also reduced in size for the sake of computational efficiency for the 2D models. Great care was exercised in the placement of the upstream and downstream boundaries. At the upstream end, the boundary needed to be placed far enough away from the bridge to ensure realistic flow patterns for the incoming water, but also in a location where the flow is approximately 1D (at least for a reasonably high flow and thus one that is outside of the channel). At the downstream end, the boundary needed to be far enough away such that the separate flows issuing from the three bridges located along Highway 75 have sufficiently recombined, and the flow is approximately 1D.

Currently, neither 2D model can accommodate pressure flow directly; both must rely on supplemental routines—HEC-RAS must use the standard 1D culvert and bridge routines, and SRH-2D must use the Federal Highway Administration's culvert analysis software, HY-8. Thus,

the discharge selected was one intended to be high enough for the flow to include the overbanks but not so high as to cause overtopping of the roadways or pressure flow through the bridges. To this end, 40,000 cfs was used as the target discharge. This value was near the “Full Valley Discharge” of 39,800 cfs listed in the KDOT as-built plans for HW 400 (96-103 K-3295-01). After the flow for the 1D HEC-RAS model was used and found to satisfactorily meet the criteria listed above, it was deemed appropriate for use in the 2D models. As was often the case for analyses included in this report, the inflow hydrographs used for the 2D models were simply ones that ramped up to the maximum discharge and maintained this constant discharge for a duration sufficient for steady state conditions to be reached. This was done primarily for numerical stability, as rapid changes in the hydrodynamics of a model may result in unrealistic flow behavior like extreme changes in depths and velocities (especially near obstructions such as piers), but also because the intermediate details are also of interest. The total hydrograph durations vary for each 2D model and will be discussed further in their respective sections. The HEC-RAS 1D model did not require an inflow hydrograph, as it was run as a steady state simulation. All models used a water surface elevation of 795 ft as the downstream boundary condition. This value was obtained from the HEC-RAS 1D model using a normal depth downstream boundary condition.

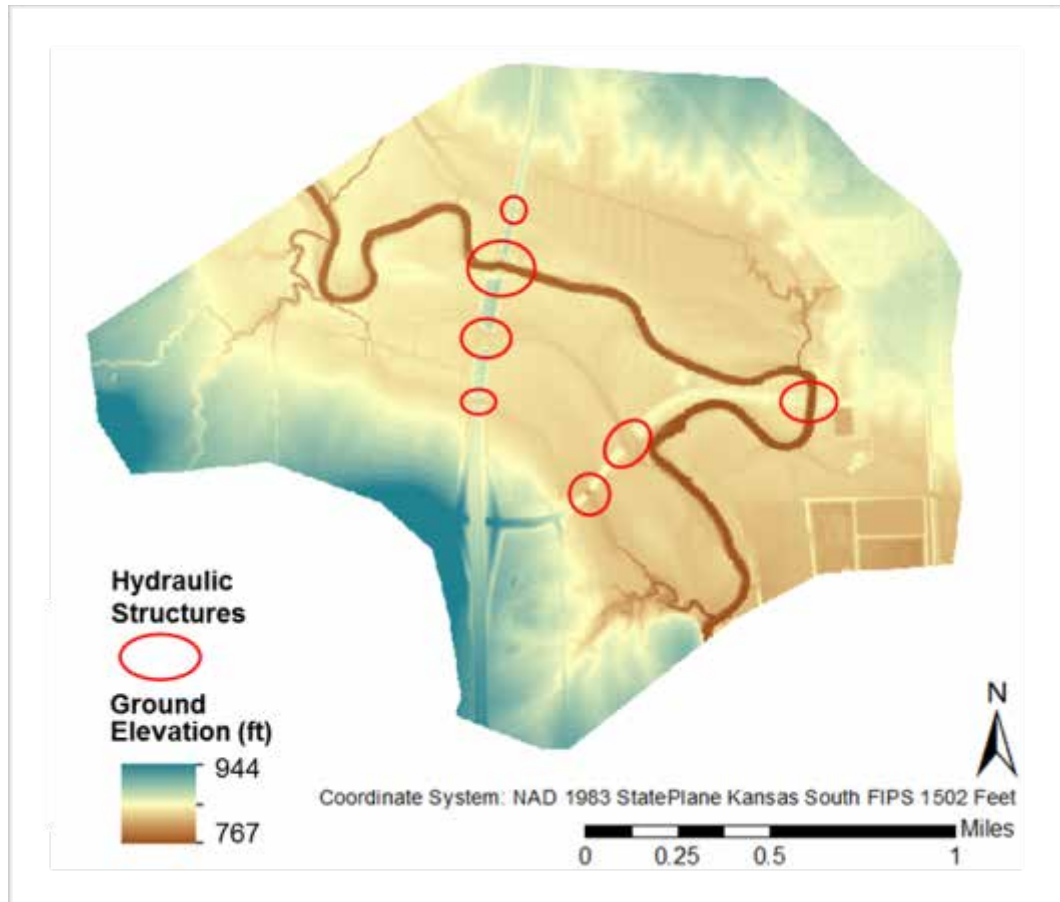


Figure 7.2: Digital Elevation Model for the Neodesha Floodplain Study

The map in Figure 7.2 shows the raster defining the terrain for the study site. Unlike the aerial imagery, this data was obtained from the Kansas Applied Remote Sensing (KARS) online resource rather than from the National Map Viewer. The elevation grid downloaded had a resolution of 1 m square, which was the highest resolution available. A raster must have a uniform grid spacing throughout its domain for the 2D models. Consequently, the 1-m raster was converted to a TIN and then resampled to a tighter grid spacing of 1 ft square. This was done to ensure that changes made to the terrain were adequately represented within each model and to facilitate acceptable modeling of the geometry of the structures. The effects of several changes can be clearly seen in Figure 7.2. Along Highway 400, the structures affected included the southernmost relief culvert, which based on the KDOT bridge plans was approximated with a 64-ft-wide opening on a plane 127 ft long and given a constant elevation of 795.20 ft. The raw elevation data (LIDAR) included only information for the road in this location, and so this

section needed to be dropped to create a channel for the flow to travel through. Also along Highway 400, a small culvert was similarly added to the terrain near the southernmost relief bridge, but since no plans were available for this structure, it was approximated using aerial imagery as being 12 ft wide, and, based on the surrounding contours, given a change in elevation from 795.87 ft to 794.92 ft from upstream to downstream over a horizontal distance of 80 ft, thus long enough to span the width of the road and its embankments. The first relief bridge south of the main channel on Highway 400 was left as it was in the raw LIDAR data. The relief bridge nearest to the main channel along Highway 75 was also left untouched. The southwestern-most relief bridge (culvert) along Highway 75 was, based upon KDOT plans, approximated with a 100-ft-wide opening on a plane 60.5 ft long and given a constant elevation of 789.10 ft. Where the main channel crosses both Highways 400 and 75, pseudo- “survey data” was created from the bridge plans. The elevations of points along the upstream face of each bridge and along the abutments were used to assign elevation values to 3D lines drawn parallel to the channel centerline. These lines were used to generate TINs with dimensions corresponding to the extents of these 3D lines. The TINs were then used to generate rasters that had a resolution of 1 ft × 1 ft. Here, as well as for the portions of the terrain mentioned above, the ArcMap Mosaic tool was used to merge the separate rasters, with the higher priority given to the newly created rasters. The results of this process for the two main bridges on this section of the Fall River are included in Figures 7.3 and 7.4.

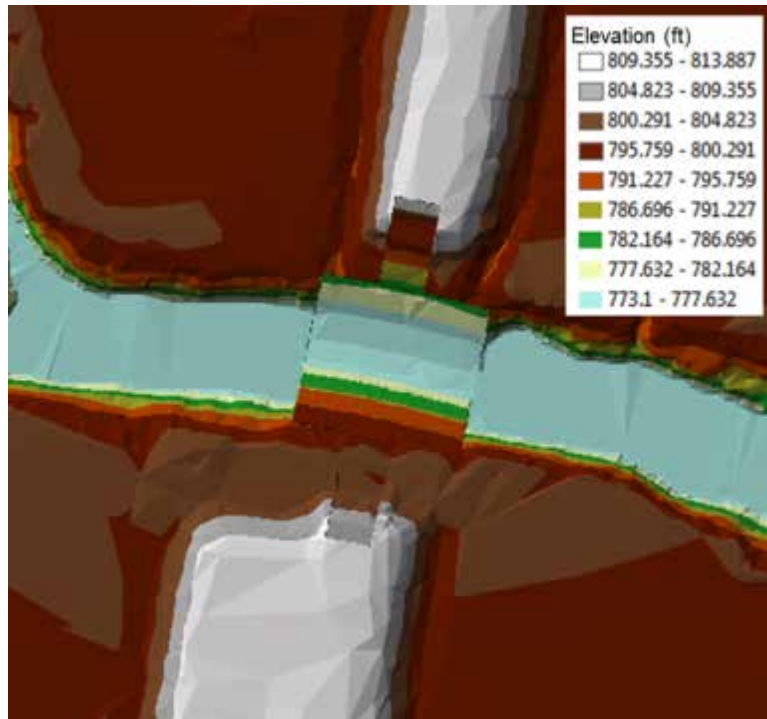


Figure 7.3: Composite TIN of Raw Data and As-Built Plan Bridge Data for Main Bridge on Highway 400

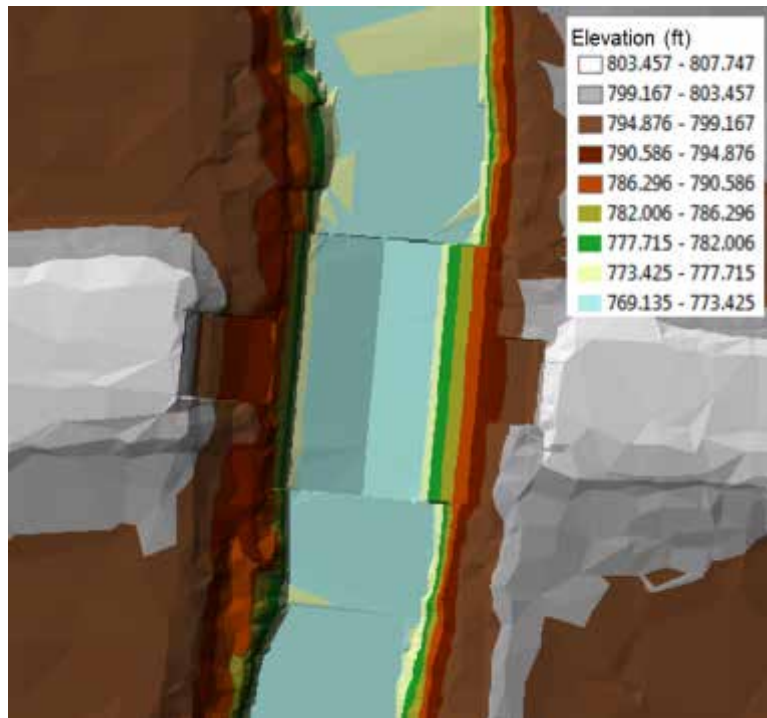


Figure 7.4: Composite TIN of Raw Data and As-Built Plan Bridge Data for Main Bridge on Highway 75

It is clear that some disagreement exists between the as-built plan data and the LIDAR, and two likely reasons exist for this. The first is that the two sources of data correspond with different dates. Several years may have elapsed between the collection of the LIDAR that was processed into the raster downloaded and the time when the field data for the bridge plans was gathered, and the channel bed is not likely to have exactly the same geometry each time data is collected because of bank erosion or soil accumulation. The second reason for the disagreement is that the flow through the river was probably different on each occasion when data was gathered. This is important because the LIDAR beams do not penetrate the water surface, and so the river bathymetry is not reflected in the dataset. The effect of this can be seen in Figures 7.3 and 7.4 in the channels away from the bridges where the channel appears unusually flat. Also, the survey included in the bridge plans actually measured the ground elevation, and so the low point of that survey data through each bridge is below that of the LIDAR, by about 4 ft and about 2.5 ft through the main bridges under Highways 400 and 75, respectively. The channel away from the bridges as represented by the LIDAR data was left intact because, while doing so artificially reduces the conveyance of the main channel, the reduction relative to the large discharge modeled was deemed sufficiently insignificant. Also, for the sake of making comparisons among the various models, what is important is that every model share the same bias if one exists. If this reach were being modeled for design purposes (or some other critical task), then it would be advisable to carve out the channel through manipulation of the DEM. This could be accomplished fairly easily within ArcMap using 3D elevation lines in a manner similar to that described in Chapter 3. These 3D elevation lines would be related to the survey data for each bridge but would also take into consideration the slope of the channel. The elevation lines could be used to generate TINs, and those could be used to generate rasters. This would be done for multiple segments of the channel. Next, carving out the channel would require a series of mosaic operations using the blend option for these multiple sections to smoothly merge the channel rasters. Then, the mosaic tool would be used again to join the merged channel rasters to the raster based on the LIDAR, but with the value priority set to minimum. Following this procedure would guarantee a greater conveyance through the main channel, but surely other methods exist to accomplish this goal.

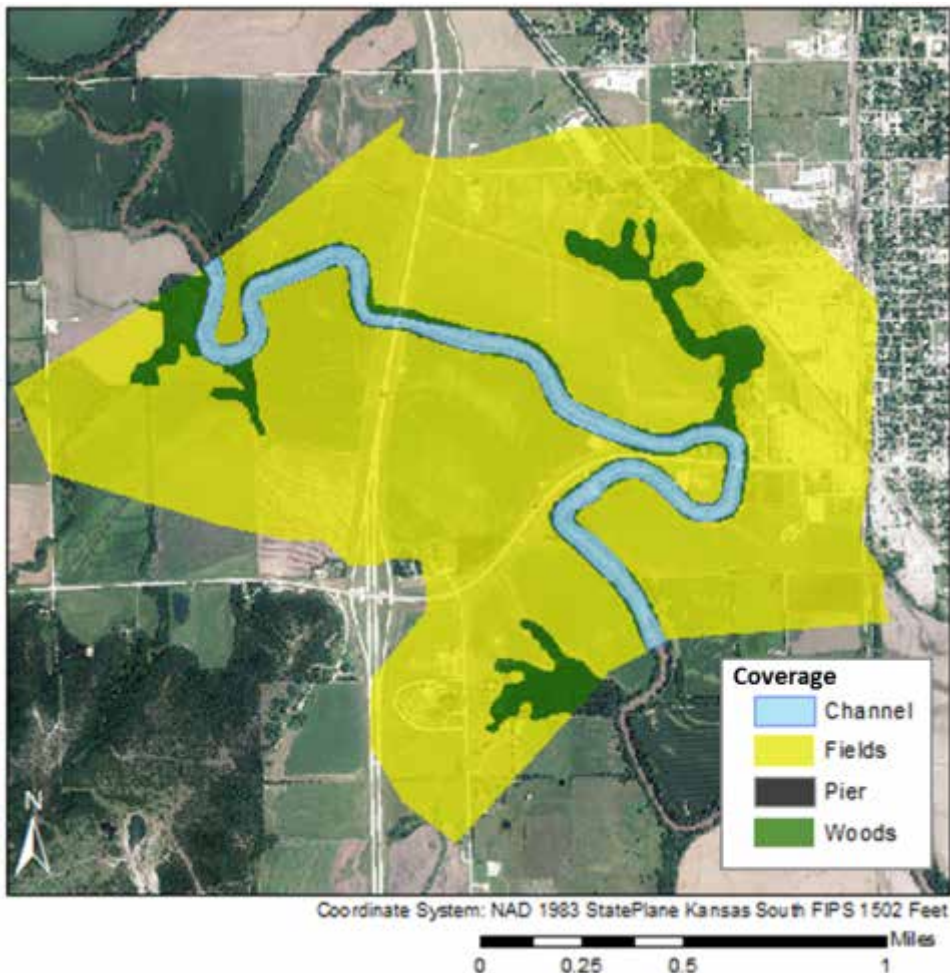


Figure 7.5: Manning's Roughness Coverage Polygons for the Neodesha Floodplain Study Site

The regions delineated in Figure 7.5 above correspond to Manning's roughness coefficients of 0.035 for the channel, 0.1 for the woods, and 0.055 for the fields; for use in the HEC-RAS 2D simulation, the piers were assigned an n value of 1,000,000 (10^6) to minimize conveyance through the piers. These polygons were drawn in ArcMap and there were assigned their respective values. Since no overtopping of the roadways was anticipated, separate roughness coefficients were not assigned to the roadways and thus the roadways are included in the "fields" category (although it should make no difference which type they belong to). The number of land use types defined was kept to a minimum in order to preserve computational efficiency and because the site was mostly fields. This coarse description of land use for the site was expected to be wholly capable of simulating the primary flow features without overly

complicating the issue of building the model. Sections 7.2, 7.3, and 7.4 describe the details and results of each model individually.

7.2 One-Dimensional HEC-RAS Model for Neodesha

7.2.1 One-Dimensional HEC-RAS Neodesha Model Setup

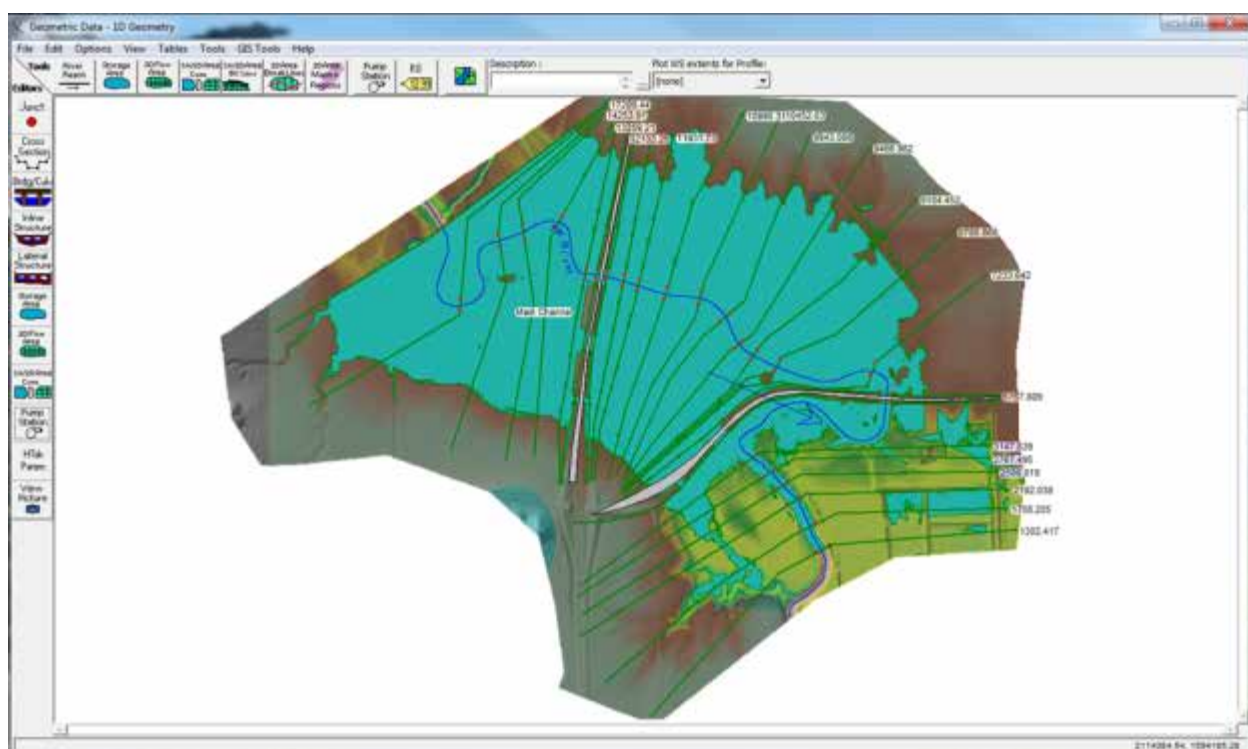


Figure 7.6: 1D HEC-RAS Geometry and Flood Map for the Neodesha Floodplain Study

The model depicted in Figure 7.6 was composed of 25 cross sections and two bridge sections. It included ineffective flow areas upstream and downstream of each hydraulic structure to account for the reduced conveyance through nearby cross sections related to the contraction and subsequent expansion of flow as it passes through these constrictions. The boundaries of each ineffective flow area were drawn at 1:1 and 2:1 ratios (longitudinal to lateral with respect to the flow direction) for the contraction and expansion sections, respectively. Blocked ineffective flow areas were used on the east sides of the three most downstream cross sections to bar the low elevation areas bounded by the levees near the water treatment plant from being used for

conveyance. Details for the bridges, such as pier sizes and distributions, opening width, roadways, and guard rails were determined from the KDOT plans. The upstream and downstream bounding bridge cross sections had their stationing and channel elevation data manually adjusted in Excel so that they lined up with each bridge opening and so that their channel elevations matched those of the field “survey data.” Figures 7.7 to 7.9 show the blocked ineffective flow areas near most downstream cross sections and the bridge cross sections from HEC-RAS 1D.

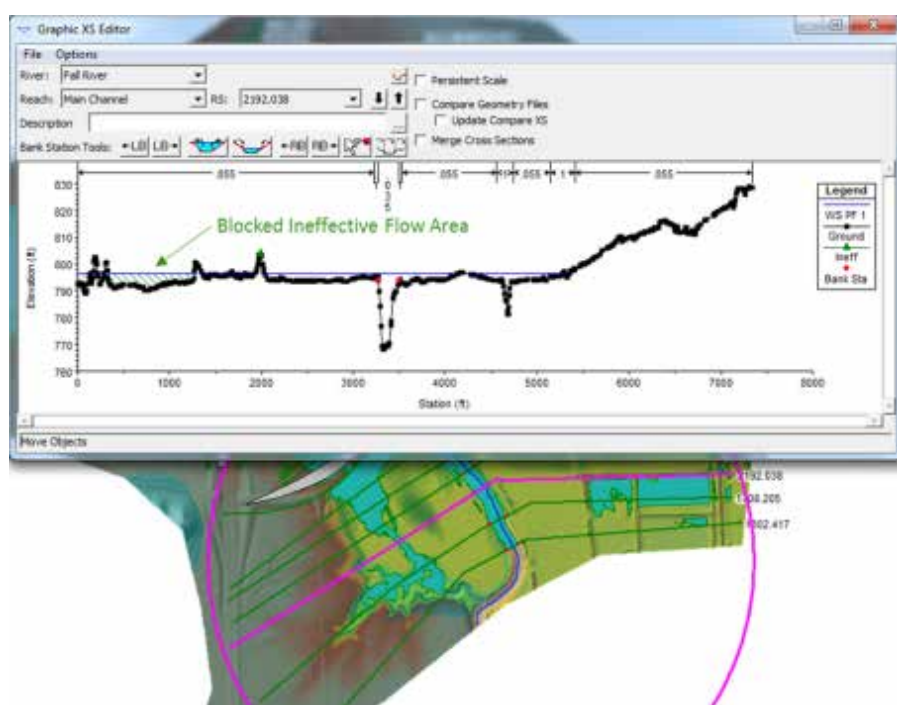


Figure 7.7: River Station 2192.038 from the HEC-RAS 1D Model for Neodesha Floodplain Study Showing Blocked Ineffective Flow Areas Typical of the Three Most Downstream Cross Sections

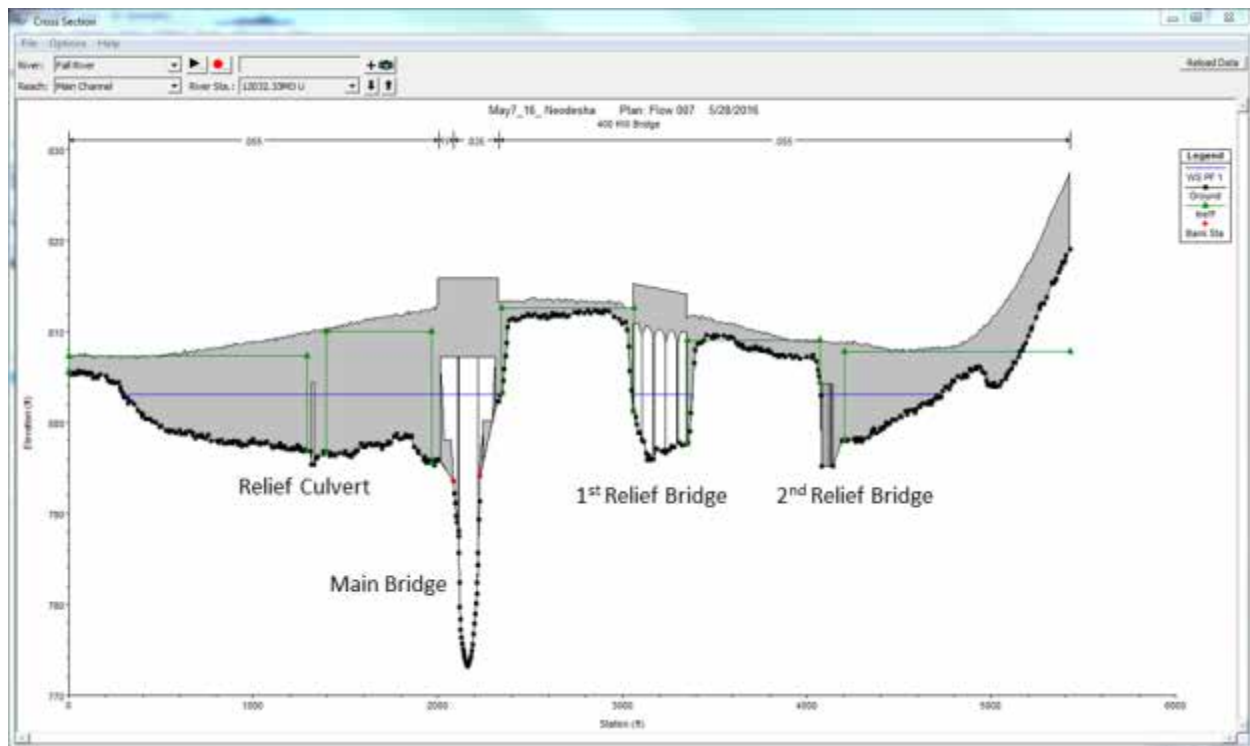


Figure 7.8: Upstream Bounding Bridge Cross Section for Highway 400

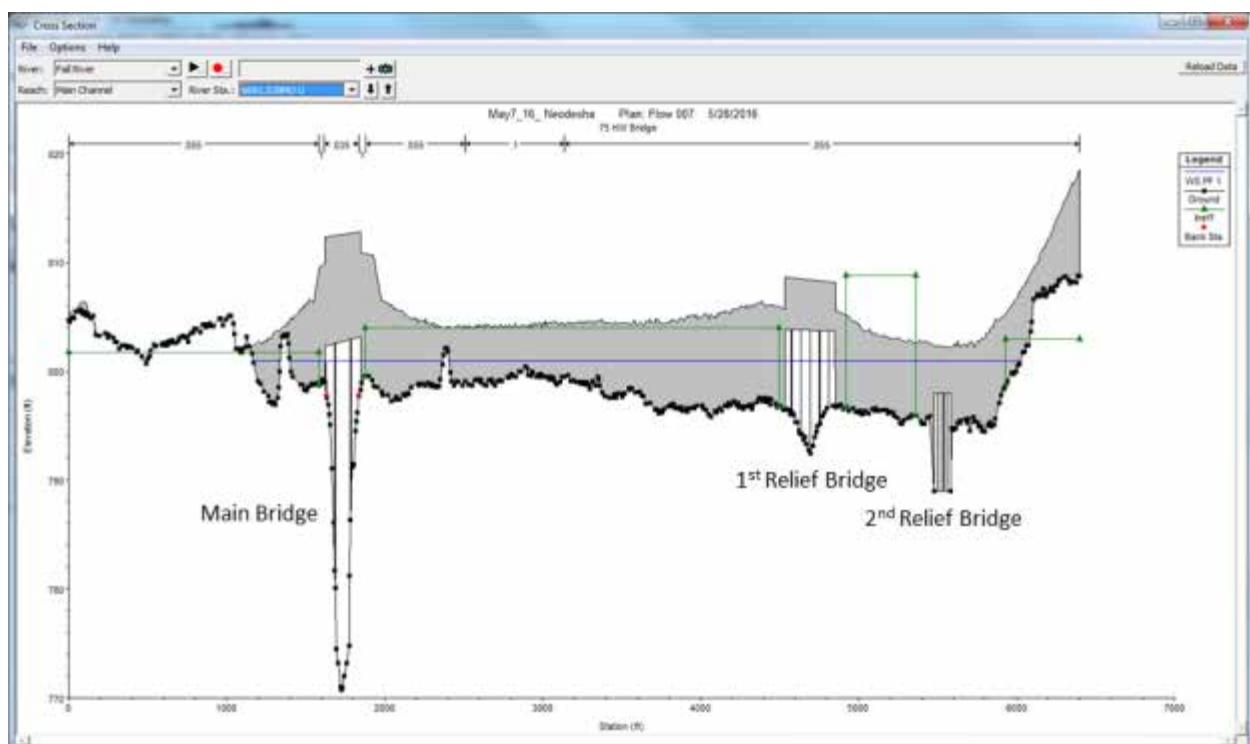


Figure 7.9: Upstream Bounding Bridge Cross Section for Highway 75

Thirty-nine piers were included for the 2D models. HEC-RAS 1D only models the upstream pier for multiple-column pier groups. At the main bridge on Highway 400, there were six piers, each with a diameter of 3.5 ft. At the first relief bridge on that Highway, there were 12 piers, each with a diameter of 2.5 ft. At the time the simulations were run, there were no plans available for the main bridge on Highway 75, and so the number of piers was estimated as 6, each with a diameter of 4.5 ft. Bridge plans have since become available, however, showing that there were actually 4 piers, each with a diameter of 3 ft. Since the 2D simulations require such a long time to run, this report presents the results that were determined using the estimated pier diameters at the main bridge on Highway 75. Finally, the remaining 15 piers were located at the first relief bridge on Highway 75, and each one had a diameter of 2.5 ft. The multiple barrels of the second relief bridges for both Highways 400 and 75 were approximated in the 2D models by using single barrels and reducing the total opening widths by amounts equal to the sum of the thicknesses of the walls separating each barrel. Taking this approach underestimates the amount of losses experienced through both relief bridges, but considering that the discharge passing through each structure is rather small relative to the total discharge, the approximation is acceptable.

7.2.2 One-Dimensional HEC-RAS Neodesha Model Results

Figures 7.10 to 7.12 and Table 7.1 below summarize the results of the 1D HEC-RAS model. The runtime for this model was 9 seconds. For the floodplain map in Figure 7.10, the disconnected flow areas produced during the “cut and fill” operation of HEC-GeoRAS were deleted in ArcMap, and then the area of the single remaining polygon was determined to be 1.35 square miles, or 63.1% of the total study area. It is vital to note that the flow did not overtop either roadway, nor did the water surface elevation exceed the height of the levee near the downstream cross sections. It is also important to note that the flooded extents were adequately bounded by the model domain.

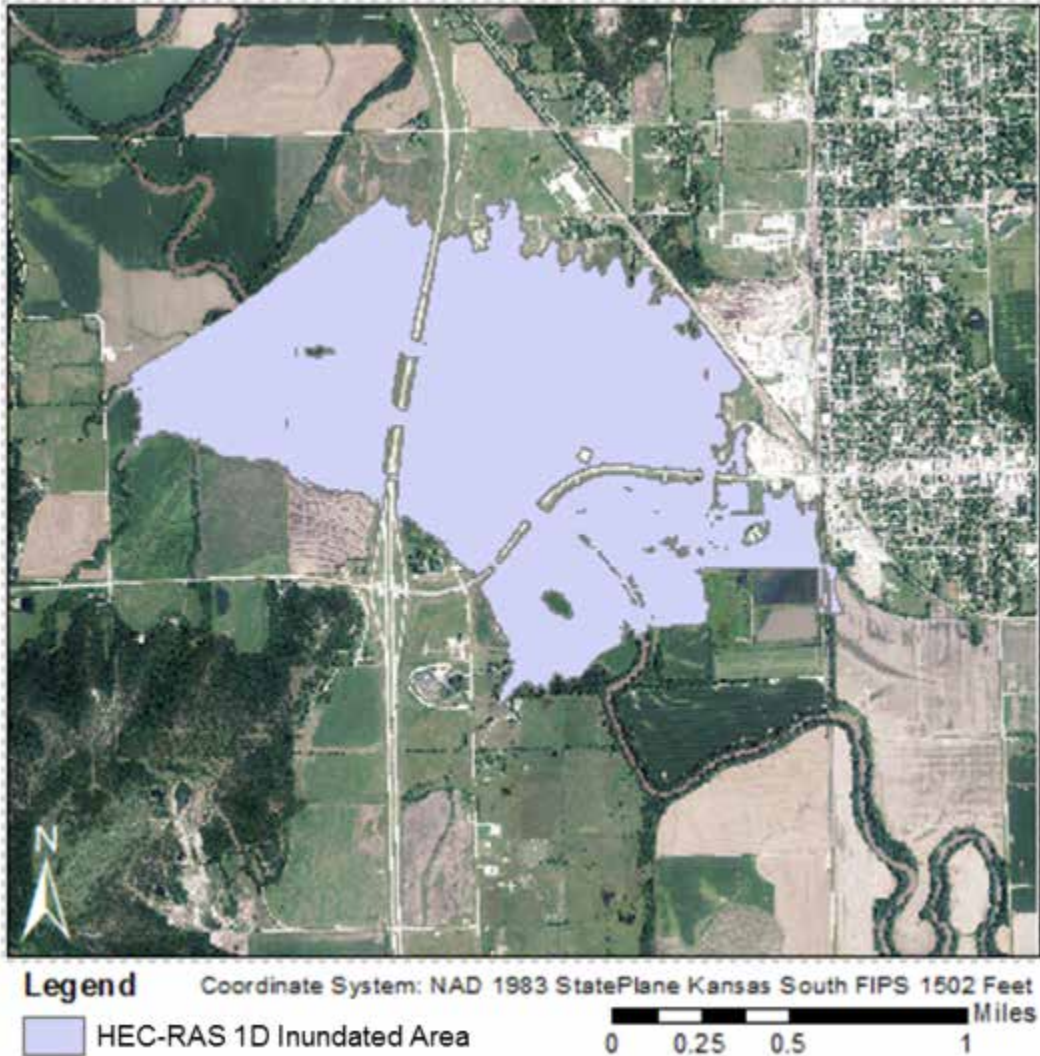


Figure 7.10: Map Showing Inundated Area from HEC-RAS 1D Neodesha Floodplain Model

The water surface profile in Figure 7.11 shows that the bed drop and subsequent rise through each bridge opening do not appear to produce suspicious results. The change in water surface elevation from two cross sections upstream of the main bridge on Highway 400 at River Station 12,276.80 feet (Station 10,974 on the plot) to two cross sections downstream of the bridge at River Station 11,676.45 (Station 10,374.03 on the plot), a distance of 160.05 feet, is 1.44 feet. This drop is reasonable given that the maximum depths at each respective cross section are 27.65 and 26.48 feet. The decrease in water surface elevation is even less distinct at the downstream bridge through Highway 75.

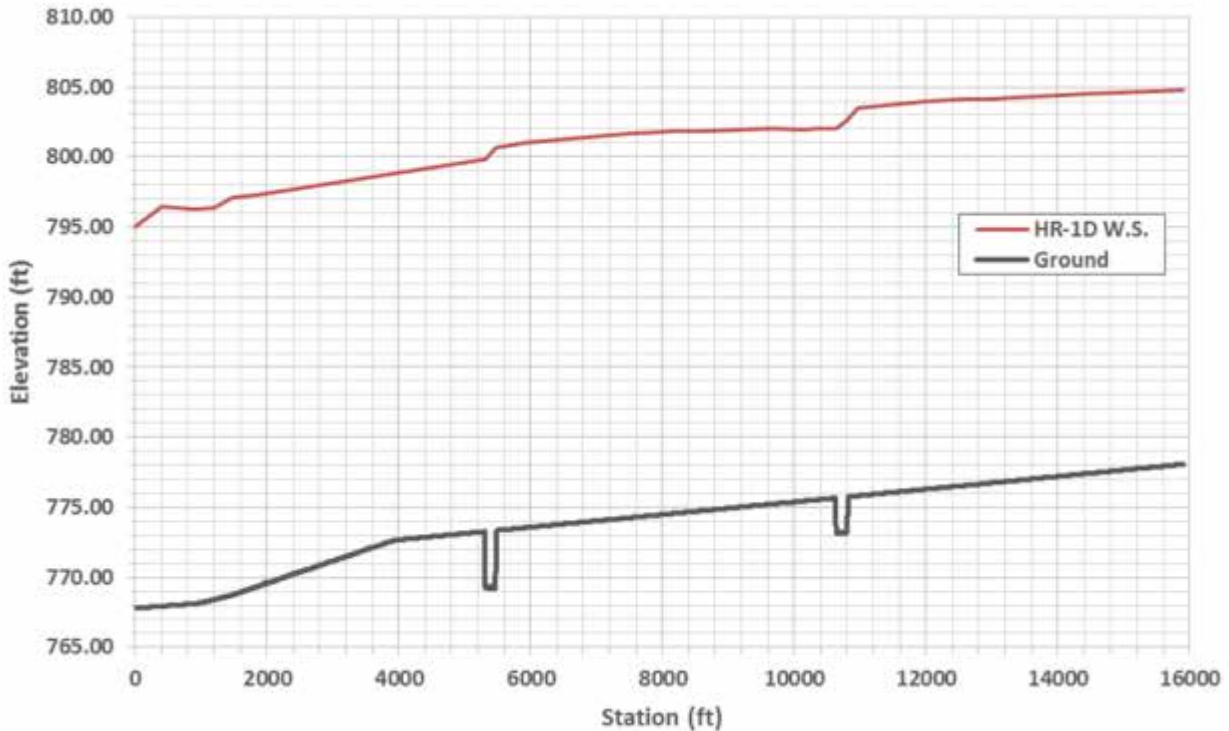


Figure 7.11: Channel Centerline Water Surface Profile from the HEC-RAS 1D Neodesha Floodplain Model

Table 7.1: Flow Divisions for the Hydraulic Structures of the HEC-RAS 1D Neodesha Floodplain Model

| Structure Designation | | Q (cfs) | Percent of Q_{MAX}^* |
|-----------------------|----------------------|------------|---------------------------|
| Highway 400 | Main Bridge | 29952 | 74.9% |
| | First Relief Bridge | 7267 | 18.2% |
| | Second Relief Bridge | 2363 | 5.9% |
| | Relief Culvert | 419 | 1.0% |
| Total Q: | | 40000 | 100.0% |
| Highway 75 | Main Bridge | 29554 | 73.9% |
| | First Relief Bridge | 6565 | 16.4% |
| | Second Relief Bridge | 3881 | 9.7% |
| | Total Q: | 40000 | 100.0% |

* $Q_{MAX} = 40,000 \text{ cfs}$

The flow splits shown in Table 7.1 were determined by entering the Geometric Editor window and left-clicking the desired bridge section to select it, choosing “Tabular Output,” and then selecting “Profile Table.” The opening of interest for the cross section must be selected from

the drop-down menu circled in Figure 7.12 below. Each Multiple Opening Output Table contains a variety of information about the particular opening, including results pertaining to the internal bridge cross sections. For example, in this table it could be determined what amount of the total discharge passed over the road as weir flow, but in this case all discharge in the vicinity of this opening passed through the bridge opening.

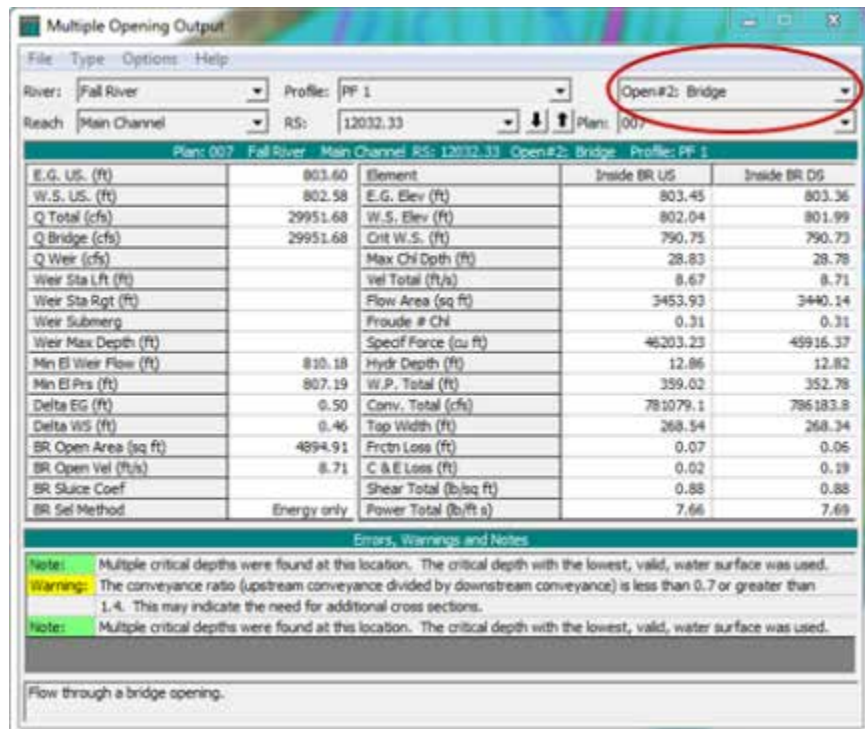


Figure 7.12: Flow Results for the Main Bridge Opening on Highway 400 for the HEC-RAS 1D Neodesha Floodplain Model

7.3 Two-Dimensional HEC-RAS Full Momentum Model for Neodesha

7.3.1 Two-Dimensional HEC-RAS Full Momentum Neodesha Model Setup

In order to more accurately account for losses through the bridge openings and the more dynamic effects of converging and diverging flow, only the full momentum equation set was considered for this fully 2D analysis using HEC-RAS 5.0.3. For a combined 1D/2D HEC-RAS model, using the 1D bridge routines to account for those losses and the 2D diffusion equation set everywhere else may be adequate, but such a case was not considered for this study. Two

different 2D plans were created for different methods of simulating the bridge piers. They were (1) High pier n -values applied in the RAS Mapper landuse layer, and (2) Raised piers applied to the RAS Mapper terrain layer.

Both full 2D plans contained 158,712 elements, with a minimum cell size of 1.07 square ft, a maximum cell size of 738 square ft, and an average cell size of 393 square ft. These cell attributes actually result in an area for the model equal to 2.23 square miles, which is slightly larger than the intended study area of 2.15 square miles. The reason for this has to do with a small area included near the downstream boundary on the east side. In this region, some rather unusual ponding occurred that was visible at the beginning of the simulation. The initial conditions of the simulation were the result of a 2-hour warmup period that used a constant discharge of 1000 cfs with the same downstream boundary as the simulation proper of a constant water surface elevation equal to 795 ft. The results from the early timesteps of the simulation show water in places it could not have flowed into and in this area, which was not intended to be part of the model domain. The velocities in this region were virtually zero, and thus the area was removed from the floodplain map that is described further within this section. The energy grade line used to establish the flow distribution at the inlet was 0.0003. The computational timestep for the model was 1 second, and the total simulated time spanned 66.7 hours. Thus, the inflow hydrograph was defined as shown in Figure 7.13.

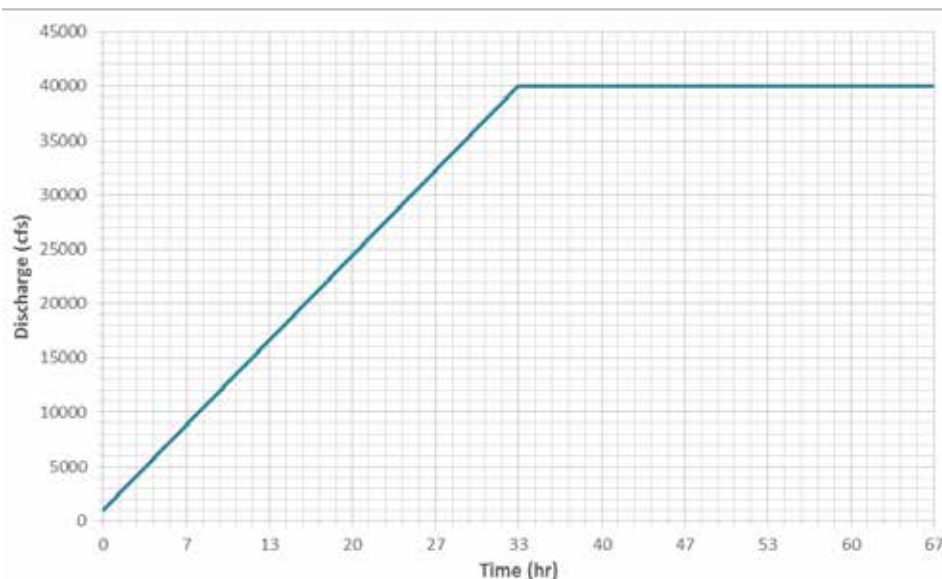


Figure 7.13: Inflow Hydrograph for the HEC-RAS 2D Neodesha Floodplain Model

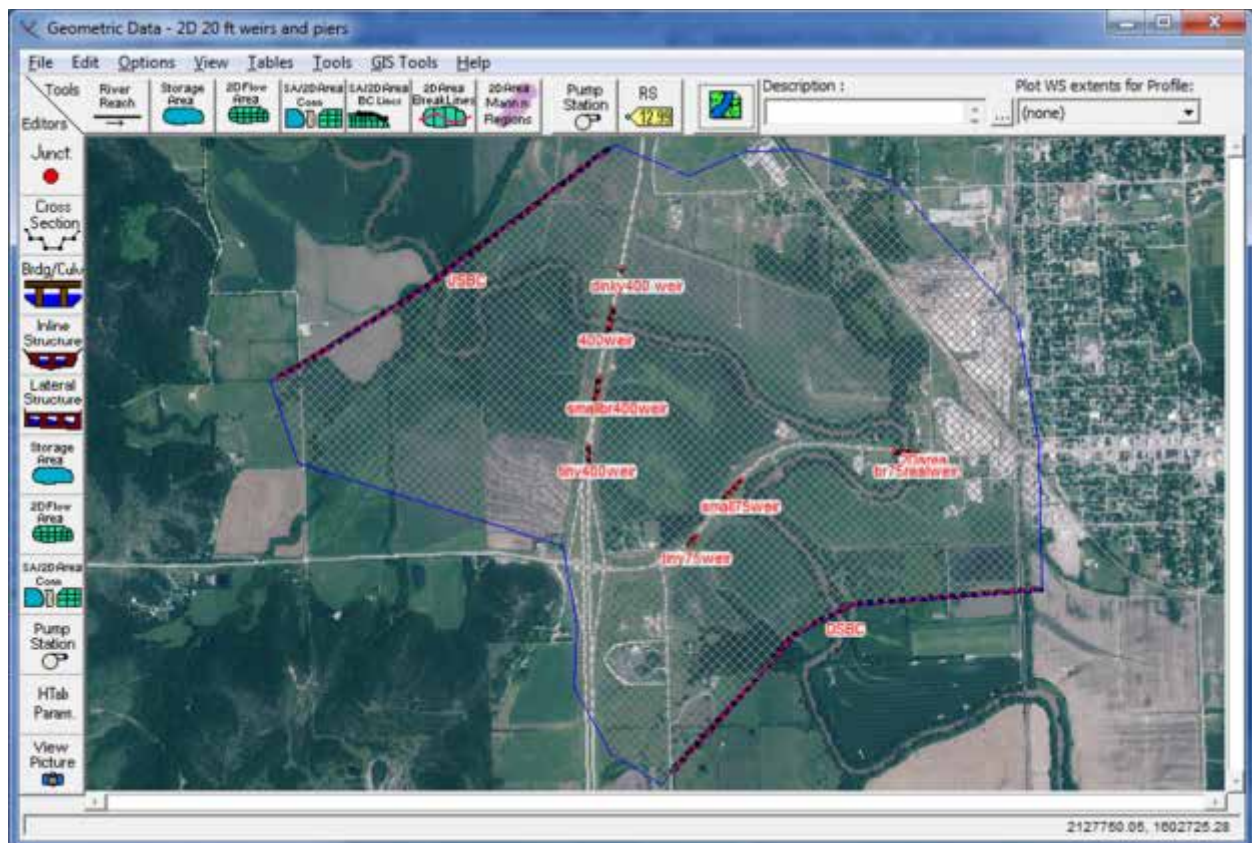


Figure 7.14: Transparent 2D Flow Area and Aerial Imagery for the HEC-RAS 2D Neodesha Floodplain Model

Both high pier n -value and raised pier approaches were used in HEC-RAS 2D to model this site. The geometry shown in Figure 7.14 was generated by enforcing a general spacing for the model area of 20 ft \times 20 ft. Individual breaklines were used to define the spacing of elements around each pier and to ensure cell faces were actually slightly inside the Manning's roughness coefficient grid cells or the raised terrain cells associated with the piers (see Chapter 6; note that the boundaries of the high n -value polygons and the raised pier rasters were buffered outside the actual pier boundaries used to create the cell boundaries). SA/2D Area Connectors were added that spanned the width of each hydraulic structure through the roadways to determine the flow through each of the seven openings. In HEC-RAS 2D there is no direct way of just measuring the flux across a line; the model does, however, record a hydrograph for the flow that passes over a weir, and a weir can be included in the 2D solution space of HEC-RAS at each of the connector locations. A weir must be drawn such that it follows the cell boundaries, and so weirs were

defined that were of the same dimensions and in the same locations as these breaklines. It would not be desirable for these weirs to have an effect on the flow characteristics, though, so they were made approximately the same height as the ground. You may get an error warning that requires you to raise the weir height just above the local ground elevation. They could not be exactly the same height as the ground, because making them thus almost invariably causes the simulation to fail in execution. For this reason, the elevation data along the breaklines was copied from HEC-RAS into an Excel spreadsheet, a value of 0.1 ft was added to every data point, and this new elevation series was pasted into the appropriate weir table. After all breaklines were enforced, a great deal of manual editing in the form of adding and moving points needed to be done to in order to avoid poor transitions in cell sizes, to reduce as much as reasonable the number of sides of each cell, to avoid thin elements, to make sure piers were properly included, and also to remove points that were too close together and violated the 1-ft spacing limit. (An alternative to this method is to create profile lines in RAS Mapper then select time series, flow to give flow plots at the profile lines.)

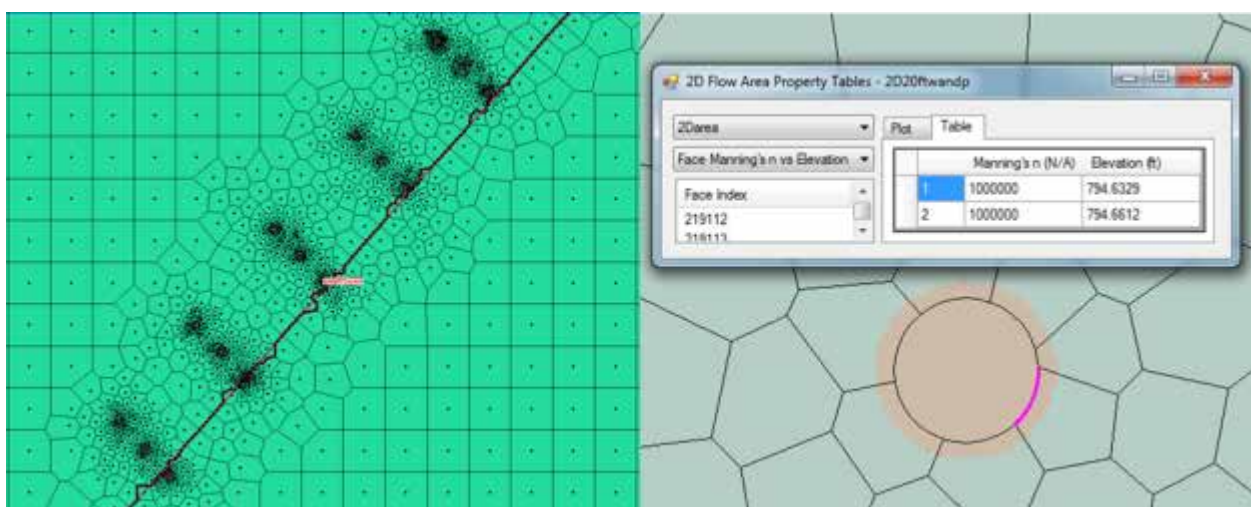


Figure 7.15: Results of Mesh Editing and Inclusion of Breaklines at the First Relief Bridge for the HEC-RAS 2D Neodesha Model

Figure 7.15 shows the results of manual editing and the inclusion of breaklines. This figure shows that after editing, the near-ground-level weir was no longer exactly on top of the breakline. This is because the weir is automatically readjusted to follow cell faces that lead from

its starting point to its end. This readjustment will not affect the flux calculations over the weir, and since the weir was raised 0.1 ft over its initial position, it should avoid any errors that may arise from the movement of the weir.

7.3.2 Two-Dimensional HEC-RAS Full Momentum Neodesha Model Results

Once all model parameters were defined and the mesh prepared, the simulation was run. The code took 27 hours 29 minutes 49 seconds and 30 hours 08 minutes 45 seconds, respectively, to completely execute the raised pier and the high pier n-value runs. Figures 7.16 to 7.22 and Table 7.2 describe the results.

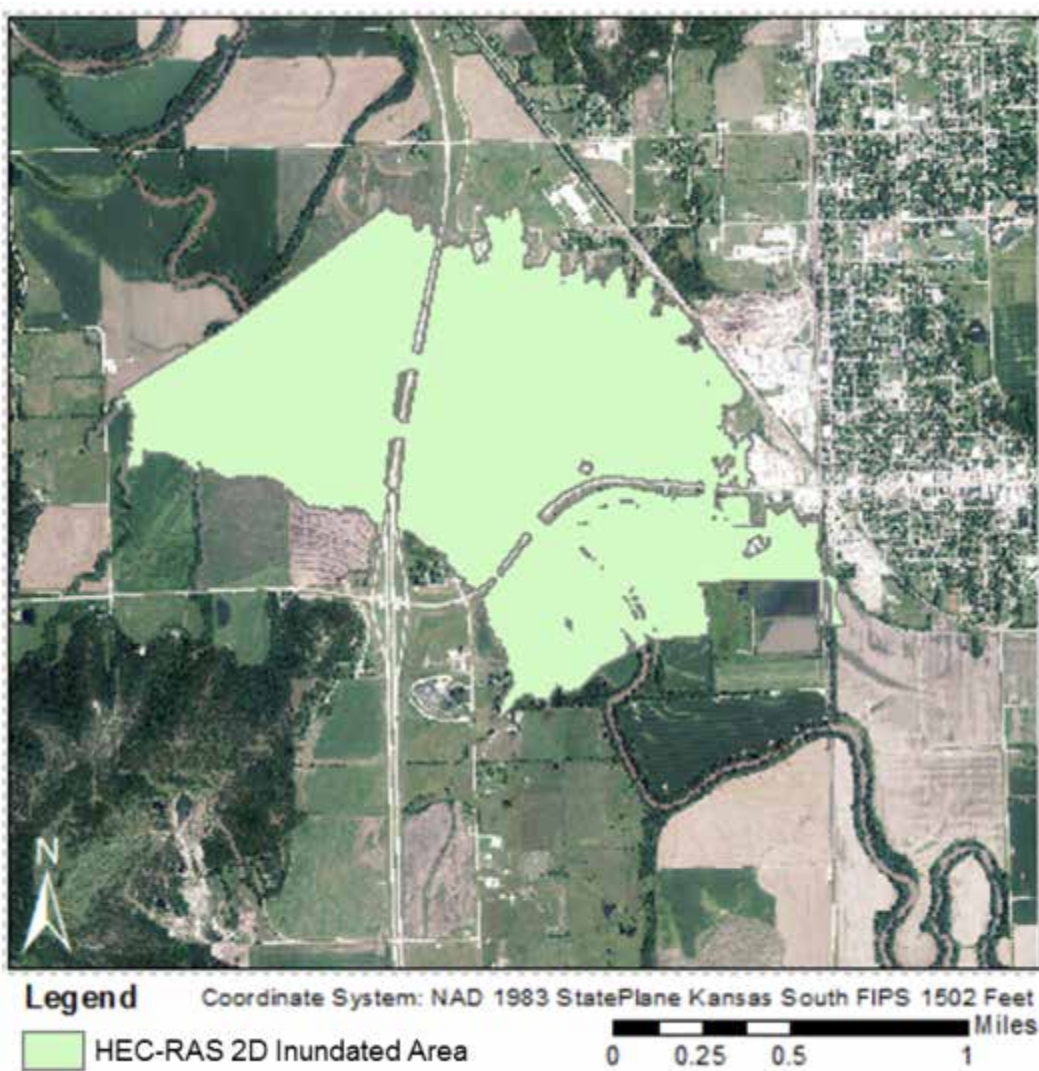


Figure 7.16: Map Showing Inundated Area from HEC-RAS 2D Full Momentum Neodesha Floodplain Model

The floodplain depicted in Figure 7.16 was determined by saving the water surface elevation raster from RAS Mapper for the final timestep of the model as a stored map. This raster was then loaded in ArcMap and the 3D Analyst tool “Raster Domain” was used to determine its extents. A few small disconnected flow areas, located in the northeastern part of the 2D flow area near the small road and train tracks that nearly form a triangle with Highways 400 and 75, were removed. Figure 7.17 shows these disconnected areas. They occurred because the 20 ft square elements in that region of the model were large enough to span the roadway from one corner to the diagonal corner across the element. Since flow is allowed to enter one mesh face of an element and then exit another, numerically the highpoint of the road centerline manifested itself merely in the stage versus storage relationship for the cell, and this interior feature of the cell was bypassed entirely by the flow. Velocities were essentially zero in this region, and viewing the results determined that the extents of the ponding due to this apparently disconnected flow area were stable. Therefore, the disconnected flow areas were deemed appropriate for removal from the final floodplain map. The problem of these disconnected areas could be easily avoided by adding a breakline along the road centerline. However, due to time constraints, this breakline was not added to the geometry, and the simulation was not rerun. The total area of this cleaned-up polygon was 1.40 square miles, or 65.0% of the total study area.

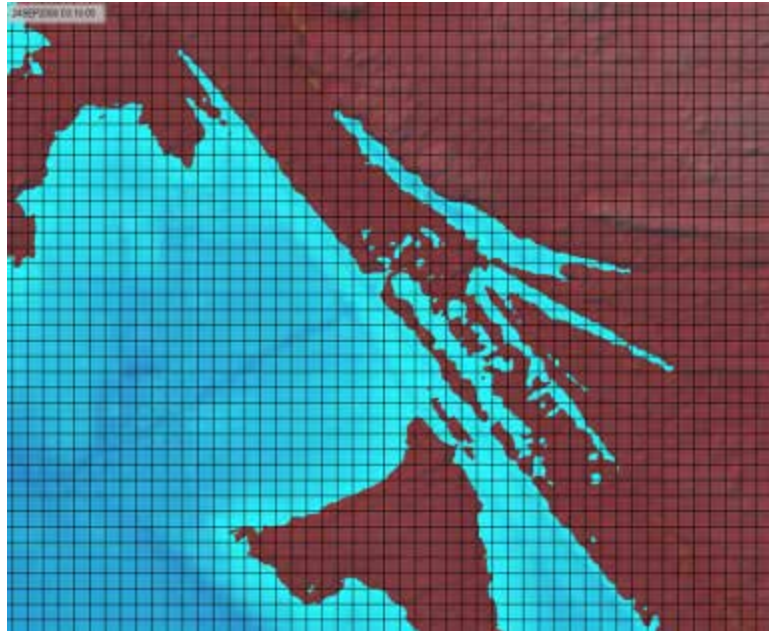


Figure 7.17: Disconnected Flow Areas from the HEC-RAS 2D Model for Neodesha Floodplain Model

Table 7.2: Flow Divisions at the Final Timestep for the Hydraulic Structures of the HEC-RAS 2D Neodesha Floodplain Models

| | | HEC-RAS v 5.0.3 2D Raised Piers | | | HEC-RAS v 5.0.3 2D High Pier n-values | | |
|---------|-----------------------|------------------------------------|-------------------------------|----------------------------------|------------------------------------------|-------------------------------|----------------------------------|
| | Structure Designation | Q (cfs) | Percent of Q _{max} * | Q _{1D} -Q _{2D} | Q (cfs) | Percent of Q _{max} * | Q _{1D} -Q _{2D} |
| HW 400 | Main Bridge | 25162 | 62.9% | 4780 | 25091 | 62.7% | 4851 |
| | 1st Relief Bridge | 10485 | 26.2% | -3218 | 10577 | 26.4% | -3310 |
| | 2nd Relief Bridge | 3688 | 9.2% | -1325 | 3686 | 9.2% | -1323 |
| | Relief Culvert | 682 | 1.7% | -263 | 639 | 1.6% | -220 |
| Total Q | | 40017 | 100.0% | | 39994 | 99.9% | |
| HW 75 | Main Bridge | 20921 | 71.3% | 8633 | 20924 | 52.3% | 8630 |
| | 1st Relief Bridge | 10574 | 14.1% | -4009 | 10587 | 26.5% | -4022 |
| | 2nd Relief Bridge | 8517 | 14.5% | -4636 | 8504 | 21.2% | -4623 |
| | Total Q | 40002 | 100.0% | | 40004 | 100.0% | |
| | Run Time | 1.15 day (desk top) | | | 1.27 day (desk top) | | |
| | No. of Cells | 158,712 | | | 158,712 | | |
| | Δt | 1 sec | | | 1 sec | | |

The flow splits shown in Table 7.2 were obtained from the HEC-RAS Stage and Flow Hydrograph tables related to plots like those shown in the following figure and compiled in Figure 7.18. The data show that steady state conditions had been reached by the 2D HEC-RAS models. The results of Table 7.2 demonstrate that the volume conservation of the HEC-RAS 2D model was quite good for the 2D simulations.

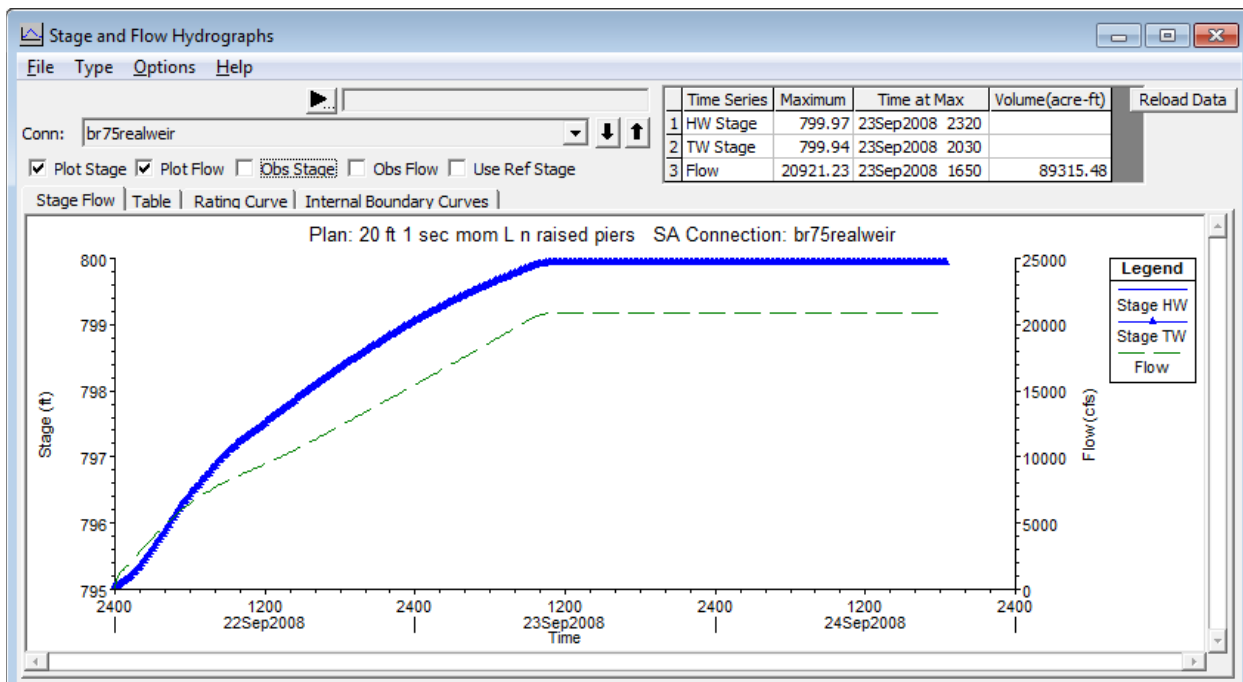


Figure 7.18: Weir Flow Hydrograph from HEC-RAS 2D for the Main Bridge on Highway 75

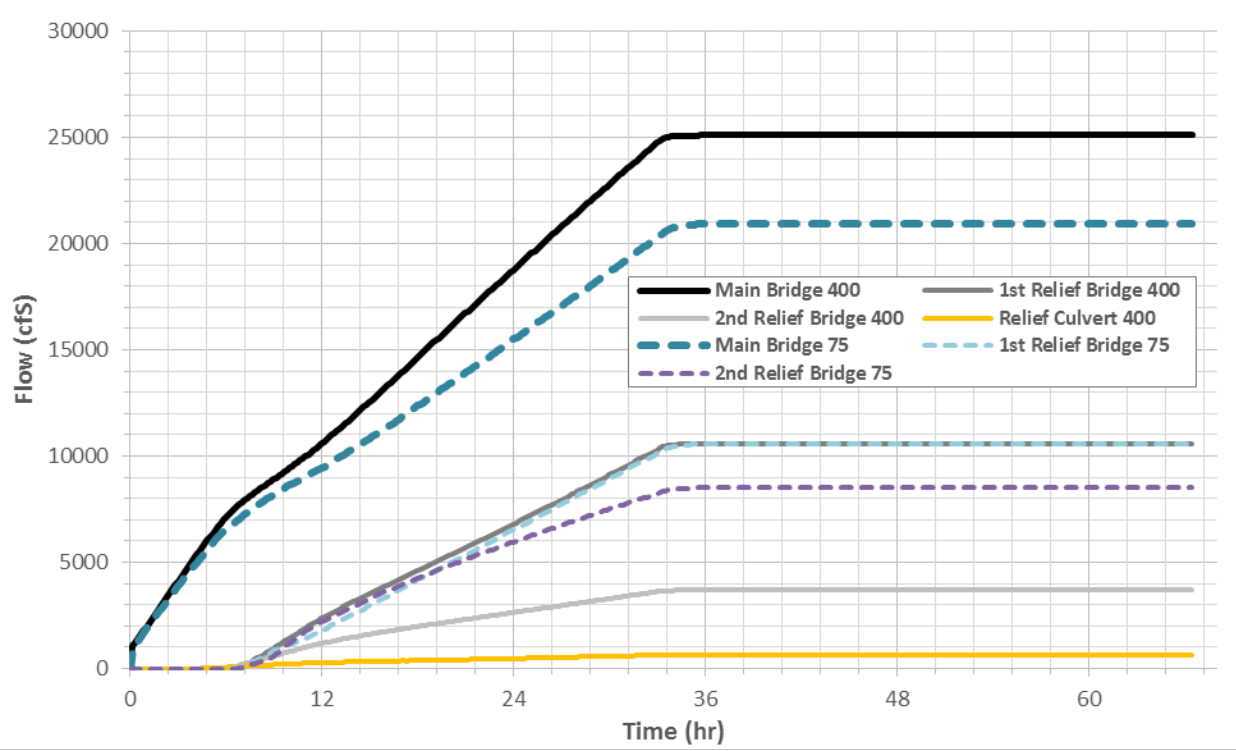


Figure 7.19: Hydrographs of the HEC-RAS 2D Hydraulic Structures for the Neodesha Floodplain Study

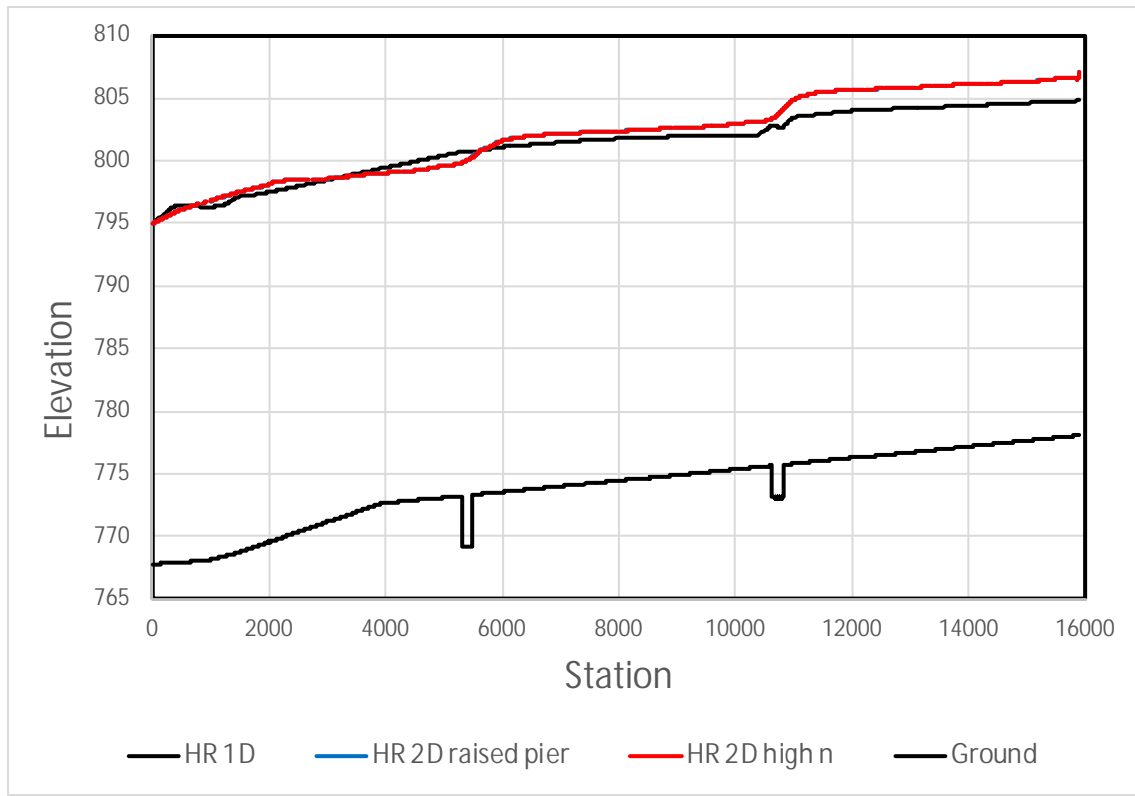


Figure 7.20: Channel Centerline Water Surface Profile from HEC-RAS 1D and 2D Neodesha Floodplain Models

The water surface profiles shown in Figure 7.20 were made from data exported from a centerline profile in RAS Mapper. Note that both of the 2D runs had virtually identical profiles verifying that at least for this site, accounting for the piers by either high n -values or raised terrain produces the same results. It can be seen that the downstream boundary condition was satisfied, and that at the upstream end, the curious behavior observed in various places elsewhere in the analyses discussed in this report was also present. The flow at the inlet entered the model space at a depth higher than seems reasonable and thus highlights the importance of placing boundary conditions far enough away from the area to be studied in detail that the boundaries do not adversely affect the results.

Figures 7.21 and 7.22 demonstrate the overall flow patterns for this model of the Neodesha Floodplain. The series of images are taken from the vicinity of each hydraulic structure. These images could be used to adjust the ineffective flow markers for a 1D model; however, this was not done here.

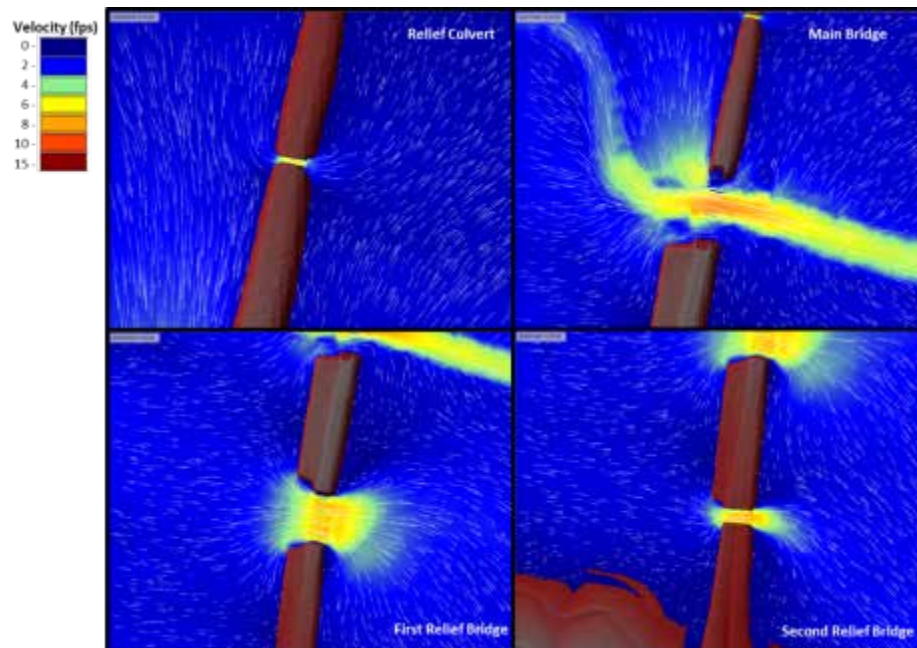


Figure 7.21: Velocity Contours with Tracers for the HEC-RAS 2D Highway 400 Openings

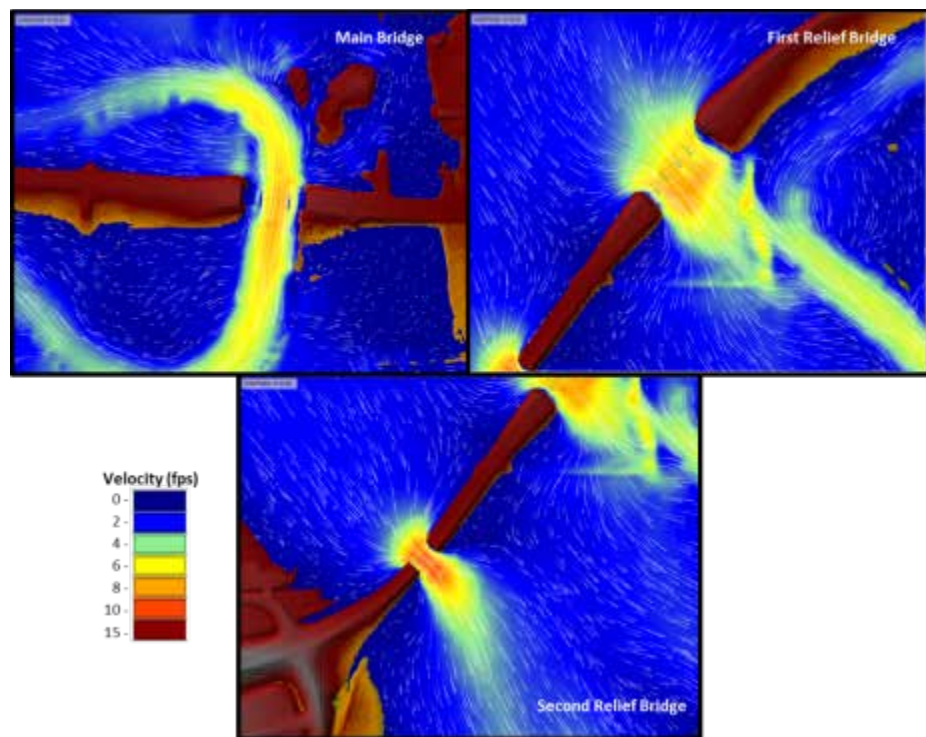


Figure 7.22: Velocity Contours with Tracers for the HEC-RAS 2D Highway 75 Openings

7.4 SRH-2D Model for Neodesha

7.4.1 SRH-2D Neodesha Model Setup

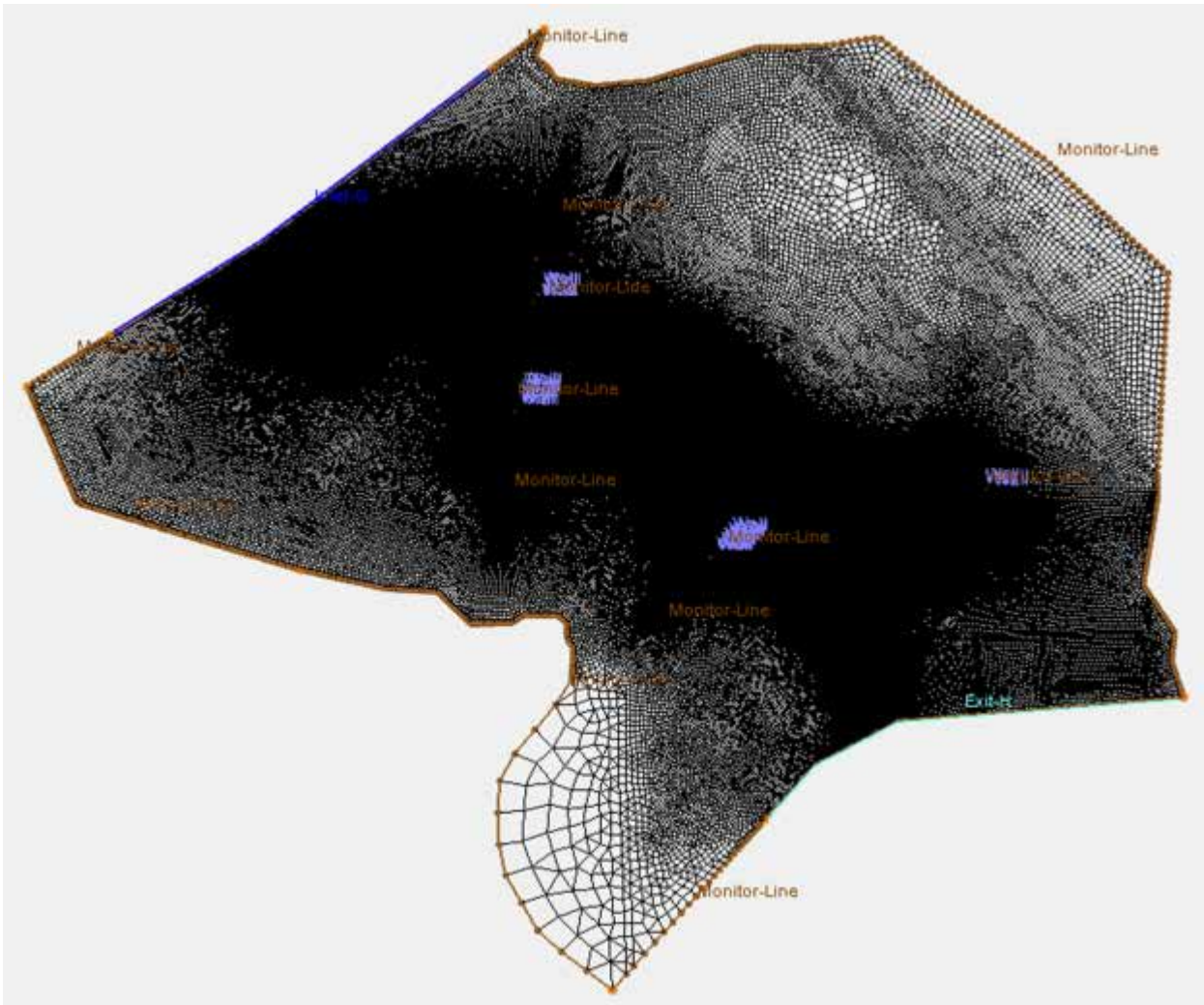


Figure 7.23: Finite-Element Mesh for SRH-2D Neodesha Floodplain Model Viewed in SMS

The mesh generated in SMS for the SRH-2D model and shown in Figure 7.23 was composed of 420,269 elements with a minimum element size of 0.34 square ft, a maximum element size of 81,956.42 square ft, and an average element size of 142 square ft. The total area for the model was 2.15 square mi and so matched that of the intended study area. The mesh contained a mixture of triangular and quadrilateral elements. The size and distribution of elements depended on the quantity of nodes along arcs defining the boundaries of the land

coverage polygons shown in Figure 7.5. The spacing of these nodes along arcs was determined manually for each arc individually with the intent of achieving an appropriate balance between computational efficiency, model stability, and precision of results. The node spacings on the arcs defining the pier boundaries were specified as 1 ft to satisfy the criteria above. Additional arcs were manually drawn, using the raster as a guide, to define key features such as the roadway embankments and the levees at the downstream boundary. A close-up view of the results of mesh generation can be seen in Figure 7.24 below. Also in this figure, two lines can be seen, each called “Monitor Line.” Seven of these lines were added to the SRH-2D boundary condition layer, one for each hydraulic structure represented within the model. When the SRH-2D code is executed, the instantaneous flux across each of these lines is written to separate text files stored in the same folder as the rest of the output from the simulation. These files can then be easily retrieved and brought into an Excel spreadsheet.

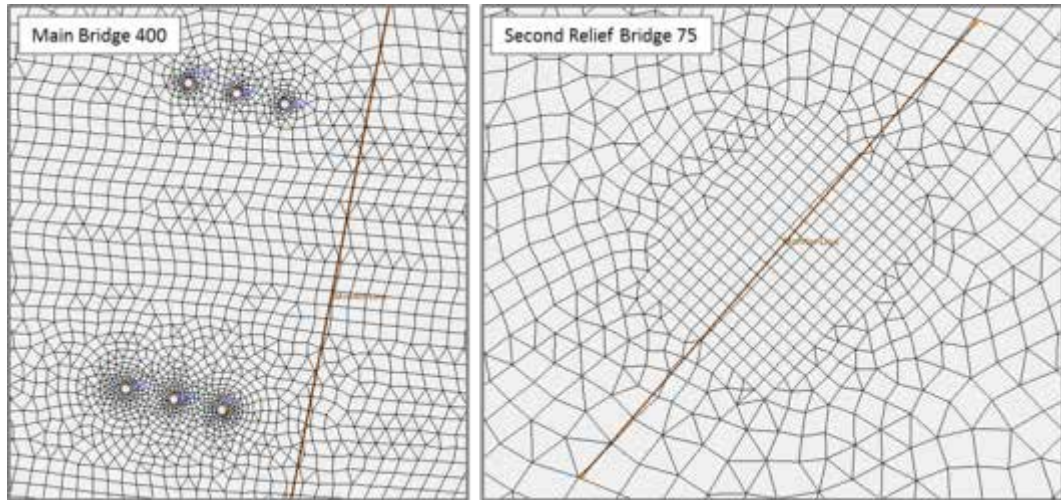


Figure 7.24: Two Plan Views Typical of the SRH-2D Mesh Construction Near the Hydraulic Structures for the Neodesha Floodplain Model

For the SRH-2D simulation the initial condition was set to “Dry.” “Conveyance” was selected as the method for distributing flow at the inlet. The computational timestep for the simulation was 0.2 seconds. The total simulated time was specified as 8 hours, and so, following a similar pattern specified elsewhere in this report, the inflow hydrograph for the model was developed as follows.

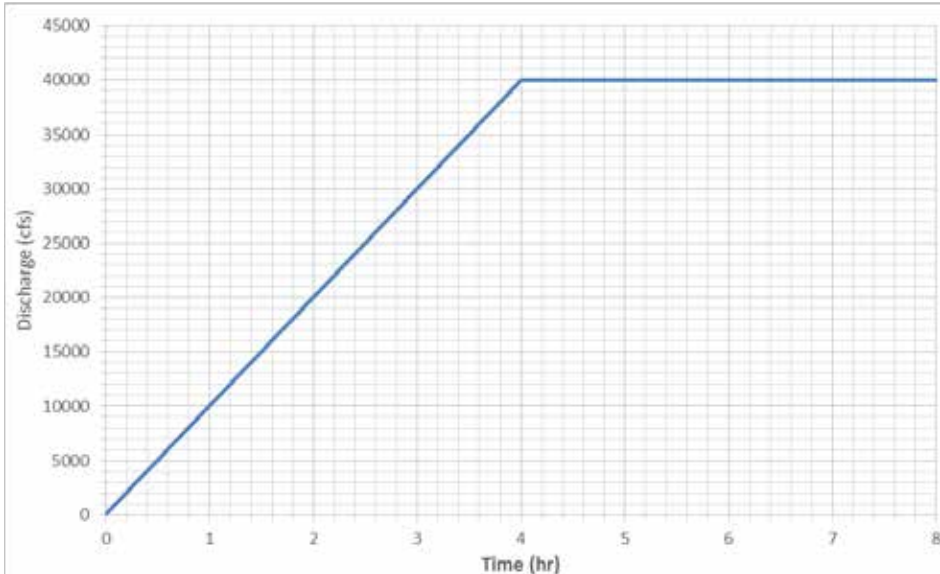


Figure 7.25: Inflow Hydrograph for SRH-2D Neodesha Floodplain Model

The total CPU time required for the model to run to completion was 166 hours 59 minutes, or 6.96 days. A restart of the model was required after about 106 hours due to an unforeseen computer shutdown. Fortunately, by default SRH-2D generates restart files that can be used to resume a model in such cases. Including the time that elapsed between the interruption of the simulation's execution and when it was able to be restarted, the model took almost 9 days to run (the shutdown occurred late at night over a weekend). This reveals one problem of using a model that involves such long computation times. Possibly the model could have used a slightly larger timestep than 0.2 seconds, but definitely not more than 1 second. Experience suggests that for numerical stability, SRH-2D requires smaller computational timesteps than the HEC-RAS 2D full momentum model. It's important to note that SRH-2D generates multiple, large restart files for each simulation run. The user must be exercise careful file management to avoid storing excessive quantities of restart data.

7.4.2 SRH-2D Neodesha Model Results

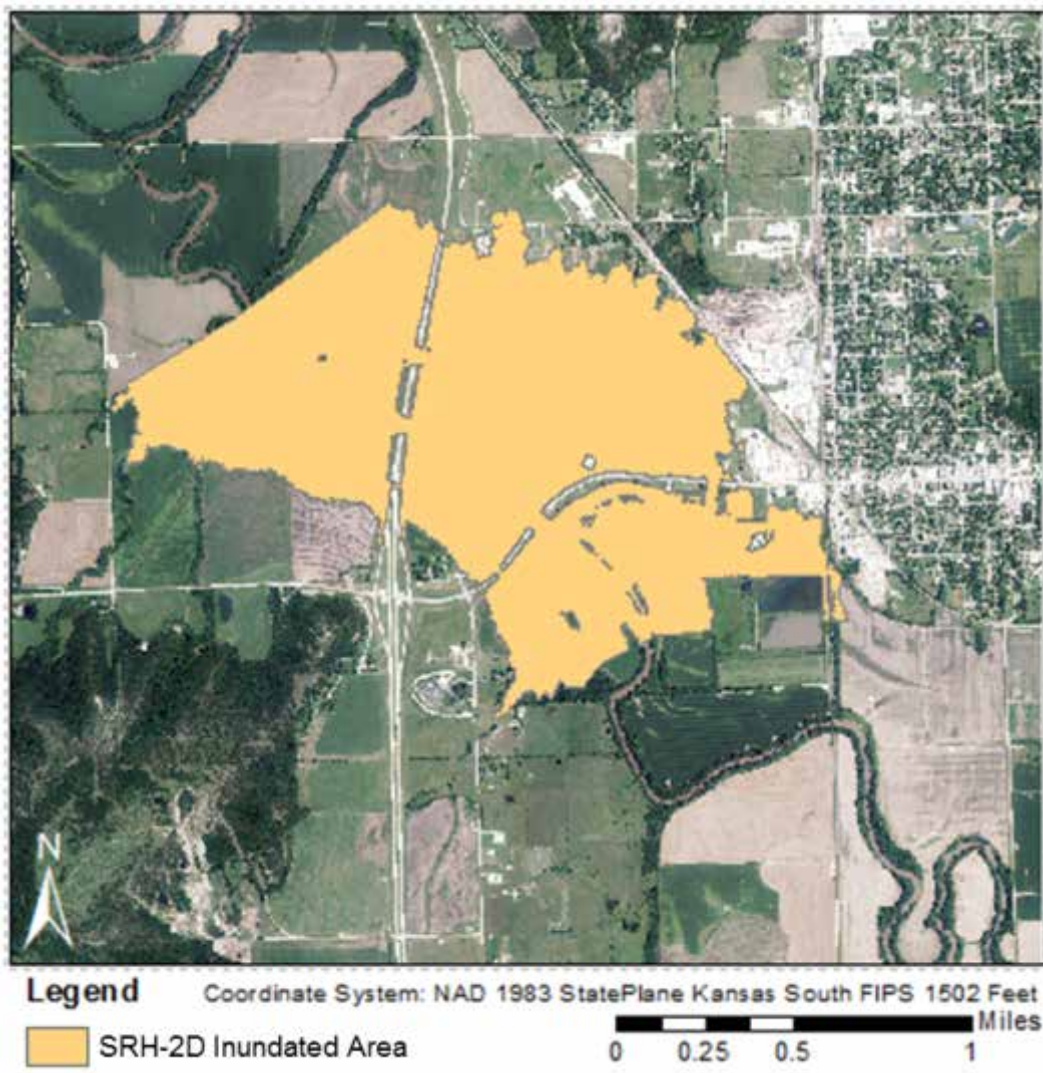


Figure 7.26: Map Showing Inundated Area from SRH-2D Neodesha Floodplain Model

In order to generate the inundation map shown in Figure 7.26 in ArcMap, quite a large number of steps needed to be performed. To summarize, the depth contour map needed its display options set to “Linear” rather than “Color Fill,” where the number of contour intervals was set to one and the single contour displayed corresponded to a depth of 0.01 ft. The contour map then had to be exported from SMS as an AutoCAD shapefile. This linear AutoCAD shapefile was brought into ArcMap containing a great number of layers and line types. The single layer that corresponded to the desired boundary was exported from its parent set so that it

would be alone and in the ArcMap shapefile format. The linear shapefile was then manipulated in a variety of ways until it was finally of the form shown in Figure 7.26. The area inundated by the final timestep equaled 1.37 square miles, thus accounting for 64.0% of the total study area.

Table 7.3: Flow Divisions at the Final Timestep for the Hydraulic Structures of the SRH-2D Neodesha Floodplain Model

| | | Structure Designation | Avg. WSE (ft) | Q (cfs) | Percent of Q_{MAX}^* |
|-----------------------|----------------------|-----------------------|------------------|------------|---------------------------|
| Highway 400 | Main Bridge | 801.81 | 27711 | 69.3% | |
| | First Relief Bridge | 803.71 | 8246 | 20.6% | |
| | Second Relief Bridge | 802.38 | 3417 | 8.5% | |
| | Relief Culvert | 801.56 | 591 | 1.5% | |
| Total Q (cfs): | | | 39965 | 99.9% | |
| Highway 75 | Main Bridge | 798.94 | 25511 | 63.8% | |
| | First Relief Bridge | 799.28 | 7535 | 18.8% | |
| | Second Relief Bridge | 798.29 | 6818 | 17.0% | |
| Total Q (cfs): | | | 39864 | 99.7% | |

While Table 7.3 may suggest that there were somewhat significant volume conservation issues with the SRH-2D model, it is more likely that the model had not yet fully reached steady state conditions. Figure 7.27 makes this appear even more likely. The series called “Exit” contains the data for the downstream boundary condition for the simulation and can be seen asymptotically approaching but not quite reaching the maximum discharge of 40,000 cfs. It is plausible that another hour of simulation time would have been sufficient to fully reach steady state conditions, but because adding another hour would have taken approximately another 24 hours to execute, this was not done. However, a visual inspection of the model results over the final half hour suggested that the floodplain extents were very nearly constant, and since the sum of the discharges through the openings were within 0.1–0.3% of the maximum inflow, these results were deemed acceptable for comparison purposes. The additional volume that would have been stored in the model at true steady state conditions is unlikely to have made any significant impact on the observed depths or floodplain extents, but this situation highlights one of the challenges involved in mathematically complex and thus time-consuming hydraulic models.

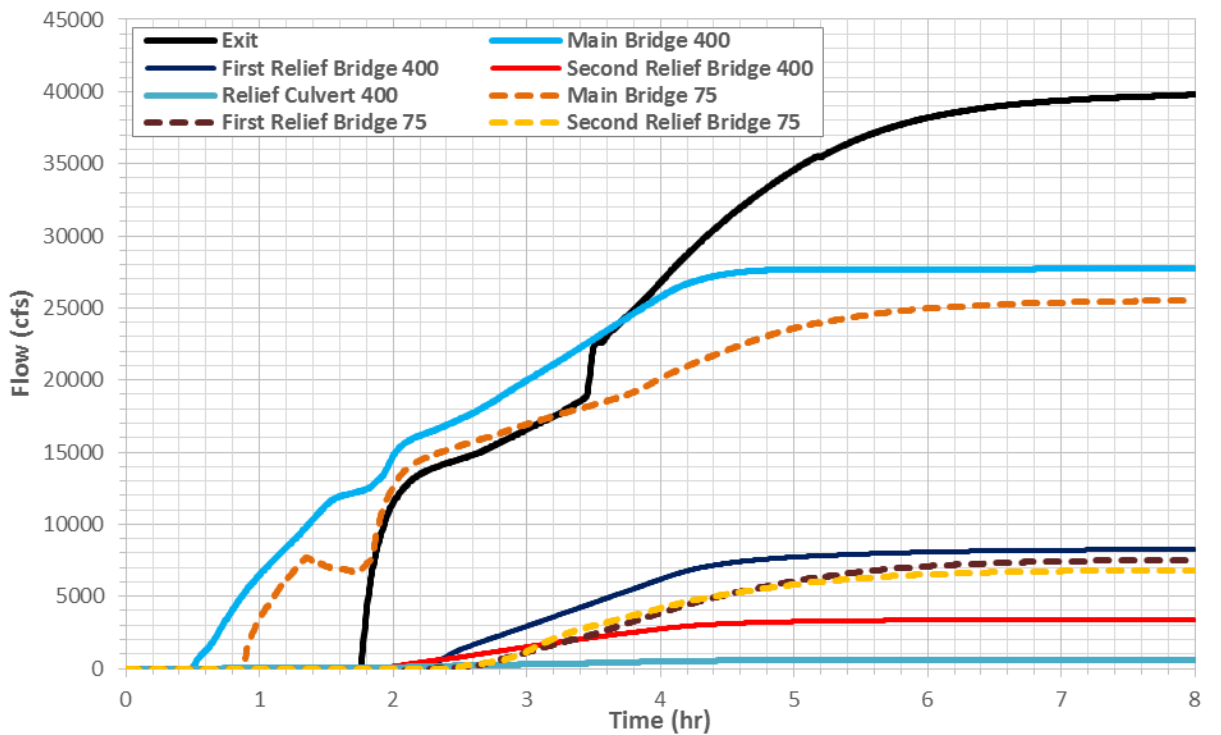


Figure 7.27: Hydrographs of the SRH-2D Hydraulic Structures for the Neodesha Floodplain Study

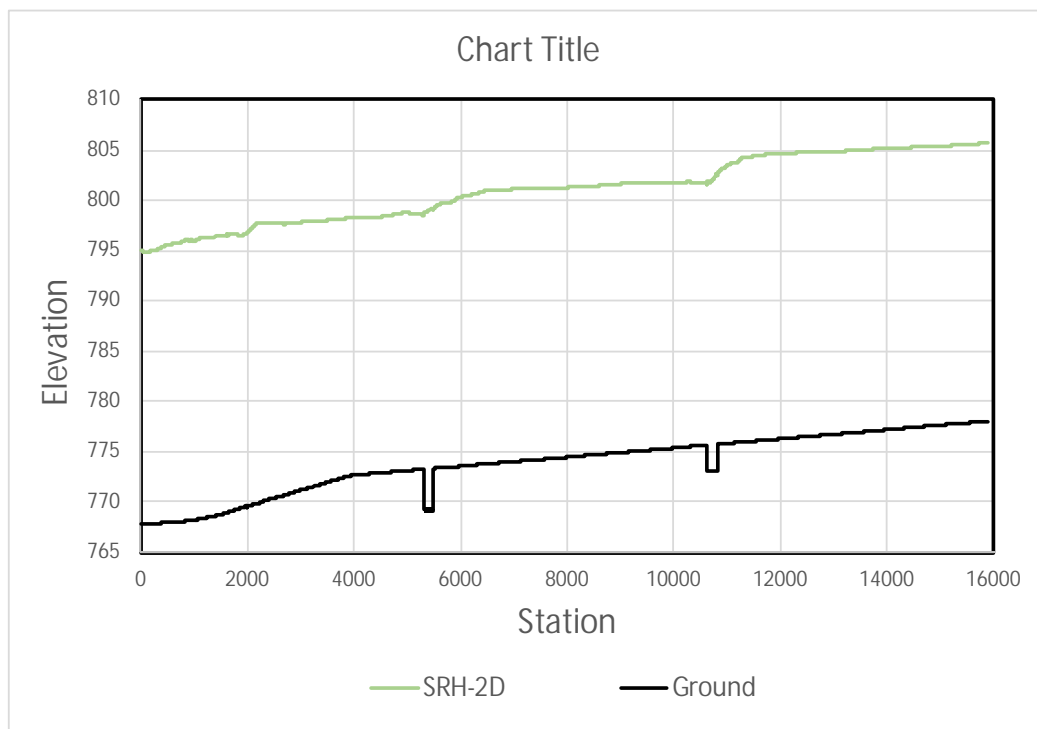


Figure 7.28: Channel Centerline Water Surface Profile from SRH-2D Neodesha Floodplain Model

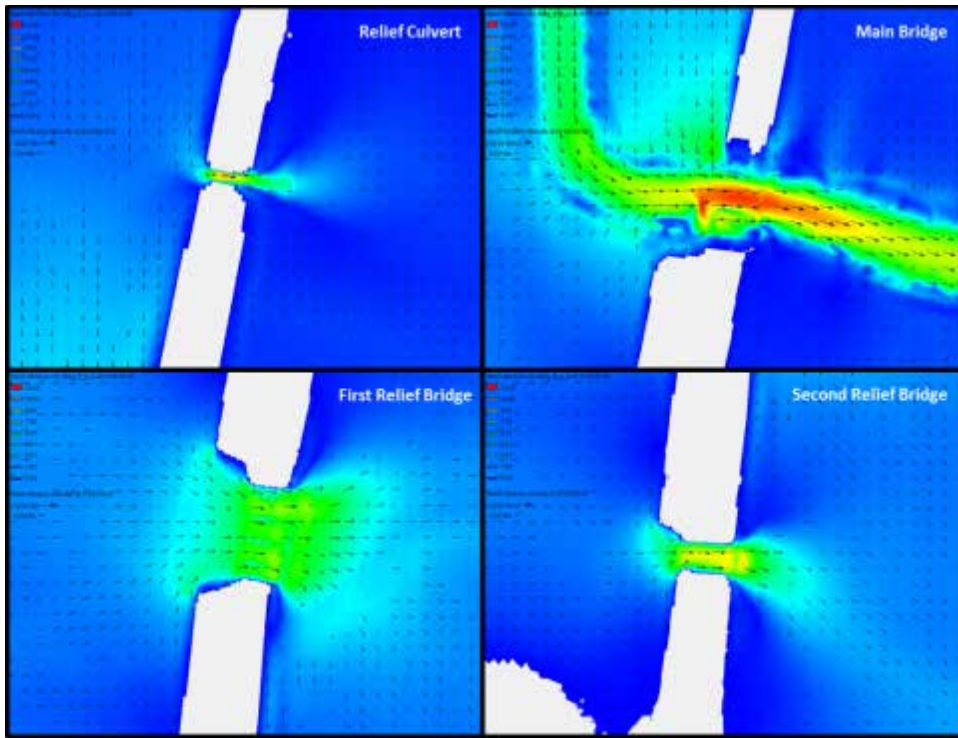


Figure 7.29: Velocity Contours with Vectors for the SRH-2D Highway 400 Openings

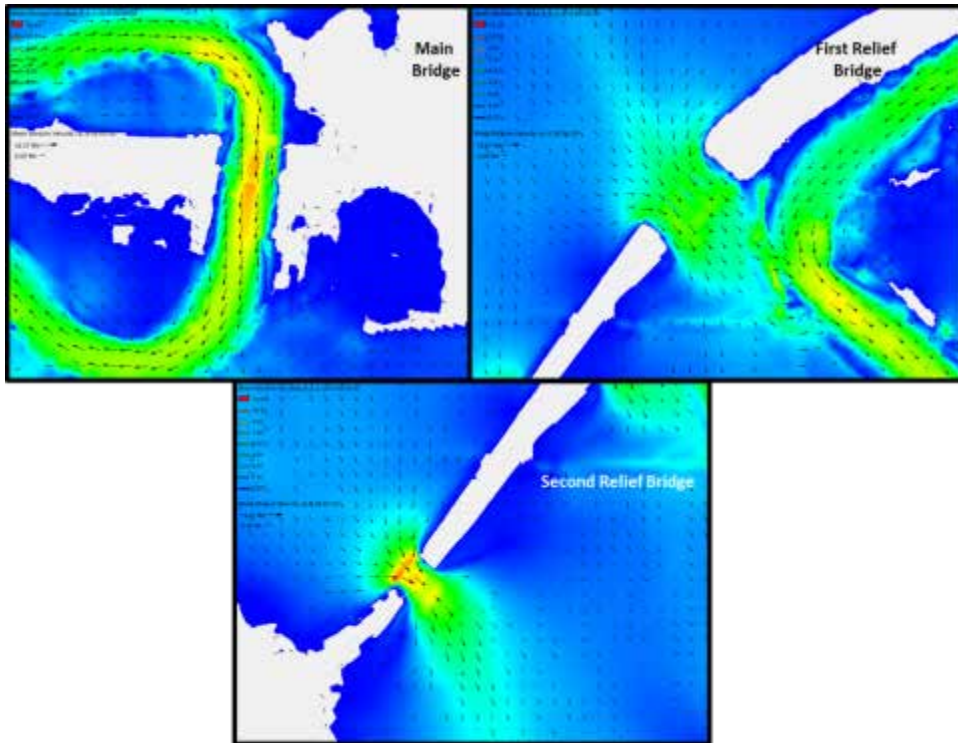


Figure 7.30: Velocity Contours with Vectors for the SRH-2D Highway 75 Openings

7.5 Summary of the Neodesha Floodplain Study Hydraulic Model Results

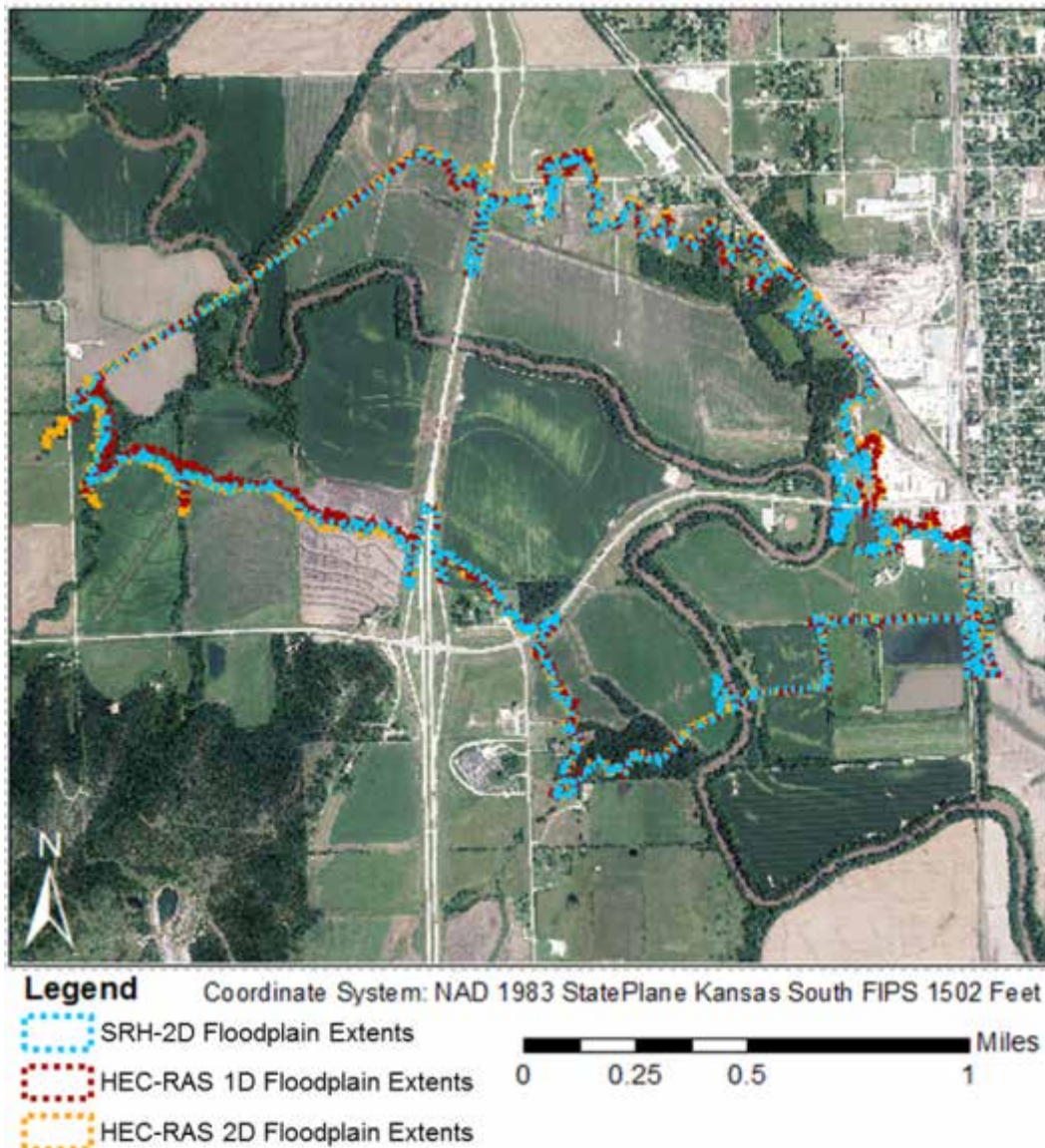


Figure 7.31: Comparison Map Showing the Floodplain Extents from All Three Models for the Neodesha Test Site

Figure 7.31 shows that the outside bounds of the floodplain are actually very similar for all three models tested: the 1D HEC-RAS model, the 2D HEC-RAS full momentum model, and the SRH-2D model. If comparing either of the 2D models' extents to those of the 2D model, it is difficult to assess which predicts a wider floodplain because sometimes the 2D floodplain extents are inside and sometimes outside. If the comparison is limited to the 2D models, however, it

appears that the SRH-2D-derived floodplain has extents either at approximately the same limits as the HEC-RAS 2D full momentum model or just inside of these limits. However, the extents are all more or less equal. This becomes even more apparent if one considers the actual portions of the model that were determined to be underwater at steady state conditions for the site. The following table contains the inundation data presented in previous sections. All models predict roughly the same amount of flooded land.

Table 7.4: Summary of Flooded Area for All Three Models for the Neodesha Test Site

| Model | Wet Area (sq.mi.) | Percent Inundation |
|--------|----------------------|-----------------------|
| - | | |
| HR-1D | 1.35 | 63.1% |
| HR-2D | 1.40 | 65.0% |
| SRH-2D | 1.37 | 64.0% |

Comparing the steady state flow from the 1D model and the final timesteps of the 2D models, shown in Table 7.5, one sees that the 1D model predicted the highest flows through both of the main bridges. Both 2D models distributed the flow more widely across the floodplain, resulting in more flow going through the relief structures present on both highways. Strikingly, the flow divisions through the openings determined by SRH-2D are more often than not closer to the conveyances determined by the HEC-RAS 1D model than those determined by the HEC-RAS 2D model. The four cases out of seven where the SRH-2D values are more similar to those given by the 1D model include, on both Highways 400 and 75, the main bridges and the first relief bridges. It is not known which division of flow is the most accurate; further testing, requiring either laboratory or field data to which the models could be calibrated, would be required to make such a claim. If the 2D models were more accurate, these could be used to guide 1D scour analyses, which may be overpredicting the amount of scour expected to occur through the main channel structures. One thing to keep in mind is that the HEC-RAS 2D model could be set up very quickly if only the raw LIDAR data were used and details such as piers

were not considered. The terrain should, however, be adjusted to include any culverts. A fairly large grid size could be used to allow one to produce a reasonable flow distribution.

Table 7.5: Summary of Flow Divisions for all Models through the Hydraulic Structures within the Neodesha Test Site

| | | HEC-RAS 1D v 5.0.03 | | HEC-RAS v 5.0.3 2D Raised Piers | | | HEC-RAS v 5.0.3 2D High Pier n-values | | | SRH-2D | | |
|---------------|--------------------------|------------------------|---------------------------|------------------------------------|---------------------------|-----------------|------------------------------------------|---------------------------|-----------------|------------|---------------------------|------------------------------|
| | Structure Designation | Q (cfs) | Percent of Q_{max}^* | Q (cfs) | Percent of Q_{max}^* | $Q_{1D}-Q_{2D}$ | Q (cfs) | Percent of Q_{max}^* | $Q_{1D}-Q_{2D}$ | Q (cfs) | Percent of Q_{max}^* | $Q_{SRH\ 2D}-Q_{2D\ Raised}$ |
| HW 400 | Main Bridge | 29952 | 74.9% | 25162 | 62.9% | 4790 | 25091 | 62.7% | 4860 | 27711 | 69.2% | -2549 |
| | 1st Relief Bridge | 7267 | 18.2% | 10485 | 26.2% | -3218 | 10577 | 26.4% | -3310 | 8246 | 20.6% | 2239 |
| | 2nd Relief Bridge | 2363 | 5.9% | 3688 | 9.2% | -1326 | 3686 | 9.2% | -1323 | 3417 | 8.5% | 271 |
| | Relief Culvert | 419 | 1.0% | 682 | 1.7% | -263 | 639 | 1.6% | -220 | 591 | 1.5% | 91 |
| | Total Q | 40000 | 100.0% | 40017 | 100.0% | | 39994 | 99.9% | | 39965 | 99.9% | 52 |
| HW 75 | Main Bridge | 29554 | 73.9% | 20921 | 71.3% | 8633 | 20924 | 52.3% | 8630 | 25511 | 63.8% | -4590 |
| | 1st Relief Bridge | 6565 | 16.4% | 10574 | 14.1% | -4010 | 10587 | 26.5% | -4023 | 7535 | 18.8% | 3039 |
| | 2nd Relief Bridge | 3881 | 9.7% | 8517 | 14.5% | -4636 | 8504 | 21.2% | -4623 | 6818 | 17.0% | 1699 |
| | Total Q | 40000 | 74.9% | 40002 | 100.0% | | 40004 | 100.0% | | 40002 | 100.0% | 0 |
| | Run Time | 5 sec | | 1.15 day (desk top) | | | 1.27 day (desk top) | | | 10 days | | |
| | No. of Cells | na | | 158,712 | | | 158,712 | | | 420,269 | | |
| | Δt | na | | 1 sec | | | 1 sec | | | 0.2 sec | | |

Comparison of the flow patterns at the first relief bridge on Highway 400, as shown in Figure 7.32, suggests that the 2D models both predict similar rates of contraction and expansion through constrictions when the model extents exist relatively far away from the site of the constriction (see Chapter 6). While the rate of contraction appears close to a 1-to-1 ratio, which was assumed for the 1D model, the flow is seen to expand much more rapidly to the south on the downstream side than was accounted for in the 1D model.

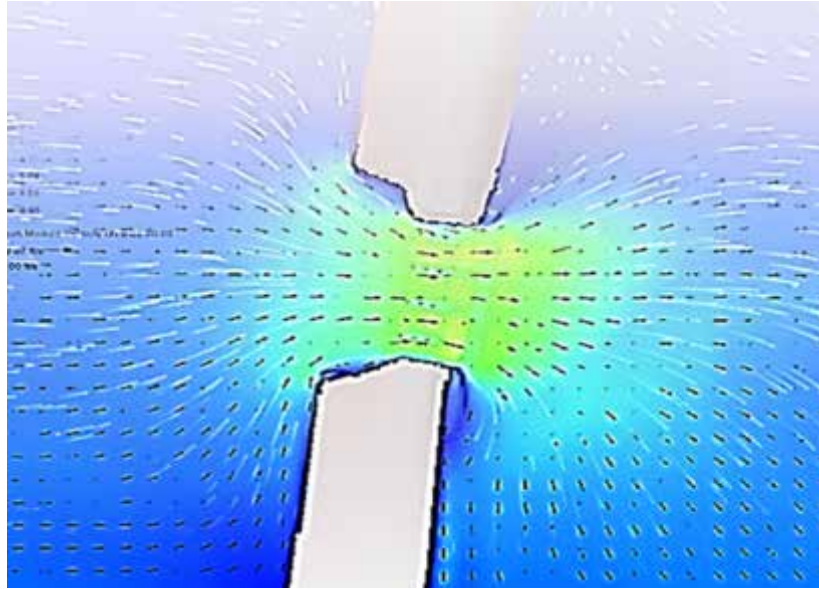


Figure 7.32: HEC-RAS 2D Flow Tracers and SRH-2D Velocity Vectors at the First Relief Bridge on Highway 400

The 2D models were used to examine the unrealistic but essential assumption inherent in the 1D HEC-RAS models that the water surface is constant across the entire length of any given cross section. Two cross sections were considered: the bounding upstream cross sections of the 1D HEC-RAS model for Highways 400 and 75. Figures 7.33 and 7.34 show the models' results. The inaccuracy of the constant water surface elevation assumption quickly becomes apparent when one looks at the water surface profiles in these figures. For all three models, the surface width of the flow at these cross sections exceeds 4000 ft. The 1D model is simply averaging properties across too great a distance. It is also clear that the HEC-RAS 2D model predicts the highest depths across the cross sections almost without exception. The water surface profiles of HEC-RAS 2D exceed those of SRH-2D by a foot or more in most locations. Interestingly, though, the overall shapes of both models' profiles are very similar to each other.

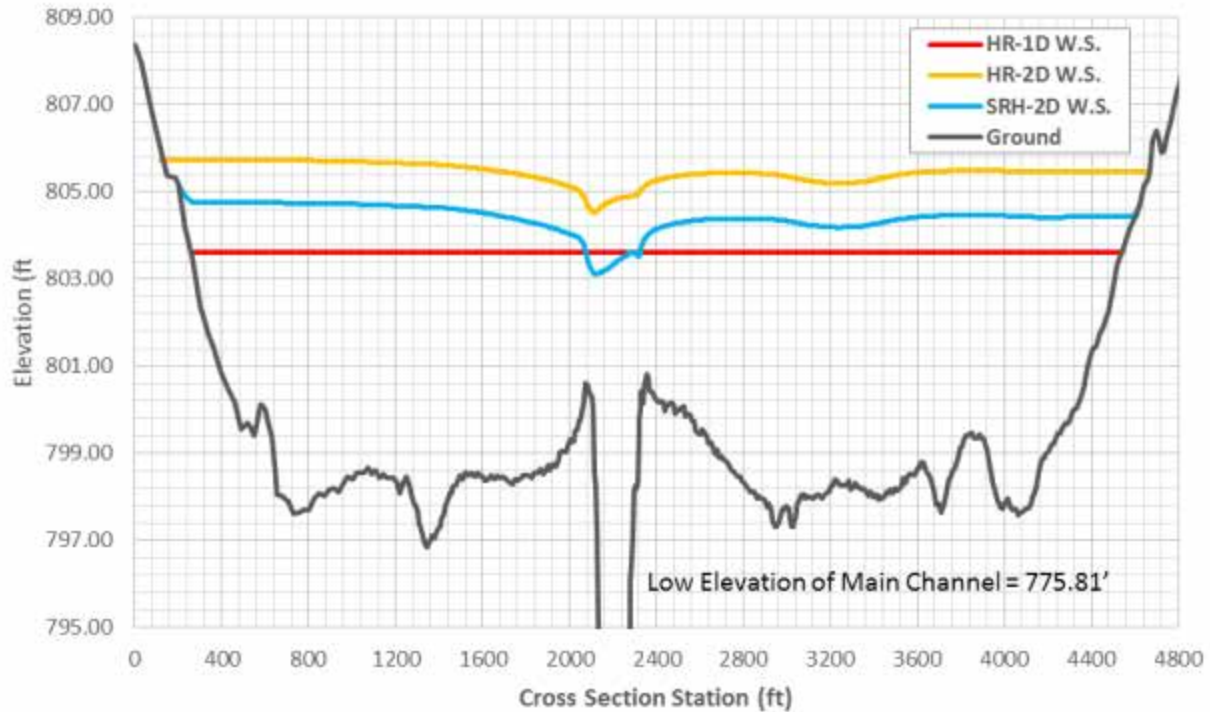


Figure 7.33: Water Surface Profiles for the Three Models at the Upstream Bounding Cross Section of Highway 400

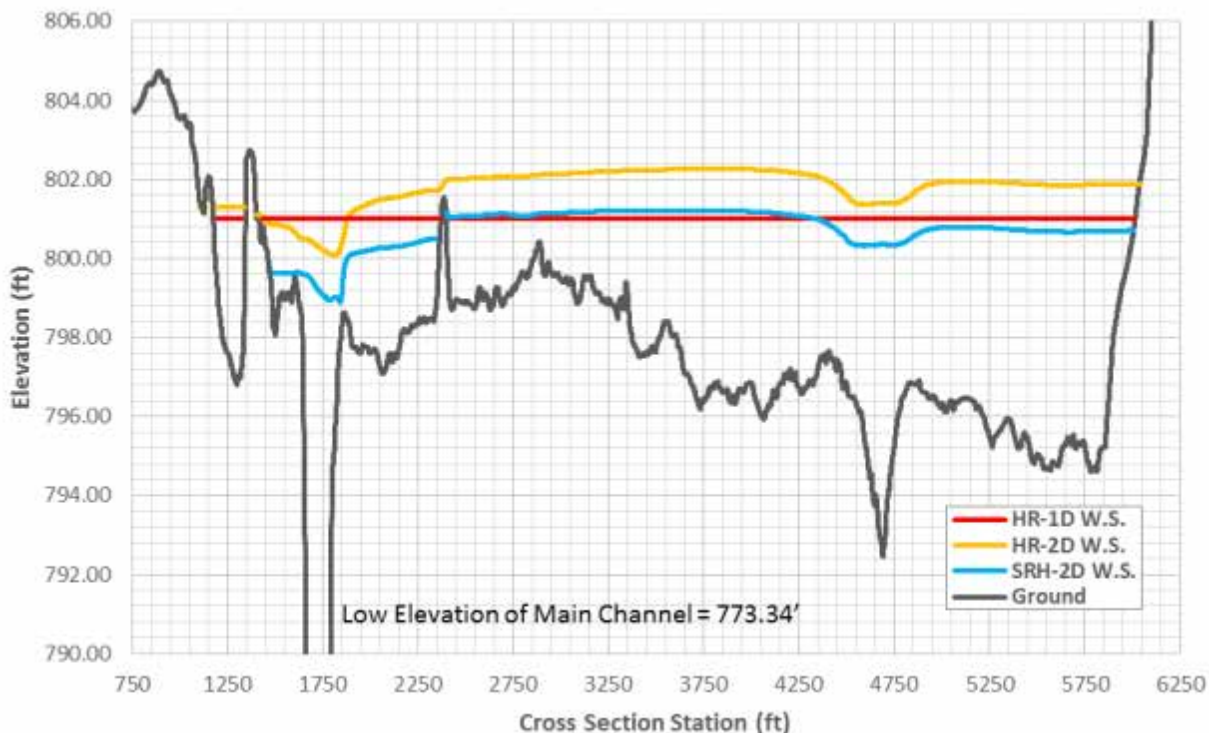


Figure 7.34: Water Surface Profiles for the Three Models at the Upstream Bounding Cross Section of Highway 75

The assumption that the energy is equal across the cross section is a much more realistic one because, in true steady state conditions, the flow will seek to balance energy losses that occur along comparable paths. So, if the cross sections are properly located, the problem becomes analogous to the well-documented situation of flow through parallel pipes between two reservoirs. This assumption is an important subject for future study, but was not addressed in regard to this site. One option that exists but was not used for the 1D HEC-RAS model is to split the flow upstream from Highway 400, having it come back with the main channel flow just downstream from the larger relief structure for Highway 75. This would require introducing two junctions and a supplementary stream that would pass through both relief bridges. This approach would also need to employ a ground-level lateral weir between the two flow fields to avoid discontinuities at the adjoining edges of the cross sections.

Lastly, the water surface profiles along the stream centerline were considered for these three models, and are included in Figure 7.35. All three profiles follow mostly the same pattern, yet those from the HEC-RAS 2D simulation exhibit a strong tendency toward higher depths than the other two models tested. The SRH-2D and HEC-RAS 1D profiles are sometimes below and other times above each other, and, to a much lesser extent, the same holds true for the HEC-RAS 2D and 1D profiles, but the HEC-RAS 2D profile is always above that from SRH-2D. This suggests that for floodplain studies, HEC-RAS 2D may be the more conservative of the 2D models, since it predicts so much higher depths than SRH-2D does, which translates to larger floodplains mapped. This has been a typical result for all tests conducted for this report. Also, the curious tendency of the HEC-RAS 2D models to let flow into the model space at unusually high depths has been a recurring issue.

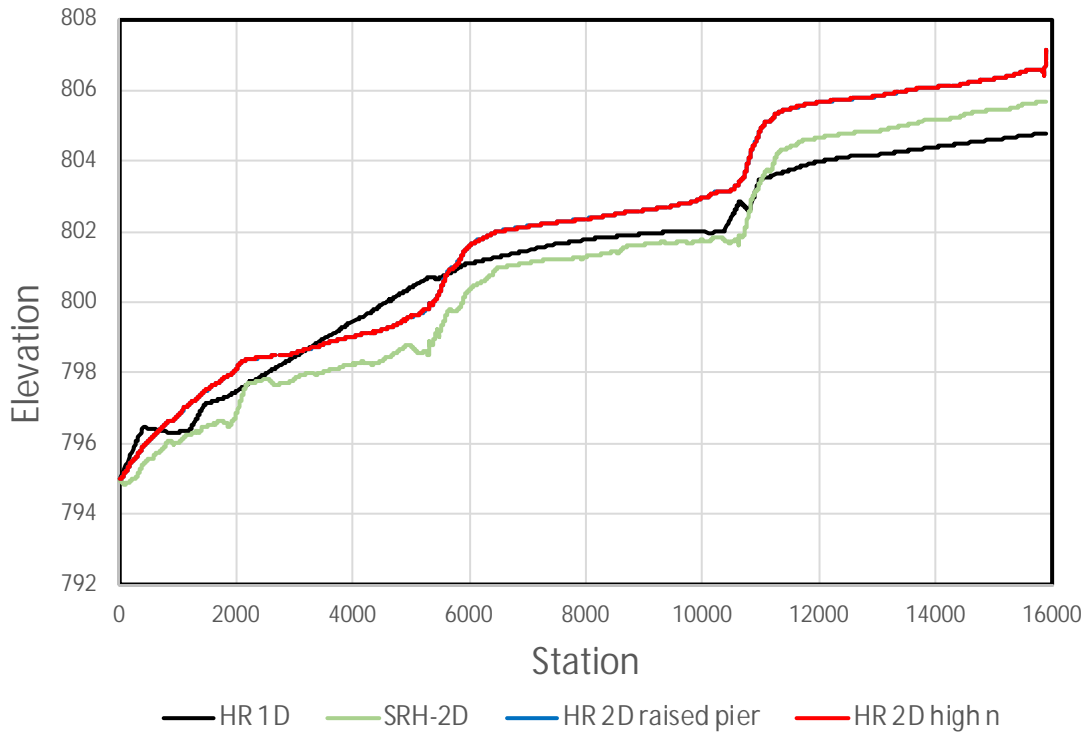


Figure 7.35: Water Surface Profiles from the Stream Centerline of the Models Tested for the Neodesha Floodplain Study – HR 1D, HR 2D (Raised Piers and High Pier n -Values), and SRH-2D

7.6 Runtime Comparison

The model runtime for HEC-RAS 2D and SRH-2D were compared for the final models in this chapter. Table 7.6 lists relevant characteristics of the two models. Note that the HEC-RAS 2D model produced good results with a larger timestep and coarser mesh (fewer cells) than the SRH-2D models. This is again due, in part, to the way that HEC-RAS 2D represents sub-grid variability. The runtimes presented are for the same computer described in Figure 6.45 (a 2.5GHz i7 laptop with 8Gb RAM). The HEC-RAS 2D model was over 28 times faster.

Table 7.6: Runtime Comparison for Neodesha

| | SRH 2D | HR 2D raised pier | HR 2D high pier n |
|-------------------|------------------------|----------------------|----------------------|
| Discharge | 40,000 cfs | 40,000 cfs | 40,000 cfs |
| Time Step | 0.2 s | 1 s | 1 s |
| Simulation Time | 66.7 hr | 66.7 hr | 66.7 hr |
| Execution Time | 10 days | 1.15 days | 1.27 days |
| Smalles Grid Cell | 0.35 ft ² | 1.07 ft ² | 1.07 ft ² |
| Largest Grid Cell | 81.956 ft ² | 738 ft ² | 738 ft ² |
| Average Grid Cell | 0.35 ft ² | 142 ft ² | 393 ft ² |
| No. of Grid Cells | 420,269 | 158,712 | 158,712 |
| Area Modeled | 2.15 mi ² | 2.23 mi ² | 2.23 mi ² |

Chapter 8: Sumner County Site

8.1 Background for the Floodplain Study

This study includes two small bridges on the East Prairie Creek in Sumner County, Kansas. Figure 8.1 shows the stream centerline and the locations of the bridges. The figure also shows cross sections and bridge sections used to model the river reach shown in HEC-RAS 1D. This type of problem is very difficult to model with confidence in 1D.

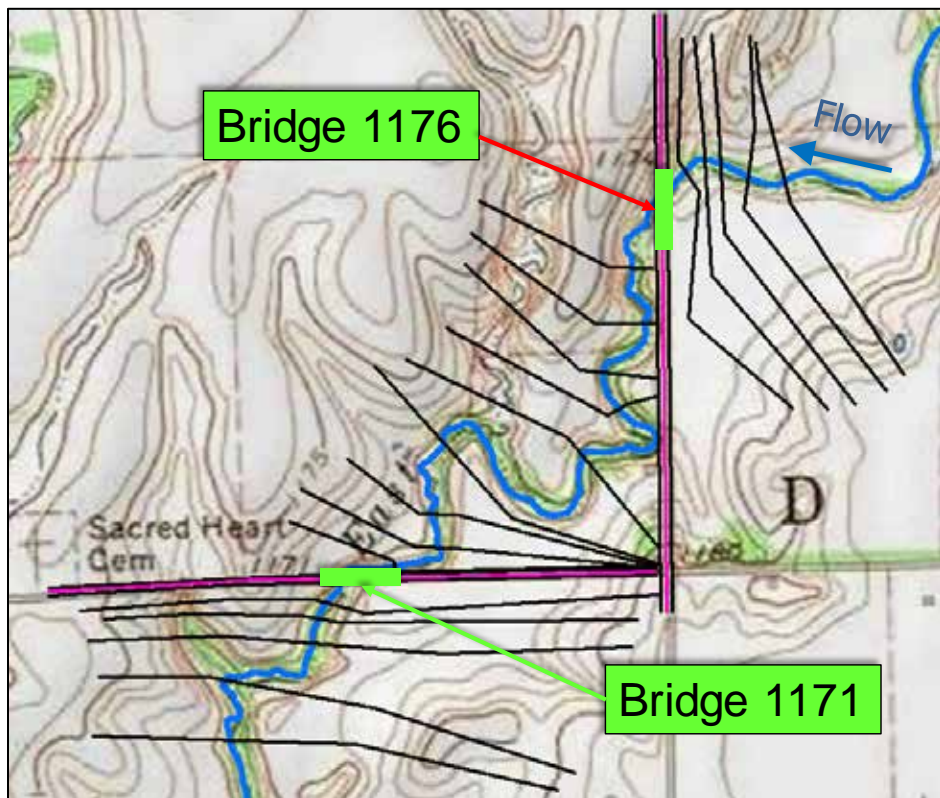
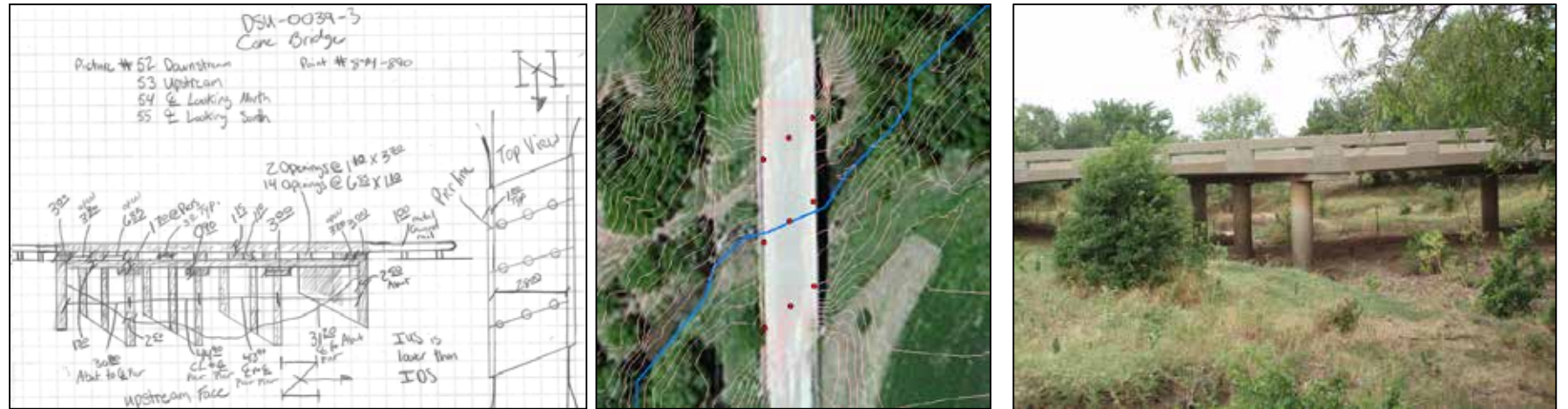


Figure 8.1: Sumner County Site

Figure 8.2 shows bridge details for the site. Bridge 1176 has three 3-column piers with a 40-degree skew angle and Bridge 1171 has two round-nosed elongated piers at a 30-degree skew angle. (Zero skew occurs when the pier axes are perpendicular to the bridge centerline.)

(a) BR 1176 Multiple Cylindrical Column Piers



(b) BR 1171 Round Nose Elongated Piers

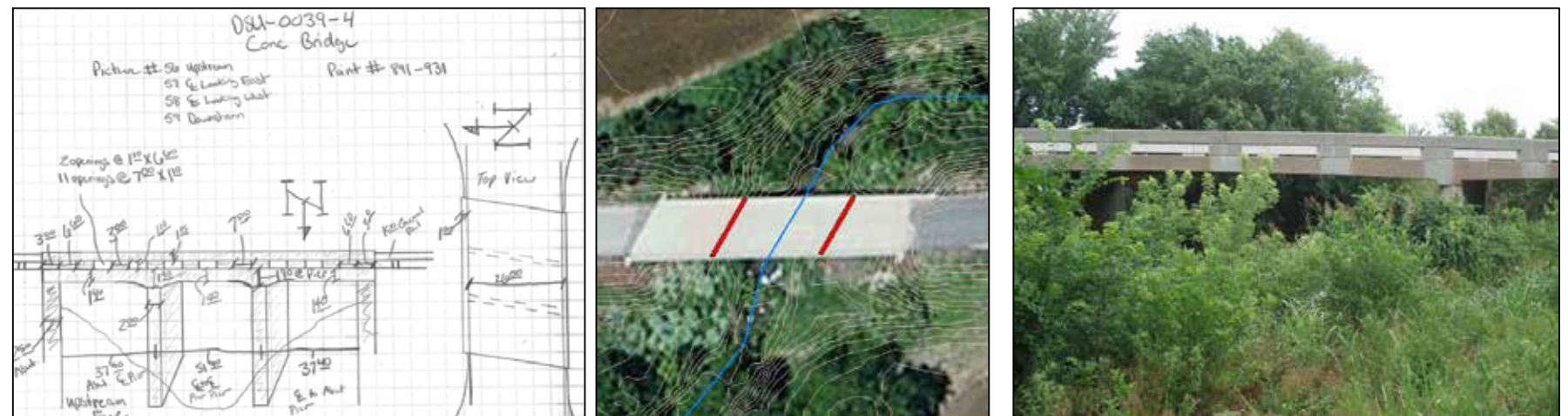


Figure 8.2: Bridge and Pier Details

8.2 HEC-RAS 1D Model

The HEC-RAS 1D model was created using the Land Use layer shown in Figure 8.3. This layer was also used in the development of the 2D model. The method used herein to account for the skew angle for the 1D model was to multiply the bridge survey station data by the cosine of 30 degrees, since the survey data were taken along the bridge face. The survey data and the corrected survey data are shown in Figure 8.4. This method assumes no change in slope through the bridge opening. The corrected data were entered into the HEC-RAS bridge data. The points called “Corrected Ground Data” were used to adjust the cross section data as cut using GIS at the upstream and downstream bounding cross sections. These adjusted HEC-RAS internal bridge cross sections are depicted in Figure 8.5 for Bridge 1171. The skew option in HEC-RAS was not used; it was considered best to leave the overbank data as it was, because overtopping water flows perpendicular to the bridge except under exceptionally high overtopping depths.

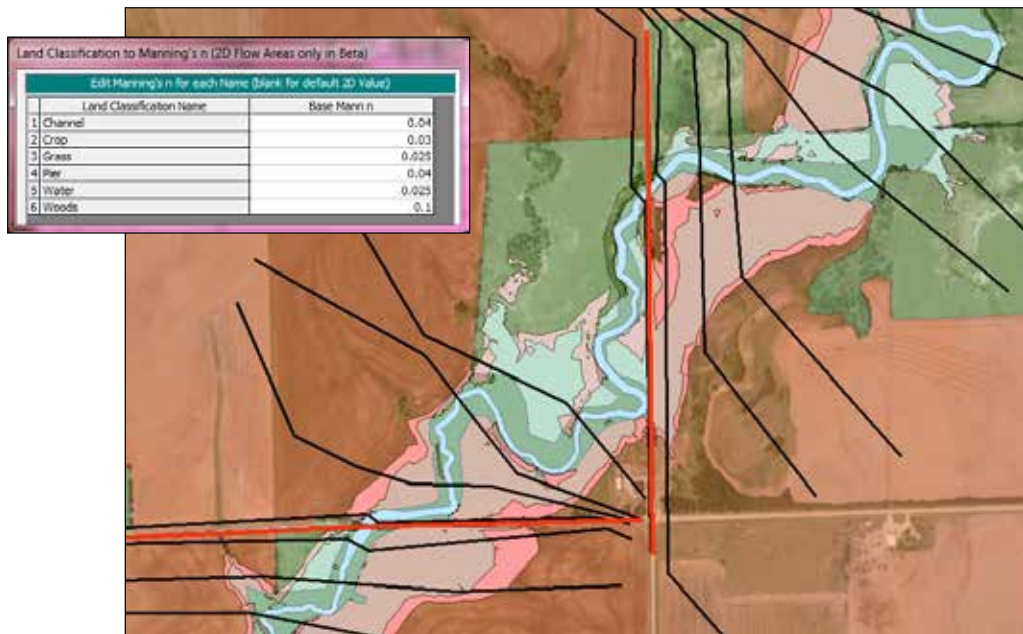


Figure 8.3: Land Use Polygon

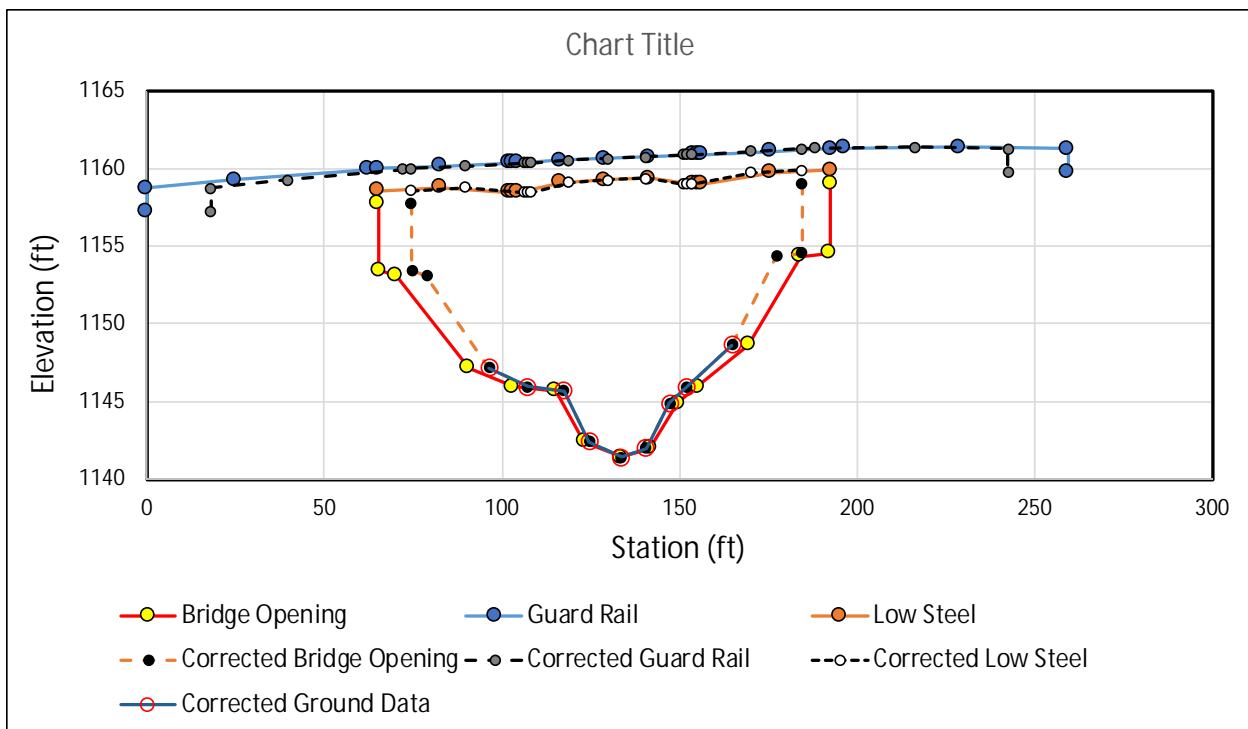


Figure 8.4: Survey Data Along Bridge Face and Corrected for Skew Angle

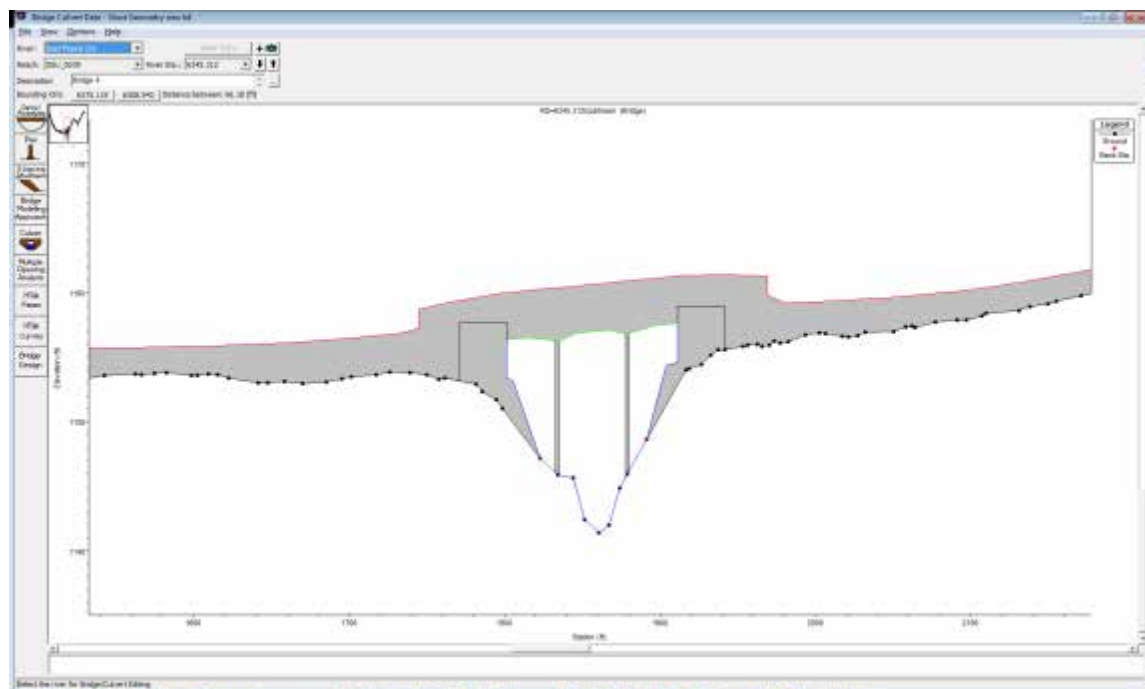


Figure 8.5: Upstream HEC-RAS Internal Bridge Cross Section for Bridge 1171

The model was run for a constant peak flow of 6,000 cfs with a normal depth downstream boundary condition whose slope was 0.00390. The floodplain based on an edge depth of 0.1 ft from RAS mapper is shown in Figure 8.6. It has not been edited to remove the unconnected portions of the floodplain.

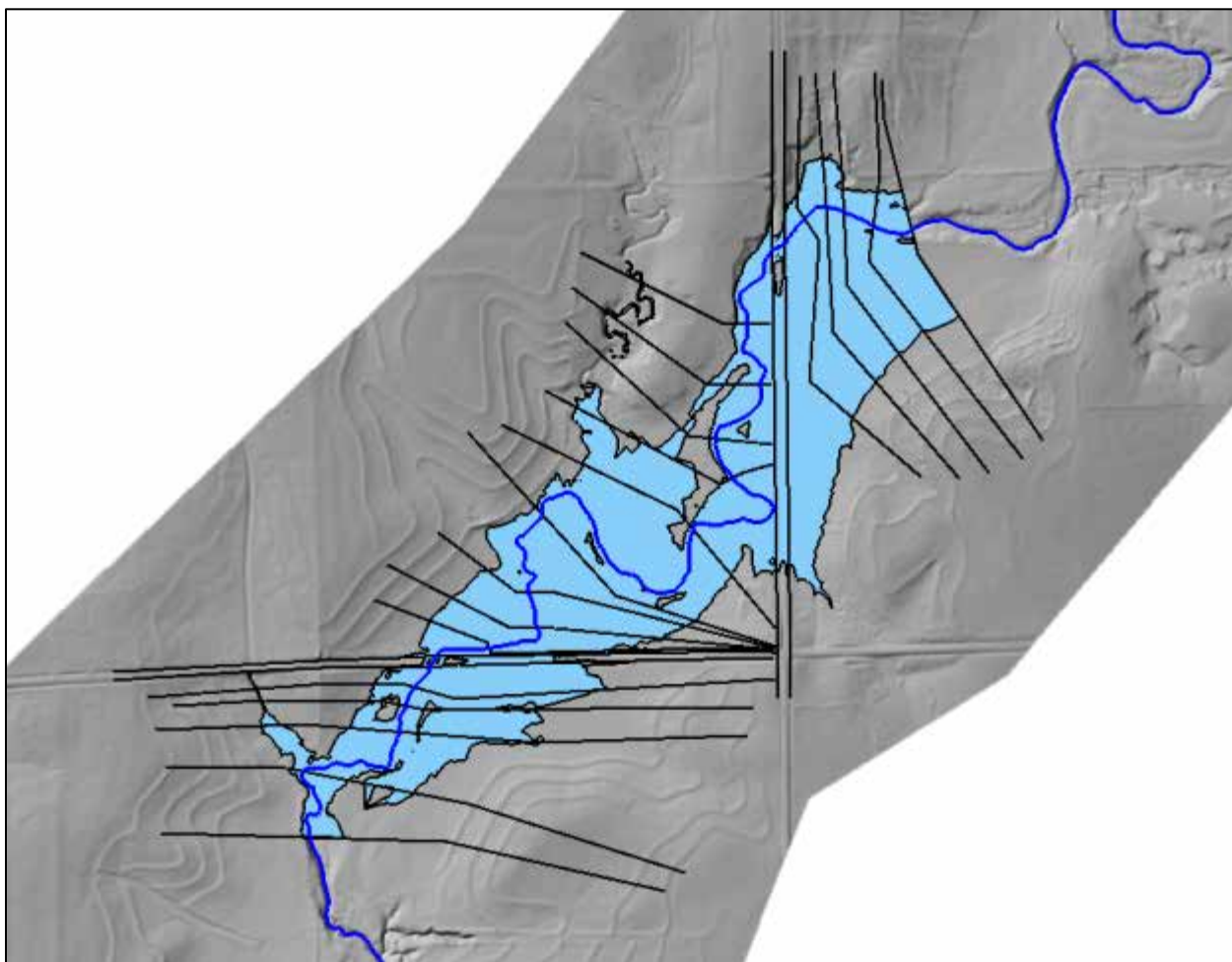


Figure 8.6: Floodplain Boundary for 1D HEC-RAS Model

8.3 HEC-RAS 2D Model

The HEC-RAS 2D model was developed using a DEM modified to reflect the bridge survey data for the skewed bridges. The 1-ft DEM was created by first making a TIN from the original 4-ft DEM and then creating a 1-ft DEM from the TIN. This DEM was modified to include the survey data extended through the skewed bridges, on the assumption that the survey data for the channel applied upstream from, through, and downstream from the bridges to reach

the locations of typical 1D model-bounding cross sections. The slope through the bridge was assumed to be negligible.

The model domain extended from the upstream to the downstream 1D cross sections, as shown in Figure 8.7. The HEC-RAS grid cell size of 30 ft was selected, with smaller cells created by breaklines in the areas of the bridge openings, roads, and piers. The breakline spacing for the bridge openings, road centerlines, elongated piers, and circular piers were 5 ft, 5 ft, 1 ft, and 1.309 ft, respectively. The tighter grid cells in the bridge opening were created to enhance scour calculations. The road breaklines were created to capture the road centerline elevation for overtopping analysis. The pier grid cells were adjusted to align as closely as possible with the pier edges, as shown in Figure 8.8. Note the cut-in survey data on the terrain.

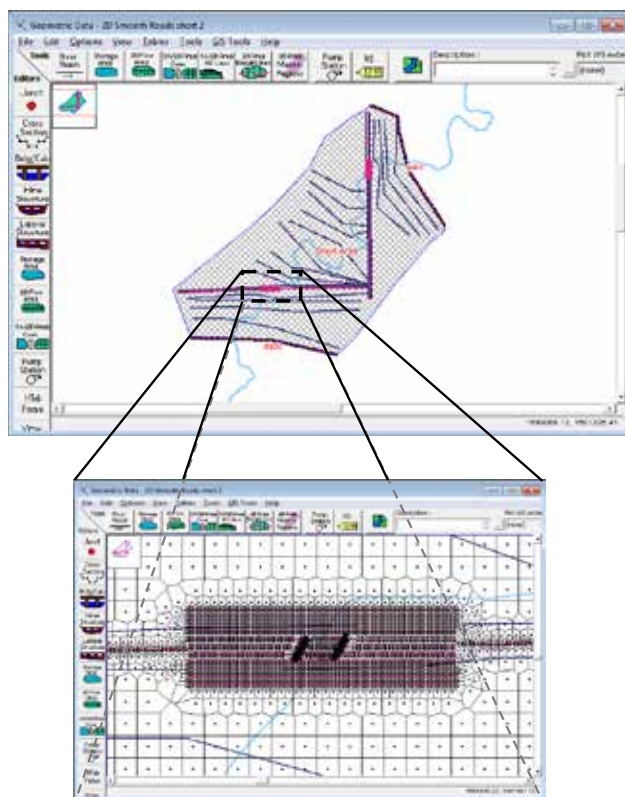


Figure 8.7: HEC-RAS 2D Mesh

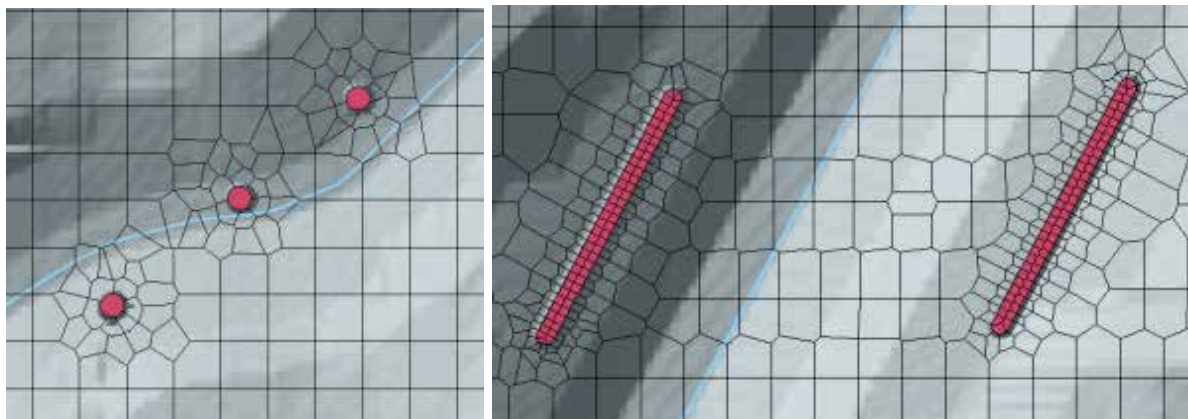


Figure 8.8: Mesh around Bridge Piers for Bridges 1176 and 1171

The HEC-RAS terrain was created in RAS Mapper by using the 1-ft grid discussed above and 0.01-ft grids for the bridge piers. The ability to use grids with different cell sizes in creating the RAS Mapper terrain enables the modeler to develop very detailed analyses in the area of hydraulic features like piers. Figures 8.9 to 8.11 show the terrain and the mesh. The method used in creating the pier grids was discussed in Chapter 6.

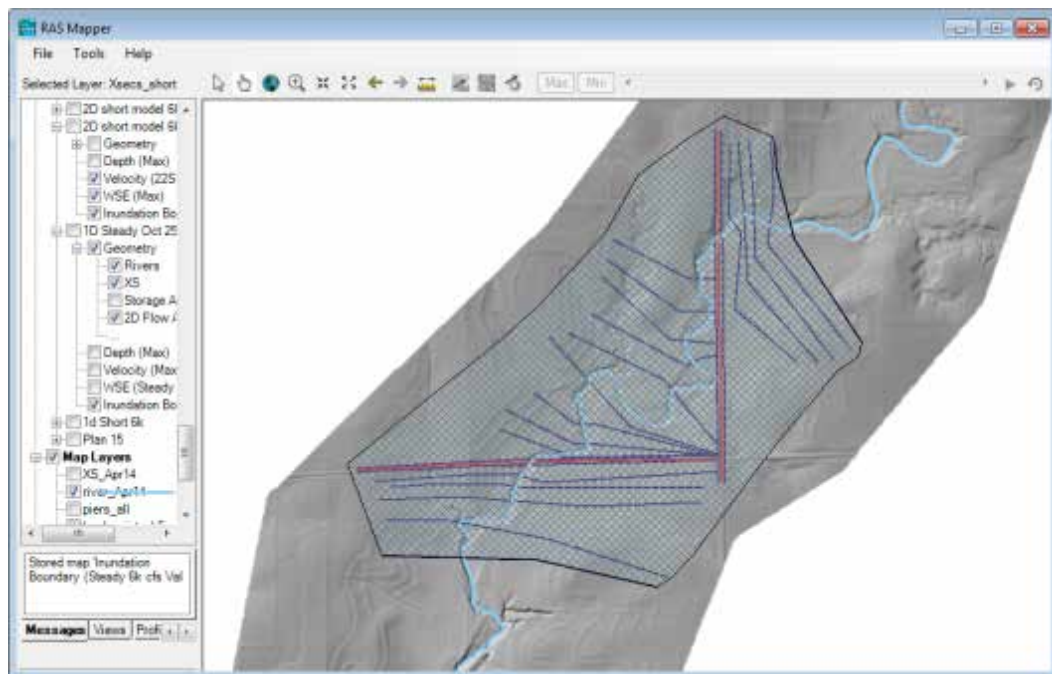


Figure 8.9: HEC-RAS 2D Terrain

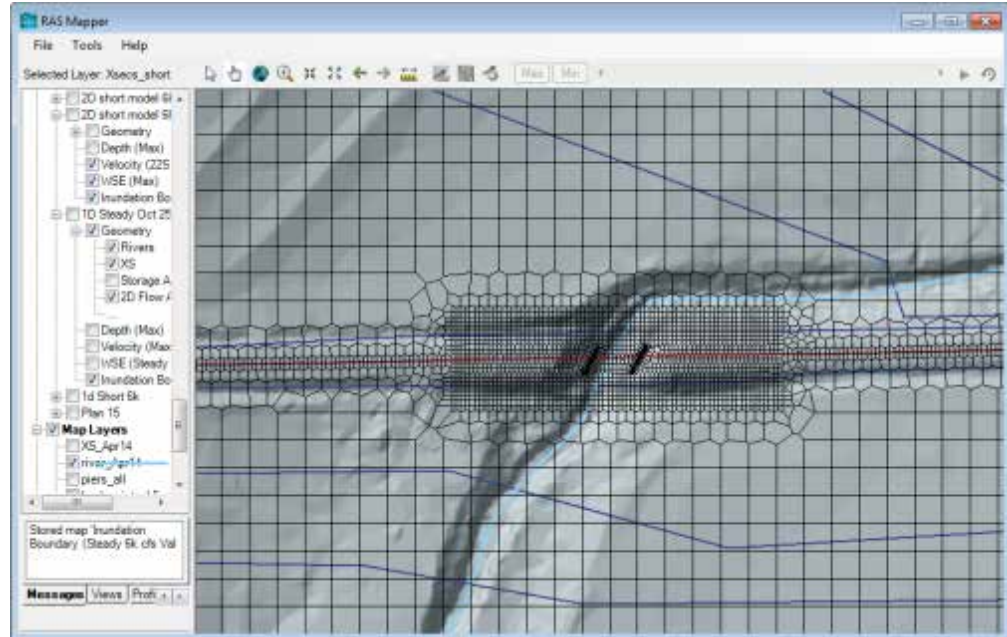


Figure 8.10: HEC-RAS 2D Terrain at Bridge 1171

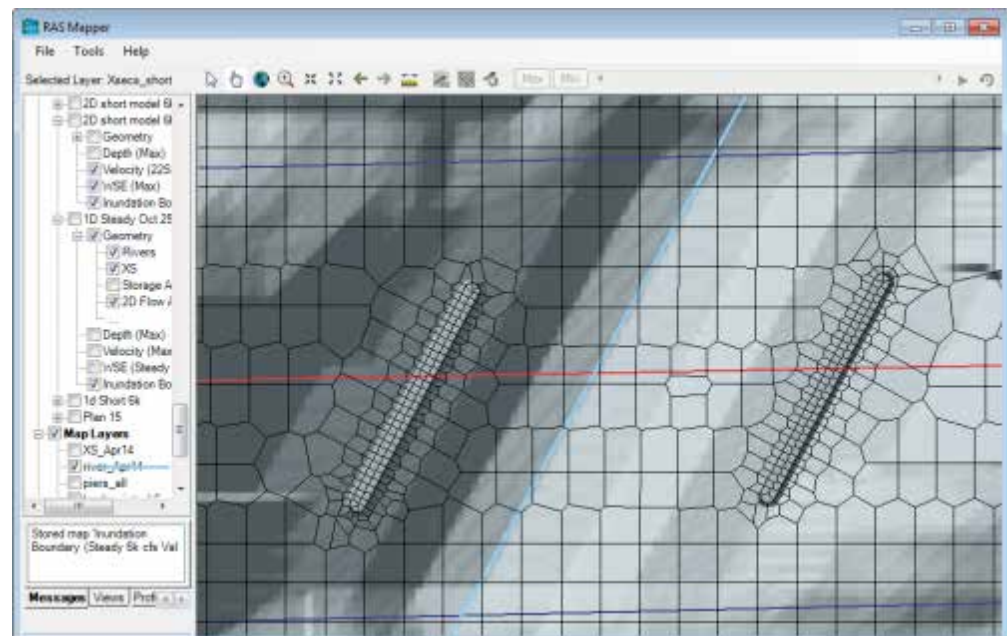


Figure 8.11: HEC-RAS 2D Terrain around Bridge 1171 Piers

The mesh statistics are shown below in Figure 8.12. There are 22,348 cells, and the average cell area is 590.34 square ft.

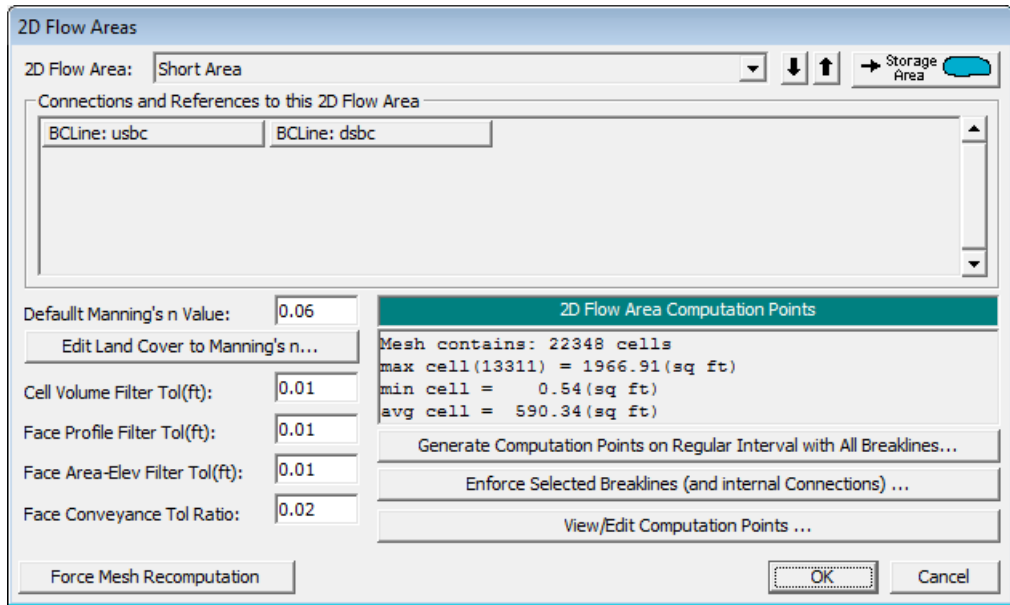


Figure 8.12: Mesh Parameters

A ramped hydrograph with a peak flow of 6,000 cfs was used to model the site at the upstream boundary condition. The slope of the EGL for distribution of flow along the upstream boundary condition line was 0.0039. The hydrograph is shown in Figure 8.13 below. This hydrograph simulates the steady flow case with the ramping serving to help stabilize the model. The downstream boundary condition was a stage hydrograph with a constant water surface elevation of 1152.57 ft. Also, the initial condition for the 2D area was 1152.57 ft. These slopes and boundary condition elevations were obtained from the steady flow model discussed previously.

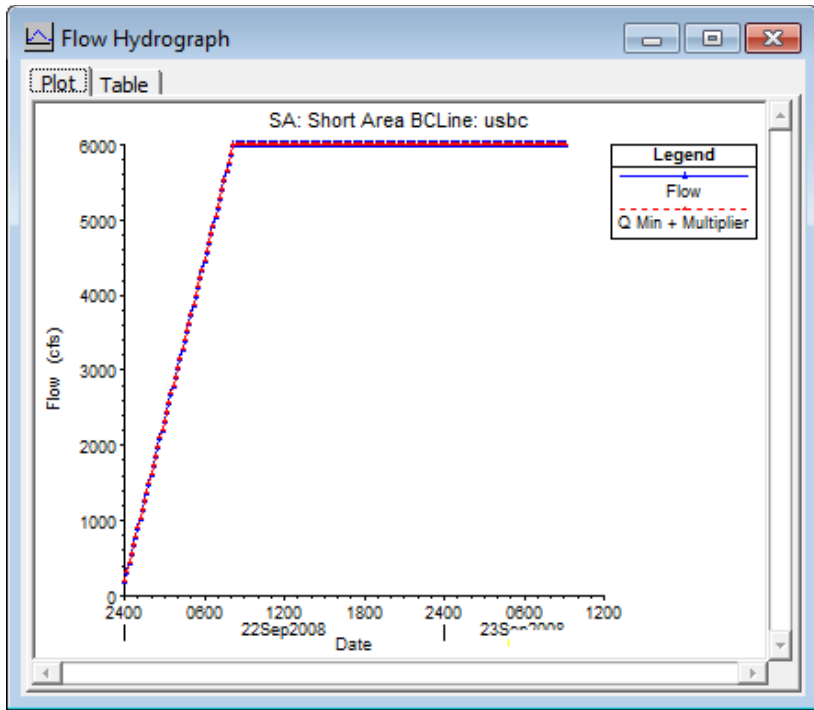


Figure 8.13: Ramped Inflow Hydrograph

The model was run for 1000 minutes for several different time steps using the full momentum equation set and a 0.25-hour ramp-up time, as shown in Figure 8.14. The average cell area of 590 square ft gives an approximate Δx of 24.3 ft or, say, 25 ft. Figure 8.15 shows the maximum centerline velocity plot for the 1-second timestep run. The average centerline velocity is about 2.55 fps, and the velocities through Bridges 1176 and 1171 are around 3 and 5 fps, respectively. Table 8.1 shows values of Δt for a Courant number of 1 for different Δx -values for velocities of 2.55 and 5 fps. The Δx -value of 5 is the cell size used through the bridge openings.

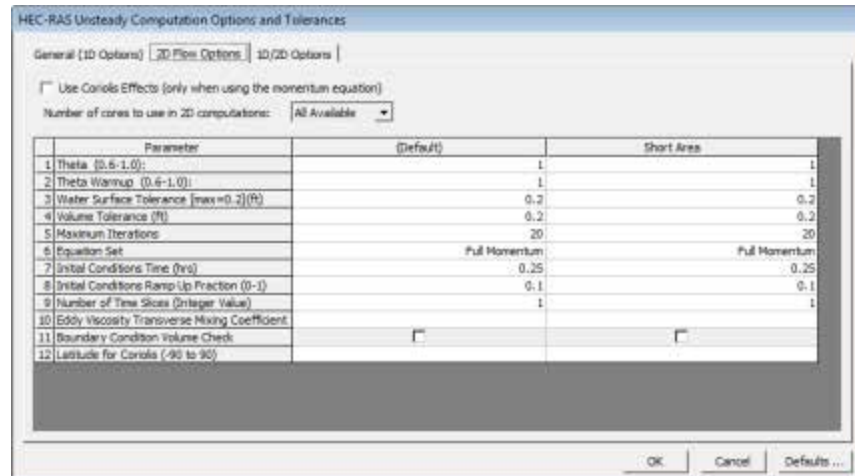


Figure 8.14: 2D Computation Options

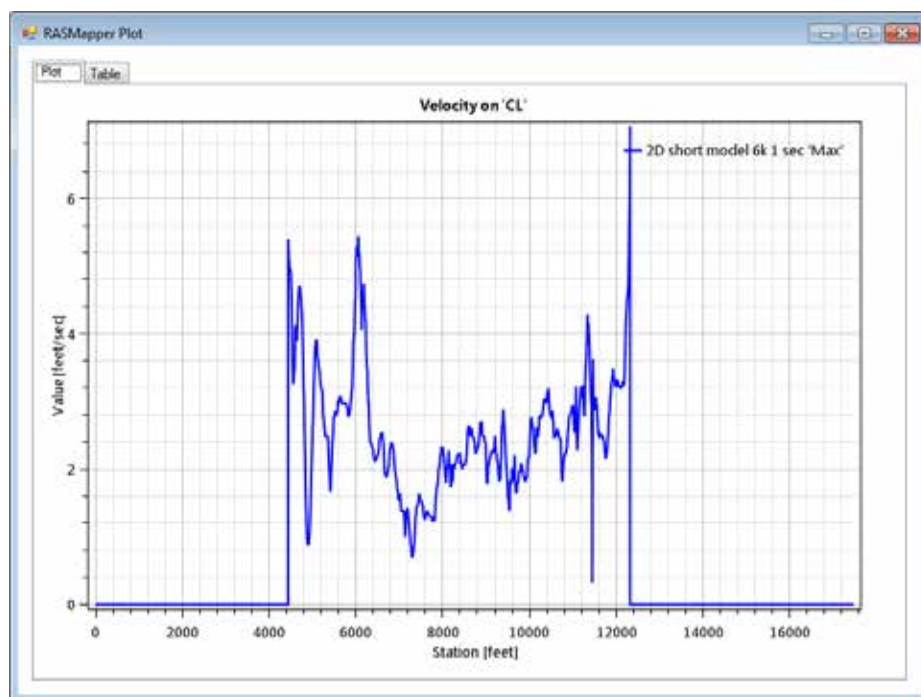


Figure 8.15: Centerline Velocities for 1-Second Timestep Run

Table 8.1: Timesteps for Different Δx -Values and Velocities

| Δx (ft) | V (fps) | Δt (sec) |
|-----------------|---------|------------------|
| 25 | 2.55 | 9.80 |
| 25 | 5.00 | 5.00 |
| 5 | 2.55 | 1.96 |
| 5 | 5.00 | 1.00 |

The stream centerline water surface profiles for HEC-RAS 2D using time steps of 0.3, 0.5, 1, 3, 5, and 10 seconds are shown in Figure 8.16. Since the differences in the profiles are difficult to ascertain in Figure 8.16, Figure 8.17 was prepared showing a plot of the Max WSE values subtracted from the Max WSE values for the 1-second timestep run. There is an obvious blip for the 10-second profile indicating that the 10-second timestep is too large. Figure 8.18 shows the water surface profile for the HEC-RAS 1D run together with the 2D profiles. It is quite different from the 2D results. This is not surprising, because this site is extremely complicated and does not lend itself to reliable 1D modeling. The 2D model results should be much more realistic than the 1D results at this site.

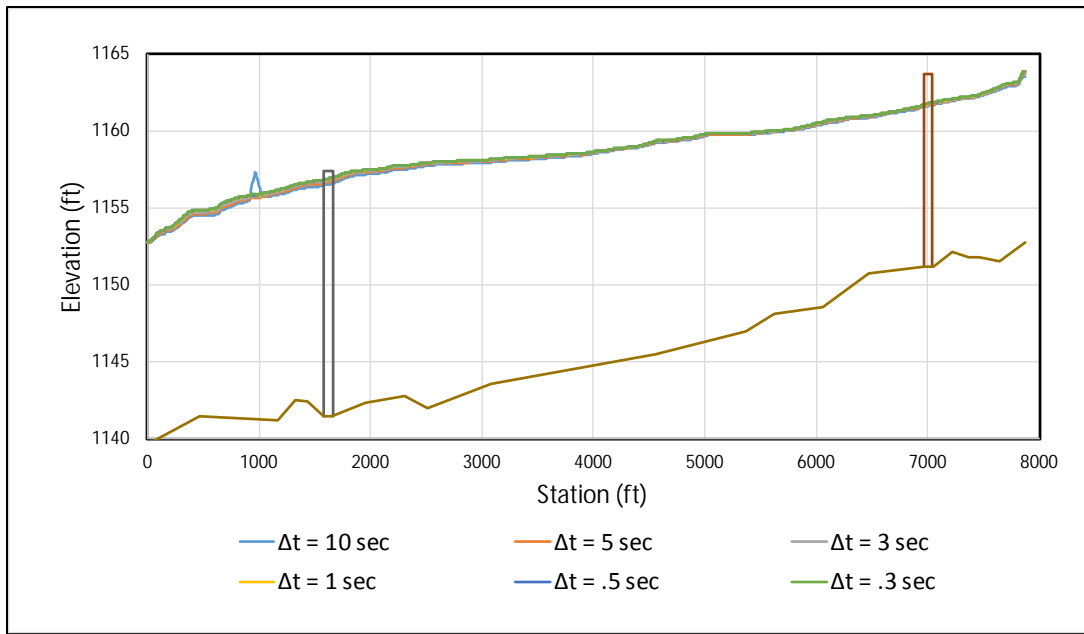


Figure 8.16: HEC-RAS 2D Max WSE for Different Timesteps

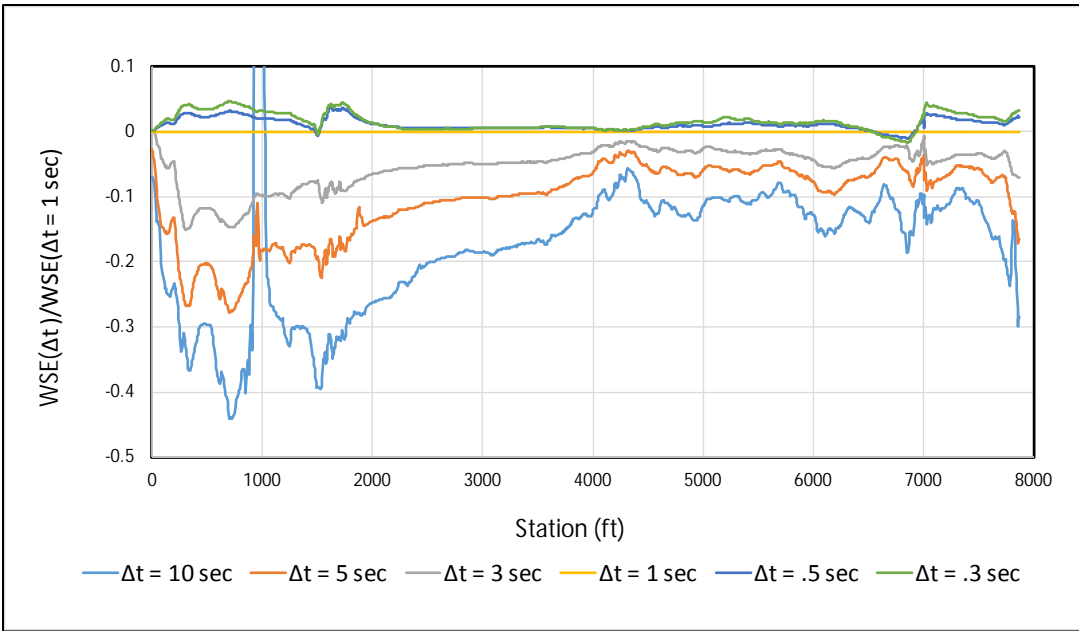


Figure 8.17: HEC-RAS 2D Max WSE (1 second) – Max WSE ($\Delta t = 3, 5$, or 10)

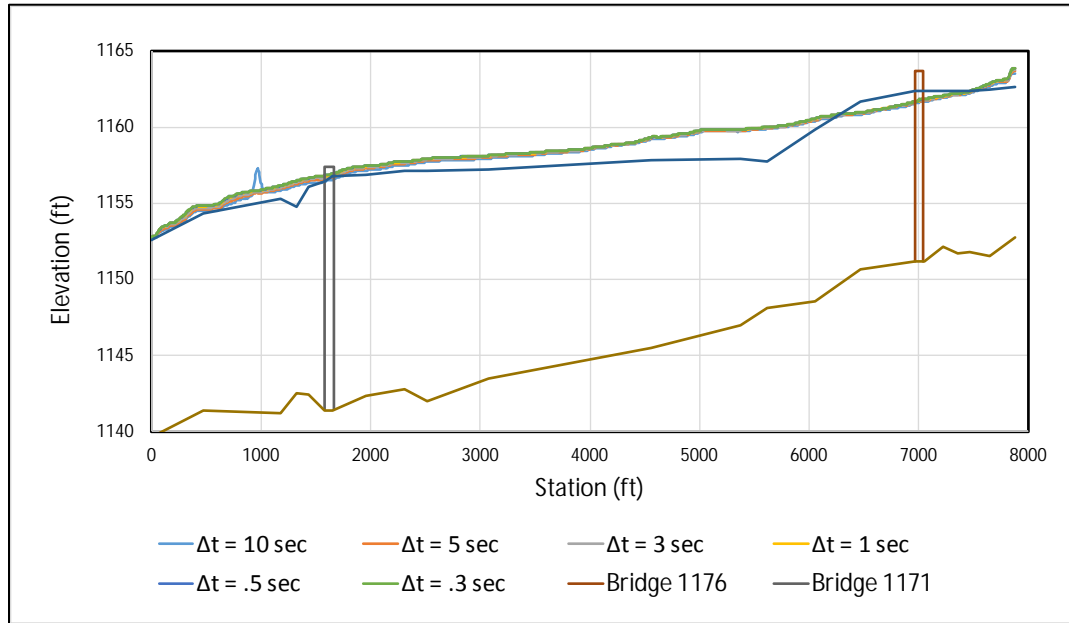


Figure 8.18: HEC-RAS 2D Max WSE for Different Timesteps with HEC-RAS 1D Profile

The floodplain for the HEC-RAS 2D floodplain run with a 1-second timestep is shown in Figure 8.19. The 1D cross sections and the stream centerline are shown for reference in Figure 8.20.

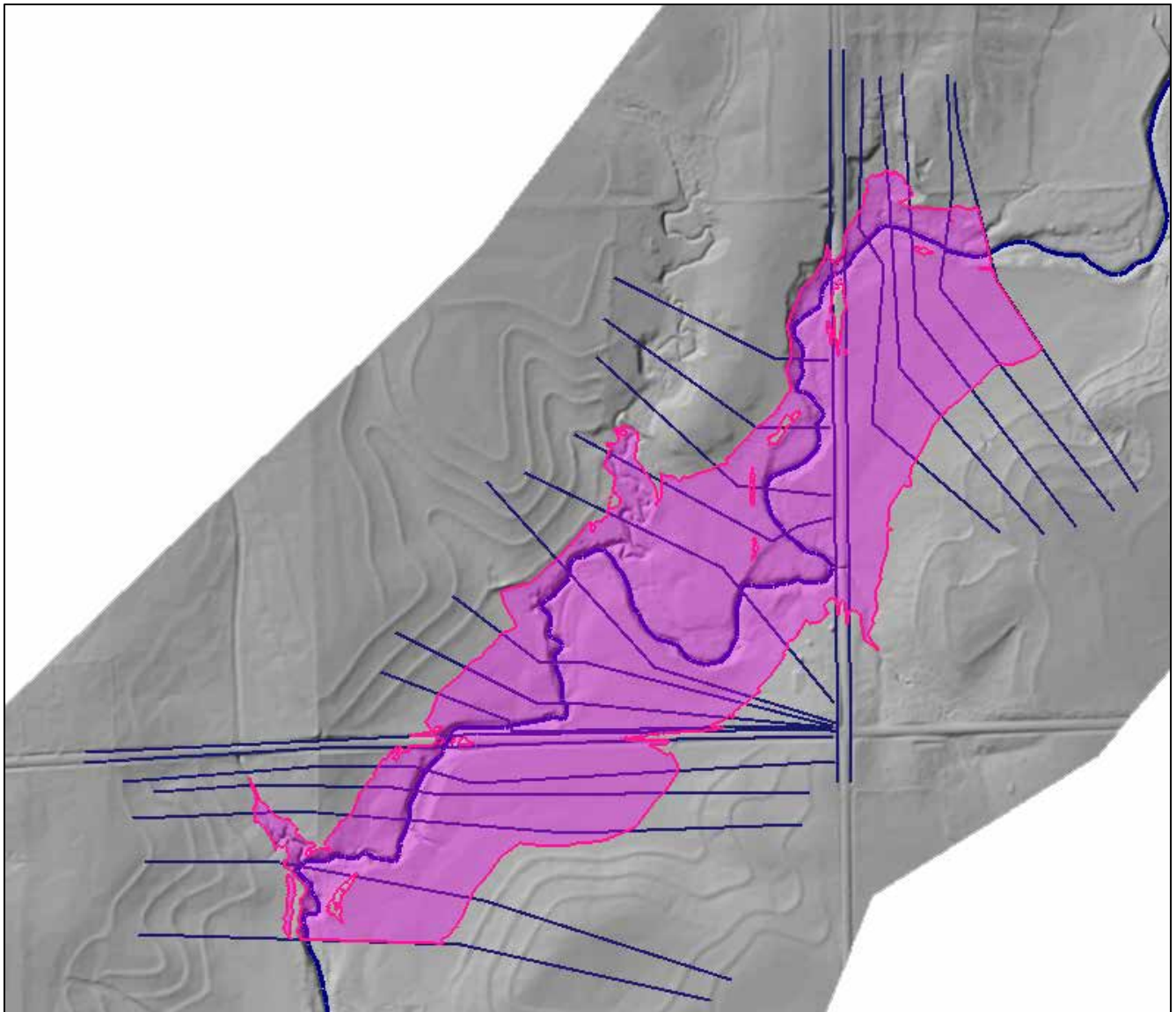


Figure 8.19: HEC-RAS 2D Floodplain for 1-second Timestep Run

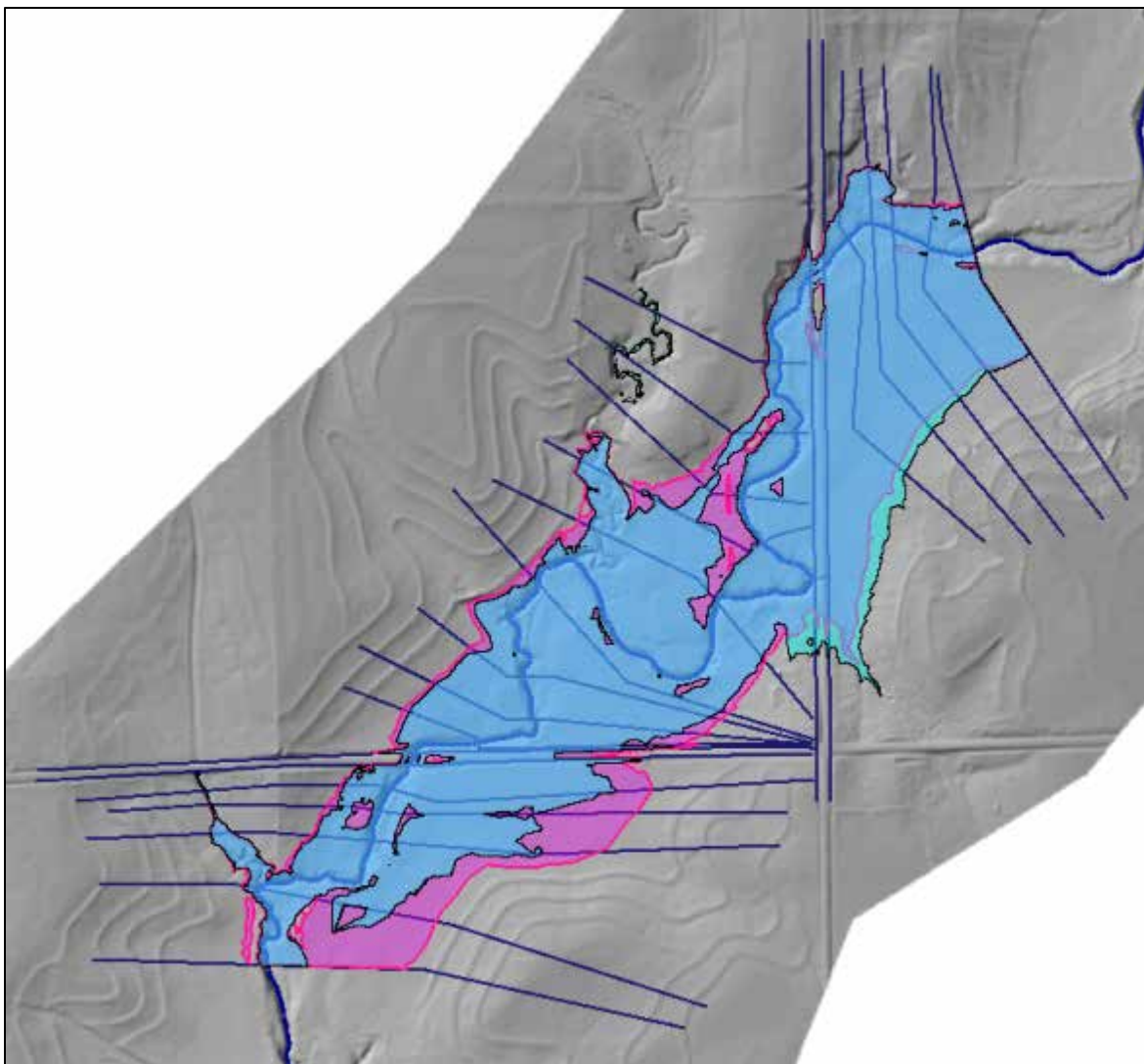


Figure 8.20: HEC-RAS 2D Floodplain for 1-second Timestep Run with 1D Floodplain Overlain

Both the 1D HEC-RAS WSE profile and 2D HEC-RAS Max WSE profiles for $\Delta t = 1$ second are shown in Figure 8.21. Of special interest is the large discrepancy between the two profiles at the downstream end of the reach. The discrepancy is reduced when the full-length HEC-RAS model is used as shown. Figure 8.22 shows the 2D HEC-RAS 1-second WSE values at the downstream boundary condition. They should be 1152.7 ft. Figure 8.23 shows the long 1D HEC-RAS floodplain and the short 2D HEC-RAS 1-second time step floodplain. The shorter model area was selected to reduce the 2D modeling time. The 2D HEC-RAS floodplain is only slightly wider than the long 1D HEC-RAS floodplain downstream from Bridge 1171.

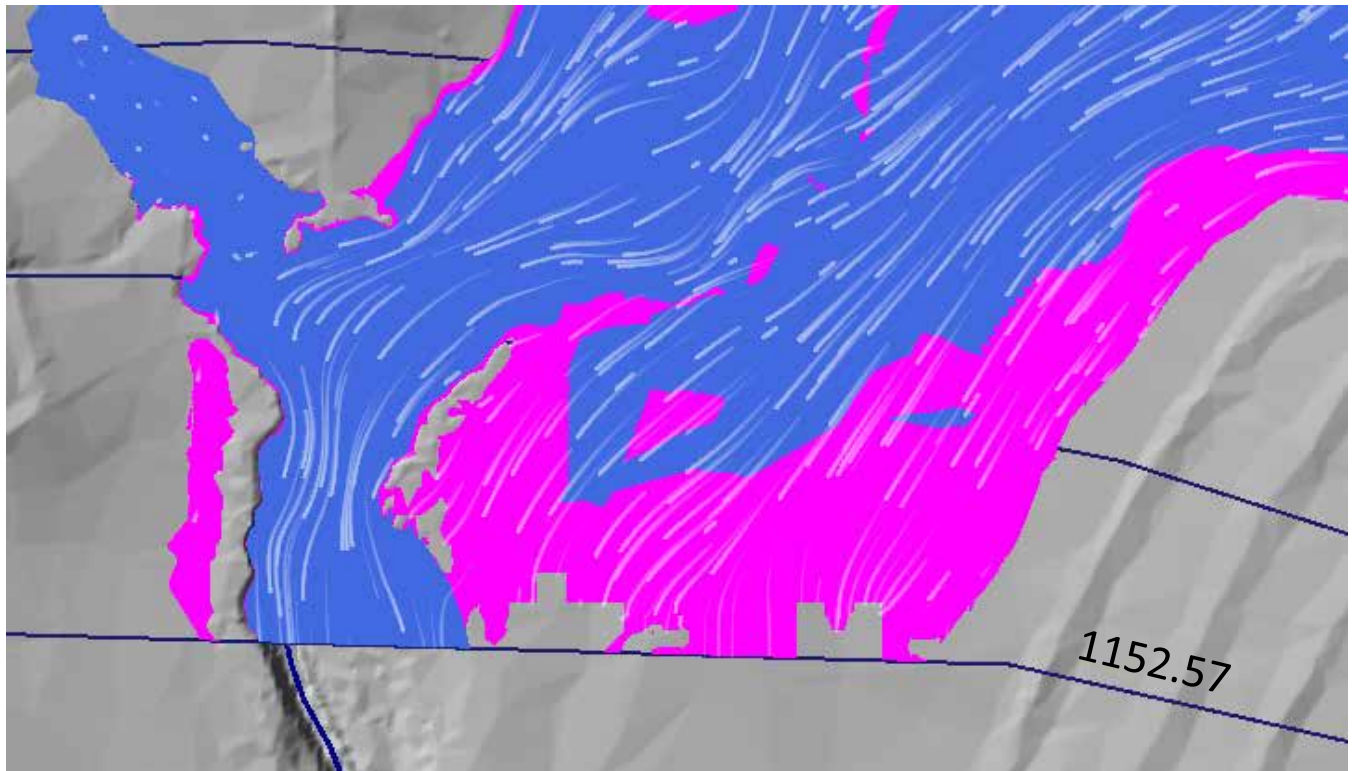


Figure 8.21: HEC-RAS 1D and HEC-RAS 2D (1 second) WSEs with 2D Streamlines

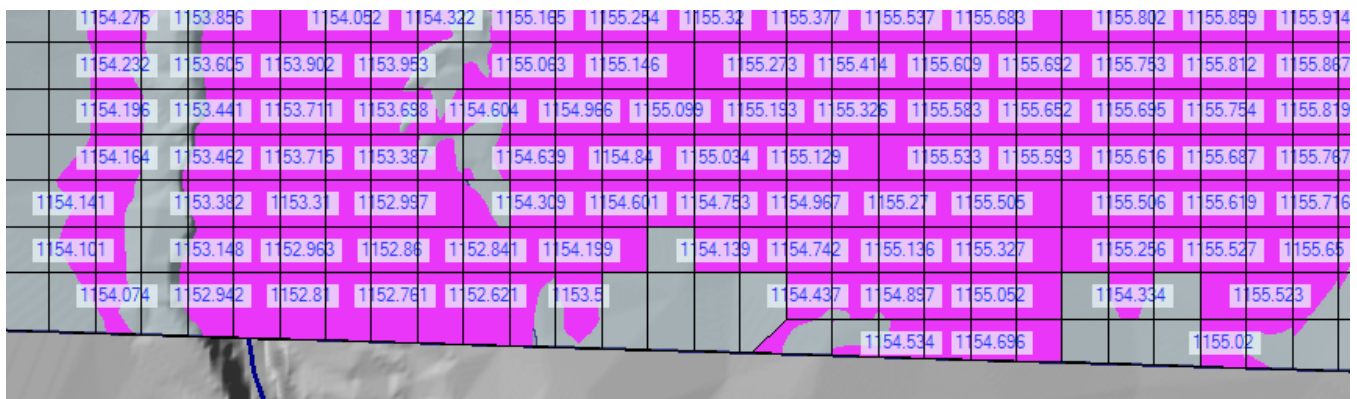


Figure 8.22: HEC-RAS 2D (1 second) cell WSEs near DS Boundary (should be 1152.57)

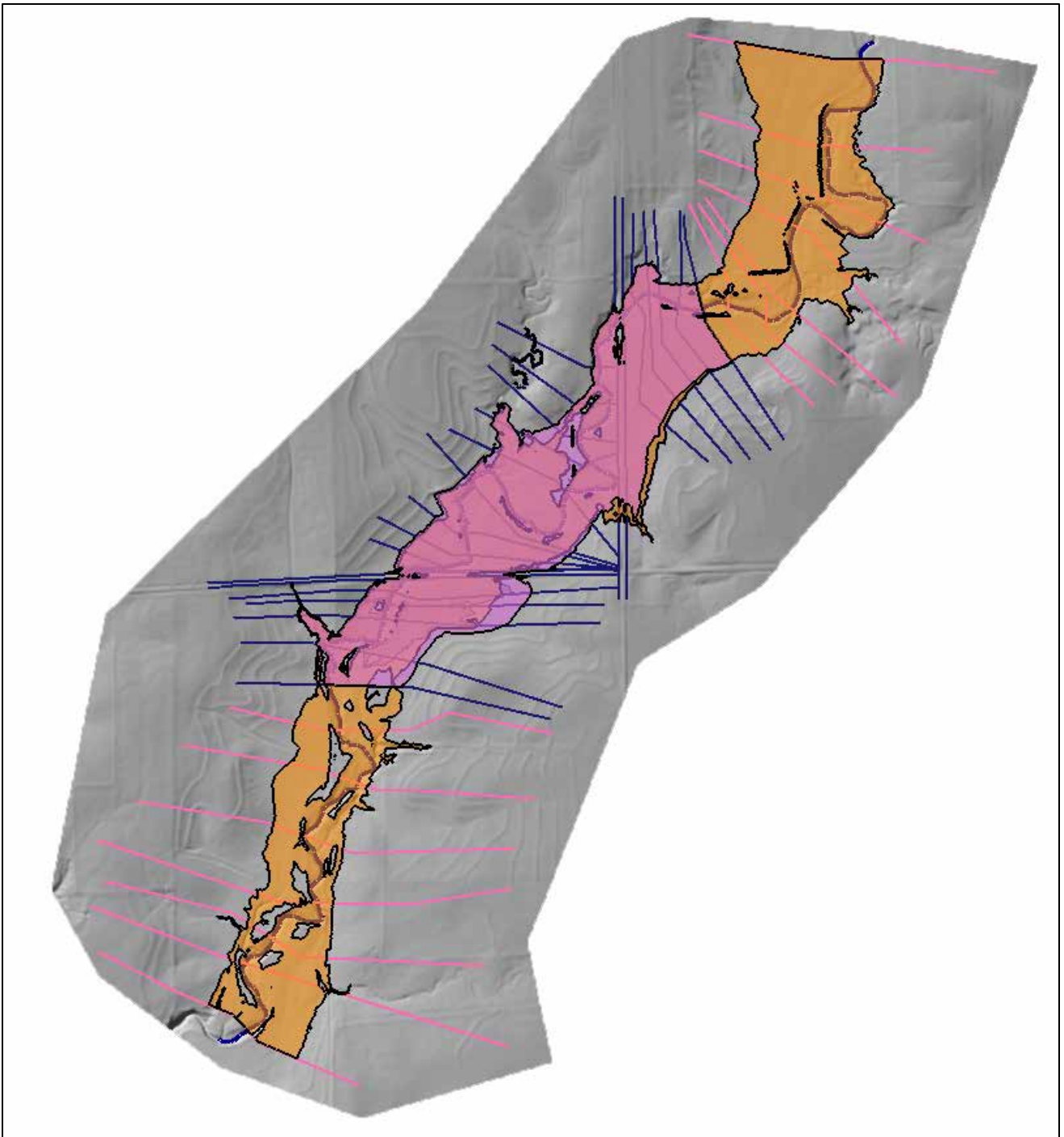


Figure 8.23: Long HEC-RAS 1D Floodplain and 2D HEC-RAS ($\Delta t = 1$ second)

Figure 8.24 shows streamlines for HEC-RAS 2D with a 1-second timestep. Note the eddies near the left overbank pier (in the right-hand side of the figure). Physically, this is what one would expect to see in the field. Figure 8.25 shows the streamlines around the left overbank pier for Δt -values of 10, 5, 3, 1, 0.5, and 0.3 seconds. The flow patterns for Δt -values of 10, 0.5, and 0.3 seconds do not appear physically reasonable (0.3 seconds being worse than 0.5 seconds). Thus, the Δt -values of 5, 3 and, 1 second appear to give the best results.

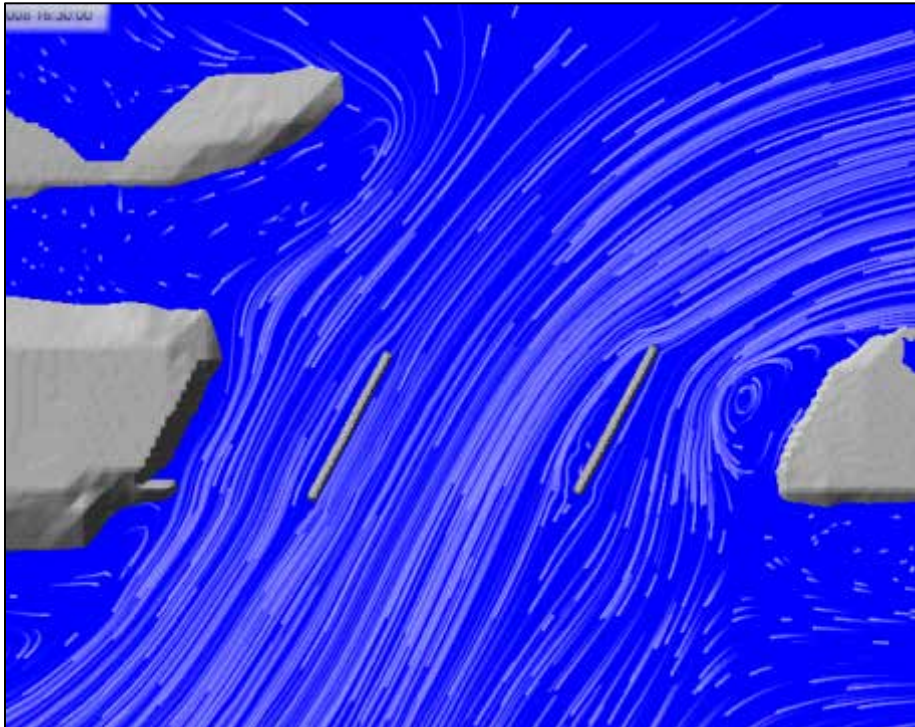


Figure 8.24: Streamlines at Bridge 1176 for 2D HEC-RAS ($\Delta t = 1$ second)

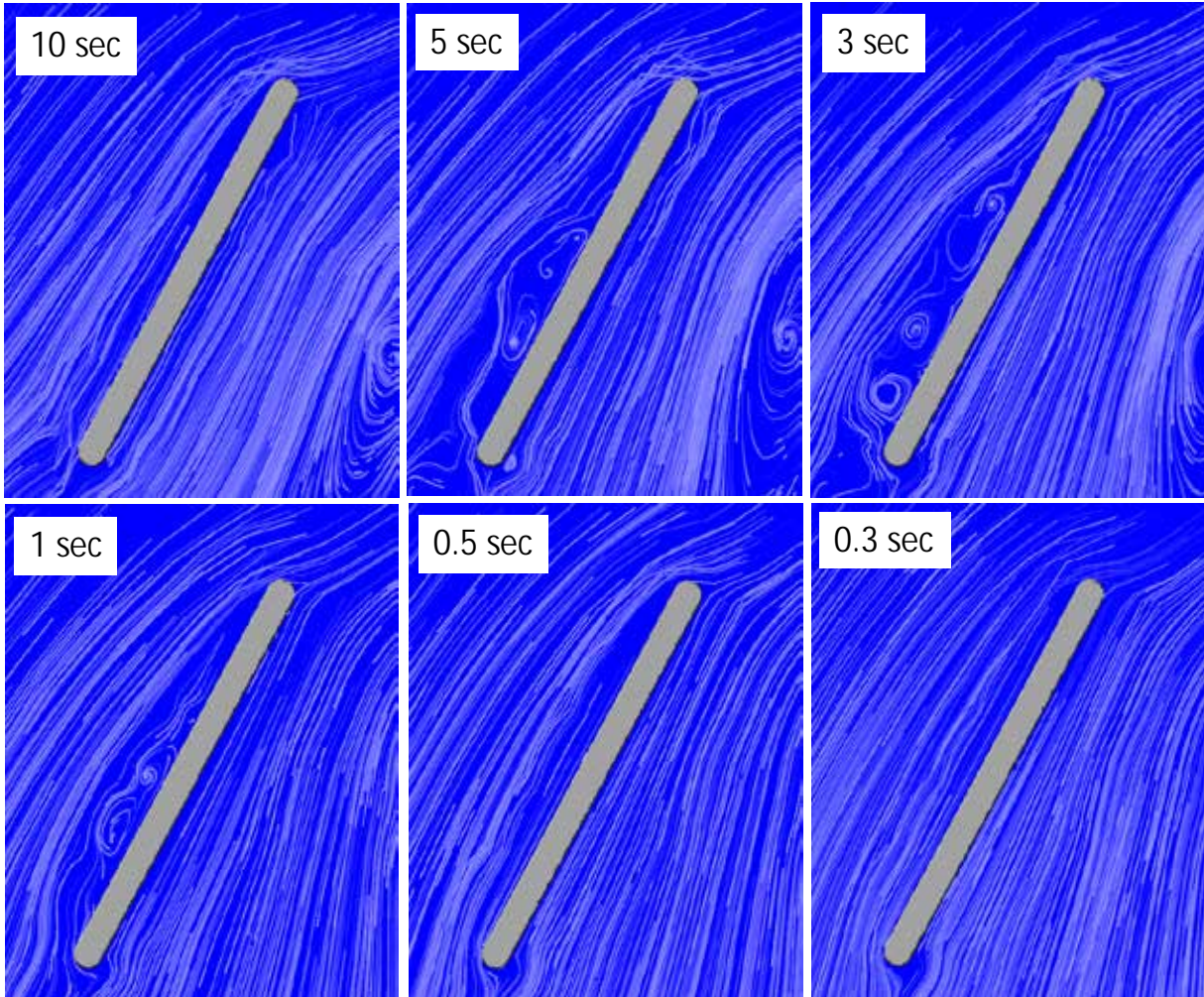


Figure 8.25: Streamlines at Bridge 1176 for 2D HEC-RAS, Several Δt -values

8.4 SRH-2D Model

The parameters for the SRH-2D model are given in Table 8.2 along with the same parameters for the 1-second timestep HEC-RAS 2D model. The SRH-2D model execution time is 12.43 hours versus 1.75 hours for HEC-RAS 2D. The Max WSE elevation profiles and floodplains are compared in Figures 8.26 to 8.28. These figures show that the two models give nearly the same results for this site.

Table 8.2: Parameters for SRH-2D and HEC-RAS 2D 1-Second Timestep Models

| | SRH 2D | HR 2D |
|----------------|--------------------------|--------------------------|
| Qmax (final) | 6000 cfs | 6000 cfs |
| Δt | 1 sec | 1 sec |
| Tsimulation | 20 hrs | 20 hrs |
| Tcpu (runtime) | 12.43 hrs | 1.75 hrs |
| CellMin | 0.086 ft ² | 0.540 ft ² |
| CellMax | 6612 ft ² | 1967 ft ² |
| CellAvg | 109 ft ² | 590 ft ² |
| No. of Cells | 97450 | 22348 |
| Model Area | 10593488 ft ² | 10593488 ft ² |

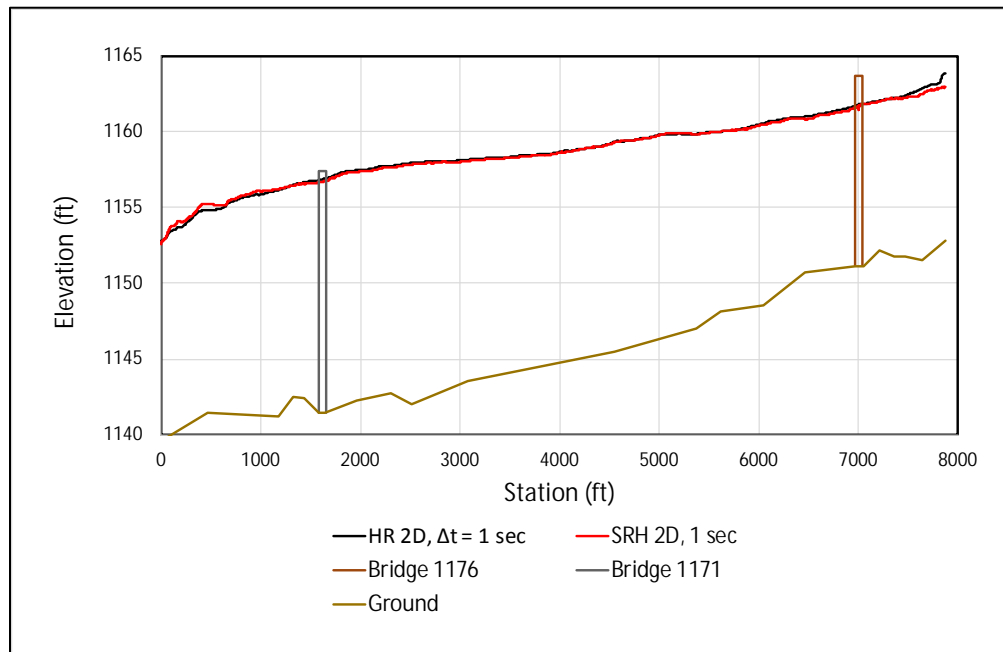


Figure 8.26: SRH-2D and HEC-RAS 2D Max WSE Profiles ($\Delta t = 1$ second)

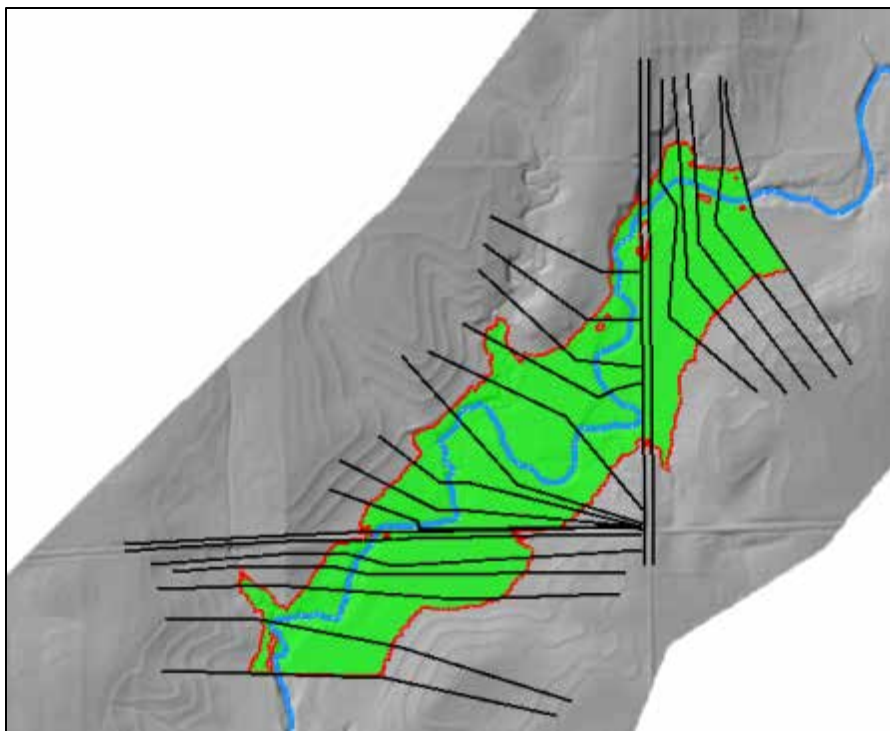


Figure 8.27: SRH-2D Floodplain ($\Delta t = 1$ second)

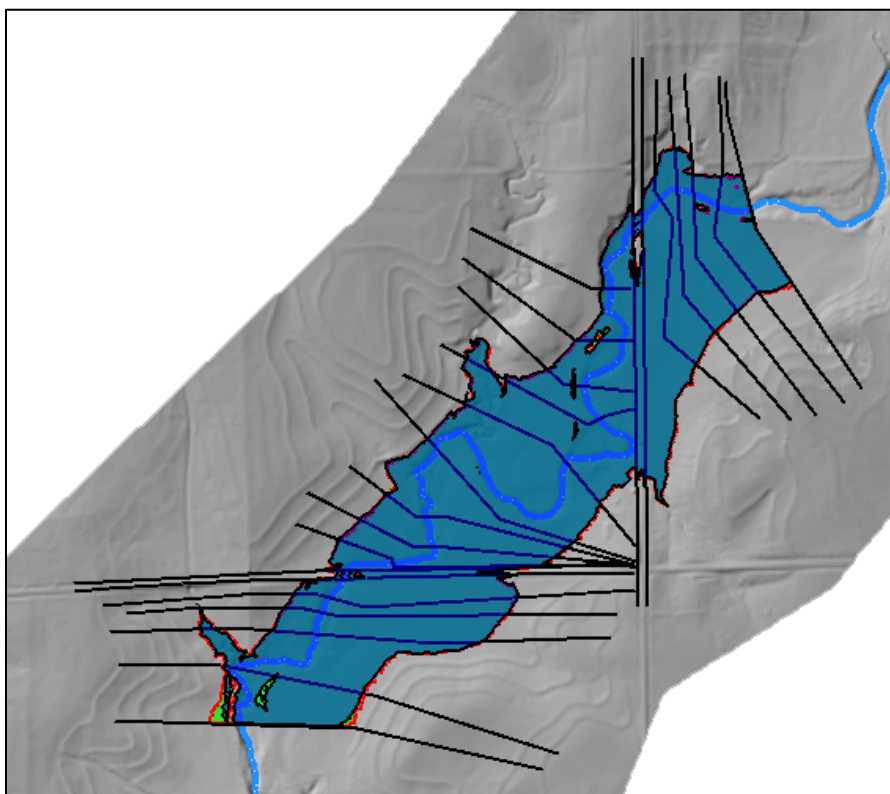


Figure 8.28: SRH-2D and HEC-RAS 2D Floodplains ($\Delta t = 1$ second)

8.5 Runtime Comparison

The model runtime for HEC-RAS 2D and SRH-2D were compared for the final models in this chapter. Table 8.3 lists relevant characteristics of the two models. Note that for this chapter, the HEC-RAS 2D model and the SRH-2D model had the same timestep (1 second) and the HEC-RAS 2D model actually had a denser mesh (more cells). As discussed in Chapter 7, HEC-RAS 2D will produce acceptable results with fewer cells and a larger timestep. Still, the HEC-RAS 2D model in this chapter was 8.5 times faster than the SRH-2D model. The runtimes presented are for the same computer described in Figure 6.45 (a 2.5GHz i7 laptop with 8Gb RAM).

Table 8.3: Comparison of Runtimes

RUN TIMES IN HOURS

| | SRH 2D | HR 2D (5.0.3) |
|--------------|-------------------------|-------------------------|
| Qmax (final) | 6000 cfs | 6000 cfs |
| Δt | 1 s | 1 s |
| Tsimulation | 20 hrs | 20 hrs |
| Tcpu | 12.43 hrs | 1.88 hrs |
| CellMin | 0.064 ft ² | 0.54 ft ² |
| CellMax | 22895 ft ² | 1967 ft ² |
| CellAvg | 273 ft ² | 590 ft ² |
| No. of Cells | 18158 | 22348 |
| Model Area | 4955563 ft ² | 4955563 ft ² |

Chapter 9: Butler County Site

9.1 Background for the Floodplain Study

This study considers the site shown below in Butler County, Kansas, on the east side of El Dorado. Figure 9.1 shows the stream centerlines of Walnut River and the West Branch tributary. The confluence of the two streams is just upstream from Bridge No. 54-8-271 on Highway 54. The discharge from the portion of Walnut River shown in the figure is the outflow from El Dorado Lake. As a consequence, the 100-year discharge is quite small for the river's drainage basin area. The effect of the reservoir is shown in Table 9.1 from the FEMA Flood Insurance Study for El Dorado Bridge No. 54-8-271.

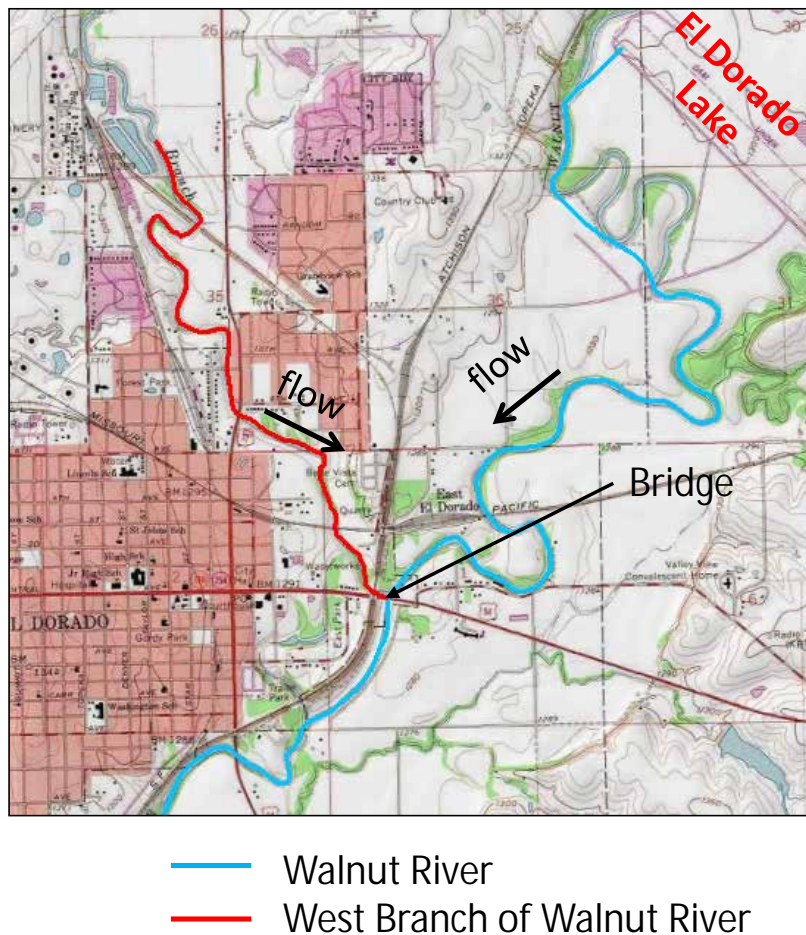


Figure 9.1: Butler County Site (El Dorado, KS)

Table 9.1: Discharges from FEMA FIS for El Dorado Bridge No 54-8-271

| FLOODING SOURCE AND LOCATION | Discharge Area (Square Miles) | PEAK DISCHARGES (CFS) | | | |
|--------------------------------------------------------|----------------------------------|---------------------------------|--------------------------------|--------------------------------|----------------------------------|
| | | 10-Percent Annual- Chance | 2-Percent Annual- Chance | 1-Percent Annual- Chance | 0.2-Percent Annual- Chance |
| Tributary to Santa Fe Lake | | | | | |
| At mouth | 1.5 | 1,080 | 1,800 | 2,120 | 2,840 |
| Approximately 1,200 feet upstream of mouth | 1.2 | 870 | 1,440 | 1,690 | 2,250 |
| Approximately 2,200 feet upstream of 70th Street | 0.7 | 590 | 980 | 1,140 | 1,510 |
| Walnut River | | | | | |
| Just below mouth of Little Walnut River | 1,345.5 | 39,500 | 75,000 | 95,000 | 150,000 |
| Just below mouth of Whitewater River | 972.1 | 30,100 | 54,000 | 73,000 | 118,000 |
| Just above mouth of Whitewater River | 454.5 | 13,400 | 25,100 | 31,500 | 49,000 |
| Just below mouth of West Branch Walnut River | 350.2 | 9,500 | 18,000 | 23,000 | 39,000 |
| Just above mouth of West Branch Walnut River | 272.7 | 4,500 | 6,650 | 8,450 | 13,500 |
| Just above mouth of Bird Creek | 247.2 | 4,500 | 4,500 | 7,000 | 7,000 |
| West Branch Walnut River | | | | | |
| At confluence with Walnut River | 77.5 | 7,900 | 15,200 | 19,500 | 32,300 |
| Approximately 1.55 miles downstream of County Road 594 | 61.6 | 6,800 | 13,100 | 16,800 | 26,800 |
| Approximately 0.95 mile downstream of County Road 592 | 43.3 | 5,800 | 11,700 | 14,700 | 24,000 |

Table 9.1 shows that the 100-year discharges upstream and downstream from the bridge are 8,450 and 23,000 cfs, respectively. The difference of 14,550 cfs is due to the inflow from the West Branch tributary. Since the 100-year discharge from the West Branch tributary is 19,500 cfs, the peak flows of the main channel and tributary are not coincident.

FEMA floodplain studies would model the main channel and the tributary separately using a separate downstream normal depth boundary condition for each channel and using the maximum 100-year discharges shown in Table 9.1. Each channel would have its own floodplain. The final composite FEMA floodplain would be the maximum extent of the two floodplains. In GIS this would be accomplished by using the Mosaic Operator *MINIMUM* to merge the two

depth rasters. The boundary of the floodplain would be the location where the depth equals 0.1 ft or less depending on the specifications.

In this chapter the goal is to compare the 1D and 2D HEC-RAS models. The approach used with regard to the discharges is to ramp the input hydrographs at the upstream ends of the modeled reaches for the main channel and the tributary. Figure 9.2 shows the area modeled and the locations of input discharge hydrographs and the output stage hydrograph for the 2D models. These are called the model boundary conditions. The ramped hydrographs for the main channel and the west branch of Walnut River are shown in Figure 9.3. The Outflow Stage Hydrographs used a constant tail water WSE of 1274.82 ft, which is the same value used for the downstream boundary condition of the 1D HEC-RAS Model.

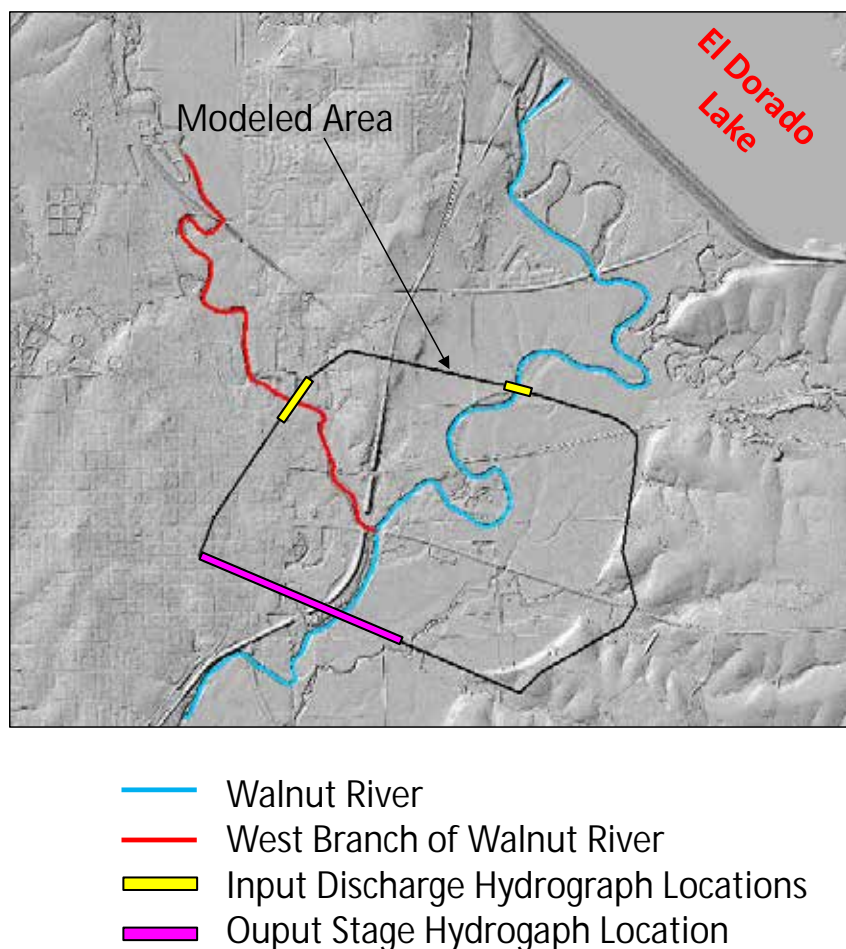


Figure 9.2: HEC-RAS Model Area

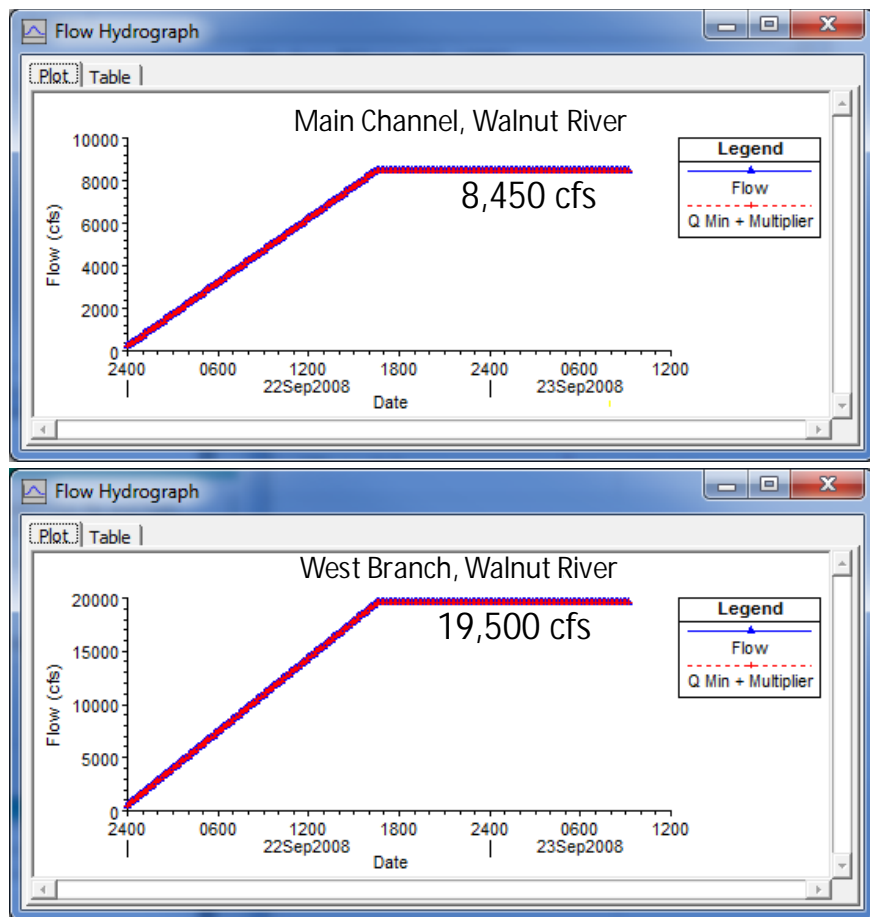


Figure 9.3: Ramped Hydrographs for HEC-RAS 2D Models

9.2 Preparation of Terrain Data

The LIDAR data for this site was modified to account for a weir located on the main channel just upstream from the confluence of the main channel and the tributary. Figures 9.4 and 9.5 show the location of the weir and a photograph, respectively. The difficulty is that the main channel appears flat for about a 3-mile reach upstream from the weir as shown in the centerline plot of Figure 9.6 which extends from the downstream end of the modeled reach to the lake outlet. This is due to the inability of standard LIDAR surveys to penetrate the water surface.

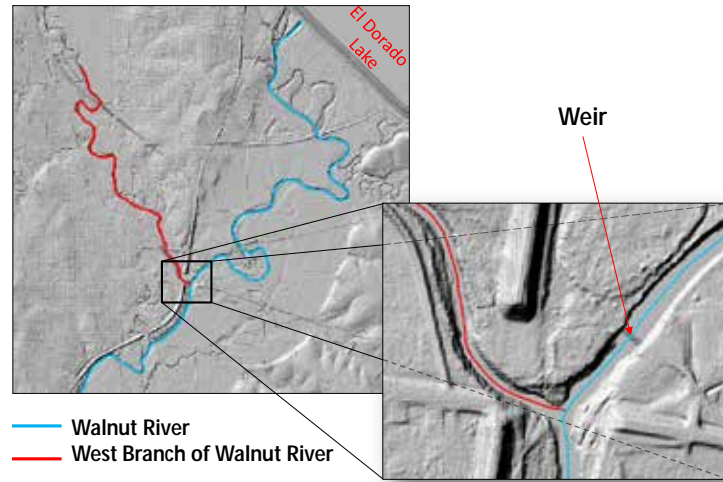


Figure 9.4: Weir Location



Figure 9.5: Weir Photograph

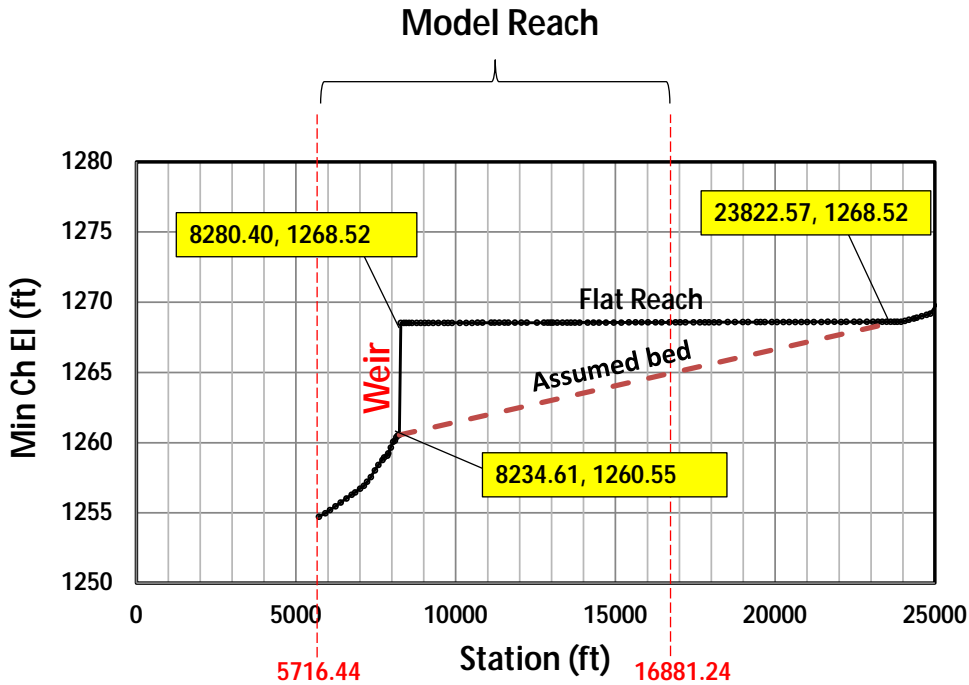


Figure 9.6: Walnut River Channel Centerline Elevation Plot from LIDAR

The LIDAR data was modified by cutting a trapezoidal channel in the flat portion of the LIDAR data. The trapezoidal channel had a base width of 40 ft and 2.5:1 (hor:vert) side slopes and the bed elevation was assumed to vary linearly in accordance with the dashed line in Figure 9.6. This was accomplished by the following steps.

1. Create a polygon shapefile to delineate the flat area of the LIDAR data.
2. Create the trapezoidal channel first as a clipped TIN then as a raster.
3. Merge the channel raster created in Step 2 and the original LIDAR raster.

9.2.1 Create a Polygon for the Flat Area of the LIDAR Data

The flat area polygon was developed by first making a 1D HEC-RAS model (call it Fake Model) from the original LIDAR data with short cross sections and a low discharge—in this case 1 cfs. Figure 9.7 shows the cross section layout through the model reach and upstream and the 0.1-ft inundation depth created with RAS Mapper. The extent of the inundation area is approximately equal to the extent of the flat LIDAR area since the depths of flow for $Q = 1$ cfs

were very small. In fact, the largest computed depth for all the cross sections was 0.45 ft. An n -value of 0.01 was used for the Fake Model.

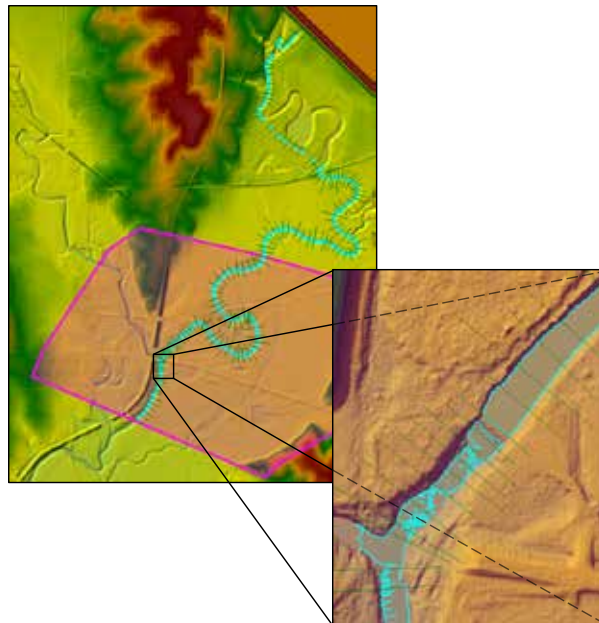


Figure 9.7: RAS Mapper Floodplain for Fake Model

The floodplain was exported to a shapefile in RAS Mapper as shown in Figure 9.8.

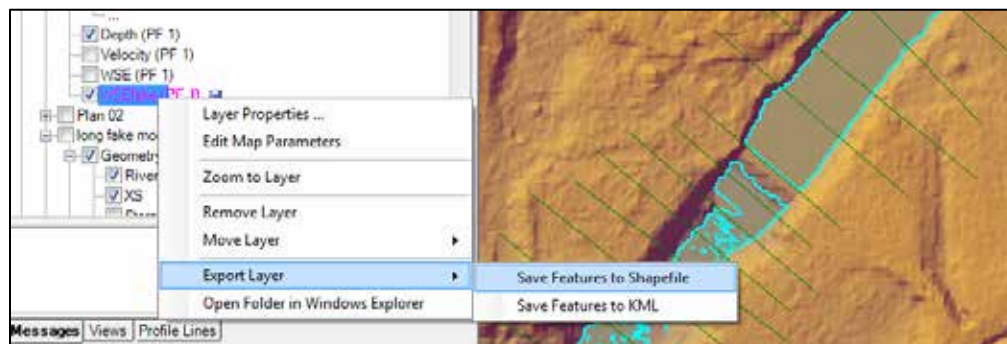


Figure 9.8: Export Inundation Area to Polygon Shapefile

This shapefile is shown in Figure 9.9a. Figure 9.9b shows that the shapefile was modified to include the elevated weir area. The resulting polygon shapefile (called *edge_edit*) is used to clip the trapezoidal channel raster to match the extent of the LIDAR flat area.

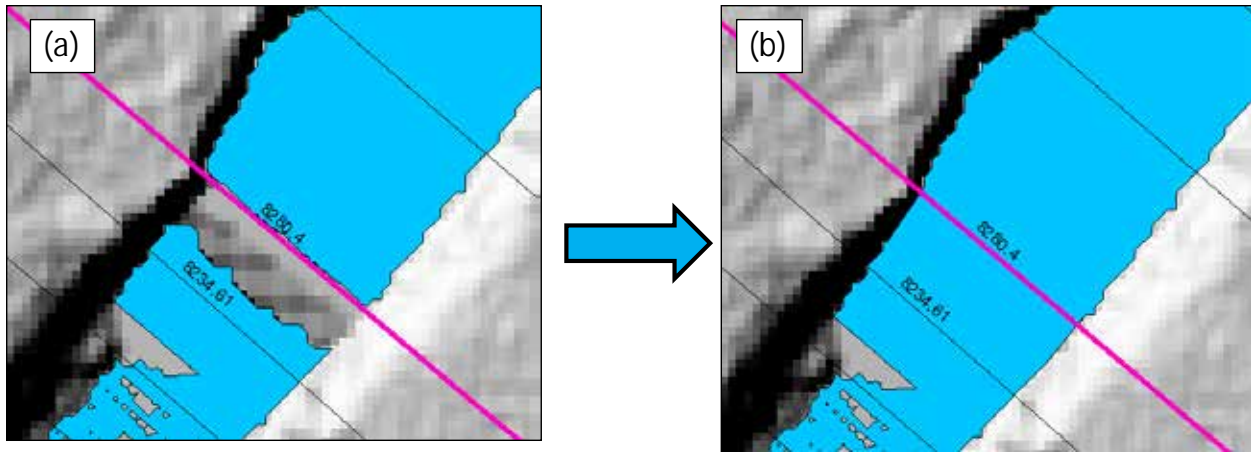


Figure 9.9: Modify Polygon Shapefile to Include Weir Area

9.2.2 Creating the Trapezoidal Channel Raster

The stream centerline was clipped to the reach defining the flat LIDAR area as shown in Figure 9.10. The centerline polyline was copied parallel 20 ft and 120 ft in both right and left directions as shown in Figure 9.11. New fields *zus* and *zds* were added to the attribute table of the shapefile then those fields were populated with the values shown in Figure 9.12a. The values for the centerline elevations are directly from Figure 9.6. The top width values are 40 ft higher than the channel base values based on the 2.5:1 side slope assumption. A 3D shapefile called *trapcline3D* was created as shown in Figure 9.12b.

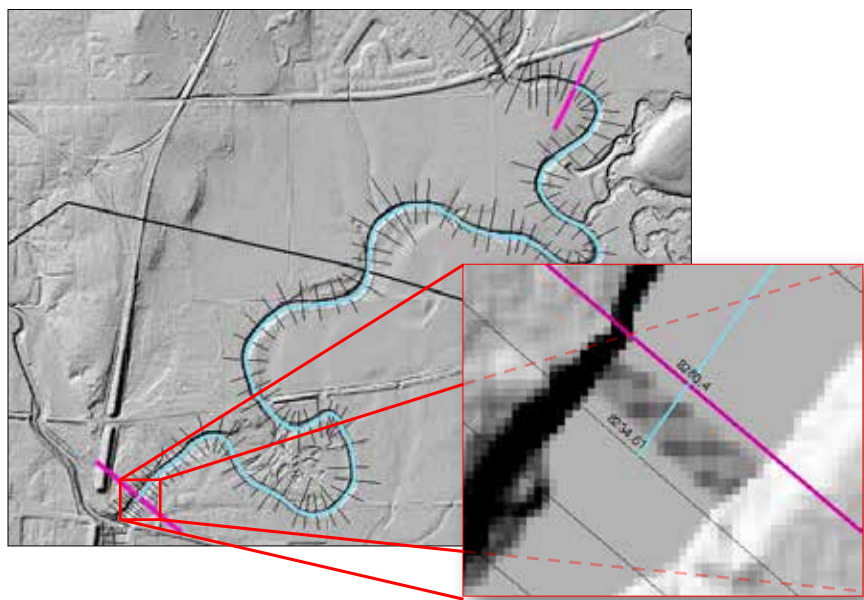


Figure 9.10: Create Centerline Shapefile Called trapchlines for Flat Reach of LIDAR



Figure 9.11: Apply Copy Parallel to Create Base and Top Width of Trapezoidal Channel

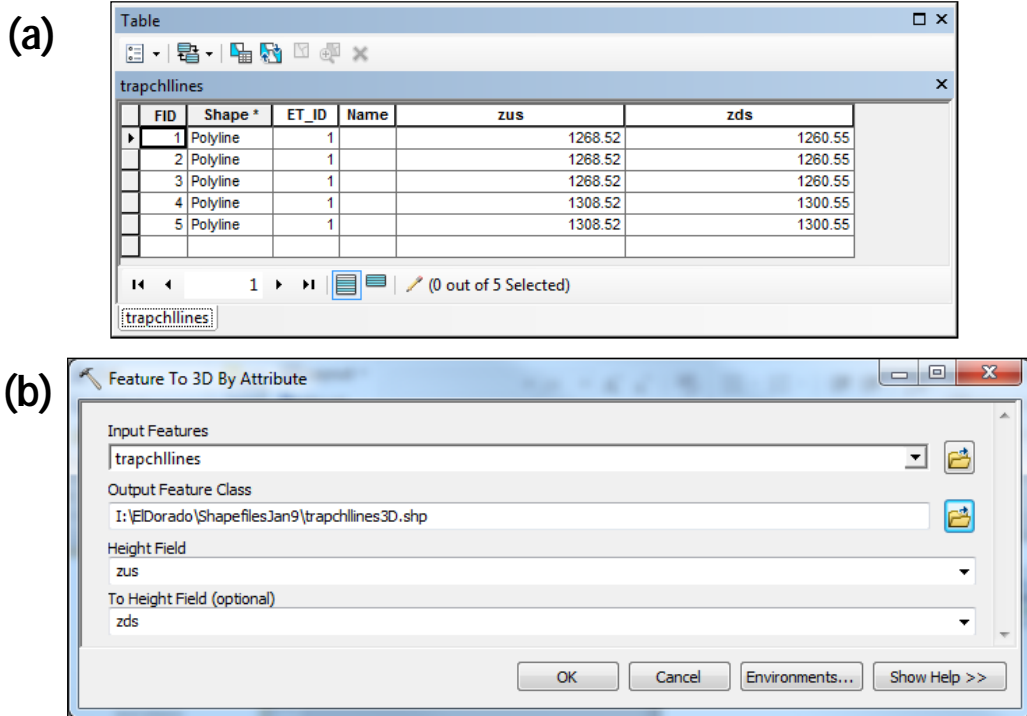


Figure 9.12: (a) Populating zus and zds fields, (b) Creating a 3D shapefile

A TIN was created as shown in Figures 9.13 and 9.14. The TIN was used to create a 4-ft raster called *chlras* in Figure 9.15.

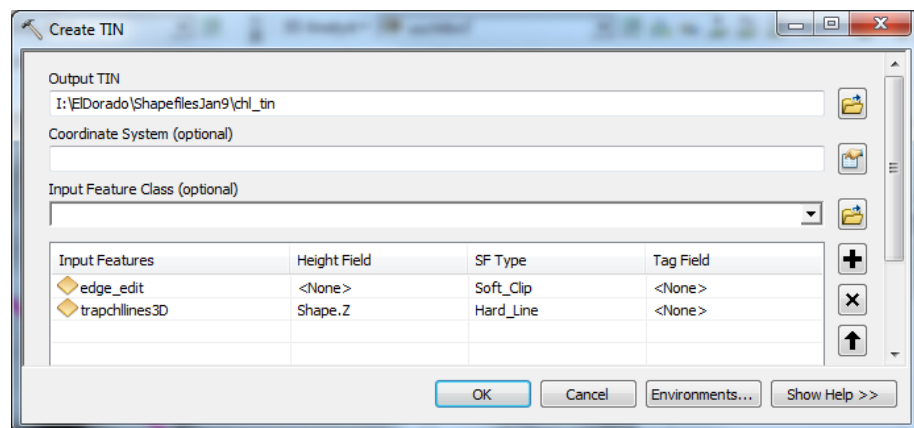


Figure 9.13: Create TIN from 3D Shapefile (chl_tin)

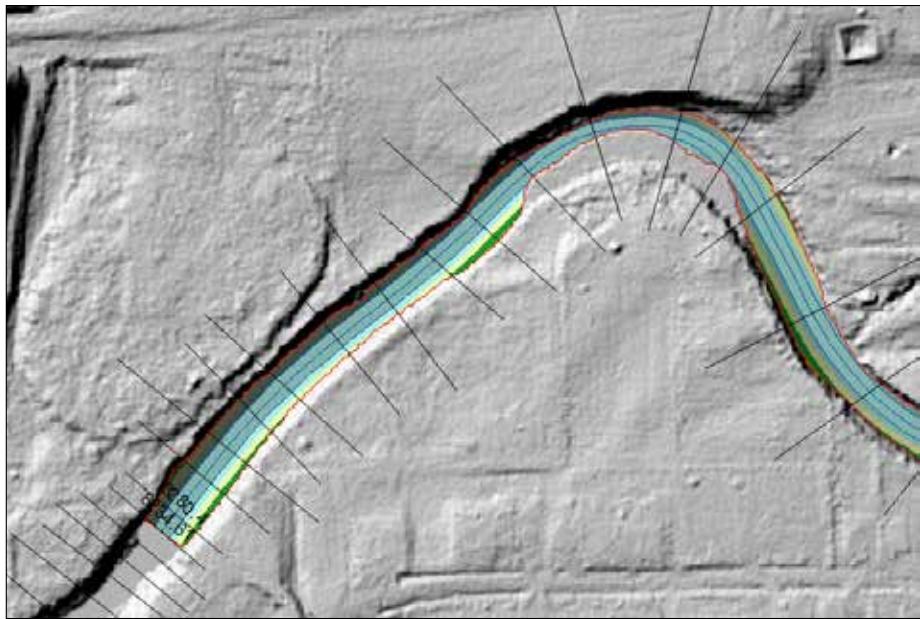


Figure 9.14: A Portion of chl_tin

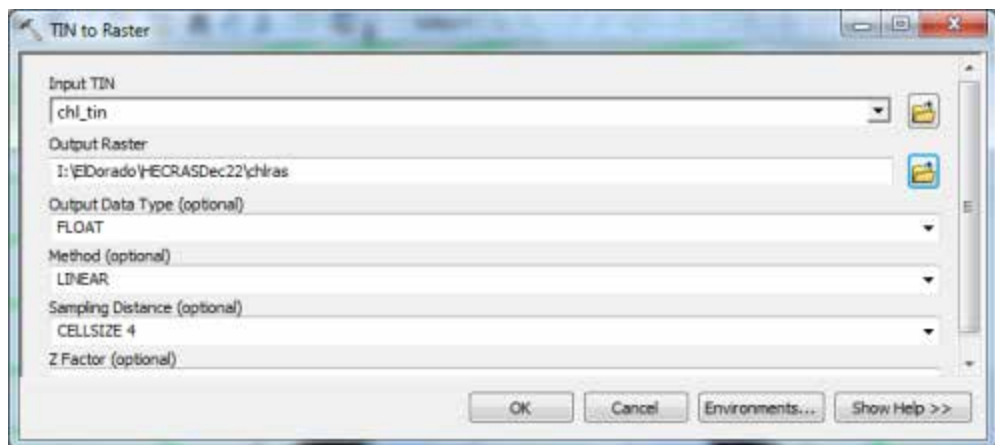


Figure 9.15: Chl_tin Used to Create chlras

9.2.3 Merge the Channel Raster and the LIDAR Raster

The channel raster, *chlras*, was merged with the LIDAR 4-ft raster called *Project4ftRAS* as shown in Figure 9.16 to create the composite raster *proj4ft_ras*. A portion of *proj4ft_ras* is shown in Figure 9.17 projected as a hillshade.

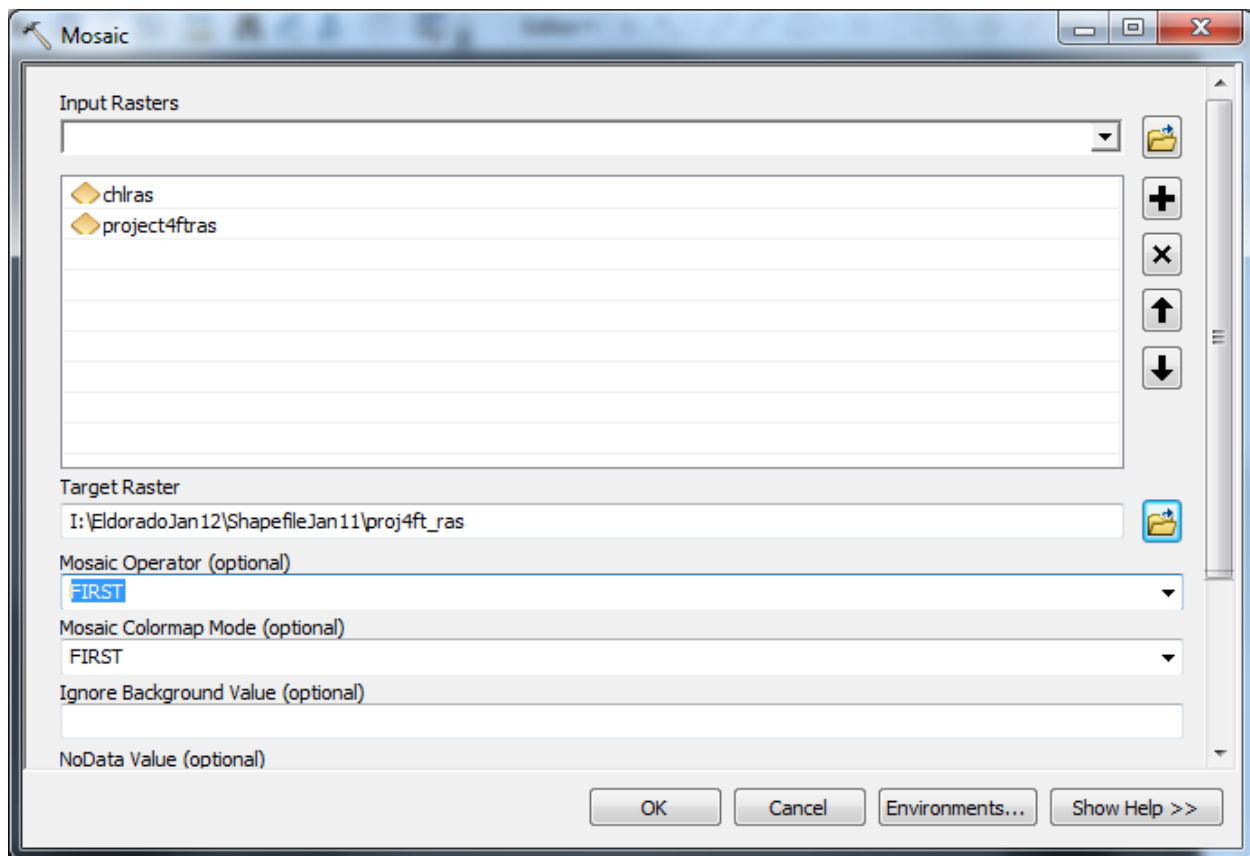


Figure 9.16: Mosaic Function was Used to Merge the Channel Raster and the Original Raster to Create the Proj4ft_ras



Figure 9.17: Final Proj4ft_ras

9.3 Create HEC-RAS Terrain in RAS Mapper

Figure 9.18 shows the area modeled in this project. Only the US-54 Bridge and the weir were modeled explicitly in HEC-RAS 1D and 2D. Ineffective flow regions and cross section spacing were used to model the railroad and the small bridges in lieu of explicit modeling within the 1D model. The US-54 bridge has seven piers. Four are elliptical 4-ft \times 6-ft piers, one is an elongated pier with 2.5-ft square columns on both ends and a 1.5-ft-wide web connecting the columns. The last two piers are two-column, 2-ft square piers. They are depicted in Figure 9.19 which is a screen shot in ARC Scene, and some of the main piers are shown in Figure 9.20. The weir discussed above is also shown. The methods presented in previous chapters were used to create 0.1-ft rasters for each pier and the weir. The pier dimensions and spacing were determined from the bridge plans.

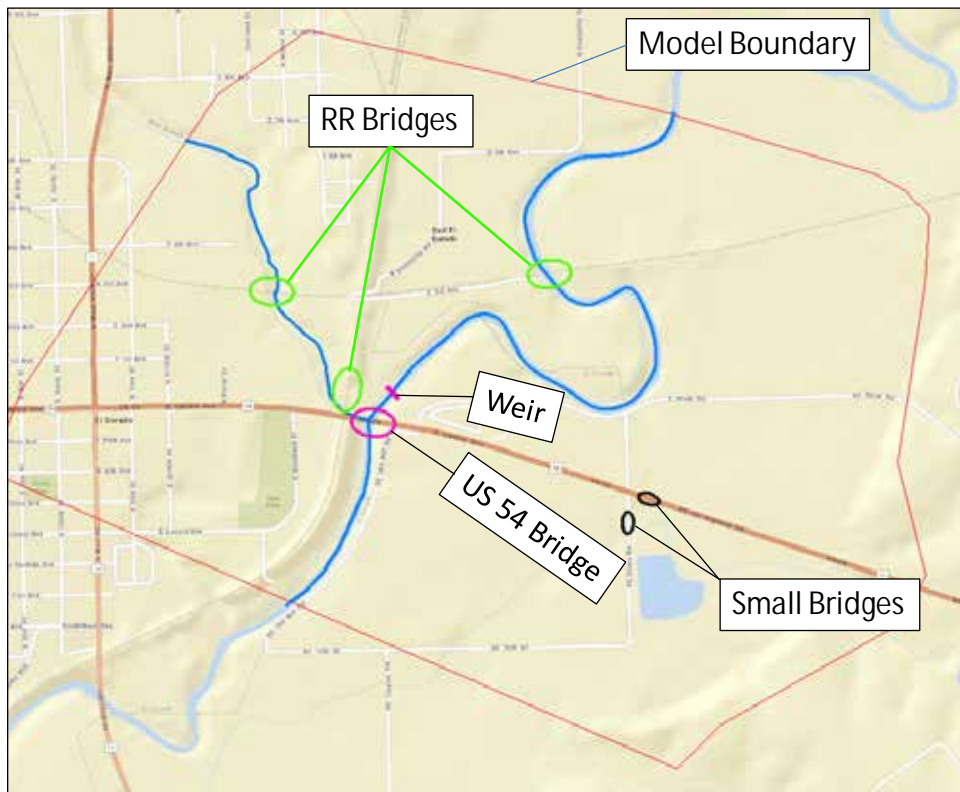


Figure 9.18: Model Site

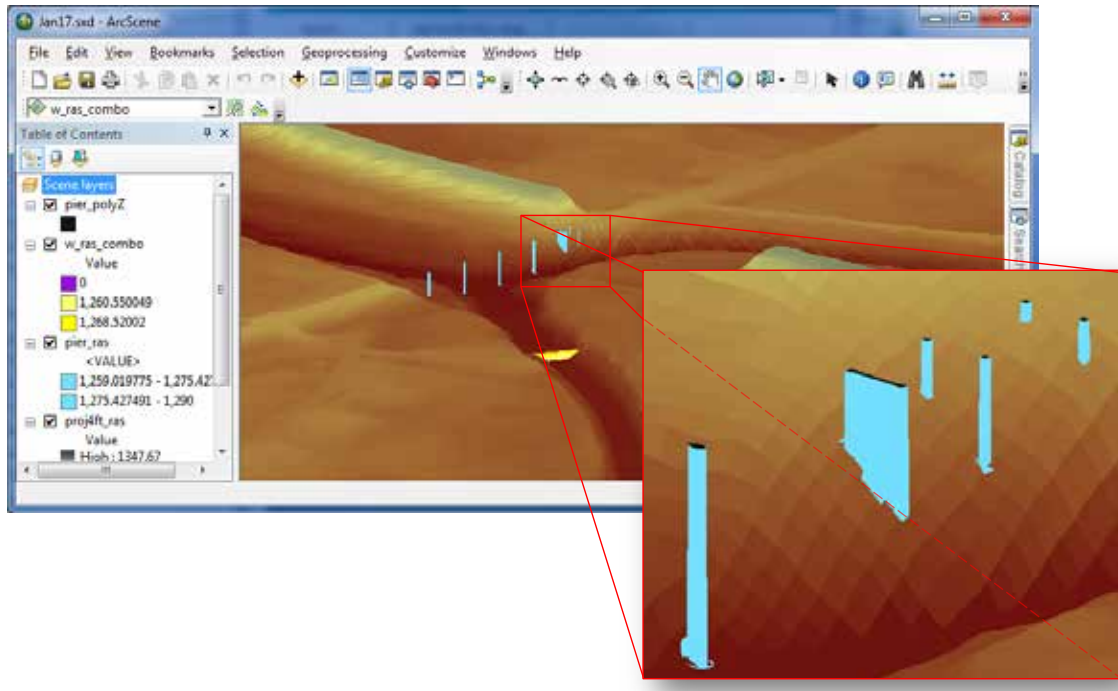


Figure 9.19: ARC Scene View of Piers, Weir, and the Proj4ft_ras



Figure 9.20: HW 54 Bridge

The terrain for the 2D HEC-RAS models was created in RAS Mapper as shown in Figure 9.21 where *w_ras_combo* and *pier_ras* are the pier and weir rasters, respectively, and *Proj4ft_ras* is the combo raster containing the cut channel described above. The resulting terrain, called *Terrain_Final.hdf*, was used for the 2D models. (Only *Proj4ft_ras* was used for the 1D model.)

The order in the window is important so the 4-ft raster was at the bottom of the list. One also needs to create a new landuse layer in RAS Mapper using a landuse polygon like those used in creating a 1D HEC-RAS model. Figure 9.22 shows a portion of *Terrain_Final* with the piers and weir in RAS Mapper.

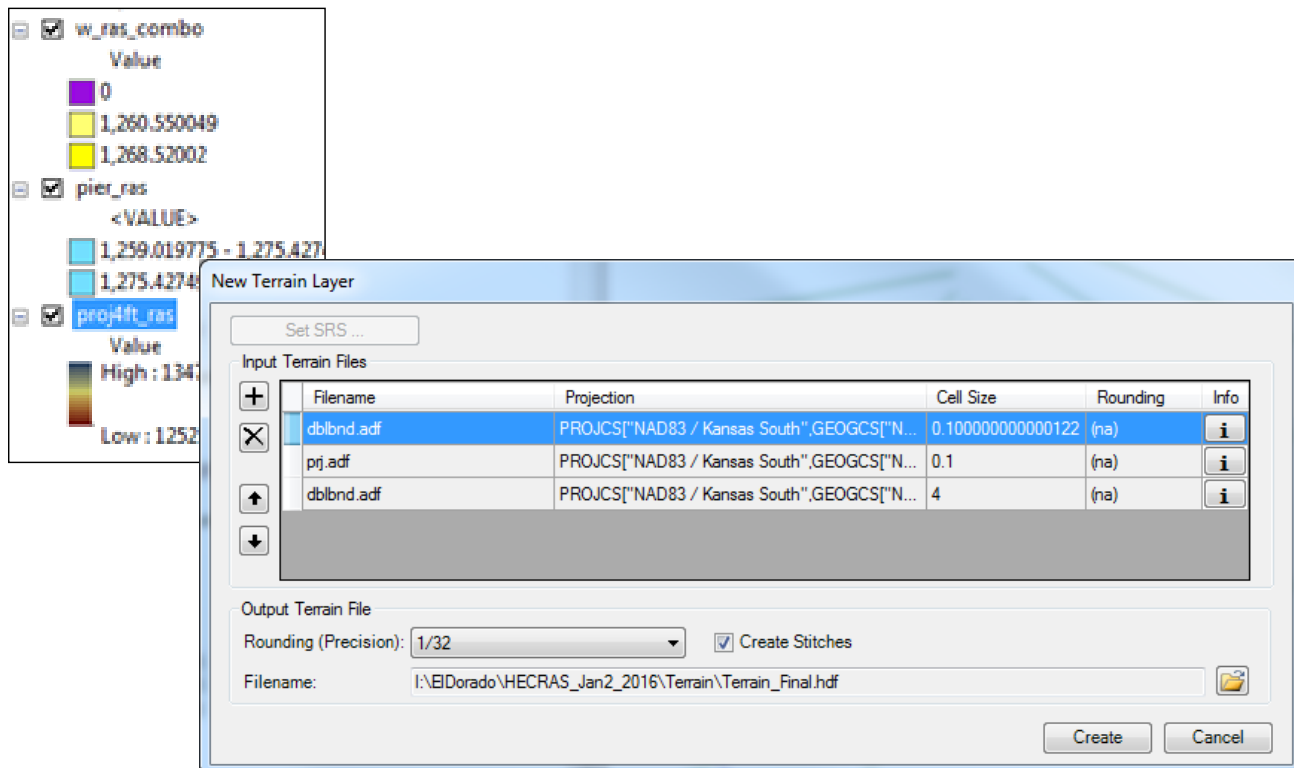


Figure 9.21: Create New Terrain in RAS Mapper

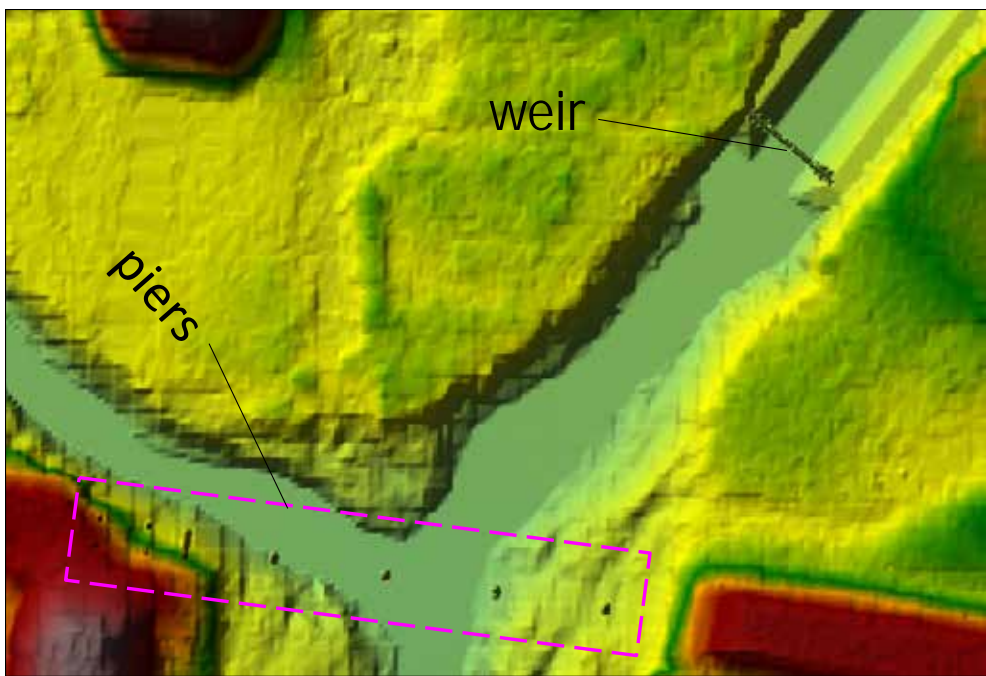


Figure 9.22: New RAS Mapper Terrain, Terrain_Final

9.3.1 1D HEC-RAS Model

The HEC-RAS 1D model was created using the raster *proj4ft_ras* and not the one created above, *Terrain_Final*. The piers and the weir were entered into the 1D model separately. A junction was created at the confluence of the main channel and the tributary to create the three reaches shown in the screen capture on the right. The 1D HEC-RAS model cross sections and river reaches are shown in Figure 9.23a together with the depth grid as determined in RAS Mapper using *Terrain_Final*. The edges of the continuous depth grid correspond to the floodplain. The regions disconnected from the main flow should not be included in the floodplain. Figure 9.23b shows the edited floodplain. Figure 9.24 shows the upstream bridge section. Figure 9.25 shows the water surface profiles for the main channel and tributary and the channel centerline ground elevation, respectively, as determined in RAS Mapper. These profiles will be compared with 2D model results in the next section.

| Avail Reaches | | |
|---------------|-----------------|--|
| Walnut River | Main Channel | |
| Walnut River | West Branch | |
| Walnut River | Main Channel DS | |

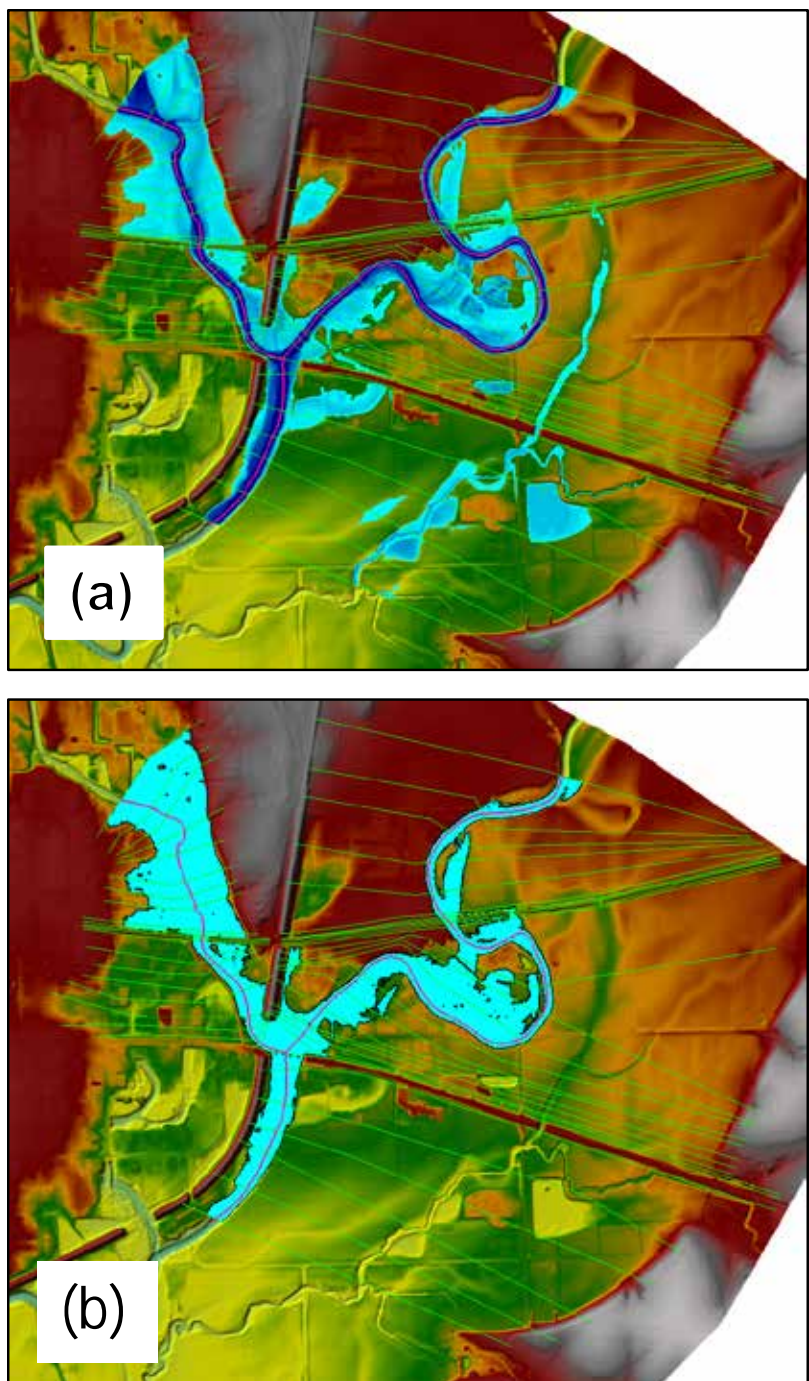


Figure 9.23: 1D HR Floodplain (a) Unedited, (b) Edited

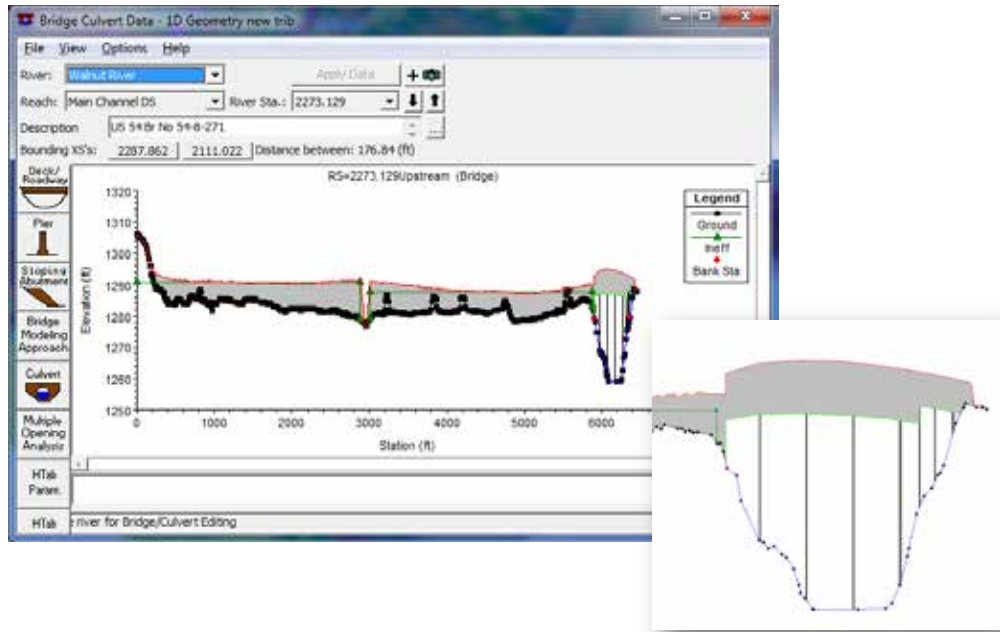


Figure 9.24: 1D HR US HW 54 Bridge Section

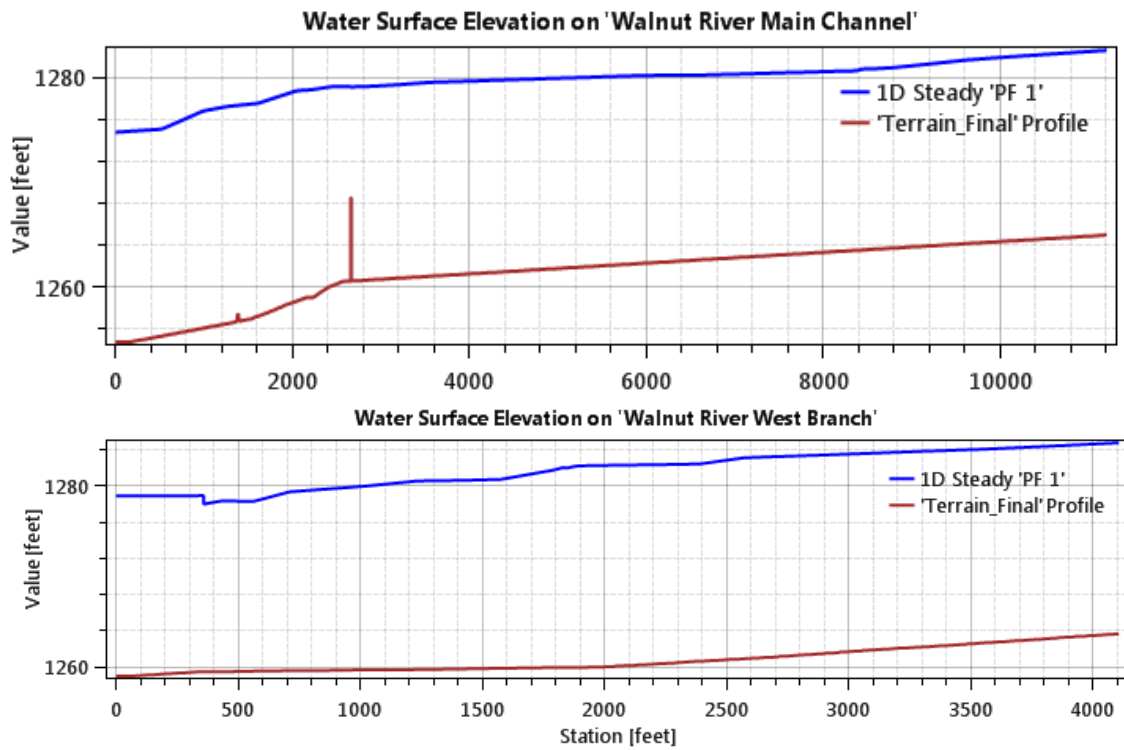


Figure 9.25: WSE and Ground Profiles for Main Channel and Tributary

9.4 2D HEC-RAS Model

The 2D model with breaklines for the streams, roads, railroads, and levee are seen in Figure 9.26 along with the two inflow hydrograph boundary condition lines and the outflow boundary condition line. Breaklines for the piers and the weir are shown in the zoomed-in view of Figure 9.27. Note that in this view you can also see the grid cells. Figure 9.28 shows zoomed-in views of the weir and selected piers displayed on the *Terrain_Final RAS Mapper* terrain. Note that the breaklines are within the buffered “Grid Tops” for the weir and the piers. This ensures that the weir and pier grid cell boundaries have the correct elevation.

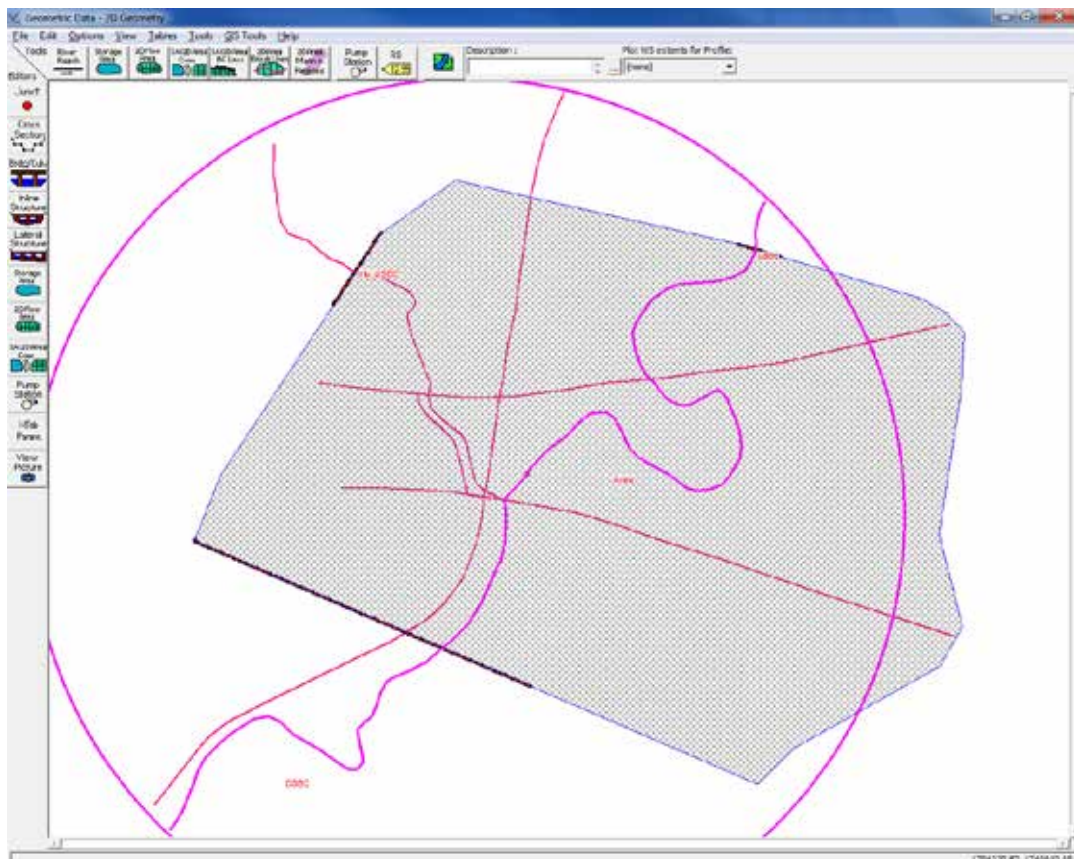


Figure 9.26: WSE and Ground Profiles for Main Channel and Tributary

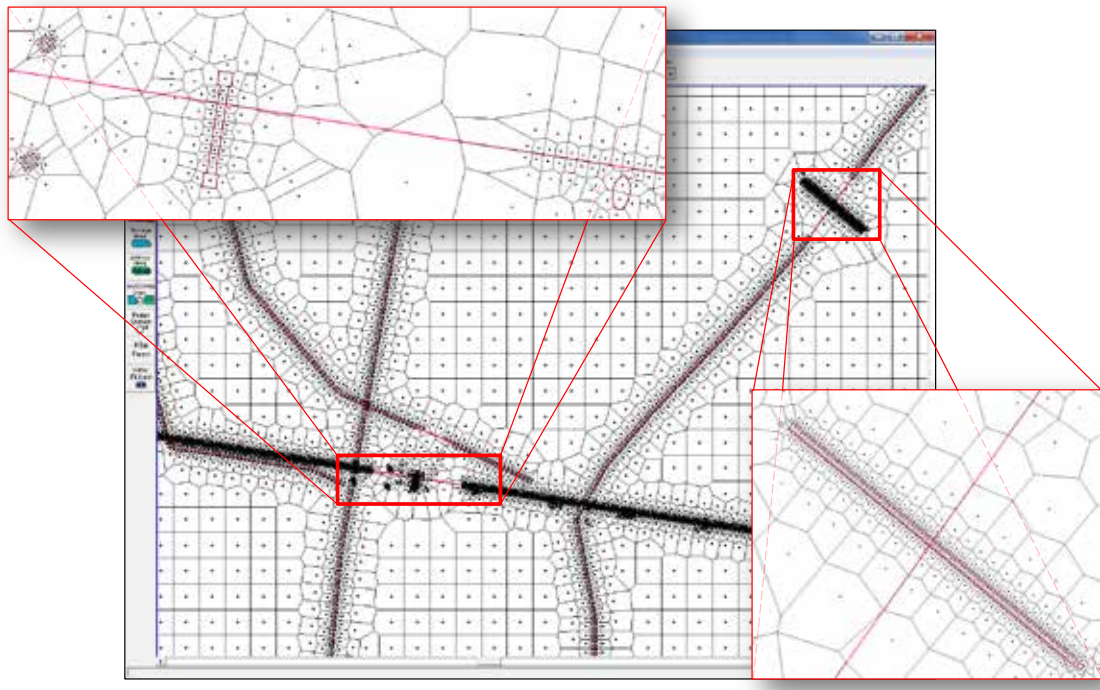


Figure 9.27: Grid in Pier and Weir Regions

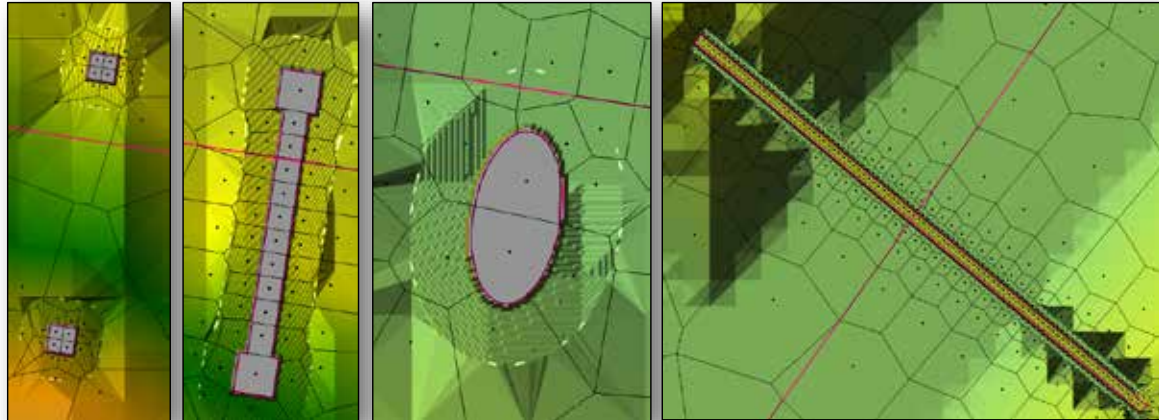


Figure 9.28: Weir and Selected Piers on Terrain_Final

The 2D model was executed for different time steps using the full momentum option. The model had 93,420 cells with maximum, minimum, and average cell sizes of 1609, 0.83, and 569 ft², respectively. According to Gary Brunner of HEC, the *n*-values used in the 2D model should be lower than the values used for the 1D model due to increased travel lengths for the 2D model.

This is evident in Figures 9.29 and 9.30 which show the computed 2D WSE profiles for Δt -values of 2, 3, 4, 5, 6, and 10 seconds for the landcover n -values used in the 1D HEC-RAS model for the main channel and tributary, respectively. All of the profiles are above the 1D HEC-RAS profile.

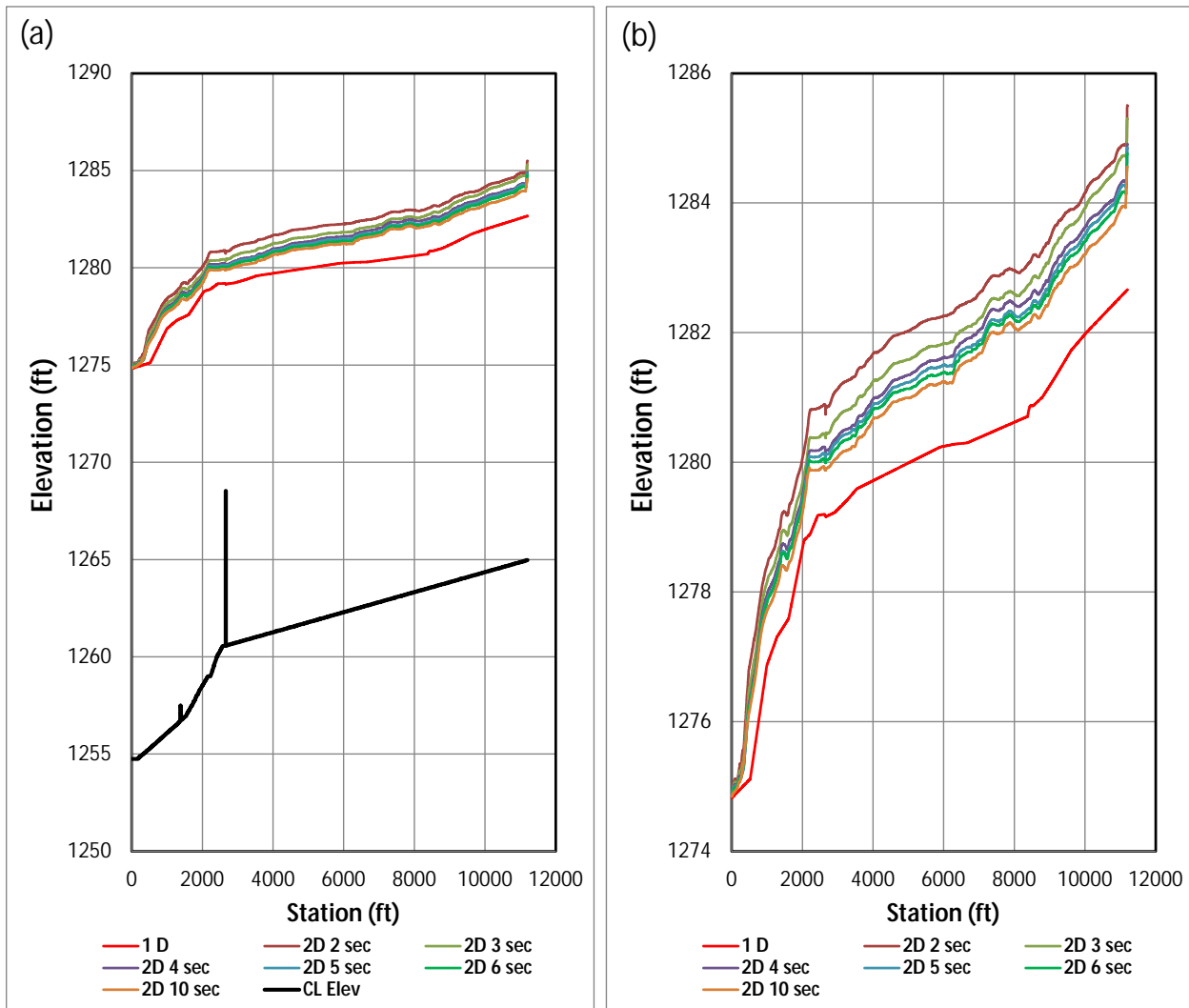


Figure 9.29: Main Channel WSE Profiles for a Range of Δt -values Using the 1D HEC-RAS n -values (a) with CL Elevation, (b) without CL Elevation

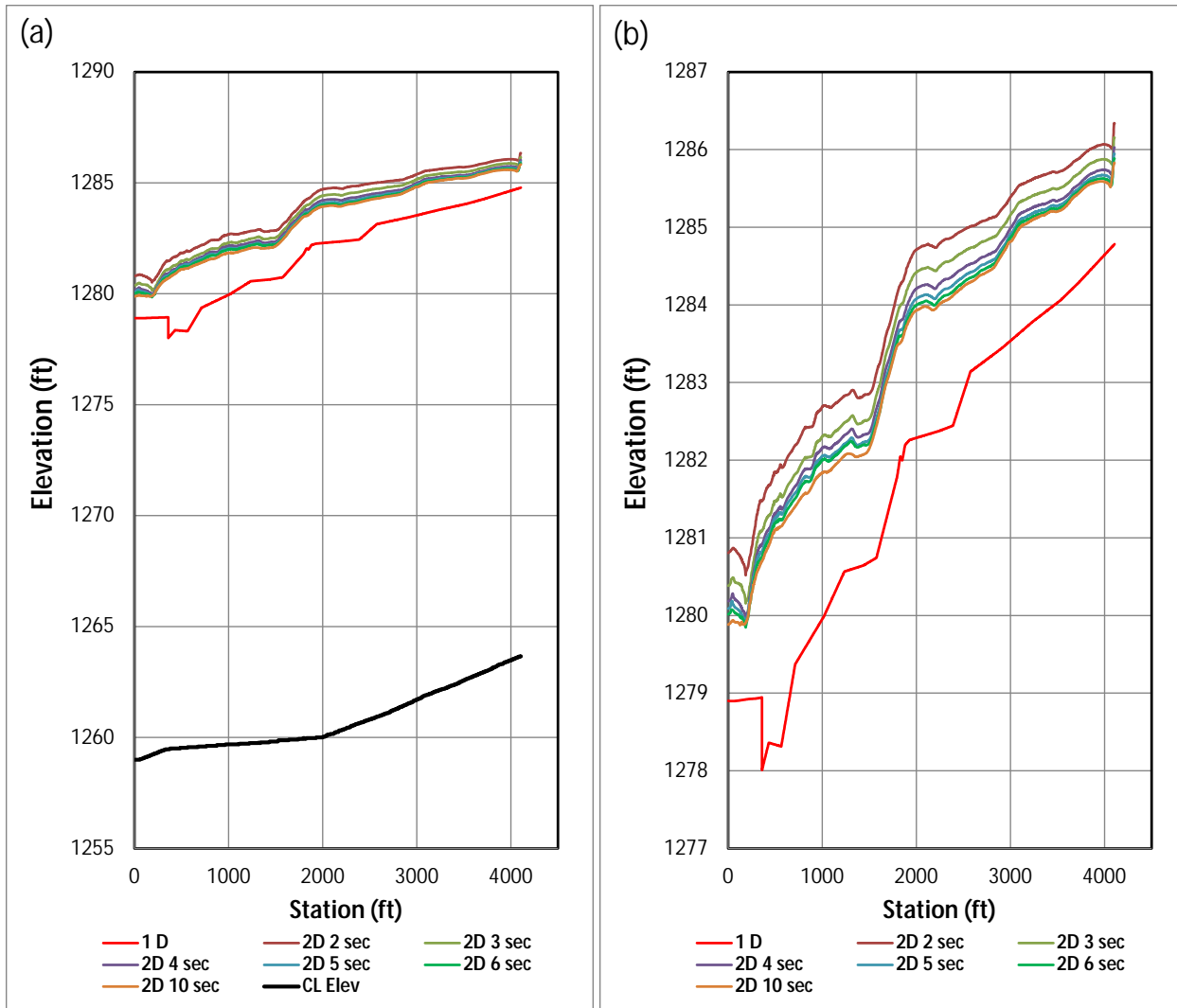


Figure 9.30: Tributary WSE Profiles for a Range of Δt -values Using the 1D HEC-RAS n -Values (a) with CL Elevation, (b) without CL Elevation

Landcover layers were created for different proportions (e.g., 70%, 60%, etc.) of the 1D landcover layer n -values to try to achieve a better agreement with the 1D HEC-RAS profile. The profiles for $\Delta t = 10$ seconds at 40, 70, and 100 percent of the 1D n -values are shown along with the 1D WSE profile in Figures 9.31 and 9.32 for the main channel and tributary, respectively. The 70 percent landcover produced the best fit with the 1D HEC-RAS profile for $\Delta t = 10$ seconds. Similar plots are shown in Figures 9.33 through 9.38 for Δt values of 5, 3, and 2 seconds. The “best fits” were found to be 60, 40, and 40 percent for $\Delta t = 5$, 3, and 2 seconds, respectively. Note that the 30 percent landcover WSE profile did not behave properly for $\Delta t =$

3 seconds and failed to run for $\Delta t = 2$ seconds. In fact, a good match was not found for $\Delta t = 2$ seconds.

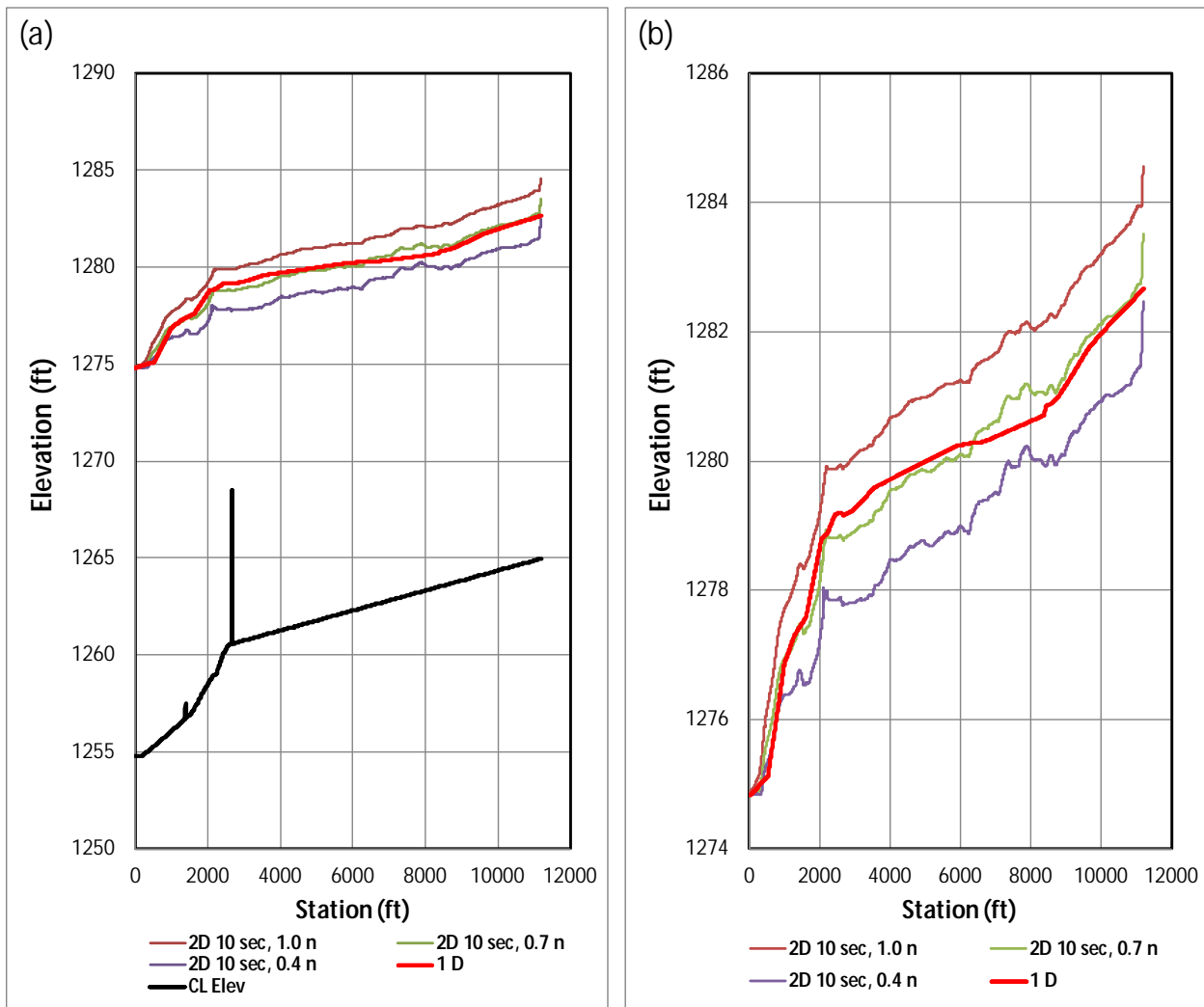


Figure 9.31: Main Channel WSE Profiles for $\Delta t = 10$ seconds

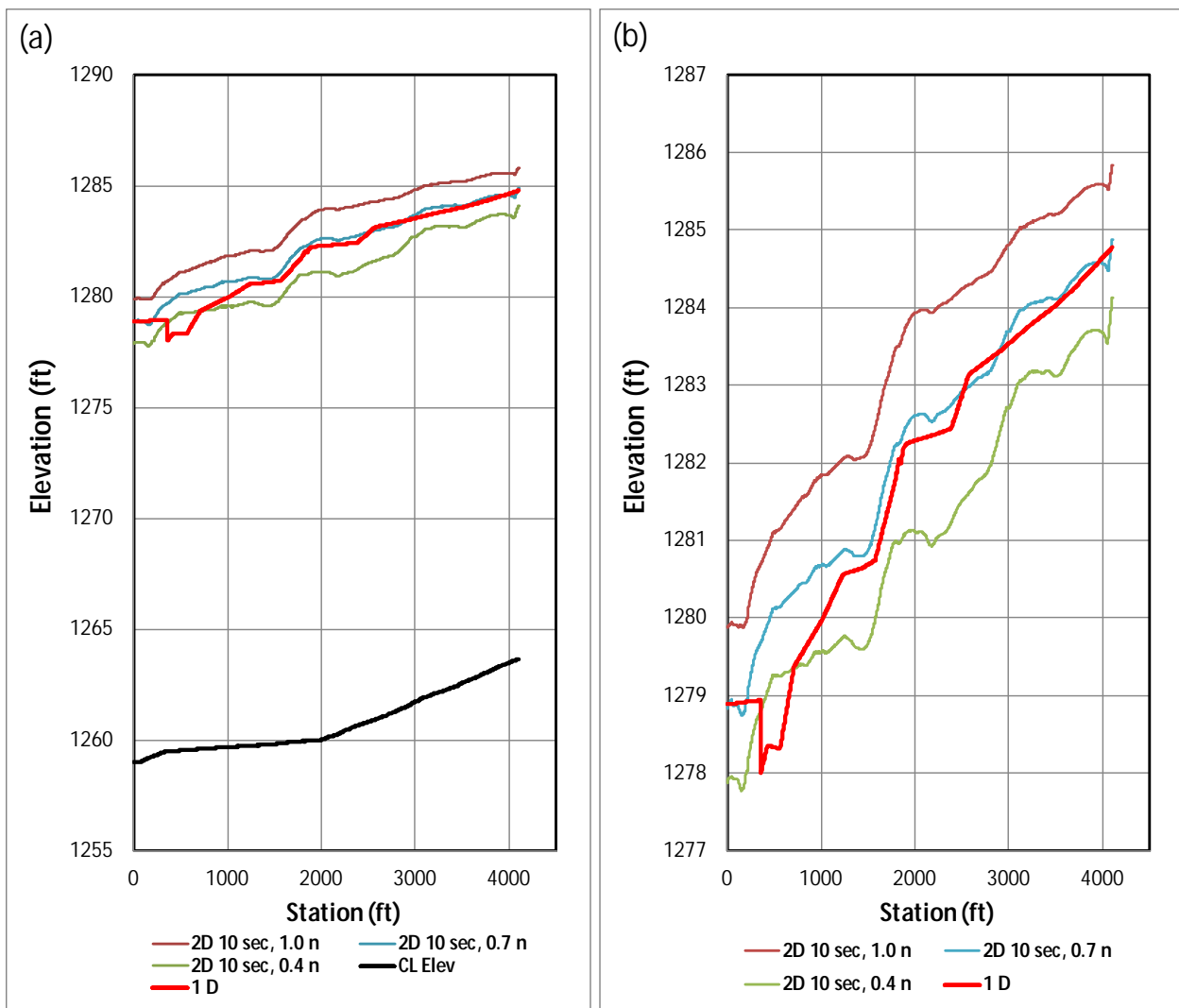


Figure 9.32: Tributary WSE Profiles for $\Delta t = 10$ seconds (a) with CL Elevation, (b) without CL Elevation

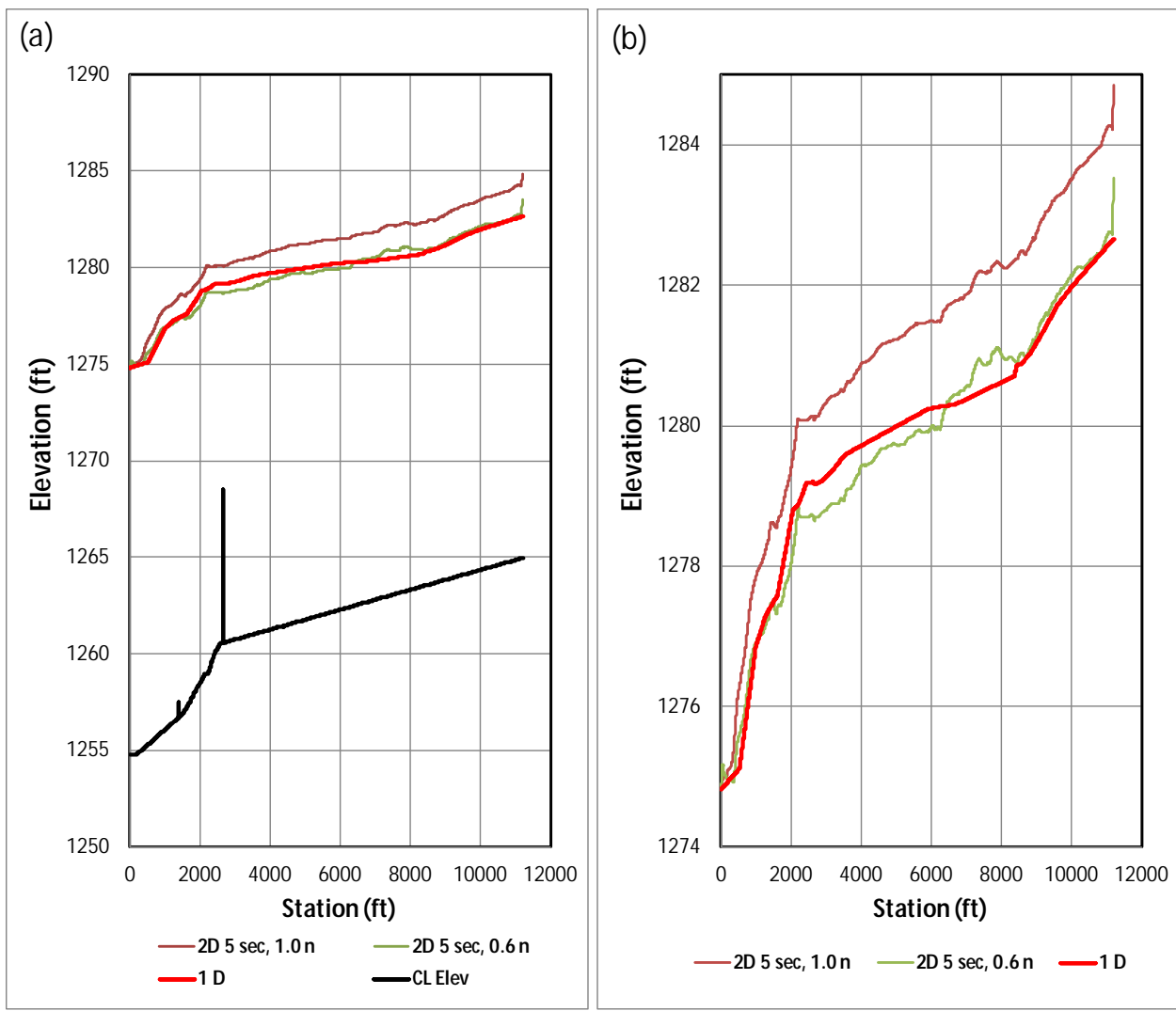


Figure 9.33: Main Channel WSE Profiles for $\Delta t = 5$ seconds (a) with Ground, (b) without Ground

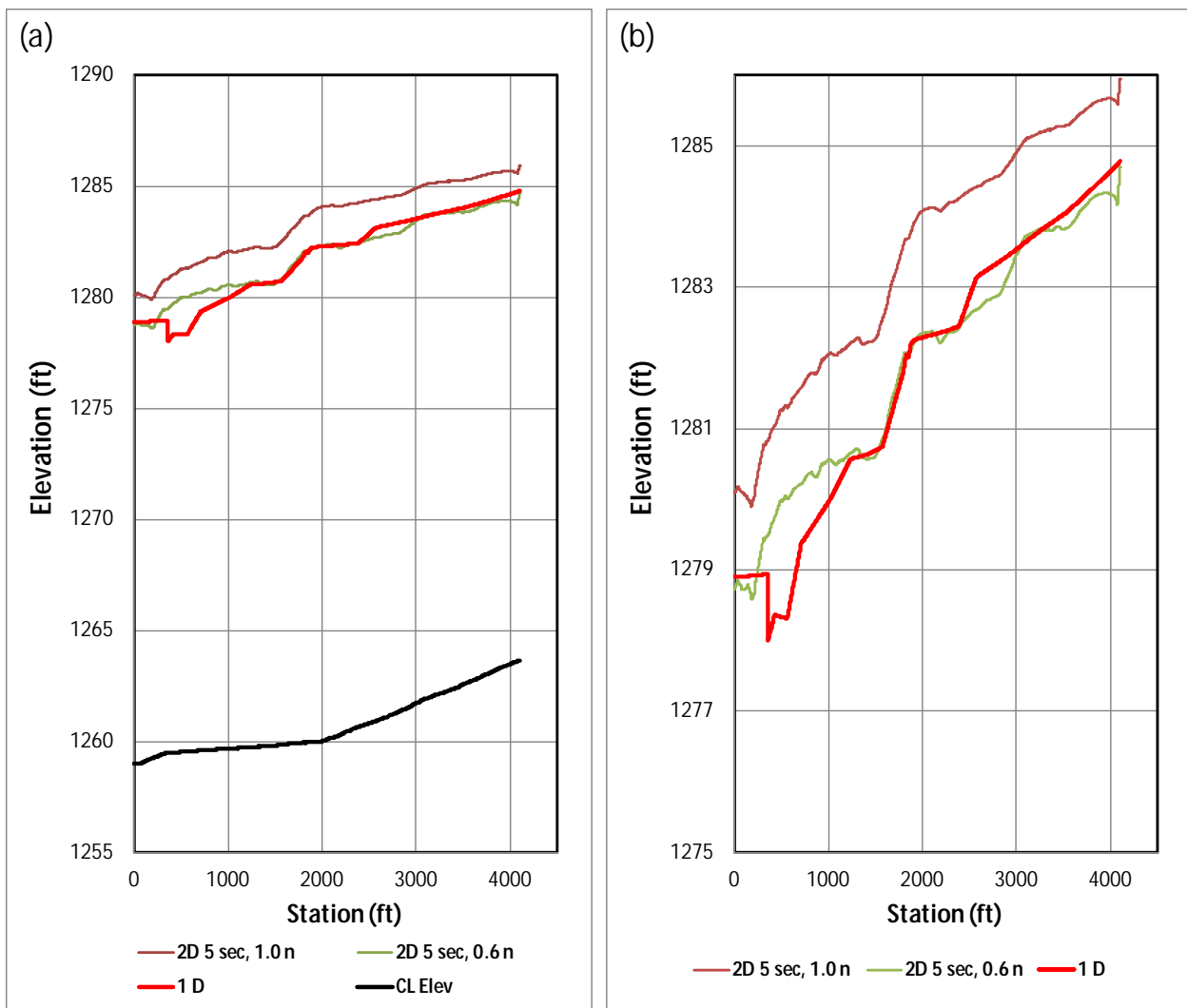


Figure 9.34: Tributary WSE Profiles for $\Delta t = 5$ seconds (a) with CL Elevation, (b) without CL Elevation

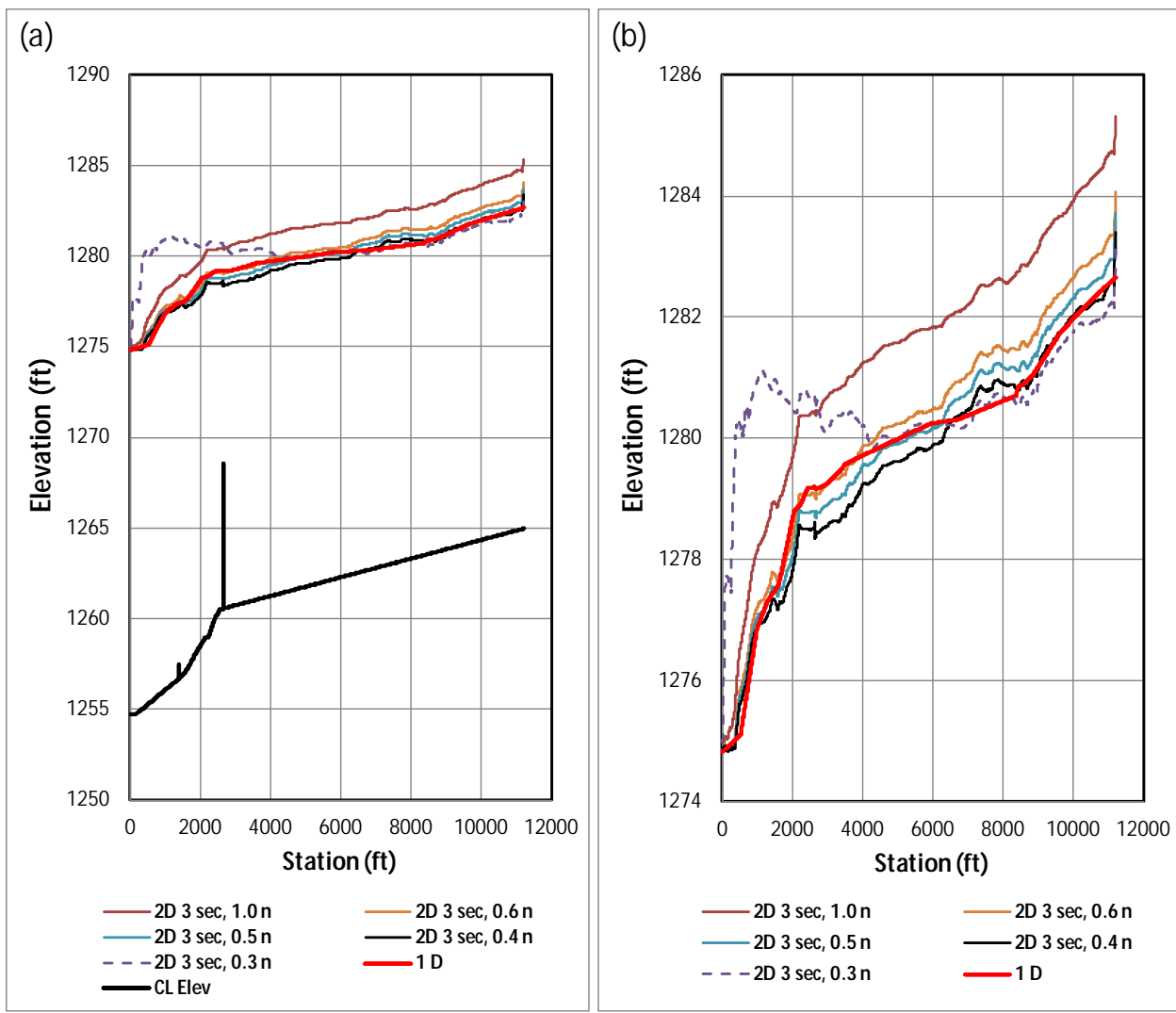


Figure 9.35: Main Channel WSE Profiles for $\Delta t = 3$ seconds (a) with Ground, (b) without Ground

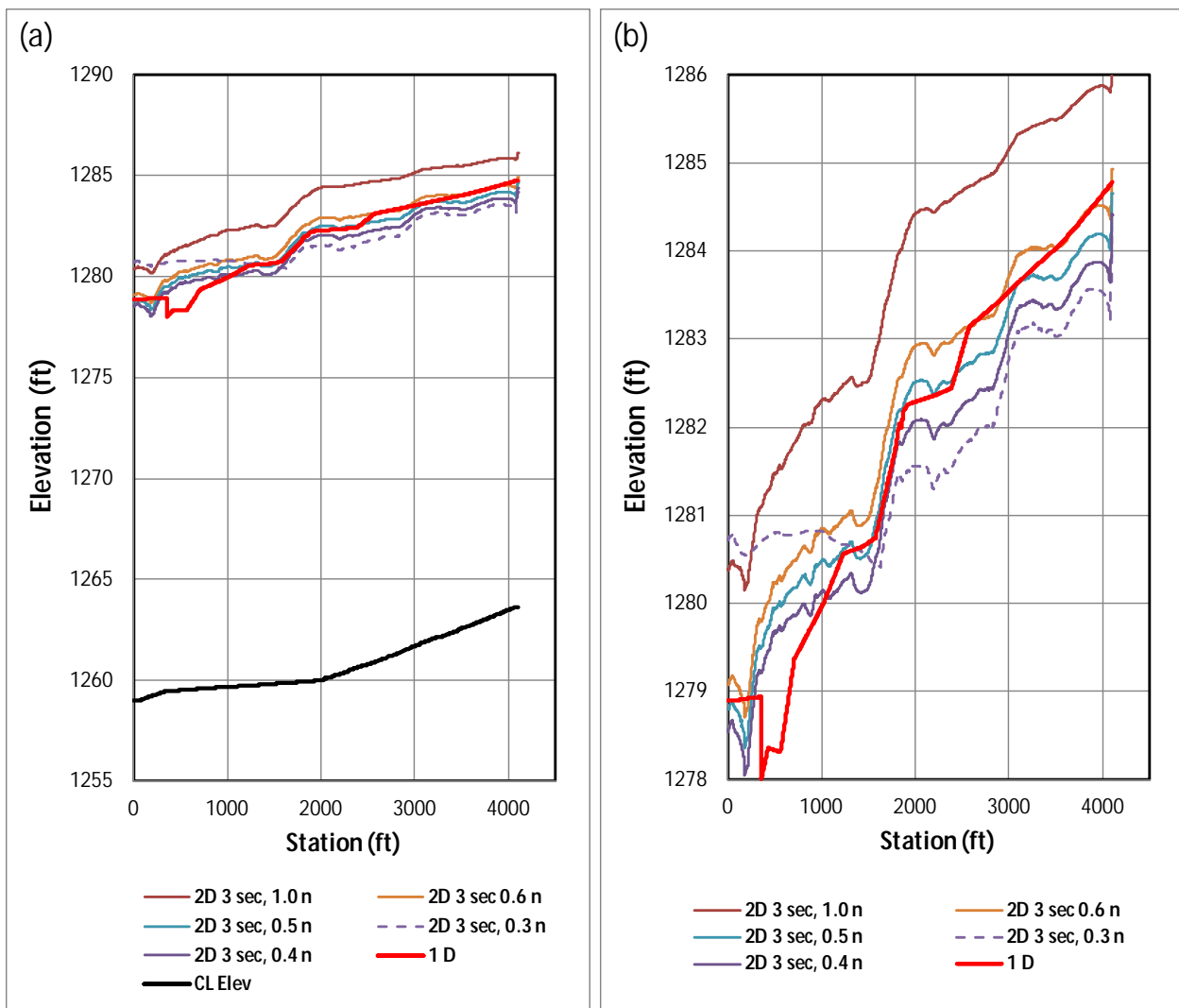


Figure 9.36: Tributary WSE Profiles for $\Delta t = 3$ seconds (a) with CL Elevation, (b) without CL Elevation

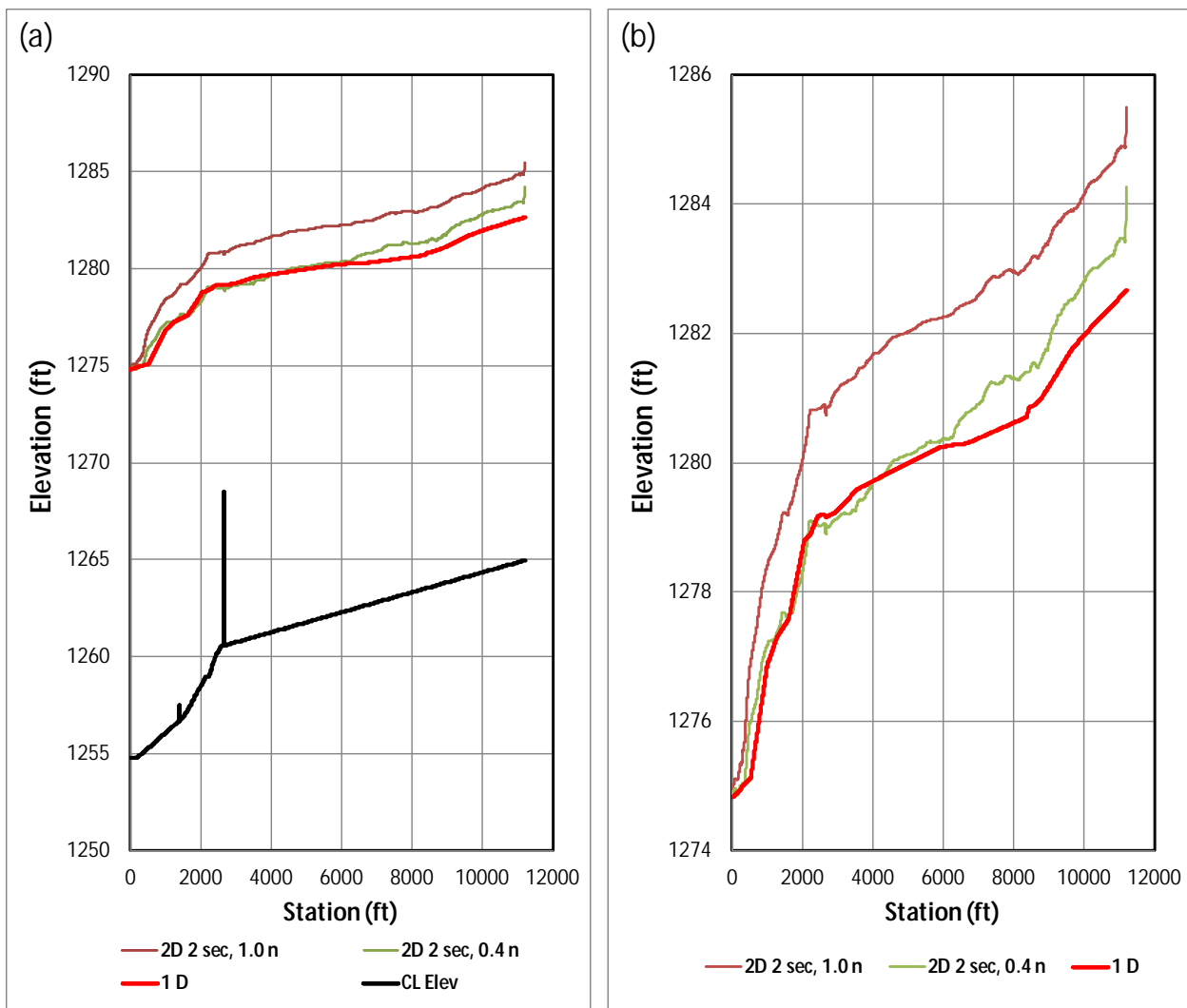


Figure 9.37: Main Channel WSE Profiles for $\Delta t = 2$ seconds (a) with Ground, (b) without Ground

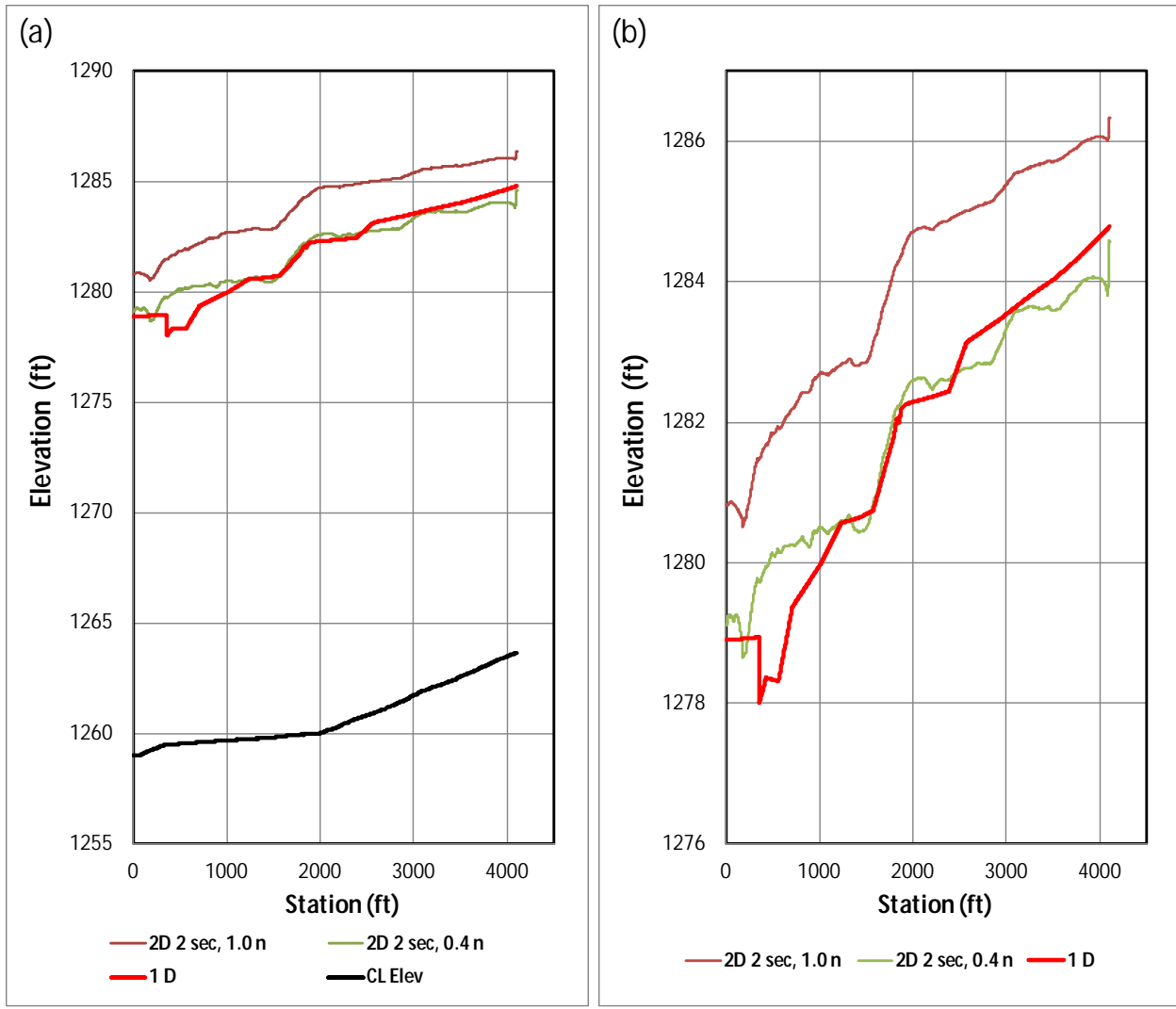


Figure 9.38: Tributary WSE Profiles for $\Delta t = 2$ seconds (a) with CL Elevation, (b) without CL Elevation

The 2D floodplains for the $\Delta t = 10, 5, 3$, and 2 seconds “best fit” profiles are shown in Figures 9.39 through 9.41, respectively, with the 1D floodplain. Table 9.2 gives the inundation areas for those floodplains. The agreement between the 1D and 2D floodplain areas were best for $\Delta t = 10$ and 5 seconds. Also, only landuse layers for even 10 percent intervals in the Manning’s roughness coefficient values were tested. Closer fits to the 1D profiles and floodplain areas could be achieved by testing tighter intervals such as 5 or even 1 percent. However, it seems excessive to seek an interval as small as 1%.

Table 9.2: Floodplain Areas

| 1D or 2D | Δt (sec) | Percent n_{1D} | Area (ft ²) | A_{2D}/A_{1D} |
|----------|------------------|------------------|-------------------------|-----------------|
| 1D | na | na | 6097260 | na |
| 2D | 10 | 70 | 6067448 | 1.00 |
| 2D | 5 | 60 | 5947997 | 0.98 |
| 2D | 3 | 40 | 5693280 | 0.93 |
| 2D | 2 | 40 | 6509720 | 1.07 |

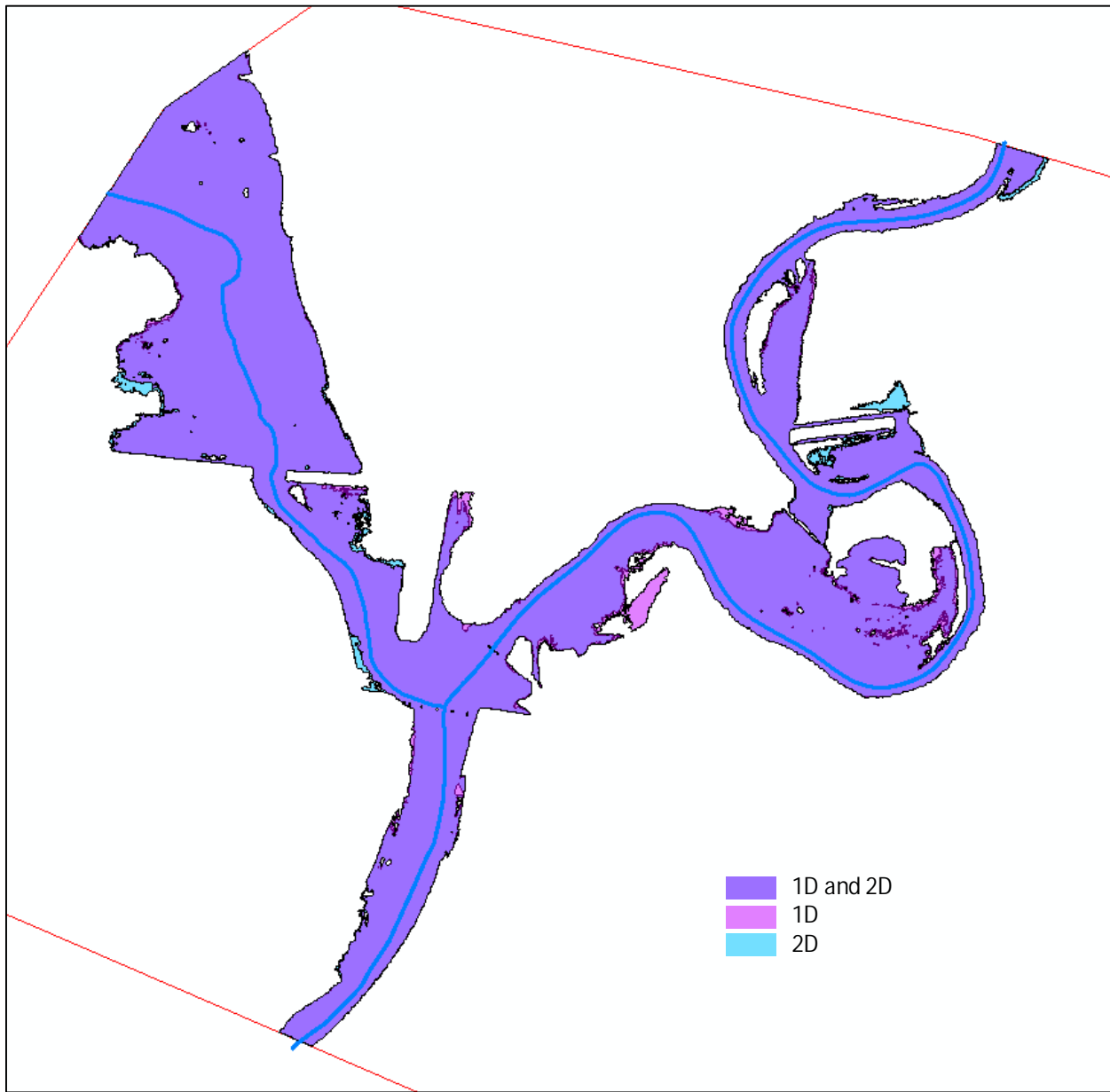


Figure 9.39: 1D and 2D Floodplain for $\Delta t = 10$ seconds, $n_{2D} = 0.7 n_{1D}$

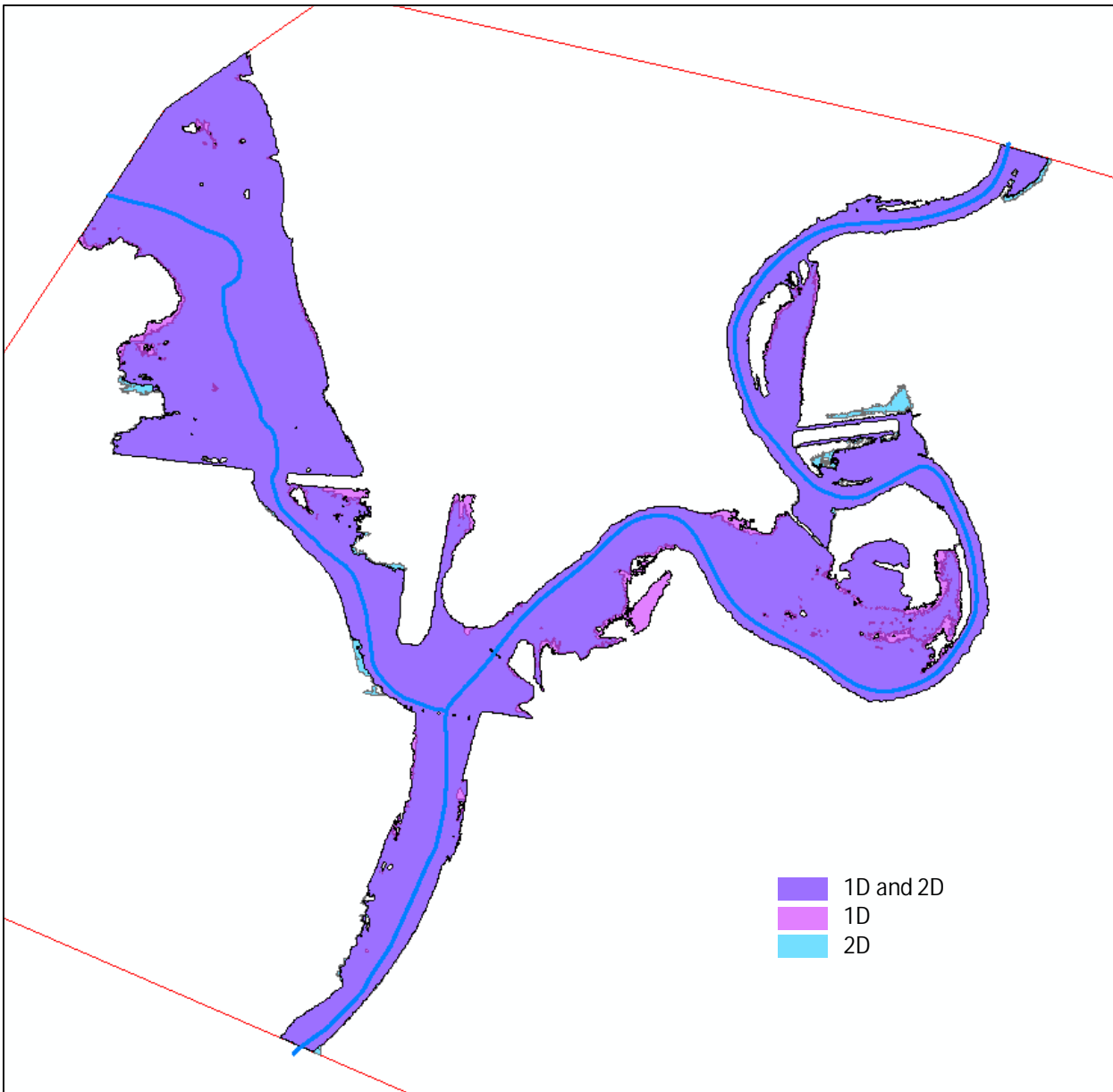


Figure 9.40: 1D and 2D Floodplain for $\Delta t = 5$ seconds, $n_{2D} = 0.6 n_{1D}$

9.5 Summary

This chapter demonstrated that 1D HEC-RAS model results can be matched very well by using 2D n -values that are lower than the 1D n -values. The fraction of the 1D n -values used is dependent on the 2D model execution time step, Δt . Since the amount by which the n -values should be lowered is not known for specific sites, calibration using a 1D HEC-RAS model is recommended. A method was also presented for cutting a trapezoidal channel into the flat, ponded region of a LIDAR coverage while maintaining most of the LIDAR bank data down to

the water edge (flat area). This application applies to inline weirs and to other sites where significant “below water surface” channel data is missing from the LIDAR data.

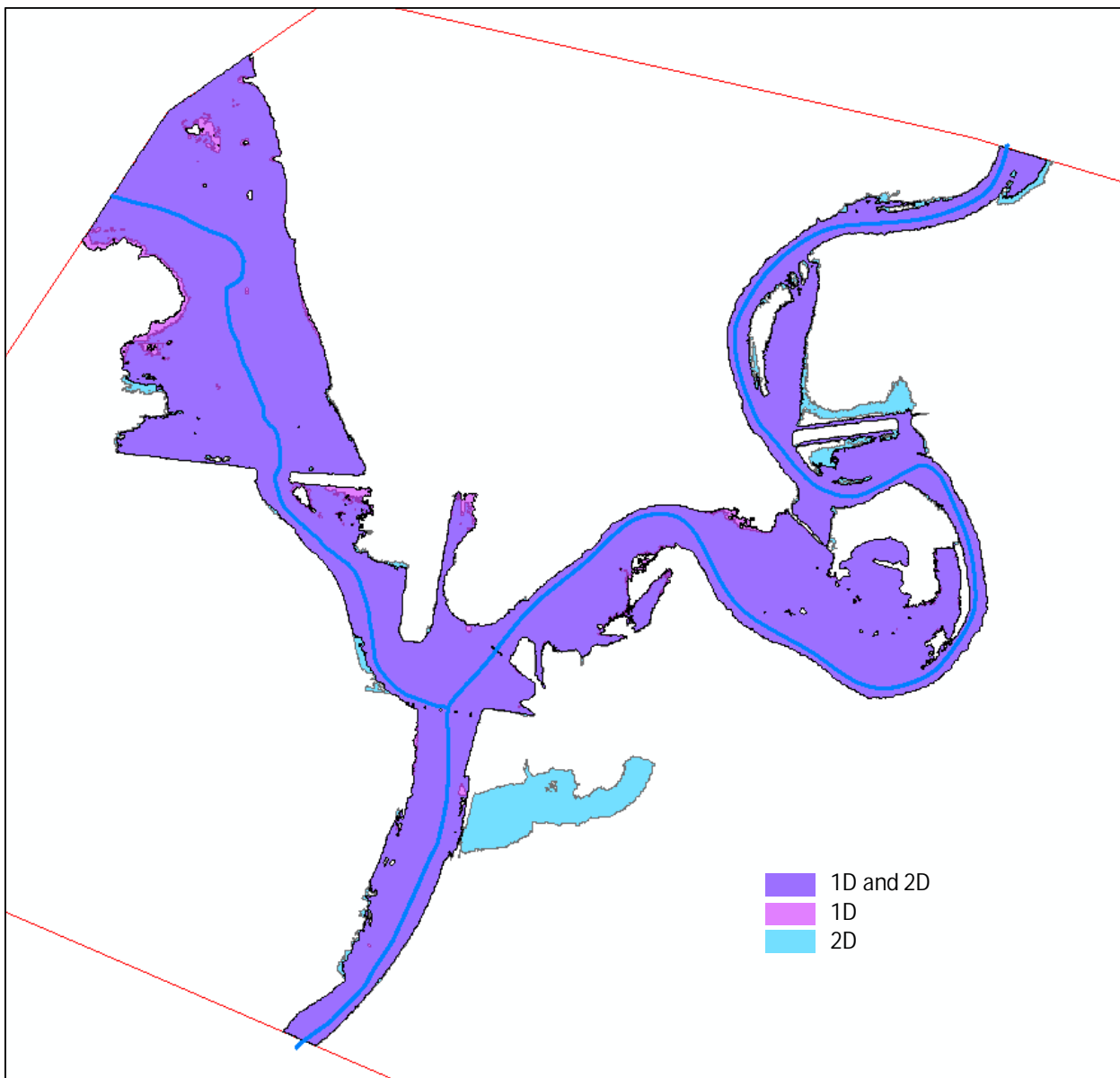


Figure 9.41: 1D and 2D Floodplain for $\Delta t = 2$ seconds, $n_{2D} = 0.4 n_{1D}$

Chapter 10: Conclusions

The work presented in this report has led to the following conclusions:

1. There is still a place for one-dimensional hydraulic models in the repertoire of the hydraulic engineer. This is in large part due to the much longer computation times required for the 2D models over 1D models. For the Neodesha test reach (Chapter 7), the HEC-RAS 1D model took 9 seconds to complete, the HEC-RAS 2D full momentum model took 24 hours, 16 minutes, and 3 seconds, and the SRH-2D model took by far the longest at 166 hours and 59 minutes. This consideration may make the two-dimensional models prohibitively time-consuming for many engineering firms for iterative bridge design projects.
2. The two-dimensional models require a great deal of judgement and editing in order to build a sophisticated representation of a site. However, even more judgement is often required for 1D HEC-RAS modeling at complex sites. In regard to the 2D models, subjectivity remains in the selection of the computational timestep as well as the mesh element locations, sizes, and distributions in order to achieve a balance between physically realistic results and computational efficiency. However, a simplified HEC-RAS 2D model could be set up very quickly using only the raw LIDAR data if details such as piers were not included.
3. The use of relatively coarse representations of a site for a simplified two-dimensional model, using either HEC-RAS 2D or SRH-2D, could greatly aid in directing the construction of 1D models by helping the engineer visualize general flow patterns for the site, flow distribution for multiple openings, and placement of cross sections and ineffective flow areas. In this manner the 2D models could help reduce the subjectivity inherent in building a proper HEC-RAS 1D model. Also, if hydraulic engineers begin to adopt this practice of using a 2D model to aid construction of a 1D

model, then the field may begin to shift towards a heavier reliance on the more mathematically advanced 2D models.

4. There are some serious concerns raised by the unresponsiveness of the 2D models to the Manning's roughness coefficient observed for the bridge model that was discussed in Section 6.5. The water depth upstream of the bridge cross section for the HEC-RAS 2D full momentum model showed no obvious connection to the value used for the channel roughness, while the SRH-2D model did—although even when the roughness coefficient for this model was reduced to all the way to 0.0001 from 0.0233, the reduction in depth was not enough to cause the 2D model to match the laboratory data. This and the fact that both two-dimensional models responded so differently to the change in the roughness coefficient when both were using the full St. Venant equations is troubling and warrants further investigation.
5. The divisions of flow through multiple opening bridges obtained from the 2D models are significantly different than those from the 1D HEC-RAS model. Thus the 2D models may be useful in guiding more accurate analyses of scour through bridges as well as sizing relief structures.
6. Virtually every analysis in this report shows that HEC-RAS 2D using the full momentum equations predicts the highest overall depths for any given site. This suggests that any analysis performed using exclusively that model to obtain results where high water levels are the critical variable would be the most conservative option. SRH-2D tends to return higher depths than HEC-RAS 1D as well, but not to such a degree as the HEC-RAS 2D full momentum model.
7. HEC-RAS 2D with the diffusion equation will underestimate losses over a reach, but for situations where local losses are relatively small this solution bears more resemblance to those from SRH-2D than from HEC-RAS 2D with the full momentum equation. This suggests a strong

possibility that a combined one- and two-dimensional HEC-RAS model using 1D routines through bridges and the diffusion equation set for the 2D flow areas would provide solutions that are a good balance between manual model set up, computational efficiency, and physically meaningful depictions of the flow behavior. Such an approach is particularly appealing for sites with highly sinuous streams that require accurate floodplain delineation.

Table 10.1 presents a qualitative comparison of HEC-RAS 2D and SRH-2D with considerations for model selection.

Table 10.1: Considerations for Model Selection

| Comparison | Notes |
|--------------------------|-------------------------------------------------------------------------------------------------------------------------------------------------------------------------------------------------------------------------------------------------------------------------------------------------------------------------------------------------------------------------------------------------------------------------------------------------------------------------------------------------------------------------------------------------------------------------------------------------------------------------------------------------------------------------------------------------------------------------------------------------------------------------------------------------------------------------------------------------------------------------------------------------------------------------------------------------------------------------------------------------------------------------------------------------------------------------------------------------------------------------------------------------------------------------------------------------------------------------------------------------------------------------------------------------------------------------------------------------------|
| Runtime | The way that HEC-RAS 2D captures sub-grid cell variability allows for larger cell size and larger timestep. Multiple comparisons of runtime were conducted throughout this study. Even when similar mesh densities and timesteps are used, HEC-RAS 2D is the faster model. For models producing comparable levels of results, HEC-RAS 2D can be up to 28x faster. Future research could further explore the acceptable limits of timestep and cell size for each model to allow for more efficient modeling. |
| Pre- and Post-Processing | ArcGIS (or other GIS software) is used to pre-process terrain data. SRH-2D, although a free program, requires expensive pre- and post-processing software (Aquaveo SMS). HEC-RAS 2D has built-in pre- and post-processing capabilities, eliminating the need for a 3 rd party program and allowing for more rapid model construction. HEC-RAS 2D interfaces with ArcGIS more smoothly than SRH-2D. |
| Setup Time | Model setup time varies greatly depending on the complexity of the site, the quality of the available terrain data, and the experience of the modeler. Both programs can be set up to run a simple scenario in less than an hour. Dealing with complexities (e.g., bridge piers) can add hours to the original model definition. |
| Accuracy | Chapter 6 presents a direct comparison of model results with laboratory observations. This is the only known comparison of the two models to actual data. In the evaluation, HEC-RAS 2D re-produces the observed laboratory data more reliably than SRH-2D (almost perfectly for 7 of the 8 runs). For the most extreme cases, HEC-RAS 2D only matches the observed data after increasing the timestep. Further research is needed to understand how to select the appropriate timestep <i>a priori</i> . SRH-2D shows a sharp break in the profiles right at the bridge for each run plus nearly horizontal profiles downstream of the bridge, indicating very small head losses in the downstream reach. In Chapter 7 and 8, HEC-RAS 2D generally produces a larger floodplain than SRH-2D and HEC-RAS 1D. Although it is not certain which model is more accurate in these comparisons (no observed data available for comparison), HEC-RAS 2D produces more conservative results. According to Gary Brunner of HEC, this is because smaller <i>n</i> -values should be used for HEC-RAS 2D than for HEC-RAS 1D. This is due to the longer particle travel lengths in the 2D model. For Manning's equation to maintain a constant friction head loss, Manning's <i>n</i> should be proportional to the square root of the length of travel. |

Table 10.1: Considerations for Model Selection (Continued)

| Comparison | Notes |
|---------------------------|----------------------------------------------------------------------------------------------------------------------------------------------------------------------------------------------------------------------------------------------------------------------------------------------------------------------------------------------------------------------------------------------------------------------------------------------------------------------------------------------------------------------------------------------------------------------------------------------------------------------------------------------------------------------------------------------------------------------------------------------------------------------------------------------------------------------------------------------------------------------------------------------------------------------------------------------------------------------------------------------------------------------------------------------------------------------------------------------------------------------------------------------------------------------------------------------------------------------------------------------------------------------------------------------------------------------------------------------|
| Flexibility | <p>HEC-RAS 2D has the ability to divide a modeling domain into 1D and 2D sections. This has the advantage of allowing 1D modeling where the river is acceptably one dimensional.</p> <p>Both models handle bridge piers easily. HEC-RAS 2D allows the use of HEC-RAS 1D bridge routines where appropriate to include overtopping and pressure flow. SRH-2D can be linked with HY-8 to simulate culvert flow. SRH-2D will allow for the simulation of overtopping in 2D at the same time a culvert someplace else on the same road is modeled using HY-8, while in HEC-RAS 2D the entire embankment must be simulated using 1D routines. At the time of this report writing, though, the SRH-2D linkage with HY-8 is unstable and difficult to work with.</p> <p>HEC-RAS 2D provides more flexibility and control of the inlet and exit boundary conditions. In HEC-RAS, the user can specify an EGL for the boundary conditions.</p> <p>Both programs allow for breaklines. The HEC-RAS 2D breaklines are easier to work with. SRH-2D requires more manual work in SRH to create the breaklines.</p> <p>HEC-RAS 2D allows for multi-sided elements (from 3 to 8). SHR-2D only allows for 3 or 4-sided elements.</p> <p>SRH-2D has the ability to model sediment transport (though this is not currently supported in the SMS interface).</p> |
| Support and Documentation | Neither model is thoroughly supported or documented. Although some documentation and training materials are available for SRH-2D, the model is being developed by the U.S. Bureau of Reclamation primarily for in-house modeling efforts. HEC-RAS 2D is being designed by the U.S. Army Corps of Engineers for the civil engineering modeling community. Although HEC does not explicitly support the model, the USACE is actively improving the model and is responsive to error reports and suggestions for improvements. |

Table 10.2: Considerations for 2D Modeling

| Issue | Notes |
|--------------------------------------|---------------------------------------------------------------------------------------------------------------------------------------------------------------------------------------------------------------------------------------------------------------------------------------------------------------------------------------------------------------------------------------------------------------------------------------------------------------------------------------------------------------------------------------------------------------------------------------------------------------------------------------------------------------------------------------------------------------------------------------------------------------------------------------------------------------------------------------------------------------------------------------------------------------------------------------------------------------------------------------|
| Manning's n Values | Additional research is needed to better understand the appropriate selection of Manning's n values in 2D models. Currently, the use of 1D Manning's n values in 2D modeling is standard practice. Due to the way HEC-RAS 2D includes sub-grid cell variability, a HEC-RAS 2D model should require smaller n values than a SRH-2D model with a similar grid cell size. For now, the greater concern in adopting 2D modeling is a more thorough understanding of mesh development, timestep selection, and boundary conditions. |
| Modeling Main Channels vs. Overbanks | Both SRH-2D and HEC-RAS 2D allow different Manning's n values for the main channel and overbanks. HEC-RAS 2D captures the sub-grid cell variability in terrain and will do a better job of capturing channel characteristics than SRH-2D. |
| Mesh Element or Cell Size | <p>Effective and efficient mesh development requires experience. Additional research could help define rules of thumb for cell size selection in HEC-RAS 2D and SRH-2D. In general, the cell size should be small enough to produce realistic results. Smaller elements are needed where the flow is moving or changing directions rapidly. For any particular model, the user can start with a coarse mesh and refine until the results do not change significantly.</p> <p>In SRH-2D, elongated rectangular elements can be used effectively when the flow direction is parallel with the long dimension of the rectangles (such as in the main channel). The use of quadrilaterals reduces the number of elements required. Triangulated elements should be used if the flow direction is uncertain or will change throughout the simulation.</p> <p>HEC-RAS 2D cell sizes can be much larger than SRH-2D cells due to the way HEC-RAS captures the sub-grid cell variability.</p> |
| Modeling Piers | <p>In SRH-2D, bridge piers should be modeled as voids.</p> <p>In HEC-RAS 2D, bridge piers can be simulated with very high Manning's n values or with raised terrain. Both approaches yield very similar results.</p> |
| Timestep Selection | The selection of timestep is challenging and requires additional research and/or experimentation by the model developer. The user wants to use the largest mesh cell size and largest time step possible while maintaining model accuracy. SRH-2D requires a Courant number ≤ 1 . HEC-RAS 2D can be used effectively with a Courant number larger than 1. |
| Adding Breaklines | Breaklines can be used in both models to help define road centerlines, toes of embankments, low points of ditches, the sides of the main channel, the centerline of the main channel, around levees, and in any other location where it is important to define a break in slope. |

Table 10.2: Considerations for 2D Modeling (Continued)

| Issue | Notes |
|------------------------------|----------------------------------------------------------------------------------------------------------------------------------------------------------------------------------------------------------------------------------------------------------------------------------------------------------------------------------------------------------------------------------------------------------------------------------------------------------------------------------------------------------------------------------------------------------------------------------------------------------------------------------------------------------------------------------------------------------------------------------------------------------------------------------------------------------------------------------------------------------------------------------------------------------------------------------------------------------------------------------------------------------------------------------------------------------------------------------------------------------------------------------------------------------------------------------------------------------------------------------------------------------------------------------------------------------------------------------------------------------------------------------------------------------------------------------------------------------------------------------|
| Hydrology | <p>To date, 1D floodplain modeling has been conducted using steady-state, peak flow conditions. Although 1D unsteady and 2D unsteady models are now available, the practice of using steady state peak discharges is likely to persist. For most situations, a steady-state simulation of the peak discharge will produce the most conservative result (storage is fully utilized). To emulate steady-state conditions in 2D models, it is advisable to use an inflow hydrograph that gradually increases from a low flow to the peak discharge and then levels out at the peak (rather than start with the peak flow, which can cause model instability). The timing of the ramp-up depends on the size and complexity of the domain and requires some experimentation by the user. The model must be run until the simulation reaches a steady-state solution. Again, this timing depends on the site and experimentation is required. Future research could develop rules-of-thumb for hydrograph input.</p> <p>The Butler County site in Chapter 9 presents a case where the stream discharge is affected by a tributary within the model domain. Currently, FEMA wants each stream segment modeled separately with a normal depth downstream boundary condition. Given the challenges of incorporating tributary flows and non-coincident peaks, 2D model application might be limited to stand-alone projects. 1D modeling might be preferred for large river systems.</p> |
| Bridge / Culvert Overtopping | Overtopping analysis should be performed using a 1D HEC-RAS model or a combination 1D/2D model where 1D is used for a few cross sections upstream and downstream from the bridge or culvert. Then, if needed, 2D modeling upstream and/or downstream from the 1D cross sections can be performed. This would be appropriate for regions with large meanders where flooding issues are prevalent. A 1D/2D combined model was used in analyzing the small culvert at the Crawford County site. The application of the 2D model through a culvert or even a bridge that is being overtopped is not recommended at this time. |

References

- Brunner, G. W. (2016a). *HEC-RAS River Analysis System hydraulic reference manual, Version 5.0* (Report No. CPD-69). Davis, CA: US Army Corps of Engineers, Institute for Water Resources, Hydrologic Engineering Center.
- Brunner, G. W. (2016b). *HEC-RAS River Analysis System user's manual, Version 5.0* (Report No. CPD-68). Davis, CA: US Army Corps of Engineers, Hydrologic Engineering Center.
- CEIWR-HEC (US Army Corps of Engineers Institute for Water Resources-Hydrologic Engineering Center). (1991). *HEC-2 Water Surface Profiles user's manual* (Report No. CPD-2A). Davis, CA: US Army Corps of Engineers, Institute for Water Resources, Hydrologic Engineering Center.
- Chow. V. T. (1959). *Open-channel hydraulics*. New York, NY: McGraw-Hill, Inc.
- Henderson, F. M. (1966). *Open channel flow*. New York, NY: Macmillan Publishing Co, Inc.
- Kundu, P. K., & Cohen, I. M. (2008). *Fluid mechanics* (4th ed.). Burlington, MA: Academic Press.
- Lai, Y. G. (2008). *SRH-2D version 2: Theory and user's manual: Sedimentation and river hydraulics – Two-dimensional river flow modeling*. Denver, CO: U.S. Department of the Interior, Bureau of Reclamation, Technical Service Center.
- McEnroe, B. M., Young, C. B., & Shelley, J. E. (2009). *Guidelines for stream realignment design* (Report No. K-TRAN: KU-08-2). Topeka, KS: Kansas Department of Transportation.
- Parr, A. D., Milburn, S., Malone, T., & Bender, T. (2010). *A model study of bridge hydraulics, Edition 2* (Report No. K-TRAN: KU-03-4R). Topeka, KS: Kansas Department of Transportation.



Kansas

Department of Transportation

